IMPROVING WAVE FORECASTING IN VARIABLE WIND CONDITIONS.

THE EFFECT OF RESOLUTION AND GROWTH RATE FOR THE CATALAN COAST.

PhD Thesis – Universitat Politècnica de Catalunya

MARTA ALOMAR

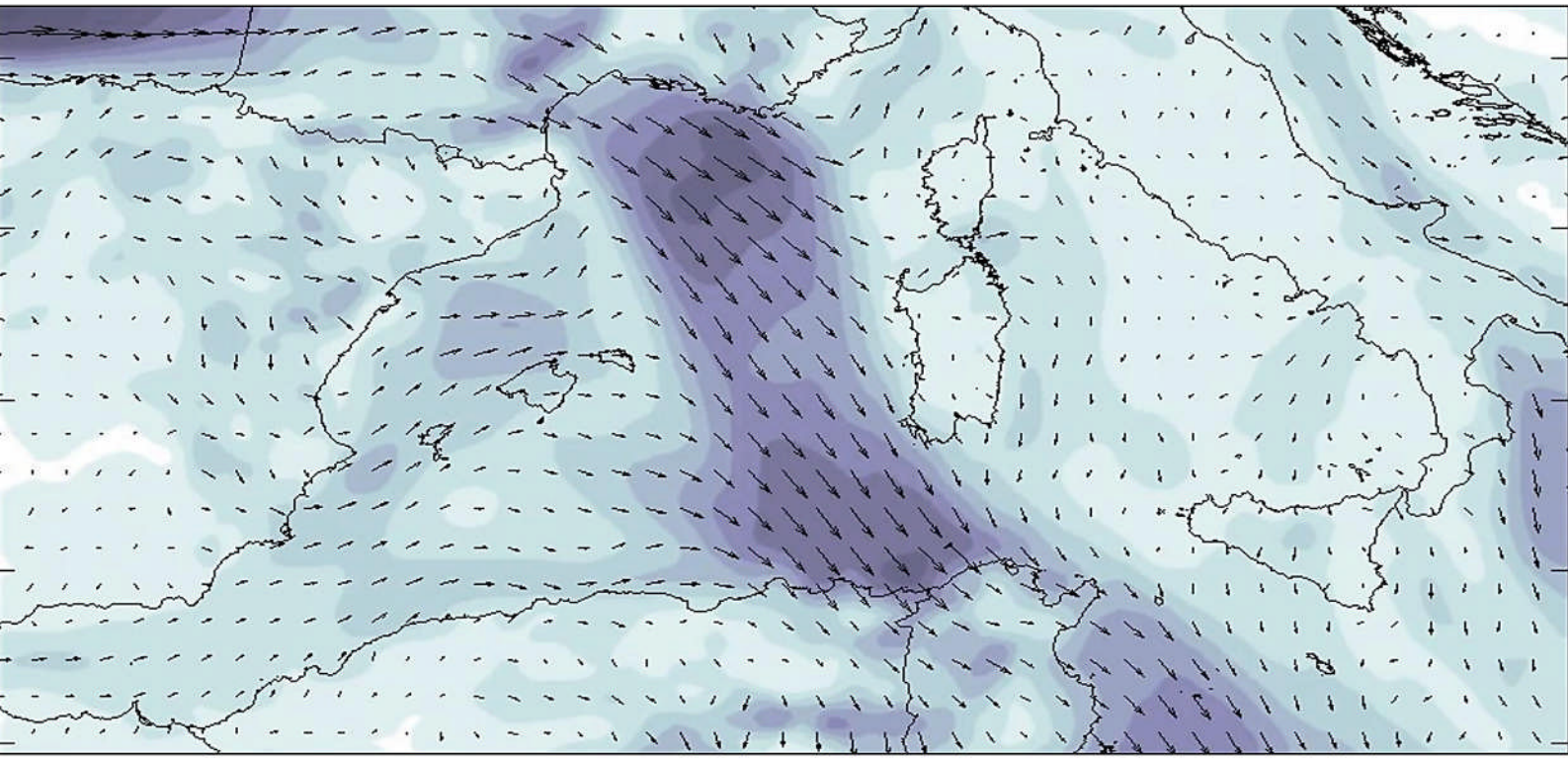

Thesis advisors
Dr. Agustín Sánchez-Arcilla
Dr. Rodolfo Bolaños
July 2012

Abstract

The main objective of this study is to improve wind wave forecasting in the NW Mediterranean Sea while focusing on the characteristic sharp gradients of the wind and wave conditions. This work was motivated by the limited accuracy of wave models in semi-enclosed-basins and orography-controlled wind conditions, especially during fetch-limited storm events. First, to reduce the commonly observed under-estimation of wave parameters, the mesoscale variability of wind and wave fields was characterized in time (1 h to 1 day) and in space (10 km to 100 km). Second, to better capture the typical sharp gradients, the grid size of the input wind fields was decreased during a characteristic storm event from 18 km to 4 km and the wind input frequency was increased from 6 h to 1 h. Third and last, the rate of wave growth in the numerical model was tuned in order to match the local rate of wave growth. The rate of non-dimensional growth in the region of study, which was calculated using measurements along the fetch, turned out to be faster than simulated using the default physical parameterizations and faster than reported in previous studies. Adjusting the wave growth rate in the model to the observations improved the estimated wave height about 18 % and the peak frequency about 4%. Decreasing the grid size of the numerical models from 12 km to 4 km improved the timing of the wave peaks but not the maximum values of the storm. Increasing the frequency of the wind input (from 6 h to 3 h) improved the estimation of the maximum wave height values (peaks) of the storm about 13%. Summarizing, the results of this work indicated that tackling wind and wave gradients in complex regions such as the study area it is posible to reduce the under-estimation of wave parameters and to improve wave forecasting.

Resum

L'objectiu principal d'aquest estudi és millorar les prediccions de l'onatge generat pel vent al Mediterrani Noroccidental enfocant-se en els forts gradients de vent i d'onatge característics de la zona. Aquest treball sorgeix de la falta d'exactitud dels models d'onatges en conques semi tancades i en condicions de vent controlades per l'orografia, especialment durant temporals d'onatge limitats pel 'fetch'. En primer lloc, per tal reduir les sub-estimacions dels parametres de l'onatge, s'ha caracteritzat la variabilitat dels camps de vent i d'onatge tant en temps (entre 1 h i un 1 dia) com en espai (entre 10 i 100 km). En segon lloc, per tal de capturar els forts gradients típics de la zona en els models numèrics d'onatge, durant un temporal característic s'ha reduit el tamany de malla dels vents d'entrada al model de 18 km a 4 km i s'ha augmentat la freqüència d'entrada dels vents de 6 h a 1 h. En tercer i últim lloc, s'ha ajustat la tasa de creixement de l'onatge en els models numèrics d'acord amb la tasa de creixement obtinguda a partir d'observacions locals. La tasa de creixement a la zona d'estudi, que s'ha calculat utilitzant mesures al llag del fetch, ha resultat ser més rápida que la predita utilitzant les parametritzacions incorporades per defecte en els models, i més rápida que les tases obtingudes en experiments anteriors. El fet d'ajustar la tasa de creixement en el model d'onatge ha permès millorar un 18% l'alçada d'ona significant estimada i un 4 % la freqüència de pic de l'onatge. Reduir el tamany de malla dels vents d'entrada de 12 km a 4 km ha permès millorar l'estimació en el temps dels pics d'onatge, però no els valors màxims del temporal. En canvi, augmentar la freqüència dels vents d'entrada (de 6 h a 3 h) ha millorat un 13% l'estimació dels valors màxims d'alçada d'ona durant el temporal. En resum, els resultats d'aquest treball indiquen que abordant els gradients de vent i onatge en regions complexes és posible reduir la sub-estimació dels paràmetres de l'onatge i millorar-ne la seva predicció.

Resumen

El objetivo principal de este estudio es mejorar las predicciones del oleaje generado por el viento en el Mediterráneo Noroccidental enfocando los fuertes gradientes de viento y oleaje característicos de la zona. Este trabajo surge de la falta de exactitud de los modelos de oleaje en cuencas semi-cerradas y en condiciones de viento controladas por la orografía, especialmente durante temporales de oleaje limitados por el 'fetch'. En primer lugar, para reducir las sub-estimaciones de los parámetros del oleaje, se caracterizó la variabilidad de los campos de viento y oleaje tanto en tiempo (entre 1 h y un 1 día) como en espacio (entre 10 y 100 km). En segundo lugar, para capturar los fuertes gradientes típicos de la zona en los modelos numéricos de oleaje, para un temporal característico, se redujo el tamaño de malla de los vientos de entrada al modelo de 18 km a 4 km y se aumentó la frecuencia de entrada de los vientos de 6 h a 1 h. En tercer y último lugar, se ajustó la tasa de crecimiento del oleaje en los modelos numéricos de acuerdo a la tasa de crecimiento obtenida a partir de observaciones locales. La tasa de crecimiento en la zona de estudio, que se calculó usando medidas de viento y oleaje a lo largo del fetch, resultó ser más rápida que la predicha utilizando las parametrizaciones incorporadas por defecto en los modelos, i más rápida que les tases obtenidas en experimentos anteriores. El hecho de ajustar la tasa de crecimiento en el modelo de oleaje permitió mejorar un 18% la altura de ola significante estimada y un 4 % la frecuencia de pico del oleaje. Reducir el tamaño de malla de los vientos de entrada de 12 km a 4 km permitió mejorar la estimación en el tiempo de los picos de oleaje, pero no los valores máximos del temporal. En cambio, aumentar la frecuencia de los vientos de entrada (de 6 h a 3 h) ha mejorado un 13% la estimación de los valores máximos de altura de ola durante el temporal. En resumen, los resultados de este trabajo indican que abordando los gradientes de viento y oleaje en regiones complejas se reduce la sub-estimación de los parámetros del oleaje y se mejora su predicción.

Acknowledgments

This dissertation would not have been posible without the support of many people and institutions, to which I am very grateful. From the funding point of view, four years fully dedicated to research were only posible thanks to the PhD scholarship received from the project RIMA (MEC, TRA2006-05132/TMAR), from the Spanish Government.

I would like to thank my supervisors Agustín Sánchez-Arcilla and Rodolfo Bolaños for their patience, guidance and advice. Also, I would like to show my gratitude to Daniel Gonález-Marco for the first months of guidance and to all the colleagues and co-workers at the Maritime Engineering Laboratory (LIM) for useful discussions and encouragement. I am especially indebted to Jordi Cateura and Joan Puigdefàbregas for their indispensable role in obtaining experimental data and to Federico Jerez for his help on obtaining data from operational simulations. I would also like to acknowledge the administrative staff at LIM and DEHMA for their precious assistance with the bureaucratic tasks and to my fellow coworkers and friends for the useful discussions and the priceless time spent together.

I owe special gratitude to Abdel Sairouni, from the Meteorological Service of Catalonia (SMC), for providing me with the high-resolution wind simulations that constitute the central part of this thesis. In this sense, the observational data obtained from the governmental networks XIOM, SMC, and Puertos del Estado, and Tarragona Port Authority also permitted to build a valuable data set to study wave growth in the NW Mediterranean.

It is a pleasure to thank the National Oceanography Centre (NOC; previously Proudman Oceanographic Laboratory) and the Centro de Investigación Científica y Enseñanza Superior de Ensenada (CICESE), two leading institutions that welcomed me and provided incalculable help and knowledge towards achieving this work. It was an honour for me working closely with Judith Wolf and Francisco J. Ocampo-Torres and their highly competent research groups.

I am grateful to Luigi Cavaleri for his useful reviews and comments on some important parts of my work, and to the external reviewers (Judith Wolf and Luciana Bertotti) and members of my committee for taking the time to read and evaluate this dissertation.

Additional financial support to present this work to the international community was provided by the Spanish project COVARIANCE (MEC, CTM2010-19709) and the European project FIELD_AC (FP7_SPACE-2009-1 nº242284).

This thesis is the result of several years of work, for which the assistance of all these people and institutions was priceless. However, not everything was easy and at some points it looked like an impossible task. Thankfully, anything is possible. Right now, and looking back, I realize there are many things to improve in the way PhD studies are carried out; just as many as within wave modelling! Improvements within doctoral studies, however, are out of the scope of this work.

The work here presented would not have been possible without the patience and support of family and friends. Thank you!

Index

1. Introduction

1.1. Motivation

Wind-generated waves are the result of wind speed blowing over water surfaces such as oceans, seas and lakes. Wind waves are usually characterized in terms of their wave height (or, alternatively, wave amplitude) and their peak period (or wave frequency); both parameters generally increase for increasing size of the water body (fetch).

Wind waves are an important element to be taken into account in many marine and coastal activities. The most common example is the role of harbours as protection structures against incoming wind waves. Harbours are designed to protect from and to resist the extreme wave heights typical of the regions where they are located. The activities inside harbours are also highly influenced by wind and wave conditions outside their boundaries. Particularly sensitive zones are the harbour entrance and loading and unloading docks, which cannot operate for wave heights above a certain limit (e.g. approximately 0.5 m depending on the location and the activity).

In coastal areas, there is also increasing pressure on beaches and near-coast structures such as housing, communication routes and other infrastructures such as power stations, which are highly vulnerable to sea level rise and strong wave storms. In the open sea, shipping, fishing and sport activities are also extremely influenced by the wind and wave conditions. Also, the activity of an increasing number of open-ocean structures such as drilling platforms and wind mills is tightly linked to the accurate knowledge of the sea conditions.

Our society is concerned with predicting sea conditions in advance to plan future activities, to recommend protection measures, to adjust working conditions, etc. To this end, numerical models are commonly used and accurate predictions are generally issued at each regional weather forecast centre at least 48 h in advance.

Wind wave modelling is the result of enormous efforts in trying to predict the surface roughness of water bodies. The first improvements in wind wave modelling were achieved during the Second World War for military purposes (e.g. Normandy landings). At present days, the wave modelling community is proud to say that successful estimations are achieved in many regions of the planet. Still, we are not happy with the level of accuracy achieved for many areas and we keep pushing the limits of knowledge in order to provide increasingly better predictions of wind waves.

The Mediterranean Sea is a good example where hard work is currently in progress due, at least, to two main reasons: the social and economic interest and the relatively inaccurate wave predictions being presently achieved. This is due to the peculiar geographical situation, being the Mediterranean Sea an enclosed basing surrounded by mountain ridges that strongly influence both the wind and wave fields.

The NW Mediterranean, in particular, is a highly populated region and there are a large number of uses and resources which require high accuracy in maritime predictions. Wind, wave and current predictions play a key role in forecasting maritime hazard situations and in supporting the corresponding management decisions for coastal, harbour and navigation authorities.

Bear in mind, for example, the ports of Barcelona and Tarragona, on the Spanish NW Mediterranean, which handled altogether close to 100 million tons of goods during 2007 (Puertos del Estado 2008). In coastal management, decision-makers are particularly interested in hazard assessment and the vulnerability of coastal systems to storm impacts. For example, beach loss is a direct consequence of storm-induced coastal processes that seriously threatens the infrastructures and housing that lie behind the coastal fringe. Sport and fishing activities, instead, strongly rely on accurate estimations of sea state parameters offshore. Additionally, the number of activities at sea in this region is also increasing; take for example the wind turbines under development in front of Tarragona.

Unfortunately, the predictability of wave fields in this region is known to be limited (Sánchez-Arcilla et al. 2008), which is often the case in semi-enclosed basins such as the Mediterranean Sea (Cavaleri and Bertotti 1997). In the NW Mediterranean Sea, in particular, wave height and period tend to be under-estimated (Bolaños et al. 2007), thus increasing the probability to miss important wave-related hazard situations. Therefore, and because of the high number of uses and resources in the coastal area, it is an economic, scientific, and engineering requirement to improve present day wave forecasts in the NW Mediterranean.

1.2. The RIMA project

The present work was a core part of the RIMA research project (Towards MAritime RIsk Reduction using High-Resolution Modelling) and their motivations were tightly related. Thus, it is of interest for the reader to be aware of the main objectives of the RIMA project in order to understand the general framework where this work was included.

The RIMA Project started in 2007 and ended in 2011. The main aim of RIMA was to calculate the wind, wave and current induced risks as a function of climatology, type of maritime activity and domain geometry. The main reason was that wind and wave risks associated to maritime or harbour activities were poorly estimated; partly because they rarely incorporated in the calculations the advanced knowledge and the tools available in the state-of-art.

The main output of the RIMA project was to be a dynamic definition of risk as a function of prevailing 'drivers' (wind, wave and currents) and the corresponding response of the activity (navigation, aquaculture, defence structures, mooring lines, etc.). This dynamic approach to risk was particularly intended to assess the sheltering potential of natural "refuge" areas.

The RIMA project started from the working hypothesis that risks due to wind, waves and currents in maritime activities were not properly estimated due to: i) the limited performance of numerical models, ii) the poor definition of equations intended to characterize the risk and identify sheltered locations, and iii) the limited use of advanced probabilistic tools to assess extreme values of the climatic parameters.

The RIMA project proposal set six intermediate goals regarding the three main sources of error mentioned above, but not all six goals were addressed in this work. In fact, this dissertation focused on only two of these goals, which were related to the limited performance of numerical models in estimating the 'drivers' (wind, waves and currents). The two RIMA goals of interest were:

1. To provide scientific advancement on the calculations of the 'drivers' at local scales (high resolution) considering the interactions among each driver and to improve the corresponding local parameterizations.
2. To validate any new parameterizations and numerical advancements with field observations from two pilot sites.

The scientific core of the RIMA project was the local interactions of wind/wave/current fields and the most suitable downscaling strategy to achieve accurate calculations at the harbour/'ria'/bay scale. RIMA considered that wind-, wave- and current-derived risks could be better estimated, and predicted in advance, if the present knowledge of their mechanics (physical, numerical and experimental) was extended to characterize in detail regions of interest at scales of a few meters and longer prediction horizons of up to one week. This achievement was expected to require an improvement of the individual (and coupled) parameterizations of wind, wave and current phenomena, and to lead to a more realistic assessment of risk and a reduction of its associated uncertainties.

The goals of the RIMA project were to be achieved using high-resolution simulations of wind, wave and current fields, and explicitly considering their coupled mechanisms and the interactions with the domain geometry. This approach was to be tested (and the resulting models validated) in two different domains: the Mediterranean basin (Tarragona) and the Atlantic Ocean (A Coruña). To this end, two intensive field campaigns were proposed at each of the study sites to additionally provide advanced and unique knowledge on the interactions among wind/wave/current fields at local scales.

The field campaign in the Mediterranean Sea (RIMA-Med) took place between the 30 Oct. 2007 and the 10 Jan. 2008. The obtained measurements are described in the following chapters. The field campaign in

the Atlantic Ocean (RIMA-Atl) started in Oct. 2008. However, none of the two instruments deployed could be recovered due to unexpected situations and no data was obtained for the Atlantic case study. Therefore, the RIMA project refocused on the observational data obtained at the semi-enclosed and micro-tidal Mediterranean basin only.

The general frame of this dissertation, in particular, was wind-wave interactions in the Mediterranean region (Tarragona Harbour). The remaining intermediate goals of the RIMA project were addressed by colleagues at the Universitat Politècnica de Catalunya (UPC), and partner institutions such as the Meteorological Service of Catalonia (SMC), MeteoGalicia, the Universidad de Santiago de Compostela (USC), and the Universidad Politécnica de Madrid (UPM).

1.3. Object of study

The objective of the present work was improving the wind wave forecasting in coastal seas, in agreement with RIMA objectives, with special focus on the region of study: the NW Mediterranean. To this end, a review of the state of the art of wave modelling, as presented in Chapter 2, was extremely important. The results from this analysis indicated, in short, that the main sources of error being commonly blamed for the inaccuracies of wave modelling in semi-enclosed regions are the limited knowledge of bimodal sea states and the variability of the forcing wind fields (Bolaños et al. 2007). In this work I focused, in particular, on the variability of the forcing wind fields during wave growth conditions for the reasons explained below in detail.

1.3.1. Fetch-limited wave growth

To understand why the focus of this work was placed on wind wave growth and not on bimodal conditions, notice first that bimodal states refer to two simultaneous wave trains with different characteristics: sea and swell. Sea refers to wind waves being actively generated by in-situ winds. Swell refers to wind waves that were generated by remote wind conditions but which are no longer growing. In other words, sea is still highly influenced by wind, whereas swell is only more residually influenced by wind. From the definition of bimodal sea states it is inferred that, if the variability of wind was a main source of error in the region of study, a previous and necessary step towards improving the prediction of bimodal conditions was to improve its wind-generated wave component (sea).

To introduce the importance of fetch-limited growth it is necessary to first introduce a few concepts related to wind sea waves and their generation process. The term wind sea refers to wave trains in the growing stage, during which energy is being transferred from the wind and the fully-developed state is not yet achieved. During the first stages of wave growth, waves are short (high frequency / short period) and their energy is low (low wave height).

Wave growth is achieved through energy transfer from the wind to those waves travelling at slower velocities than the wind. Note that wave speed is directly proportional to wave period and, thus, waves

speed up as they grow. In fully-developed wave conditions it is assumed that wind has blown long enough (in time) and over a long enough distance (fetch) so waves run as fast as the wind and they do not grow any more. Within the wave growing stages two different conditions may happen: fetch-limited and duration-limited waves. Fetch-limited waves are not fully developed because the fetch (distance) is not long enough). Instead, duration-limited waves are not fully developed because the wind has not blown long enough (time).

Wave growth in general is more easily studied in offshore-blowing wind conditions for which the length of the fetch is 'known' because it can be approximated with the distance to the coast along the wind direction. Note, however, that this approximation weakens in variable wind conditions during which wind may not blow uniformly from the coast towards offshore thus deviating from the more homogeneous conditions of wave growth. In fact, the accuracy of wave forecasting in fetch-limited conditions and variable wind conditions such as the region of interest is known to be limited (Bolaños and Sánchez-Arcilla 2006). For the above reasons, the focus of this work is wave growth in fetch-limited conditions (sea wave trains), as a preliminary step before addressing bimodal conditions in the future.

1.3.2. Mesoscale variability

First of all, one needs to be aware that the wind variability commonly blamed for the inaccurate wave predictions in the NW Mediterranean is mainly due to the complex orography of the coastal areas. Consequently, according to Bolaños (2004), the spatial scales involved are tenths of kilometres (width of river valleys) and the temporal scales are shorter than 12 h (mean duration of storms). It is important to bear in mind that these were the scales aimed at, as opposed to the much smaller scales of gustiness-induced variability (in the order of minutes). This clarification is essential because the scale of the target variability is a main novelty of this work.

In fact, gustiness as a source of variability affecting wave growth and wave forecasting was already addressed by several authors before (see for example Ponce de León and Ocampo-Torres (1998) and Abdalla and Cavaleri (2002)). The results from their work indicate that the higher variability induced by gustiness results in increased wave parameters (wave height and peak period). Inspired by this promising outcome, in the present work the goal was to improve wave estimations by including in the wave model the wind variability at larger scales both in time (hours) and space (kilometres). The mesoscale aimed in this study is a major contribution to the state of the art, which at present is focused in climate change, storm-length scales and gustiness. This study focused on temporal scales within short-duration storm events and the spatial scales associated to fetch-limited wave growth conditions.

1.4. Approach

Wave forecasting can be affected by wind variability in two different ways. On the one side, too coarse numerical resolutions (in time and in space) are prone to miss the high temporal and spatial variability of

the forcing wind fields. On the other side, the physical rate of wave growth (as currently implemented in wave models for rather uniform and constant wind speed) might differ significantly in highly variable wind speed conditions. Such physical differences could be related e.g. to a different drag coefficient (Babanin and Makin 2008) or to a different balance of energy (Ponce de León and Ocampo-Torres 1998).

In the present work, the approach taken to improve the estimation of wave growth in the region focused on the two groups defined above:

1. The spatial and temporal resolution of both the forcing wind and the wave model was increased to capture the mesoscale variability typical of the region. The higher variability of the wind fields and its overall improvement resulted in improved wave predictions, as it is shown below.
2. The different physical response of waves to variable winds was explored using a well known method: the non-dimensional wave growth curves, i.e. using observed data to derive empirical relationships between wind and waves. Previous authors usually used the rates of wave growth resulting from this method to calibrate wave models. In this work, characterized by the highly variable wind conditions of the region, higher rates of wave growth were derived in comparison with previous studies. To match the faster growth of the observations and to reduce the common under-estimation of wave parameters in the region, the wave model was accordingly tuned.

1.5. Specific objectives

Summarizing the previous sections, the aim of this work is to improve wave estimations in fetch-limited wave growth conditions by including variability-related processes in spectral wave models (i.e. increasing the variability of the forcing wind fields and adjusting the physics in the wave model to experimental data). A set of specific objectives, or milestones, were defined and were addressed in the process that lead us to improve wave estimations in the region. They are enumerated below:

- Describing the characteristic variability of wind and wave observations and simulations at the scales of interest: 1 h to 1 day and 10 to 100 km.
- Assessing the improvement achieved in wave forecasting by increasing the spatial and temporal resolution of the wind input fields. The models' grid size was reduced from 18 km to 12 and 4 km, and the wind input frequency was increased from 6 h to 3 and 1 h.
- Calculating the wave growth rate in the region of study from experimental data.
- Exploring different situations that could influence wave growth in the region (e.g. stability of the atmosphere, wind speed, etc.).
- Improving wave forecasting by tuning the wave model to the local rates of wave growth.
- Discussing the limitations of the present approaches.

1.6. Structure of the document

The present work was stimulated by the limited accuracy of wave models in the region. The present chapter introduces the main justifications for the approach taken in this work towards improving wave forecasting. The next Chapter 2 reviews the state of the art of each one of the approaches selected, including an overview of the problem of wave modelling and the possibilities to improve wave forecasting in the region of study.

In Chapter 3, the region of study is described and the wind and wave instruments with the observed datasets used to support this work are introduced. Also, the main characteristics of the wind and wave models used are presented. Chapter 4 is dedicated to basic methodologies employed throughout the document. The specific subjects addressed are the accuracy assessment of the numerical simulations (statistics and visual analysis), the identification of hazard situations (storm identification), and the performance assessment of operational wave models.

In Chapter 5, the particular features characteristic of the sharp gradients in the region of study and their implications for wave modelling are described. This is the first step towards including enhanced variability into wave models and characterizing the so-called mesoscale variability.

In Chapter 6 the spatial and temporal resolution of wind and wave models is increased and the improvements of wave predictions are assessed. Special attention is paid to the accuracy of the simulations in estimating the characteristic features of regional variability. The results indicated that the better estimation of the forcing wind variability in fetch-limited conditions resulted in over-estimated wind speeds but consistent under-estimation of the wave parameters.

The estimation of the non-dimensional wave growth curves from experimental data is presented in Chapter 7. Wave growth is explored in terms of different wind and wave conditions possibly affecting the growth rate (e.g. atmospheric stability, wave age, etc.). Chapter 8 presents the results from tuning the dissipation coefficient in the wave model to match the growth rates calculated experimentally; in this way, the under-estimations of wave parameters were slightly reduced and the predictions were improved.

Although the overall results were promising and confirm that improving wave forecasting is possible if wind variability is also taken into account, the remaining under-estimation of wave parameters indicated that there still is physical and numerical work to do. A critical evaluation of the methods employed in this work is included in Chapter 9. This chapter addresses, both, the limitations of increasing the resolution of wind and wave models and the restrictions of the physical parameterizations presently implemented in wave models. The discussion is completed with a review of the shortcomings associated to using the non-dimensional wave growth curves to study wave growth in variable wind conditions. The overall discussion suggested that the weakest point in wave forecasting is the parameterization of physical terms. This conclusion supports the path recently followed by other authors, which lead to newly developed

parameterizations (e.g. Ardhuin et al. 2010). The results presented also claim for further research towards increasing the understanding of wave growth in variable wind conditions.

The future work, main conclusions and the core findings of this work are enumerated in Chapter 10. The Annexes compile additional work that was done to either support or assist the achievement of the main advances of the dissertation. Annex I explains in detail the method employed to extrapolate wind speed at 3 m height to 10 m height. Annex II is dedicated to the quality control that was performed on the spectral data analyzed in Chapter 7. Note that the MATLAB function specifically written for this purpose (QC_raw.m) is submitted along with the dissertation. Annex III is dedicated to reviewing some of the existing sea/swell partitioning and identification processes. The MATLAB function that was specifically written for this purpose (ID_seaswell_1D.m) is also submitted along with the dissertation. All the references mentioned in this work are provided in last Chapter 11, including the references in the Annexes.

2. State of the art

Wind wave modelling is not a new subject and a lot of work has been, and is being, done towards improving wave predictions in a wide variety of regions and wind conditions. Nowadays, wave modelling in operational applications relies on spectral wave models, which are being used in a broad range of spatial scales from global to regional and local scales. The average accuracy obtained is quite good (4% bias and 0.11 scatter index from the global wave model being run operationally at the ECMWF; see Cavaleri et al. 2007). The situations/regions where spectral wave modelling is known to be inaccurate are sharp gradient conditions, such as short duration storm peaks associated with extreme events, and in enclosed basins such as the Mediterranean Sea, where fetch-limited generation often occurs (Cavaleri et al. 2007; Ardhuin et al. 2007). In this chapter I review the present knowledge of wind wave modelling that is relevant to the region of study (the NW Mediterranean Sea) and which further justified, both, the need to improve regional wave forecasting and the approach taken to achieve it.

2.1. Wave modelling in semi-enclosed regions: the NW Mediterranean

The Mediterranean Sea is a semi-enclosed sea for it has limited exchange of water with the outer ocean. It can be considered a big lake in the sense that it is highly influenced by the coastline and the surrounding orography. The Mediterranean region has been extensively studied because of the large number of social and economic interests. Wave forecasting in this region is not an exception and important progress was achieved in the past. All in all, in this region the under-estimation of wave parameters is not only common but it is also generally accepted (Cavaleri and Bertotti 2003, 2004). Note, however, that in other regions and under different conditions, under-estimating the wave parameters is no longer generalized and some authors report good wave estimations (Ardhuin et al. 2007, Rogers et al. 2003) and even overestimations (Bottema and van Vledder 2008, Bottema and van Vledder 2009).

Predictability limits in the NW Mediterranean lead to, generally speaking, under-estimation of wave height maximum values (in storm conditions) and over-estimation of wave height during calm periods (Bolaños 2004). The reasons for the limited predictability of wave fields in the Mediterranean region in general, and the NW Mediterranean in particular, are several. According to Cavaleri and Sclavo (2006) and Sánchez-Arcilla et al. (2008), these reasons are, mainly, the frequent offshore-blowing winds (with very small fetches along the land to sea direction) and the short-duration and veering wind fields, which

result in double peaked wave spectra. Additionally, loss of accuracy in wave estimations is due to the sharp gradients in orography and topography, which produce acute variations in the forcing wind fields.

The limitations of wave models in the NW Mediterranean region, in particular, were thoroughly addressed by Bolaños et al. (2004), Bolaños and Sánchez-Arcilla (2006), Bolaños et al. (2007). These authors identified the large gradients and high variability of the wind fields, on the one side, and the bimodality of the wave fields, on the other side, as the main sources of error in regional wave models. To reduce the importance of wind variability, these authors increased the models' spatial and temporal resolution. To address the bimodality of local sea states (mixed sea/swell), Bolaños and Sánchez-Arcilla (2006) derived a new parameterization of the drag coefficient.

In spite of the considerable efforts invested in improving regional wave forecasting, Sánchez-Arcilla et al. (2008) and Bolaños et al. (2009) acknowledge that wave predictions are not yet accurate enough. Bolaños et al. (2009)'s work was based on the previous work from Bolaños (2004), Bolaños and Sánchez-Arcilla (2006), Bolaños et al. (2007) and insists that the errors of operational models are due the sharp gradients of the region. Bolaños et al. (2009) stress, again, the importance of using high wind input frequency and high spatial resolution. High wind input frequency is necessary due to the faster (than 6 h) response of waves to wind change and to prevent information losses in short-duration storms. High spatial resolution is necessary to better resolve coastal processes such as wave diffraction, wind shadowing, etc.

In the literature, the very demanding met-oceanographic conditions are repeatedly blamed for the difficulties of predicting wind and wave conditions in the Mediterranean region. Evidence of these limitations were provided, for example, by Cavaleri and Bertotti (2004), who observed larger errors of model estimations in the northern coast of the Mediterranean Sea compared to the Southern coast. They attributed this difference in wave model performance to the more complex orography to the North (Pyrenees, Alps). In spite of the numerous references to the role of the high variability of the wind and wave fields as a main limiter of wave forecasting in the Mediterranean region, variability was insufficiently addressed if compared with other sources of error, especially in terms of mesoscale variability. For example, there were not enough detailed characterizations of the temporal and spatial gradients in the region. Also, no exhaustive approach was taken to reduce the influence of such variability in wave forecasting (physics and numerics).

For all the reasons above, the starting point of this work (working hypothesis) was to consider the sharp wind and wave gradients in the region as the main limitation of wave estimations. In this study, wave observations and simulations were addressed from the point of view of wind and wave variability, thus approaching wave modelling in the region from a quite different perspective.

2.2. Effects of wind variability on wave growth

Sánchez-Arcilla et al. (2008) point to wind variability as the main source of error in wave forecasting in the region because of the high sensitivity of wave models to wind field variations. However, so far, most of the work carried on towards including the effect of wind variability in wave predictions focused on the smaller temporal scales and gustiness. For example, the sensitivity of wave models to increased gustiness (small scale variability) was explored numerically by authors such as Ponce de León and Ocampo-Torres (1998) and Abdalla and Cavaleri (2002), among others.

On the one side, Ponce de León and Ocampo-Torres (1998) compared the effects of gustiness on wave estimations using two simulations for which the wind input time step was set, first, to 6 h and then to 5 min (white noise). Their results indicated that wave heights increase due to increased variability of the forcing wind fields (white noise/gustiness). In fact, a 24% increase of white noise results in a 10% increase of wave height. Ponce de León and Ocampo-Torres (1998) also reported additional effects of gustiness on wave modelling such as the broadening of the directional spectra and the presence of secondary energy peaks (bimodal spectra). These effects were attributed to the relative importance of young waves in the energy-transfer term from wind to waves in wave models.

On the other hand, Abdalla and Cavaleri (2002) compared the effects of gustiness on wave modelling using two time series with added gustiness. In this case, gustiness was not random but it was coherent in time. Gustiness was added at intervals of either 15 or 3 min. Abdalla and Cavaleri (2002) expected the presence of higher winds due to gustiness to, at least, increase the possibility of higher sea states. Indeed, their results indicated that, due to enhanced gustiness, wave height increases up to 20% after 3 days of simulation. According to these authors, the effects of gustiness are only relevant after almost two days of simulation and thus, the importance of gustiness in enclosed regions and dominant fetch-limited conditions (young waves) is limited, as explained below.

According to Abdalla and Cavaleri (2002) three different mechanisms can explain the enhanced wave growth due to gustiness: 1) the energy transfer from wind to waves increases when winds are faster than the waves, but it does not decrease proportionally in the opposite situation (waves faster than the wind); 2) the mean friction velocity (which depends on gustiness and drives wave growth) increases faster than the mean wind speed for increasing wind speeds; and 3) the energy input from wind to waves has a concave dependence on friction velocity, thus slightly enhancing the transfer energy due to gustiness for high wind speed conditions. According to these authors the first mechanism considered is not active during the first stages of wave growth (during which the wind is always faster than the waves) thus explaining the limited effect of gustiness on increasing wave height in enclosed regions.

Abdalla and Cavaleri (2002) also considered the possibility that the effects of gustiness were already indirectly included in physical formulations of wave growth. They concluded that the effects of gustiness

included in present-day formulations are limited and it is therefore meaningful to additionally include them in wave forecasting. In agreement with these results, Abdalla et al. (2003) calculated a new growth rate, which accounts for gustiness and is greater than the traditional one, whose impact on the model performance was, although positive, rather limited.

In addition to the mechanisms mentioned above, Babanin and Makin (2008) point to an increased drag coefficient in gusty wind conditions, which enhances the transfer of energy from wind to waves. However, it is important not to forget that an increased drag coefficient could also reduce surface wind speed (due to increased roughness) and, thus, the energy transfer from wind to waves might be instead reduced. In any case, note that the temporal scales explored in these previous gustiness-related experiments were much higher than the hourly time scales aimed at in this work.

Negative impacts of gustiness on wave forecasting (enhanced under-estimations) were considered by Bauer and Weisse (2000), who pointed out that the shorter duration of gusty winds reduces estimated H_s. These authors observed that the internal sensitivity of the wave model does not produce a noticeable response to wind frequencies higher than 3 h. All in all, Komen et al. (1994) stated that wave growth is indeed affected significantly by both the temporal and spatial variability of the wind fields (not necessary gustiness), thus justifying the interest to focus on wind and wave gradients in order to eventually improve wave forecasting.

2.3. Previous characterizations of wind and wave variability

Characterizing wind and wave variability requires high frequency measurements both in time and space. Ideally, spatial variability should be studied using remote sensing instruments. In the coastal zone, work in this direction was done, for example, within the SCAWVEX project (Wyatt 1998a). To infer variability of the wave fields in coastal zones, the SCAWVEX project used observations from radars and remote sensing instruments (Wyatt 1998a, Wyatt 1998b).

Wyatt (1998b) described in detail the results from the HF radar data in the SCAWVEX project and the comparison with buoy data and satellite-mounted radars. HF radar observations result in broader directional spectra, compared to measurements from floating instruments. In spite of their quality constraints (Wyatt et al. 2011), HF radars are much more suitable to study spatial variability, as opposite to the limited accuracy and suitability of point measurements (i.e. buoys). HF radar data can also be used to study wave development and decay but they are limited in terms of spatial coverage (distances up to 20 km offshore, approximately). Satellite-mounted radars, instead, provide good spatial coverage but are limited in terms of the temporal resolution (which depends on the orbital frequency).

Ocampo-Torres (2001) also addressed the spatial variability in the coastal zone using satellite radar altimeter and synthetic aperture radar (SAR). In spite of the limited temporal resolution of the data used,

these authors successfully described wave propagation processes in shallow waters; namely, refraction, diffraction and ‘groupiness’ (wave groups).

For the same purpose of describing the spatial variability, Queffeulou and Bentamy (2007) used remote sensing instruments (altimeters) in the Mediterranean Sea. Their analysis focused on seasonal, interannual and intrannual variability both in time and space and they looked for common patterns in the different Mediterranean sub-basins. In the short-scale, the results revealed sea state features associated with the meteorological patterns characteristic of each basin, such as the sharp gradients in off-shore blowing wind conditions in the NW Mediterranean area. However, this study also manifested the unsuitability of using remote sensing data to capture the time scale of the characteristic events due to its large sampling frequency (up to 9 days).

In the Catalan Coast (NW Mediterranean), in particular, the characteristic features of the spatial and temporal variability of the region were qualitatively described by Sánchez-Arcilla et al. (2008). Regional wind storms are typically short (less than 12 h), with veering winds and short fetches. Wind fields are characterized by the shadowing effect of coastal capes and mountain ranges. The typical wave climate is as complex as the wind fields, reproducing the gradients of the forcing winds and tending to develop bimodal wave spectra. Sánchez-Arcilla et al. (2008) use the word ‘torrential’ to describe the wave climate and to refer to the predominance of impulsive and discontinuous wave storms which are more energetic than the preceding calm periods. In terms of wind during torrential storms, in this document the expression ‘coastal wind jet’ is used to refer to the typical wind gusts, fuelled through river valleys and blowing over coastal waters. The description performed by Sánchez-Arcilla et al. (2008) addresses the general features of the region, but it lacks a more detailed description of the spatial and temporal gradients and mesoscale variability of wind and waves and their implications for wave forecasting.

In the present work, an array of floating instruments is used to further characterize the typical features of wind and wave gradients in the region and to analyse the capabilities of wave models in capturing and simulating the observed variability. Wind data from remote sensing sources was also used, but due to their coarse spatial resolution it was difficult to isolate the spatial scales of interest. Note also that even though coastal radars were not available in the region of study, their spatial coverage would not have been sufficient to describe spatial variability at distances as far as 50 km. Consequently, in Chapter 5 the time series recorded at the different instruments are compared. The time series were evaluated considering the position of the instruments in the directions parallel and normal to the coast. The differences between instruments permitted to effectively identify typical features of wind and wave variability in the area, such as coastal wind jets.

2.4. The resolution of the input wind fields

The most direct physical method to increase wind variability in wave forecasting is to increase the temporal and spatial resolution of the forcing wind fields. High resolution input winds are expected to, at least, prevent information losses in short-duration storms (e.g. peak/minimum values). In fact, in basins where the orography plays a substantial role, Signell et al. (2005) already indicated that high resolution wind models provide stronger and more accurate wind speeds overall, thus reducing the generally observed wave height under-predictions.

In the past, many authors reported improved wave predictions with high resolution models: some of their contributions are reviewed in this section. Summarizing, these past studies indicate that it is indeed possible to improve wave forecasting, and to better capture spatial and temporal gradients, by increasing the resolution of the models. Note, for example, that Cavaleri and Bertotti (2003) increased the resolution of the wind and wave models from 190 km to approximately 31 km to better represent the orography along the coast. They specifically aimed to better reproduce the sharp wind and wave gradients of the Mediterranean region. They concluded that although higher resolution models increase wind speed and reduce wave height under-estimations, further improvements should be related to reducing horizontal diffusion of wave models, improving their numerics or including data assimilation; all of which require increasing the computational power.

Also Cavaleri and Bertotti (2004) described, in semi-enclosed basins, decreasing wave errors with higher resolution models (up to 25 km). Additionally, Cavaleri and Sclavo (2006) performed a systematic increase of the resolution of wind and wave models (up to 25 km). They concluded that the maximum wind speeds increase asymptotically with higher resolution models, but the improvements are less important for sufficiently high resolutions. These results confirm that increasing the resolution infinitely will not necessarily improve wave estimations. These results also indicate that the description of the physics in extreme events is still inaccurate.

Besides the overall improvement of wave estimations for increasing resolutions, note that the minimum grid size considered by the authors above (e.g. Cavaleri and Bertotti 2003, 2004, 2006) is not enough to resolve the spatial scales of river valleys along the Catalan coast (about 10 km according to Bolaños 2004). In the region of study, decreasing the grid size of wind and wave models was already addressed by Bolaños (2004), among others. Bolaños (2004), in particular, assessed the improvement of predictions when using higher resolution wind (decreasing the grid size from approximately 28 km to 9 km) and wave models (from 28 km to 2 km). Bolaños (2004) highlighted the suitability of increasing the spatial resolution of the wind and wave models, especially during fetch-limited conditions (see also Bolaños and Sánchez-Arcilla 2006).

In addition to improving wave estimations in general, do not forget that the focus of this work was better estimating the regional wind and wave gradients. The ability to capture strong gradients using increased resolution models was addressed by Bertotti and Cavaleri (2009) who decreased the wave model's grid size to 7 x 5 km (the wind input frequency was 3 h). These authors confirmed that wind estimations improve when increasing the resolution of the wind models because smaller scale features are better estimated. However, they also concluded that the overall performance of wind and wave models still produce generalized under-estimations of both wind speed and wave height, when compared with remote sensing instruments. The resolution increase carried out in the present work complemented the results from the previous authors because, although also using high spatial resolutions, the wind input frequency was increased even more (up to 1 h instead of 3 h) in order to capture the short-duration of the local storm events. Also the characteristic features of sharp-gradients regions were specifically looked for (e.g. coastal wind jets).

2.5. Experimental wave growth curves

Wave growth is significantly affected by both the temporal and spatial variability of the wind fields (Komen et al. 1994) via, for example, an increased drag coefficient (see section 2.2 above). The exact physical processes are not yet well known but it seems clear that enhanced wave growth should be expected in variable wind conditions.

Wave growth is usually described as the non-dimensional evolution of wave parameters along the fetch. In this direction, the first similarity law was suggested by Kitaigorodskii (1962) (see, e.g. Kahma and Calkoen 1992; hereafter KC92) and it describes the growth of dimensionless wave energy (and peak frequency shift) along the dimensionless fetch. Since then, parametric wave growth curves have been commonly used to empirically calculate wave height under fetch limited conditions (e.g. inner basins, lakes). The reference study of wave growth along the fetch is the JONSWAP experiment (Hasselmann et al. 1973). It provided valuable evidences on the shape of the growing wave spectra and the downshift of the peak frequency along fetch.

The experimentally measured wave growth functions have also been used to tune the source functions of spectral wave models (e.g. Van der Westhuysen et al. 2007) and to validate the wind wave generation processes implemented therein. However, there is not a unique wave growth function and many deviations from the first similarity law for growing seas were reported (KC92). The first parameterizations were calculated assuming uniform and steady wind blowing perpendicular offshore (ideal fetch-limited conditions). Alternative parameterizations were derived under physical conditions that deviated from the ideal conditions such as the stability of the atmosphere (KC92), the morphology of the fetch (Pettersson 2004), and strongly varying wind conditions in time (Donelan et al. 1985; hereafter DO85). In this last case, both wind speed and wind direction were variable in time. Notice that DO85

considered it more valuable to describe wave parameters in terms of local conditions and they used the inverse wave age instead of the non-dimensional fetch as the independent variable. In KC92 they recalculated the development rates suggested by DO85 in terms of the more common scaling law of Kitaigorodskii (1962) and showed that the development rates along dimensionless fetch are comparable, in spite of the variability of the wind conditions and the differences of the data set. The effects of swell on wave growth were addressed, among others, by Ardhuin et al. (2007).

Overall, wave growth under spatially varying wind conditions has received comparatively limited research attention. The limited knowledge of wave growth in varying wind conditions is of great concern in coastal regions such as the study area, which is characterized by sharp spatial and temporal gradients of both wind and waves. I suspected that wave growth in variable conditions might differ from the more homogeneous conditions generally used to tune the wave models for several reasons (see also section 2.2 above). First, the performance of wave models in the region of study is seen to be limited, and wave parameters are often under-estimated (e.g. Sánchez-Arcilla et al. 2008). Second, temporal variability at small scales is already seen to numerically affect the simulated wave parameters. And third, it is physically possible that an increased variability increases, for example, the roughness of the sea surface which, in turn, may increase the transfer of energy from wind to waves (Babanin and Makin 2008).

2.6. Tuning wave growth in wave models

The non-dimensional wave growth curves are a valuable and easy-to-use tool to approximate wave growth along the fetch and to calibrate wave models. For example, the development rates derived by KC92 were used to calibrate recently developed expressions for wave energy dissipation (e.g. Van der Westhuysen et al. 2007, Ardhuin et al. 2010). The calibration of the wave model showed good agreement with the observations even though KC92's growth rates are relatively slow compared to the rates derived by other authors (such as DO85 and JON73). Also, the results presented by Hwang et al. (2011) showed that wave models tuned for idealized conditions still work well in real, but variable, situations.

Wave growth in SWAN wave model can be calibrated in many different ways, for example, increasing the amount of energy input from the wind or decreasing the amount of dissipation due to whitecapping; i.e. adjusting the energy balance. Because the generally less well-known process is whitecapping dissipation, this term is commonly adjusted to balance wind input (which is generally better understood). Indeed, whitecapping dissipation is right now the focus of many recent works which attempt to improve it in spectral wave models (e.g. Ardhuin et al. 2010, Banner et al. 2010). In spite of all previous efforts, a definitive expression for dissipation due to whitecapping was not yet agreed on. Therefore, adjusting the amount of whitecapping for local applications still is a practical alternative to calibrate wave models locally (Babanin and van der Westhuysen 2008).

3. Region of study and data used

3.1. The region of study

The area of study is located on the Southern Catalan coast, in the NW Mediterranean Sea (Figure 3.1). This region is characterized by a complex coastal orography, with the Pyrenees, to the north, as the main orographic feature running in an E-W direction and several abrupt mountain ranges parallel to the coast i.e. in a NE-SW direction (see Figure 3.2). During regional northerly winds, the orography favours wind channelling down the Ebro River and off the Ebro Delta. The same applies to smaller river valleys, which are associated with 'breaches' in the coastal mountain range and are expected to produce jet-like wind patterns over the coastal sea area.

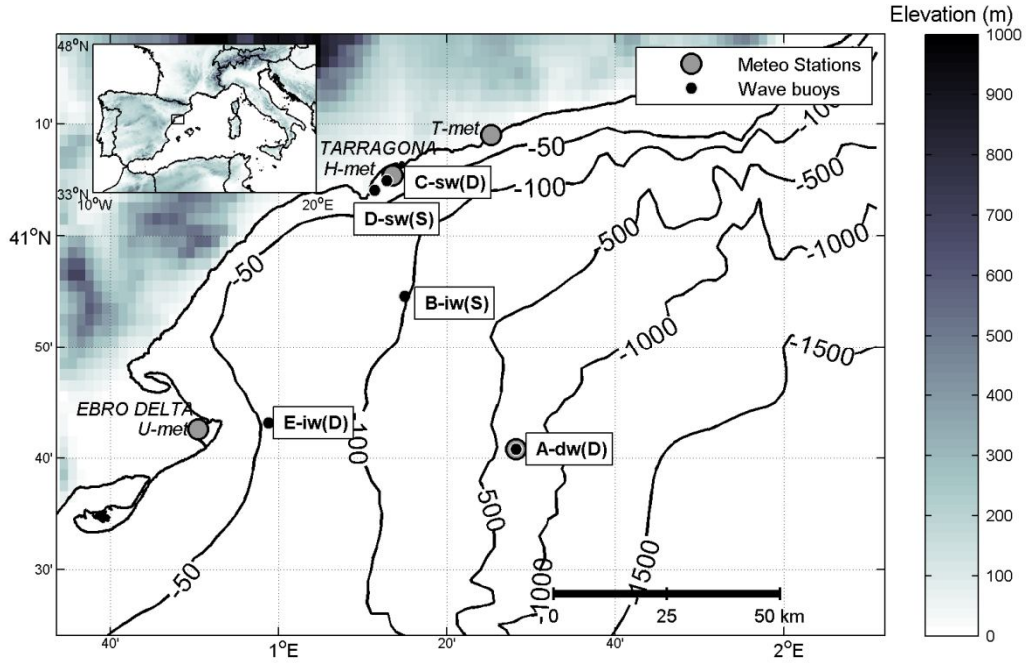

Figure 3.1 Location of the measuring instruments in the study region. B-iw(S), C-sw(D), D-sw(S) and E-iw(D) are wave stations (see Table 3.1). T-met, U-met and H-met are meteorological stations (see Table 3.2). A-dw(D) is simultaneously a wave and a meteorological station.

The characteristic northwest land-to-sea winds (Mestral in the local vernacular) are particularly intense and persistent, especially during the fall and winter seasons. In winter, eastern wind conditions (highest wind speeds) are also characteristic of the local wind climate; they are usually generated by a low-

pressure centre over the western Mediterranean. In summer, south-westerly winds predominate (Sánchez-Arcilla et al. 2008).

The directional distribution of waves in the region agrees with the wind climate and shows a predominance of northwest and eastern wave conditions, and some southern wave systems. The largest waves come from the east and northeast, which are the directions along the longest fetch. Double peaked (bimodal) wave conditions are often observed under strong local north-western winds and offshore easterly (or southerly) winds (Sánchez-Arcilla et al. 2008), especially in the Ebro Delta region, where these bimodal spectra can occur more than 50% of the time (Bolaños et al. 2009).

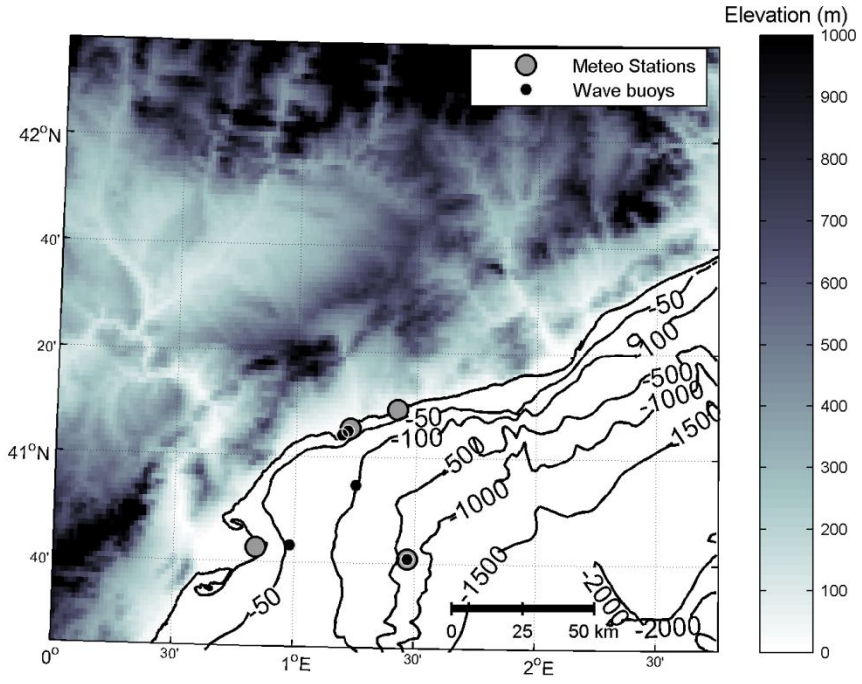

Figure 3.2 Orography of the Catalan Coast. Note that maximum height values are above 2000 m and are located in the northern mountain range, the Pyrenees. Nonetheless, the colour scale was set to maximum 1000 m to permit a better representation of the river valleys along the coastal mountain range.

The bathymetry presents a narrow continental shelf right in front of Tarragona's harbour: the 600 m isobaths is only 60 km offshore. Towards the south, the Ebro Delta is a geographical feature characterized by a gently sloping bathymetry which results in a wider continental shelf. In both regions, because depths are large relative to the prevailing wave lengths, deep-water growth conditions could be assumed for any waves being generated by offshore winds (and thus, fetch limited).

The variations of sea level in the Mediterranean Sea due to tiedes are not as important as in other larger seas or ocean domains (Bolaños et al. 2009). According to these authors, the tidal oscillations are in the order of 10 - 30 cm and thus, the area of study could be considered as a micro-tidal environment. These authors also reported a mean current intensity at 100 m depth of about 10 cm/s, although winter

intensifications reached 40 cm/s. Therefore, in this work, tidal levels and currents were not further considered because they were not expected to affect significantly the estimation of the wave fields (Bolaños et al. 2011).

3.2. Observational data

The data used in this work was classified in two groups: oceanographic and atmospheric data. Oceanographic data contained measurements of the sea characteristics, mainly surface wind waves and sea surface temperature. Atmospheric data referred to measurements of the atmosphere; namely, wind speed, wind direction and air temperature. The observations taken and used in this work are described below for each of the two groups of data.

3.2.1. Oceanographic measurements

In the region of study there were two permanent instruments monitoring Tarragona's wave conditions: A-dw(D) and D-sw(S). These two instruments were part of a national network that was being managed by the Spanish organization Puertos del Estado (EPPE). To make it easier for the reader to identify, at a glance, the characteristics of the wave instruments, keep in mind that their name consisted of a capital reference letter, which was followed by a pair of lower case letters that indicated the depth of the instrument (dw - deep waters; iw - intermediate waters; sw - shallow waters), and a bracketed letter indicating whether the measures taken were directional (D) or scalar (S). EPPE referred to A-dw(D) as 'Boya de Tarragona (Exterior)'; and to D-sw(S) as 'Boya costera de Tarragona'. A-dw(D) was a Seawatch meteo-oceanographic buoy that also measured water temperature at 1 m depth. D-sw(S) was a Datawell scalar Waverider buoy.

In order to provide a detailed description of wave storms along a perpendicular coastal transect, from November 2007 to January 2008 we carried out a field campaign called RIMA-Med. During RIMA-Med we deployed two additional wave measuring instruments in front of Tarragona's harbour: B-iw(S) and C-sw(D). C-sw(D) was deployed at the entrance of the harbour, and B-iw(S) was deployed 22 km offshore. B-iw(S) was a Datawell scalar Waverider buoy and C-sw(D) was an Acoustic Doppler WAve and Current profiler (AWAC).

Additionally, observations from another permanent instrument located south of buoy A-dw(D), and over a wider continental shelf, were also used to assess the spatial variability of the region along a horizontal coastal transect. This instrument was denoted as buoy E-iw(D) and it was a Datawell directional Waverider buoy. E-dw(D) was especially useful because of its directional measurements and because there were no data gaps during the RIMA-Med campaign. E-iw(D) was part of the regional XIOM network for oceanographic and coastal meteorological measurements (Bolaños et al. 2009). It belonged to the Catalan regional government under the name 'Cap Tortosa'.

The wave instruments, except C-sw(D), were wave-following buoys that measured the acceleration in the vertical direction (scalar and directional buoys) and in the north-south and east-west directions (directional buoys only). The acceleration data were converted to sea surface elevation using the buoys' own software which, first, filtered the signal using a low-pass filter with a cut-off frequency that depended on the sampling frequency. Second, the acceleration signal was integrated twice to get three translation values in the x, y, and z directions in the frequency range (see for example Datawell BV 2009).

Table 3.1 Description of the wave measuring instruments in Figure 3.1. Note that the buoys' name is a reference to its location and measuring characteristics (see the text). The 'record length' refers to the time during which the instrument was sampling and the 'record frequency' refers to the number of integrated measures every hour.

Instrument	Position (latitude/ longitude)	Depth (m)	Period of observation (dd.mm.yy)	Distance from the coast (km)	Sampling frequency (Hz)	Burst length (s)	Burst frequency (1/h)
A-dw(D)	40°41.0N 1°28.1E	672	19.11.07 – 10.01.08	48	1.28	1600	1
B-iw(S)	40º 54.7N 1º 14.9E	93	4.12.07 – 10.01.08	17	2.56	1200	3
C-sw(D)	41°04.9N 1°12.8E	23	30.10.07 – 30.11.08	1	2	1024	1
D-sw(S)	41°04.1N 1°11.3E	24	30.10.07 – 10.01.08	1	2	2560	1
E-iw(D)	40º43.3N 0º 58. 9E	60	30.10.07 – 10.01.08	10	1.28	1199.2	1

The wave data set were analysed using several integrated parameters of the energy spectrum: significant wave height (H_s), peak period (T_p), mean wave direction (θ_m) and peak wave direction (θ_p). The integrated spectral parameters were chosen over the statistical parameters to differentiate wave trains from different directions and origins (e.g. sea and swell). Spectral parameters describe the amount of energy in each frequency and direction (where available) whereas classical statistical parameters do not. Also, operational wave models were of spectral type and their common outputs were the integrated parameters as above.

The wave energy spectrum was calculated from the sea surface elevation time series, which were thought of as discrete Fourier sums. The amount of energy associated to each discrete frequency was calculated using a mathematical analysis called the Fast Fourier Transform (FFT). More information on how to calculate the energy spectrum can be found in Tucker and Pitt (2001).

The integrated parameters H_s and T_p were calculated from the momentums (m_n) of the energy spectrum using the following expressions:

$$H_s = 4\sqrt{m_0} \qquad T_p = \frac{m_{-2} \cdot m_1}{m_0^2} \qquad \textbf{[3.1]}$$

The direction from which the most energetic waves were coming from (peak of the energy spectrum) was denoted as θ_p and the mean direction (coming from) of all the waves registered was denoted as θ_m. Note that the peak frequency (f_p) is the inverse of the peak period. The integrated parameters were obtained using each instrument's own software, when available. Otherwise, WAFO Matlab toolbox was employed (Brodtkorb et al. 2000). WAFO is a MATLAB toolbox that calculates the energy and directional spectra and the integrated wave parameters from the raw data time series of surface elevation. WAFO was also used to calculate the frequency and directional spectra from the free surface elevation measurements at each instrument.

The raw time series and the corresponding energy spectra were submitted to a strict quality control to remove possibly erroneous records. The quality control on the raw data and the frequency spectra was mainly taken from Casas-Prat and Holthuijsen (2010), and it is described in detail in Annex II.

3.2.2. Atmospheric measurements

During the period of study and within the area of interest, wind speed, wind direction and air temperature were recorded at four different meteorological stations: the deep water meteo-oceanographic buoy A-dw(D), a coastal-sea station located on Tarragona's harbour breakwater (H-met), and two coastal-land automatic meteorological stations T-met (north of the port), and U-met (south of the port). H-met data were provided by Tarragona's Port Authority during the RIMA-Med field campaign. T-met and U-met were provided by the Catalan Meteorological Service (SMC). The location of each station is shown in Figure 3.1 and their characteristics are summarized in Table 3.2.

A-dw(D) wind data were measured at a height of 3 m and were extrapolated to 10 m elevation using a shear stress formula to calculate the friction velocity. The drag coefficient was taken after the Smith and Banke (1975) drag law, and the roughness length was calculated after Charnock (1955) relationship (Charnock's constant equal to 0.04) assuming a logarithmic profile of the atmospheric boundary layer (see Komen et al. 1994). The method used is described in Leake (2007) (see Annex I) and it is widely used and validated in the literature. Note additionally that Bolaños and Sánchez-Arcilla (2006) derived an alternative drag coefficient for the region of study, whose main feature was the consideration of mixed sea conditions.

In Chapter 6, an additional source of winds at sea is used: real time blended surface wind data provided by IFREMER (2007). In this case, wind data over the sea were obtained by blending ECMWF analysis data with remotely sensed data every 6 h at 0.25º (degrees) spatial resolution. Remotely sensed wind data were derived from near real time measurements from Seawinds (scatterometer onboard QuikSCAT

satellite) and from three Special Sensor Microwave Imagers (SSM/I; onboard DMSP satellites F13, F14, and F15). More details on the blending process can be found in Bentamy et al. (2007).

Table 3.2 Characteristics of the meteorological stations in the region of study (Figure 3.1).

Station	Position (latitude/ longitude)	Burst length (s)	Burst frequency (h^{-1})	Height relative to sea level (m)	Height relative to the ground (m)	Location
A-dw(D)	40.68°N 1.47°E	600	1	0	3	Offshore buoy
H-met	41.09ºN 1.23ºE	600	1	2	10	Tarragona Harbor's breakwater
T-met	41.15°N 1.42°E	1800	2	2	10	Torredembarra
U-met	40.71°N 0.84°E	1800	2	0	10	Illa de Buda – Ebro Delta

3.3. Simulated data

In this work I used the spectral wave models currently used at the Maritime Engineering Laboratory (LIM) and the atmospheric models used at the SMC. Below, I describe the different numerical models used throughout this work to estimate waves from forcing wind fields.

3.3.1. Wave models

There exist mainly two different types of numerical models presently used to simulate waves: phase-resolving models and spectral wave models. Phase-resolving models are used, as its name indicates, to resolve the exact value of the free surface and the individual waves. These models are very expensive computationally and, thus, are commonly used for very small scale applications (in the order of hundreds of meters and tenths of minutes, at most). Spectral wave models, instead, consider the sea surface as a discrete sum of regular waves and calculate the evolution of the energy spectra which is representative of the sea surface. Spectral models are not able to resolve the exact shape of the free surface but are much less expensive computationally and can be used for larger areas and longer periods of time. Also, they easily permit to calculate the generation of waves from winds. For all these reasons, operational predictions of wind waves are mainly conducted using spectral models.

There are three main spectral wave models being used world-wide by the wave modelling community: WAM, SWAN and WAVEWATCH. Each model has advantages and disadvantages but their accuracy is comparable in relatively homogeneous wind wave situations such as those encountered in open seas (see for example The WISE Group 2007). In this work I focused on the first two models because they have been traditionally used in the region of study and they produce acceptable results (see for example Bolaños et al. 2007).

The wave model running operationally for the Catalan coast at the time of the study was WAM Cycle 4 (Günther et al. 1992), modified for coastal applications by Monbaliu et al. (2000) and adapted for the Catalan Coast (Bolaños 2004). SWAN (Simulating Waves Nearshore; version SWAN 40.72ABCD), is specifically designed for coastal areas (Booij et al. 1999, Ris et al. 1999) and, in the study region, it was implemented and adapted for comparative purposes (see e.g. Bolaños et al. 2007).

Both models are based on the action balance equation for given source and sink functions. However, SWAN uses an implicit scheme for wave propagation, which is computationally more economic in shallow waters than other state-of-the-art third generation models (including WAM), and claims to provide additional robustness to the model. In WAM, wind input and dissipation formulations depend on the existing sea state and are taken from Janssen (1989, 1991), hereafter referred to as JAN. SWAN deep water physics are taken by default from a previous version of the WAM model and are due to Komen et al. (1984), hereafter referred to as KOM. In SWAN it is also possible to use JAN formulations, as well as the modification of KOM to improve the dissipation term such as it was introduced by Van der Westhuysen et al. (2007), hereafter referred to as WESTH.

For the Catalan coast, WAM was operationally forced with wind input from MASS atmospheric model (see below) every 6 h. Wave predictions were issued twice a day with a spatial resolution of approximately 18 km (1/6º) and a forecasting horizon of 48 h (further details in Bolaños et al. 2009). Previous assessments of WAM's performance in the region reported a 0.36 m root mean squared error and - 0.075 m bias (Bolaños et al. 2007, Bolaños et al. 2009). In this work, the performance of the operational wave prediction system was recalculated again, for reference purposes, in Section 4.5.

In this work, I ran SWAN with ad-hoc settings at different resolutions and using forcing wind fields from both MASS and MM5 atmospheric models. Further details are given in Chapter 6, where I improved wave estimations by increasing the resolution of the wind and wave models.

3.3.2. Atmospheric models

In this work two atmospheric models were used: MASS and MM5. At the SMC, during the RIMA-Med campaign, the operational wave prediction system consisted of MASS (Mesoscale Atmospheric Simulation System) atmospheric model and WAM Cycle 4 wave model. The geographical grid of both models covered the western Mediterranean Sea and spanned from 34º N to 45º N in latitude, and from -4.83º W to 18.17º E in longitude. The wind input frequency to the wave models was 6 h and the spatial grid resolution was 1/6º (approximately 18 km) (see Bolaños et al. 2009 and Sánchez-Arcilla et al. 2008).

The MASS 5.13 atmospheric model is a 3-dimensional hydrostatic primitive mesoscale model designed to be implemented using 20 to 40 levels in the vertical, and horizontal spatial resolution ranging from 10 km to 100 km (Codina et al. 1997). The planetary boundary layer parameterization used in MASS was a high resolution Blackadar type. Surface energy and moisture budgets included the parameterization of

surface hydrology and evapo-transpiration. The model forecast's variables included both cloud water/ice and precipitation, and the parameterization of its interaction with water vapour and with long and short wave radiation. The interaction of long and short wave radiation at the surface and within the atmosphere was also included in the parameterization. To account for the effects of sub-grid scale cumulus convection in high resolution simulations, the Fritsch-Chappell scheme was used in order to avoid over-estimating convection in mountainous areas.

To parameterize some of the processes accounted for in the MASS model, the use of global and regional databases was needed. The sources of these data are described in Table 3.3. The observational data for initialization and boundary conditions were interpolated from the Aviation global model (AVN) to the model grid using optimum interpolation. MASS ran twice a day with an output frequency of 6 h and a 48 h forecasting horizon until the end of 2008, when it was substituted operationally at SMC by the MM5 atmospheric model.

Table 3.3 Databases used in the parameterizations of the MASS atmospheric model (after Codina et al. 1997**).**

Parameterization	Source
Terrain elevation	U.S. Central Intelligence Agency 5 minute x 5 minute (about 9 km resolution) topographical database
Land/water boundaries	U.S. Navy 10 minute resolution data set
Normalized Difference Vegetation Index (NDVI)	Monthly Global Vegetation Index (GVI) from the Global Ecosystems Database CD-ROM at 10 minute resolution
Soil type	Webb global soil texture class from the Global Ecosystems Database CD-ROM at 1 degree resolution
Land use and land cover data	Olson World Ecosystems Database CD-ROM at 30 minute resolution
Climatological Sea Surface Temperature (SST)	Bi-weekly U.S. Geological Survey SST climatology at 12 minute resolution

At the time of this work, the operational wave system at the SMC used the MM5 atmospheric model and the WAM wave model in the same domain (Mediterranean Sea). MM5 vs.3.5 is a nonhydrostatic primitive-equation model that uses terrain following sigma coordinates (Grell et al. 1994). It was running operationally for the Catalan coast at the SMC, since 2008, with a spatial resolution of approximately 15 km; output wind fields were provided every 6 h.

For the present work, the SMC simulated a specific 7-days storm event using ad-hoc settings to provide the best wind estimations possible. For this purpose, three MM5 simulations were nested with horizontal resolutions of approximately 36 km, 12 km and 4 km. The mother domain covered southwest Europe and was initialized every 24 h with wind data from the European Centre for Medium Range Weather Forecasts (ECMWF) re-analysis data at 0.5° spatial resolution. The second domain covered Catalonia and south France and the finer domain covered only Catalonia (northeast Spain). Each simulation of the

model assimilated surface observations (METAR, SAO, SHIP) and upper air sounding data (RAOB data). The output frequency was 3 h for the coarser domains and 1 h for the finer grid. The output wind speed from MM5 at height 7 m was extrapolated to height 10 m using the same shear stress formula that was used for the observations at buoy A-dw(D) and assuming a logarithmic wind profile (see section 3.2.2 above and Annex I).

Note that the simulations from the two wind models, MASS and MM5, could not be compared because they were run for different purposes and with different input data. MASS wind fields were operational predictions whereas the initial conditions in MM5 assimilated local observations to further improve the accuracy of the wind fields at sea.

3.4. Periods of time explored

The present dissertation and the work presented herein use four main data sets. Each data set contains wave data for specific periods of time and/or using different wind and wave data, as summarized in Table 3.4. In order to avoid later confusions, the four data sets are briefly presented here, and are described again in more detail in the corresponding chapters (see last column of Table 3.4).

Table 3.4 Data sets for different periods of time as used throughout this document.

Data set	Period of time	Wave instruments	Meteorological stations	Used in
RIMA-Med	30.10.2007 – 10.01.2008	A-dw(D) B-iw(S) D-sw(S) E-iw(D)	A-dw(D) H-met U-met T-met	Chapter 4, 5, 6
Storm nº3	7.12.2007 – 13.12.2007	A-dw(D) B-iw(S) D-sw(S) E-iw(D)	A-dw(D) H-met U-met T-met	Chapter 5, 6
Fetch-limited	7.12.2007 5h – 8.12.2007 15h & 9.12.2007 20h – 11.12.2007 20h	A-dw(D) B-iw(S) D-sw(S) E-iw(D)	A-dw(D) H-met U-met T-met	Chapter 6
Long-term reference	20.08.2004 – 25.11.2009	A-dw(D)	A-dw(D)	Chapter 6

3.4.1. The RIMA-Med field campaign

The RIMA-Med field campaign was designed to measure wave data under fetch limited conditions and double-peaked sea states in front of Tarragona Harbour, as described above. The RIMA-Med study period started on the 31 Oct. 2007 and finished the 10 Jan. 2008. The period of observation was monitored by the five wave-measuring instruments and the four meteorological stations described in section 3.2 and depicted in Figure 3.1. Note however that, due to operational reasons, simultaneous observations from all wave instruments could not be obtained. In November, no data were available at A-dw(D) and B-iw(S)

during an interval of 15 to 30 days, respectively. From December to January no data were available at C-sw(D). Details on the period of observation of each wave instrument are given in Table 3.1.

3.4.2. Selected storm event

During the RIMA-Med field campaign I was lucky enough to record the different wind and wave conditions characteristic of the region of study, as described below in Section 4.1. In this work, however, I was specifically interested in wave growth in fetch-limited conditions and, thus, at some points I focused on a specific storm event that complied with certain basic requirements; namely, wind blowing offshore and no, or little, opposing swell trains. This event, which started on the 7 Dec. 2007 and finished on the 13 Dec. 2007, is described in more detail in Chapter 6 where it is simulated using forcing wind fields at different resolutions.

3.4.3. Fetch-limited dataset

The so-called 'Fetch-limited dataset' was a selection of the data measurements recorded during the fetch-limited storm event above (7-13 Dec. 2007). Indeed, some data measurements during the storm event were seen to deviate from what could be considered as 'ideal wind wave growth conditions' either because wind was not blowing approximately perpendicular to the coast or because interfering swell systems were masking 'pure' wind wave growth. Remember that this work focuses in the simplest processes of wave growth in sharp gradient regions because they constitute the previous but necessary step before addressing more complex sea and swell states.

As it is shown further on, during the selected storm event (Storm nº3) the instruments registered a 'calm period' during which winds were very weak and a small onshore-coming swell was recorded. Also, during the last days of the fetch-limited storm event, additional swell energy was recorded. Once these situations were conveniently removed, the remaining fetch-limited data set consisted of the periods 7 Dec. 5 h – 8 Dec. 15 h and 9 Dec. 20 h – 11 Dec. 20 h (see Figure 7.1).

3.4.4. Long-term reference (5 years)

Last, but not least, in Chapter 7, I additionally used a 5-year long data record to explore, with statistical reliability, different processes that might affect wave growth such as the stability of the atmosphere or the wind speed trend. For this reason, I used wind and wave data from buoy A-dw(D) recorded between 20 Aug. 2004 and 25 Nov. 2009. This dataset contains approximately 5 years of hourly measurements both meteorological and oceanographic (excluding the gaps due to maintenance or malfunctioning). The measurements on buoy A-dw(D) data were also taken through the same quality control and data processing used for RIMA-Med data (see Annex II). The different wave systems recorded during the 5-years long data set were classified as sea or swell using the methodology in Annex III; the results are presented in the next chapter.

4. Analysis and evaluation tools

This chapter is dedicated to the different analysis and evaluation tools that are further used in the present dissertation. In section 4.1 of the present chapter, the storm events during RIMA-Med field campaign were identified using quantitative and qualitative methods as explained below. The resulting storm conditions were further addressed in Chapter 5, where they were used to characterize the spatial and temporal gradients of wind and wave fields in the region of study. Section 4.2 is dedicated to the methodology used to separate sea and swell conditions during, both, the RIMA-Med dataset and the 5-year long data set. The statistical tools used to assess the performance of the different numerical simulations (*slope-1* and *R2*) are presented in section 4.3. The statistical analysis was commonly followed by a visual analysis that was routinely performed to complement the assessment of the numerical simulations (see section 4.4). Lastly section 4.5 evaluates the performance of the at-the-time operational wave prediction system (MASS atmospheric model and WAM wave model) during RIMA-Med data set. This evaluation was provided here for reference purposes only because it justified the need to improve wave estimations in the region and because it provided the starting point or reference values to be improved.

4.1. Storm definition and identification

The methodology used in this work to identify intervals of time characteristic of 'storm periods' within RIMA-Med dataset was based on quantitative and qualitative arguments. Remember that the focus was set on storm periods because it is then that most of the danger situations occur and it is then that the wind-wave-sea interaction processes are enhanced.

The quantitative method was based on the criteria locally employed to define a coastal storm; see for example Sánchez-Arcilla et al. (2008). In this work, storm conditions were defined for wave heights exceeding 1.5 m (threshold) during more than 6 h. The maximum time span in between independent storms during which the threshold was not to be exceeded was set to 24 h.

The qualitative method is based on a visual identification with the objective of matching the start of the storm with H_s sharp increase, and the end with H_s decrease. One of the interests of this work is studying the storm build up and decay. For modelling purposes, the initial start time was as important as the peak value of the storm. Therefore, the start and the end of the event were qualitatively chosen as those moments where wave height first sharply increased and then decreased again to an energy background

level set to approximately 0.5 m. The qualitative analysis was based on the wind and wave data time series during the last month of 2007, which are plotted in Figure 4.1 and Figure 4.2. Resulting from the quantitative and the qualitative analyses, five storm periods were isolated from the RIMA-Med data set (Table 4.1).

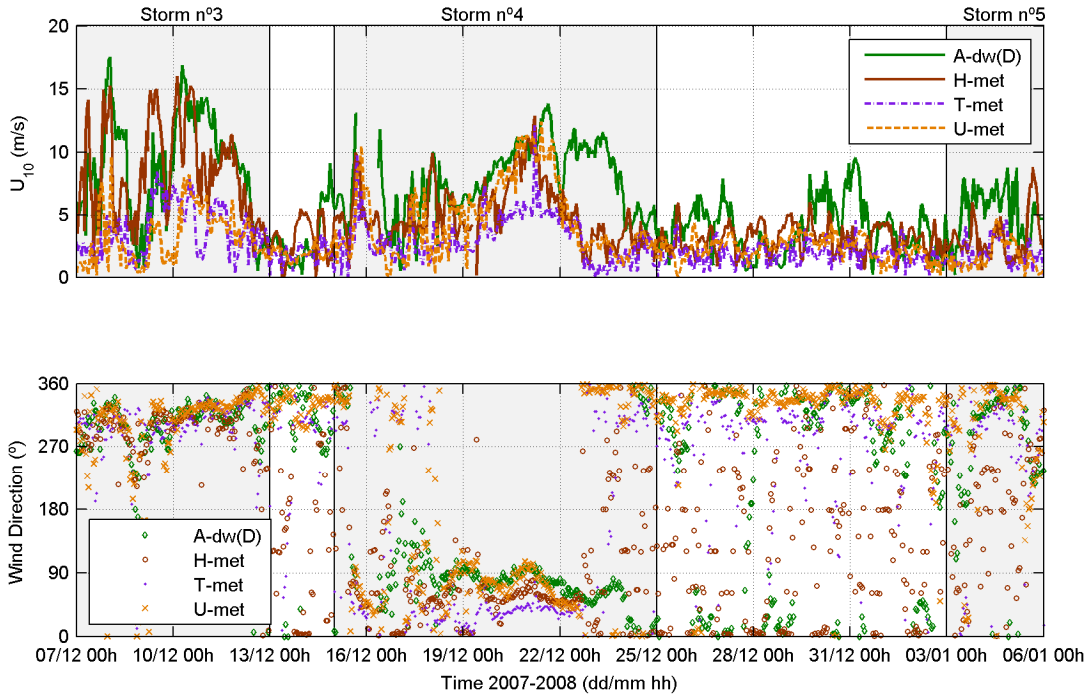

Figure 4.1 Wind speed (upper panel) and wind direction (lower panel) during RIMA-Med's last month (from 7 Dec. 2007 to 6 Jan. 2008) at the four meteorological stations neighbouring the area of study. Shaded areas correspond to wave storm periods.

The analysis of the energy spectra (not shown) indicated that, during the RIMA-Med field campaign, three out of five storm periods presented mixed sea and swell conditions, in agreement with what was reported by Sánchez-Arcilla et al. (2008) and Bolaños et al. (2009). These authors refer to characteristic double peaked spectra in this region, which usually consist of pre-existing eastern or southern swells and, superposed, northwest, and eventually south, wind-waves.

The first two storms in Table 4.1 (nº1 and nº2) recorded within RIMA-Med agreed with the typical bimodal events in the region: a northwest wind blowing over a pre-existing, although not very important, eastern swell. The last storm (nº5) started with a swell train from the south, and then incorporated a swell train from the east. Local wind speed was blowing from the northwest direction thus generating an additional low energy sea system that was propagating towards offshore.

Storm nº3 was characterized by fairly unidirectional spectra, which were originated by offshore blowing winds that generated growing wind-waves in fetch-limited conditions. H_s increased with fetch and reached maximum values of 2.4 m and 2 m at stations E-iw(D) and B-iw(S), respectively, for

approximately 20 km of fetch. At the most offshore station A-dw(D), with 55 km of fetch, H_s reached 3.5 m during the peak of the storm.

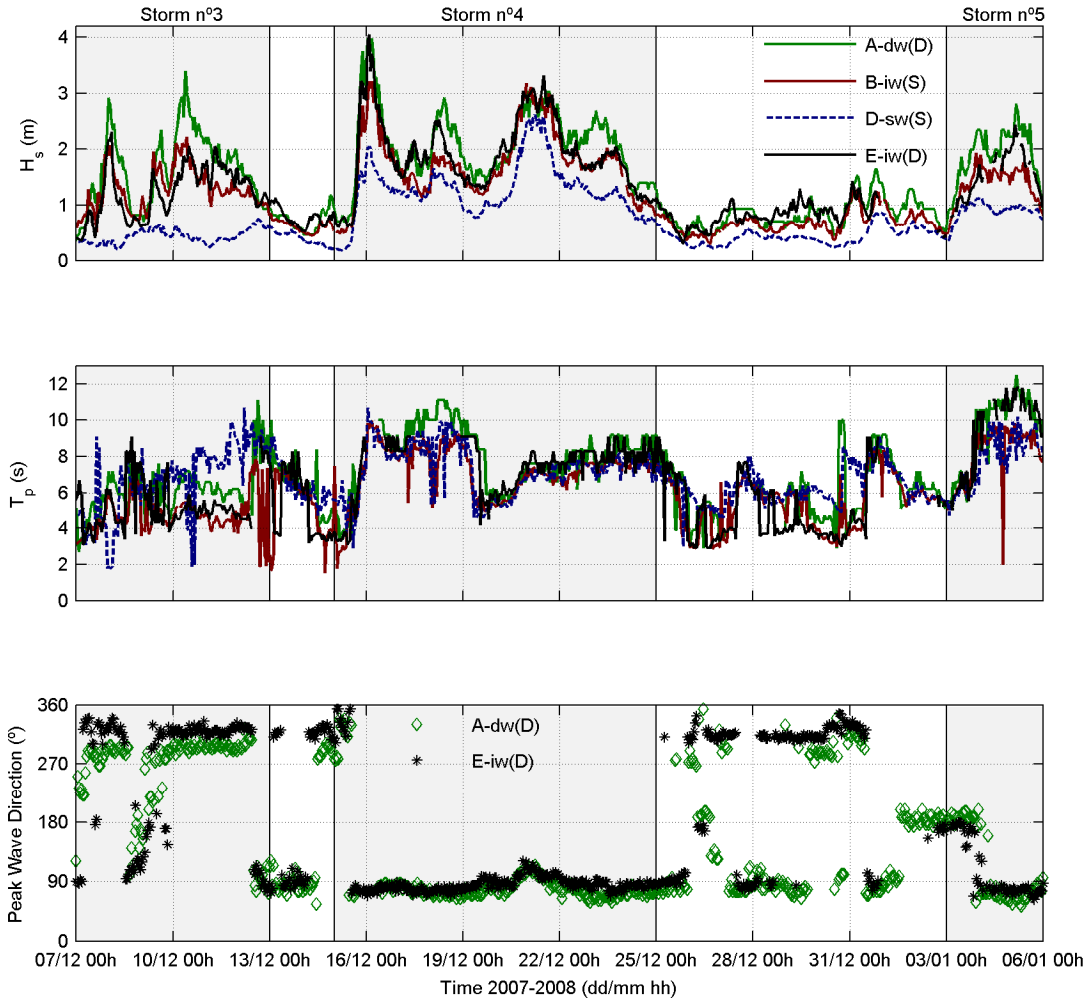

Figure 4.2 Significant wave height (upper panel), peak period (middle panel), and peak wave direction (lower panel) during RIMA-Med's last month (from 7 Dec. 2007 to 6 Jan. 2008) at the different wave instruments at the instrumental set. Shaded areas correspond to wave storm periods.

Storm nº4 recorded in RIMA-Med was unidirectional. Wave trains came straight from the east (80º±30°), with large peak periods (T_p > 10 s associated to swell) and the highest energies of the field campaign ($H_{s,max}$ > 4 m). The fact that similar values of H_s and T_p were recorded at all buoys confirmed that the main energy system was a swell event. During Storm nº4, the local wind was also blowing from the east which meant that, although the main energy system was swell coming from the east, local wind speed was still inputting energy at high frequencies. Consequently, sometimes two or more energy peaks from the same direction appeared at higher frequencies. The secondary (and narrower) peaks were observed to

merge from time to time with each other (or with the main peak). Consequently, the energy spectra became markedly broad along frequencies.

Table 4.1 Characteristics of the selected wave storm periods. The directions of wave provenance (θ_p) are NW: Northwest; E: East; S: South;

Storm period	Start and end time (dd.mm.yyyy)	Spectral type	θ_p	Maximum H_s at E-iw(D)
1	14 - 18.11.2007	Mainly bimodal	NW + E	2.1 m
2	24 - 30.11.2007	Mainly bimodal	NW + E	1.7 m
3	07 - 13.12.2007	Mainly unidirectional / sea	NW	2.3 m
4	15 - 25.12.2007	Unidirectional / swell	E	4.1 m
5	03 - 06.01.2008	Slightly bimodal	S+NW + E	2.4 m

4.2. Sea and swell separation

Separating sea and swell is a common procedure in disciplines such as numerical modelling, maritime engineering and structural design, coastal protection, fishing activities and marine sports (e.g. surfing). More recent applications include the identification of seismic noise within wave records (see Ardhuin et al. 2011) and wave data assimilation in operational models (Tolosana-Delgado et al. 2010). In this work sea/swell separation was required to estimate the rate of wind wave growth (sea) and to adjust the numerical model accordingly, as presented in Chapters 7 and 8.

Pure wind sea is not easily found in Nature because a sea state is the combination of a large amount of wave components being generated by different wind conditions and travelling at different speeds and in different directions. Nonetheless, wave components being generated by similar wind events have similar frequencies and directions. Thus, the spectral representation of a sea state results in main energy peaks which correspond to main wind events. Spectral peaks of young sea states are fairly sharp and are aligned along the mean wind direction (see section 6.3 in Holthuijsen 2007). In other words, sharp, narrow and unidirectional wind sea peaks are the closest one can get to pure wind sea conditions.

Wind sea peaks can also coexist with swell conditions, i.e. broader energy peaks that are no longer being actively generated and that propagate at faster velocities and lower frequencies. Swell is not being generated by local wind, and it is thought to be relatively independent of wind and wind sea (see e.g. Ardhuin et al. 2007). Because the interaction between wind sea and swell is not yet fully understood, in chapters 7 and 8, the two types of wave systems were separately considered. To this end, I calculated the frequency spectra of wave energy from the sea surface measurements, I separated independent energy systems and I classified them into four different groups: wind sea, swell, and wind sea in either a wind sea-dominated or a swell-dominated bimodal spectrum. All data records were used in this analysis in both storm and calm conditions. The details of the separation method are given in Annex III. Nonetheless, this

section also aims to provide a brief overview of the amount of data records within each group, in particular at buoy A-dw(D) during the 5-year long data set.

The results from the separation procedure are depicted in Figure 4.3 and Figure 4.4 and show the amount of spectra classified within each of the four groups mentioned above, during both the RIMA-Med data set and the 5-years long dataset. Notice that not all data records are plotted in the figures: the wave systems in energy spectra with more than two superimposed wave systems are not plotted.

Notice that after separating sea from swell only 80 data records were classified as pure wind sea during RIMA-Med. Within the 5-year long data set, instead, about 5,630 frequency spectra corresponded to pure wind sea, out of almost 90,000 spectra (5 years of hourly data). Notice, however, that in Chapter 8 pure wind sea data was further reduced because the wind direction was also constrained to a range of directions around the shore-normal direction. For wind directions within 315±15º the amount of wind sea spectra was reduced to less than 1,500 (not shown).

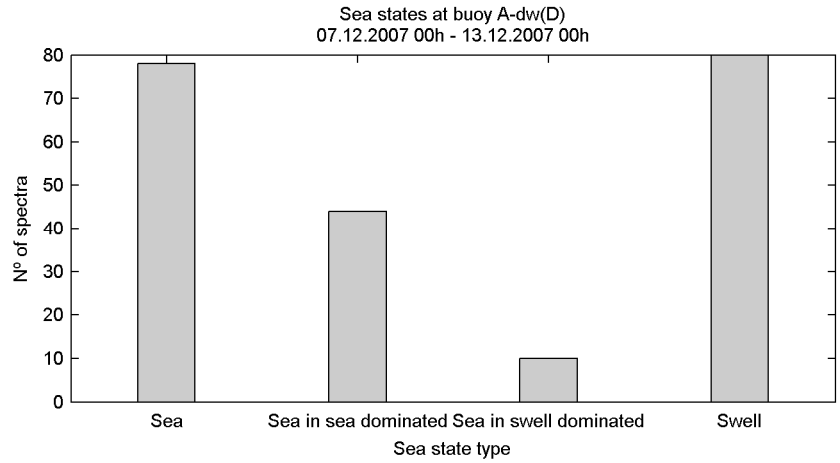

Figure 4.3 Amount of spectra classified as sea, swell, or sea in either a sea-dominated or a swell-dominated bimodal spectra from data records at buoy A-dw(D) during the RIMA-Med dataset.

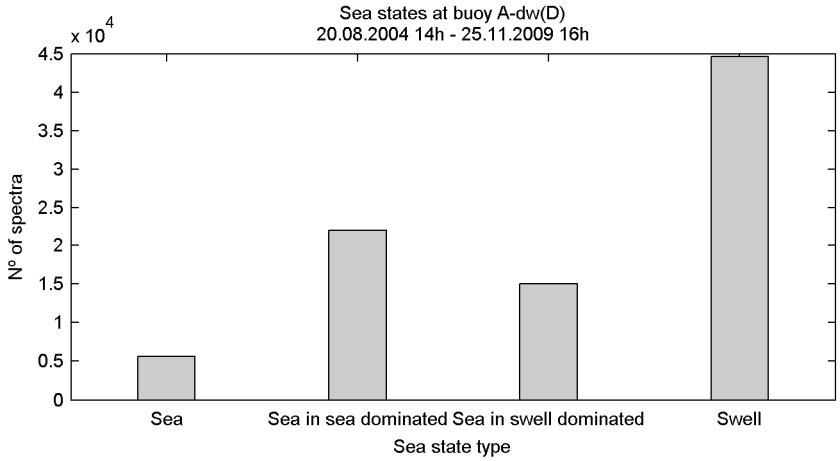

Figure 4.4 Same as Figure 4.3 but for the 5-year long dataset. Note the different scale on the y axis compared to Figure 4.3.

4.3. Statistical analysis

Throughout this work, the accuracy of the numerical simulations was evaluated fitting the simulated data to the observed data and calculating the statistical accuracy of the fit. In MASS and WAM, the simulated data at each buoy's location were interpolated using the simulated data at the four closest model nodes using the Inverse Distance Weighting method with a power of 2. This method consists of multiplying the value at each node by a weight factor which corresponds to the inverse of the squared distance between the node and the point to be interpolated. The time series were built up using the +6 h and +12 h predictions.

The statistical parameters used to assess the goodness of fit were *slope–1* and *R2*, as explained below. Note that the data were log-transformed because they are bounded and always positive (U_{10}, H_s, and T_p). The detailed reasons and benefits of long-transforming the data can be found in Tolosana-Delgado et al. (2010), for example. The regression equation of the log-transformed simulated data (dependent variable; *y*) versus the log-transformed observed data (independent variable; *x*) looks like:

$$\log(y) = slope \cdot [\log(x)] \quad \textbf{[4.1]}$$

Transforming equation [4.1] back into natural values, the parameter *slope* turns out to be the exponential of the independent term in a regression equation where the slope is forced to be **1** and the variables are log-transformed.

$$y = x^{slope} \quad \textbf{[4.2]}$$

The parameter *slope-1* used in this work is equal to the slope of the regression equation minus **1**, as follows:

$$slope\text{-}1 = slope - 1 \quad \textbf{[4.3]}$$

A direct result of the log-transformation is that the parameter *slope-1* can be conveniently used as a measure of the proportion of over/under-estimation (bias) of the forecast model (dependent variable) versus the observations (independent variable).

The coefficient of determination *R2* measures the percentage of variability of the forecast model (the fit f_i) consistent with the buoy data (y_i), and it is expected to be independent of the scale of the phenomena compared. Therefore, the larger the *R2* value the more natural variability is captured by the forecast model. Compared to the standard coefficient of determination, *R2* could be largely negative indicating that the fit explained the variability of the forecast model worse than the mean of the model data ($\bar{y}$). Mathematically, negative *R2* values indicate that the differences between the fit to the forecast model and

the measurements (denominator of *R2* equation) are larger than the differences between the mean of the measurements and the measurements themselves (quotient), as shown below:

$$R2 = 1 - \frac{Var[residuals]}{Var[total]} = 1 - \frac{\sum_i (y_i - f_i)^2}{\sum_i (y_i - \bar{y})^2} \quad \textbf{[4.4]}$$

Note that the number of data points used to calculate the fit of simulated versus observed data during individual storm periods was sometimes limited (in the order of 5 - 7 days). Therefore, although the statistical tools are very useful to quantify the differences between similar numerical runs, the limited amount of data might bias the results. Consequently, in this work, the statistical parameters were handled with care and they were supported by careful analyses of the time series.

4.4. Visual analysis

The time series of simulated and recorded data at the buoys were generally carefully analyzed to complement the statistical comparisons for several reasons. On the one side, the periods of time compared were relatively short and the amount of data for comparison was limited, compared to other long-term and larger-scale studies such as those performed by and Ardhuin et al. (2007), Cavaleri and Bertotti (2003). For limited amount of data sets the reliability of the statistical parameters decreased. On the other side, in this work I was not only interested in the overall statistical performance of the simulations, but also on their 'physical' ability to reproduce the maximum (peak) and minimum (calm) values of the storm events and the temporal variability of the time series. These parameters were not easily calculated statistically. For these reasons, the statistical assessment was not always enough and the visual analysis was also required.

A good example of the inaccuracy of the statistical analysis was presented in Section 4.5 below. It was shown that the predictions issued by the operational models were less variable and they under-estimated the peaks of the storm, but presented better statistical fit parameters than the predictions issued by the higher resolution models (see for example Figure 6.4). All in all, the visual analysis is a qualitative tool only. Thus, it is not always suitable to use it to evaluate the performance of some datasets compared to others.

4.5. Performance assessment of operational models

To conclude this chapter I assessed here the performance of the wind and wave operational models during RIMA-Med field campaign. The main objective of this section is to further justify the need of improving the estimation of wave parameters in the region of study, especially during fetch-limited wave growth conditions, and to explore the capability of the operational system to capture temporal and spatial variability of wind and waves. To this end I performed a standard statistical and a visual analysis of the

overall performance during the 5 storms selected in section 4.1. The variables considered were wind speed (U_{10}), wave height (H_s), mean period (T_m) and mean wave direction. The results revealed some of the limitations of wave forecasting in the region.

For comparison, bear in mind that previous studies reported consistent under-estimations of H_s and T_p in enclosed basins (such as the Mediterranean Sea; see Cavaleri and Bertotti 2004). Also, in the region of study, Sánchez-Arcilla et al. (2008) reported a general overestimation of mean period, but they did not observe a clear pattern of H_s over- or under-estimation because the differences depended on the location (buoy) of comparison.

4.5.1.1. Wind speed

During the RIMA-Med period, the results shown in Table 4.2 indicated that the MASS wind model considerably over-predicted U_{10} at all meteorological instruments. The largest U_{10} over-estimations occurred at the two coastal-land stations (T-met and U-met), in agreement with the results from Bolaños et al. (2007), who attributed this behaviour to an inaccurate parameterization of the surface roughness over land (poorly resolved orography). In open sea conditions, instead, Bolaños et al. (2007) reported U_{10} under-estimations (compared to QuikSCAT data).

Instead, the presented results indicated that at sea (buoy A-dw(D)) the MASS wind model under-estimated U_{10} but only during Storm nº4 (wind and waves coming from the east). The under-estimation was very slight and much less important than the over-estimation reported for offshore wind conditions (blowing from the north-west). These results confirmed that offshore wind conditions were more demanding in terms of wind modelling than onshore wind events. A common explanation is the complexity of the coastal orography compared to the homogeneity of the sea surface (as already pointed out by Bolaños et al. 2007).

Table 4.2 Statistical comparison of the logarithm of the modelled wind speed (U_{10}) using MASS atmospheric model and the observations during RIMA-Med. Boldfaced values correspond to the slope of the regression equation minus 1 (*slope-1;* positive/negative values indicate an over/under-prediction). Regular values correspond to the determination coefficient *R2*.

U_{10}	All data		Storm 1		Storm 2		Storm 3		Storm 4		Storm 5	
A-dw(D)	**0.1**	0.01	**0.22**	0.27	**0.24**	-2.32	**0.19**	0.37	**-0.05**	0.34	**0.72**	-6.18
H-met	**0.29**	-0.38	**0.20**	-1.17	**1.13**	-3.09	**0.23**	-0.95	**0.34**	0.17	**0.80**	-0.88
T-met	**1.3**	-0.71	**1.83**	-1.18	**2.02**	-7.83	**1.73**	-3.22	**1.88**	-1.22	**2.81**	-1.84
U-met	**2**	-0.59	**2.59**	-0.55	**1.75**	-0.64	**2.78**	-2.21	**0.93**	-0.34	**4.31**	-2.12

4.5.1.2. Wave height

Note in Table 4.3 that also H_s were both over- and under-estimated during the whole RIMA-Med period, compared to available instruments. A closer look at the values in Table 4.3 indicated that different

behaviours existed depending on the buoy location and the storm event (in agreement with Bolaños et al. 2007's work).

Table 4.3 Comparison of the logarithm of the wave height (H_s) simulated using WAM wave model and the observations during RIMA-Med. Boldfaced values correspond to the slope of the regression equation minus 1 (*slope-1;* positive/negative values indicate an over/under-prediction). Regular values correspond to the determination coefficient *R2*.

H_s	All data		Storm 1		Storm 2		Storm 3		Storm 4		Storm 5	
A-dw(D)	**-0.17**	0.74			**0.21**	0.25	**-0.18**	0.5	**-0.18**	0.74	**-0.23**	0.29
B-iw(S)	**-0.23**	0.78					**-0.31**	0.41	**-0.09**	0.74	**-0.18**	0.52
D-sw(S)	**0.13**	-1.04	**0.23**	-0.53	**0.60**	0.42	**0.57**	-0.38	**0.13**	0.80	**0.06**	0.60
E-iw(D)	**-0.19**	0.68	**0.02**	0.60	**0.10**	0.13	**-0.29**	0.54	**-0.19**	0.71	**-0.17**	-1.29

The statistical analysis showed that H_s over-estimations were only reported during the first two bimodal events. However, a close look at the time series indicated that these over-estimations were either apparent, or could be easily explained through the lack of temporal variability of the wind fields, as explained below. During Storm nº 1, measured wave data for comparison was only available at buoys E-dw(D) and D-sw(S). Over-estimations at D-sw(S) were persistent, probably because this buoy was located only 1 km offshore and it was largely affected by the model's sea-land boundary. Instead, over-estimations at E-dw(D) were only statistical because a visual analysis of the time series revealed that wave height at this buoy was rather accurately predicted (not shown).

During Storm nº2, a very pronounced H_s peak was over-estimated due to a considerable, although only instantaneous, over-estimation of U_{10} (see Figure 4.5). Because the temporal resolution of the wind field was coarse (6 h), the high, although instantaneous, wind speed peak influenced wave growth exaggeratedly. Wave height was allowed to grow constantly during 6 h thus generating the unreal wave height peak.

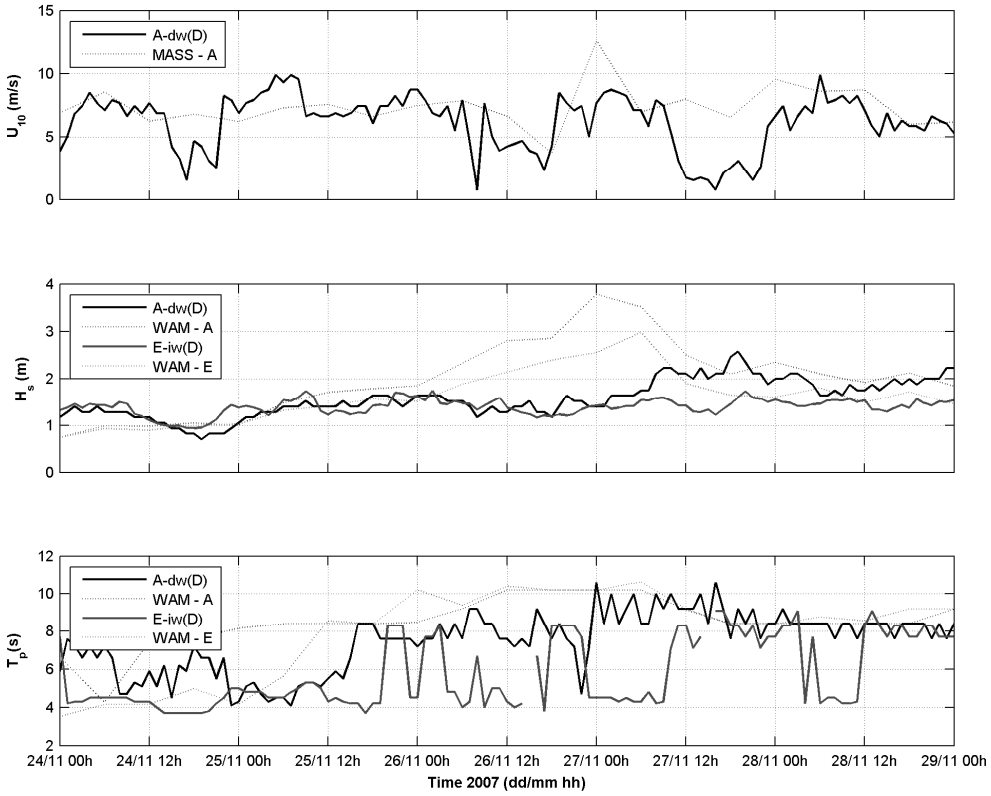

Figure 4.5 Observed and simulated wind speed (top figure), wave height (middle figure) and peak period (lower figure) at buoys A-dw(D) and E-iw(D) during Storm nº2 (from 24 Dec. to 29 Dec. 2007).

These results indicated that the coarse wind input frequency produced unrealistic over-estimations of wave height in the region of study. Similarly, the coarse resolution could also produce under-estimations of wave parameters. The main reason is the temporal features in the region, which time scales were less than 6 h (e.g. coastal wind jets). In fact, wave height under-predictions were reported during the last three storms: in fetch-limited growth conditions (Storm nº·3), in swell propagating situations (Storm nº 4), and in a mixed sea/swell event (Storm nº5).

Simulated H_s time series were very similar at all the instruments and they did not reproduce the large variability characteristic of the observations. The only differences were in terms of magnitude and due to the different fetch at each buoy (see for example Figure 4.5); i.e. no sharp spatial gradients were captured.

4.5.1.3. Mean period

Although statistical estimators in Table 4.4 suggested that T_m predictions were more accurate than H_s predictions, the fit values were not consistent, meaning that both over- and under-estimations occurred without a clear and systematic reason. *R2* values for numerous fits were negative, which meant that the fit slope was not 100% reliable. Remember that *R2* measures the percentage of variability of the forecast

model consistent with the buoy data. Negative values of *R2* indicate that the fit explained the variability of the forecast model worse than a constant function crossing the data points along their mean value. In these situations the visual analysis of Figure 4.2 becomes especially valuable.

Table 4.4 Comparison of the logarithm of the mean period (T_m) simulated using WAM wave model and the observations during RIMA-Med. Boldfaced values correspond to the slope of the regression equation minus 1 (*slope-1;* positive/negative values indicate an over/under-prediction). Regular values correspond to the determination coefficient *R2*.

T_m	All data		Storm 1		Storm 2		Storm 3		Storm 4		Storm 5	
A-dw(D)	**-0.06**	0.35			**0.15**	-0.72	**-0.12**	0.28	**-0.06**	-0.17	**-0.11**	0.64
B-iw(S)	**0.03**	0.21					**0.07**	-0.13	**-0.03**	0.13	**0.14**	-3.24
D-sw(S)	**-0.07**	0.24	**-0.01**	0.56	**0.15**	-0.07	**-0.29**	-0.15	**-0.04**	-0.37	**0.10**	0.38
E-iw(D)	**0.05**	-0.14	**0.06**	0.46	**0.37**	-0.50	**-0.07**	0.32	**-0.03**	-1.81	**-0.06**	-0.32

The time series of the simulated mean period show that most of the temporal variability was missed, although sharp changes of mean period in bimodal sea states were simulated, which is a promising result. The accuracy in time of the changes was slightly mis-estimated but, given the coarse temporal output of the model (6 h), the result was no big surprise. The frequency downshift of growing waves moving away from the coast was, however, not properly simulated. In other words, the simulated mean period (which inversely corresponds to the frequency) at A-dw(D) was not longer than at B-iw(S) or E-iw(D), which were located closer to the coast, as it was expected to be according to wind wave growth observations. In fact, the operational system tended to over-estimate short mean periods and to under-estimate longer ones. Possible reasons causing these errors were thought to be the limited number of grid nodes along the fetch (too coarse spatial resolution), the lack of smaller scale physical processes in the model parameterizations, and an inaccurate parameterization of the downshift rate, thus justifying, again, the hypothesis and the approaches taken in this work.

4.5.1.4. Mean wave direction

The simulated wave direction time series were evaluated in terms of the differences between the measured values at two buoy locations: A-dw(D) and E-iw(D). As shown in the next chapter, in this region a consistent difference of wave direction between the two buoys is not uncommon. For this reason, in this section the ability of the operational wave model to estimate these differences is evaluated.

In the following chapters, a few mechanisms causing the difference in wave direction at the two buoys are addressed: wind directions along each buoy's fetch being different from each other, refraction and diffraction and/or slanting fetch. The limitations to predict wave direction within wave models were addressed, again, in section 6.5.2. In this chapter the aim is to explore and show that differences in wave direction were indeed simulated by the at-the-time operational models.

In this section, wave direction differences were calculated separately for each of the three characteristic directional sectors (north-west, east and south), as summarized in Table 4.5; the differences simulated were between 4º (eastern wave trains) and 13º (southern wave trains). These results indicated that simulated wave direction was able to adjust to the particularities of each buoy location, thus capturing part of the spatial gradients of the region. In next chapter I show that these differences also existed in the observations.

Table 4.5 Average simulated mean wave direction for the three characteristic directional sectors: east, south and northwest. Data were numerically calculated using WAM spectral wave model. The output was linearly interpolated at the location of buoys A-dw(D) and E-iw(D).

Buoy location	East $0º \leq \theta_m \leq 130º$	South $135º \leq \theta_m \leq 225º$	North-west $270º \leq \theta_m \leq 360º$
A-dw(D)	64.8º	190.9º	321.5º
E-iw(D)	68.5º	177.0º	333.5º
Difference	3.7º	13.9º	12º

5. Spatial and temporal gradients in the NW Mediterranean

The strong gradients of the wind regimes and the complex orography of the region were important limitations of regional wave models (Sánchez-Arcilla et al. 2008). For this reason, I believe that characterizing the spatial and temporal variability of extreme wave conditions in the NW Mediterranean Sea is crucial to improve wave predictions in the area. In this chapter I describe the mid-scale variability features of characteristic storm events from observations registered during the RIMA-Med campaign.

Compared to the work carried on by previous authors (see Chapter 2), the present work, instead, tackles the time scale of storm conditions (hours to days), and spatial scales from 10 – 100 km. Moreover, it focuses on the time series during particular storm events, rather than looking at the problem from a statistical, generalist, point of view. The evolution of the time series was investigated using point-measurements rather than comparing spatial-resolving remote-sensing observations offshore. The reason is that this study is intended for the coastal zone, for which coastal features are of the order of kilometres, and for regional wave forecasting, for which prediction horizons usually are 48 h. The aim of this chapter is not only to narrow down and to better characterize the general processes mentioned in the work of Sánchez-Arcilla et al. (2008) but, also, to set the starting point to better approach the improvement of wave estimations in following chapters.

I believe that a more thorough description of the characteristic gradients would permit to identify the more demanding situations to be captured by wind and wave models and would lead to improved wave forecasting in the region. Describing the spatial and temporal gradients in the Catalan region is the first step before attempting to reproduce the gradients in the next chapter, using improved input wind fields and higher spatial and temporal resolution.

Although the main aim of this dissertation as a whole is fetch-limited conditions for reasons such as the large errors in their prediction and its role in the even more demanding bimodal sea states, in this chapter in particular, I describe the whole set of observations registered during the RIMA-Med field campaign and I address their implications for wave modelling. The main reason, or aim, is laying the ground for improving wave forecasting in sharp gradient regions and all wind wave situations. Particular attention was given to the simple unidirectional events, both in wave growth conditions (storm nº3) and in swell dominated situations (storm nº4).

This chapter is organized in three main sections. First, I characterize the spatial gradients recorded. Second, I describe the temporal gradients from the observations. Third, I discuss the results in terms of their implications for wave modelling. A summary of the results is provided at the end of the chapter to sum up the valuable information that should be kept in mind in subsequent chapters.

This chapter describes the wind and wave observations taken during the RIMA-Med field campaign (November 2007 - January 2008) just in front of Tarragona Harbour (see Chapter 3). Wave data was taken from the four wave buoys A-dw(D), B-iw(S), D-sw(S) and E-iw(D) depicted in Figure 3.1. Wind data was taken at the four meteorological stations U-Met and T-met (over land) and H-met and A-dw(D) at sea.

5.1. Spatial gradients in the observations

The spatial variability of the wind and wave conditions was assessed through a detailed inspection of the recorded time series and a comparison of the observations at the different instruments. At the first glance, wave data time series agreed with the most basic behaviour of wave generation and propagation in homogeneous conditions, for the different wind conditions. In other words, higher wave heights and longer peak periods occurred for the longer fetch wind conditions (e.g. Storm nº 4 from the east; see Figure 4.2). During situations of wind blowing offshore (wave growth conditions like Storm nº 3) the highest wave heights and longer peak periods were recorded at the longest-fetch buoy (A-dw(D)). Also, the wave conditions recorded at the two buoys located at similar depths and with similar fetches (B-iw(S) and E-iw(D)) were generally similar.

The shape of the wave energy spectra recorded at the different instruments along the direction perpendicular to the coast behaved, in general, as expected for homogeneous and stationary wind conditions. During northwest events (fetch-limited growth conditions) the wave energy increased and the peak frequency decreased for increasing fetch distance. During eastern events (fully-developed wave conditions) the shape of the spectra and the peak frequency were very similar at all the recording instruments. During bimodal wave states, the characteristics of growing wind sea waves and fully-developed conditions coexisted in single two-peaked energy spectra.

At station D-sw(S), only 1 km offshore, the energy peaks in the frequency spectra were less energetic than at the other locations due, in part, to the somewhat sheltered location of the buoy (between the port, to the northeast, and Cape Salou, to the west) and, in part, to the existing shallow water depth (24 m). In other words, the short north-west and south fetches (due to the sheltered location of the buoy) produced low-energy wind seas. Also, bottom friction due to shallow water depth dissipated the incoming swell from eastern sectors (not sheltered). Altogether, energy spectra at D-sw(D) were generally multi-peaked: they contained high-frequency growing waves from the coast and predominant low frequency (about 0.1 Hz) eastern swells.

Directional spectra from buoys A-dw(D) and E-iw(D) indicated that double peaked spectra did not only exist during opposing eastern/south swell and northeast sea; but they also existed when two wave trains from similar but slightly different directions, and peak frequencies, coexisted within the same sea state. In this kind of bimodal situations, very common in changing wind directions, it became difficult to use the terms sea and swell in its traditional way. Also, it became necessary to employ the terms 'young' and 'old sea', depending on the maturity of the energy peak. In the region of study, this duality was addressed by Bolaños (2004), who used the wave age to separate the frequency components of the energy spectra in young and old sea components.

In spite of the well-known behaviour of wave growth and wave propagation generally observed, the detailed inter-comparison of the time series at available instruments highlighted some interesting differences characteristic of the regional gradients. Below, the observed differences are discussed in terms of wave height and peak wave direction.

5.1.1. Wave height differences

In the region of study, the spatial gradients in the wind fields are generated by the irregular coastal orography that generates jet-like wind patterns over the sea. This behaviour was already mentioned in section 3.1 and it was described in Sánchez-Arcilla et al. (2008), for example. Comparatively, the spatial gradients of the wave fields were expected to be less sharp because of the slower response of waves to winds and because wave energy spectra are the integrated effect of wind on waves. This subsection explores the differences in wave height recorded at the available instruments in order to characterize more precisely the existing spatial variability of the wave fields. Although this approach could not be as extensive or comprehensive as radar measurements (see Wyatt 1998a, 1998b) it does provide useful information of the existing variability in scales larger than tenths of kilometres, as shown below. In short, I observed two main features characteristic of sharp gradient regions in the wave height time series: the effect of coastal wind jets, and the attenuation of easterly swell due to the orientation of the coastline and associated refraction/diffraction.

5.1.1.1. Coastal wind jets

The imprint of coastal wind jets in waves was seen to cause some of the differences in wave height between the available buoys. An example is the remarkable difference in wave height between buoys B-iw(S) and E-iw(D) recorded on the 9 Dec. 2007 during Storm nº3, an offshore blowing wind event. In this case, H_s at buoy B-iw(D) was seen to increase from 0.8 m to 1.2 m (peak) and to decrease again in less than 6 h (see Figure 5.1 – left). Even though both instruments had a similar fetch for northwest winds, no such wave height peak was registered at E-iw(D). The wave height difference between the two buoys was 0.5 m (50%).

To investigate the reasons of the reported difference, note first that the measured waves were generated by wind and, thus, they were expected to be, in general, tightly linked to wind speed patterns. Also, waves in growing conditions (offshore blowing winds) were not expected to interact with the bottom and be affected by bottom-related wave propagation mechanisms. Therefore, the existing wave height differences between buoys B-iw(S) and E-iw(D) were most probably caused by spatial differences of the wind fields rather than by bottom effects.

In this case, however, a straight forward comparison of the wind field at each buoy was not an easy task because meteorological measurements were not available at each buoy's location. Consequently, I used the meteorological station closest to each instrument to infer the local wind speed at the instrument's location. U-met data were used to analyze wind conditions at E-iw(D) and measurements at H-met were used to reconstruct wind conditions at B-iw(S) (see Figure 3.1). T-met was used to support the data from H-met, but wind data at this location was expected to be less representative of wind speed at B-iw(S) than data from H-met because T-met was not located along the wind direction but offside.

On the 9 Dec. much higher U_{10} values from the northwest were recorded at H-met (compared to U-met), which explained the H_s peak at B-iw(S) (compared to E-iw(S)). Wind speed at H-met was 8 m/s (700%) higher than at U-met (1 m/s). These values confirmed the presence of a coastal wind jet at H-met that was responsible for the high energy sea peak at B-iw(S) (see the energy spectrum in Figure 5.1 - right). The wave height difference was a clear sign of the spatial variability of the wind and wave fields along the coast (the buoys were only 30 km apart).

The referred wind speed peak from the northwest was also recorded at the offshore buoy A-dw(D), which was located along the same direction perpendicular to the coast as B-iw(S). However, wind speed was 50% less intense (4 m/s) which indicated that the wind jet was already decaying at distances shorter than 50 km from the coast (see Figure 5.1 – left). The local nature of this wind jet was obvious because the energy of the sea peak recorded at buoy A-dw(D) was much lower, compared to B-iw(S) (see Figure 5.1 - right). Buoy A-dw(D) and B-iw(S) were only 30 km apart and, in this case, along the same fetch. But U_{10} peak values along the fetch were not strong (or 'long') enough to increase wave energy at the distant position of buoy A-dw(D). Note that by 'long', I refer to the spatial persistence of the wind jet up to a certain distance offshore. The features of wind jets over the sea were a clear example that wind and wave variability was not only important along the coast, but also along the fetch.

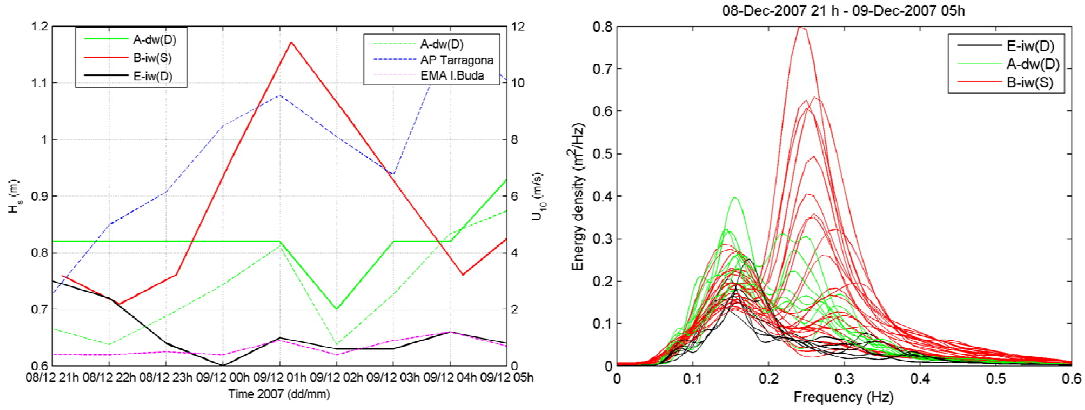

Figure 5.1 (Left panel) Wave height (solid lines; axis on the left-side) and wind speed (dashed lines; axis on the right-side) time series during the coastal wind jet observed on the 9 Dec. 2007 01 h. (Right panel) Frequency spectra at the three buoys from 8 Dec. 21 h until 9 Dec. 5 h. Notice the higher energy of the sea at B-iw(D).

The effect of wind jets on wave height was also an example of the persistence of local wind features on the sea state. In fact, locally high wind speeds were able to increase wave height locally (only) for a short period of time. The particular wind peak discussed above lasted about 6 h. It increased from 2.5 m/s to 9.5 m/s in 4 h, a growth rate of almost 1.8 m/s every hour. The corresponding wave peak lasted 6 h as well, but it started to increase 1 h later and kept decreasing 1 h after the wind speed stopped decreasing (see Figure 5.1 – left). Wave height increased from 0.7 m to 1.2 m in 3 h (and decreased at the same rate of almost 0.17 m every hour). This kind of strong short-lived wind jets could have a relevant impact on maritime activities due to their sudden occurrence and the high wave heights they generate. Right now coastal wind and wave jets are rarely considered or predicted due, in part, to the low spatial and temporal resolution used in numerical models, as discussed in next section 5.3.

5.1.1.2. Swell attenuation

Another example during which wave height was considerably different at the two buoys B-iw(S) and E-iw(D) occurred on the 18 Dec. for onshore blowing winds (coming-from direction of approximately 80º). In this case, however, H_s at E-iw(D) was much higher (2.5 m) than at B-iw(S) (1.9 m), which represented a 32% difference. This difference could not be explained through the wind speed difference at the available meteorological stations: wind speed at U-met was much slower compared to H-met (or A-dw(D)); Note that wind speed at U-met did not even increase above 4 m/s. The analysis below, however, indicated that the difference in wave height was due to an effect of the mechanisms of wave propagation in the regional scale.

The inspection of the energy spectra in Figure 5.2 (left panel) indicated that, at the time of the measurements, the buoys were mainly recording wave trains from the east-northeast (70 - 80º) that were very much attenuated at buoy B-iw(S). Note that because local wind speeds were also blowing from the

east the energy spectra were markedly bimodal with both sea and swell trains coming from the same eastern direction.

The comparison of the frequency spectra recorded at each buoys indicated that the attenuation of the wave energy focused on the swell peak (see in Figure 5.2 – right panel). Three possible effects could cause swell attenuation at buoy B-iw(D): wind-wave interaction, bottom friction (associated to refraction and shoaling), and coastal geometry (shape effects).

The first effect, wind-wave interaction, was explored in terms of the wind speed and direction at the meteorological stations closest to each instrument. On the 18 Dec. the wind direction at H-met was approximately 30º deviated towards the north-east compared to A-dw(D), while the wind direction at U-met was constantly changing (possibly due to the low wind speeds registered). If the wind direction was different at each meteorological station, it was also possibly different at each buoy. Therefore, it was likely that the wind direction at B-iw(S) was different from the wind direction at E-iw(D), and different from the wave direction. If the wind speed at this position was indeed blowing at an angle to the wave direction, new energy would be entering the system at high frequencies in the wind direction. A new energy peak (sea) in this position would confirm that wind was strong enough to interact with swell and, eventually, attenuate it. There were three main reasons to reject this hypothesis. First, the limited knowledge of wind-wave interactions could not explain the mechanism itself without a great deal of uncertainty. Second, no significant energy peak was recorded in B-iw(S) at high frequencies (> 0.3 – 0.4 Hz) and, thus, it is not possible to confirm that wind at B-iw(D) was strong enough to interact with swell and attenuate it. Remember that no directional wave data were available at buoy B-iw(S), or in-situ wind speed measurements neither at B-iw(S) nor at E-iw(D). And third, similar swell differences between the buoys existed in different (and milder) wind conditions (i.e. 5 Jan. 2008). These observations confirmed that other mechanics of swell propagation were probably more important than the influence of wind speed on swell attenuation.

The second effect possibly causing swell attenuation at B-iw(S) was thought to be bottom friction during wave refraction and shoaling (see e.g. Holthuijsen (2007) for a review about coastal water processes). Wave refraction refers to the reorientation of the wave trains towards a direction perpendicular to the bathymetric isolines due to lateral changes of the phase speed, which are in turn caused by the interaction of wave trains with the bottom as the waves approach the coast (or, in this case, the buoy's location). Shoaling refers to the variation of wave direction due to changes in group velocity in that direction, which occurs in decreasing water depths due to bottom friction. Shoaling also generally results in an increase of wave amplitude ('energy bunching'). Both refraction and shoaling are directly related to friction of wave trains with the bottom due to insufficient water depth. Bottom friction results in energy dissipation and wave energy decrease, and wave direction reorientation (perpendicular to the bathymetric lines). Note that, according to linear theory, peak period is conserved under refraction and shoaling.

To assess the importance of bottom friction in swell attenuation, I compared the wave energy spectra at buoys E-iw(D) and A-dw(D). Because A-dw(D) was located in deep water, it was not affected by refraction processes, and could be used for comparison. This comparison was useful because both instruments were directional and the effect of refraction (wave direction changes) could be explored. Also, and more important, E-iw(D) was located in shallower waters than B-iw(S) and, therefore, swell trains at the first buoy were more prone to energy dissipation than at the second buoy. However, wave energy and direction from buoys E-iw(D) and A-dw(D) were not significantly different. This result implied that, because water depth at B-iw(S) was larger than at E-iw(D), swell attenuation at B-iw(D) could not be only due to refraction/shoaling of swell approaching the buoy from offshore sectors.

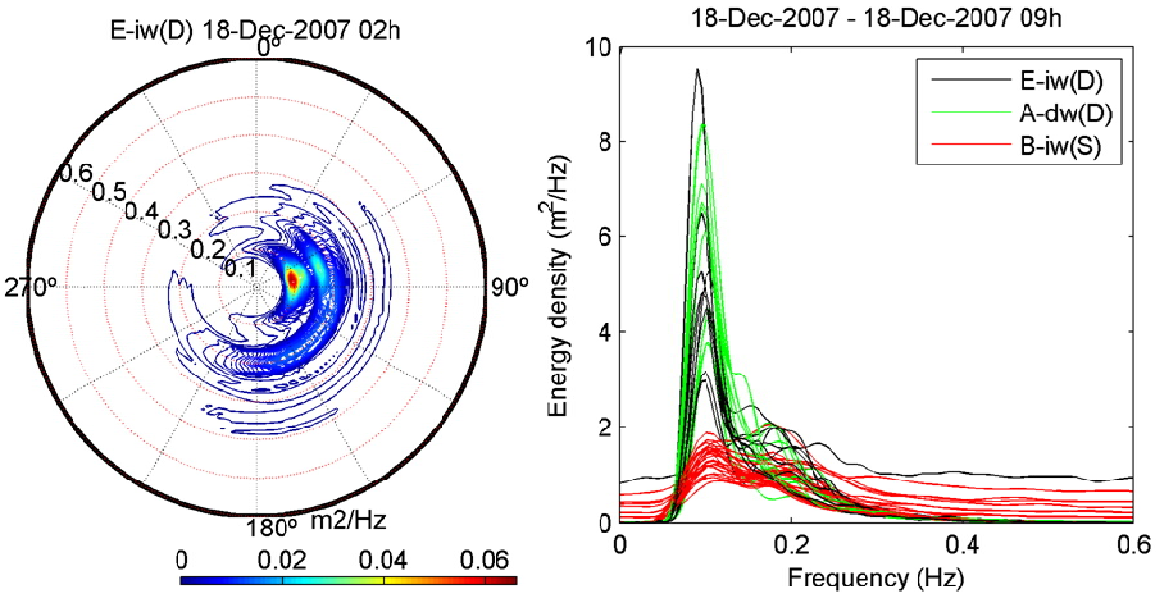

Figure 5.2 Directional (from) energy spectrum at buoy E-iw(D) (left). Frequency spectra from buoys A-dw(D), B-iw(S) and E-iw(D) from 18 Dec. 2007 at 00 h until 9 h (right). This plot clearly shows the attenuation of swell at buoy B-iw(S).

The third effect possibly causing swell attenuation at buoy B-iw(S) was the influence of the coast to the north of the buoy. In fact, the attenuation at B-iw(D) could be a shadowing effect due to the proximity of the coast to the north, even though water depth at the buoy was not deep enough to dissipate as much swell energy, as discussed above. Note that, although the bathymetry close to the buoy was orientated approximately perpendicular to the incoming swell (0º), the coastline was orientated along the swell from-direction (70º). Thus, for about 80 km along the eastern direction the bathymetry of the coast favours swell refraction. Aftwerwards, the coast shifts (reorientates) towards a more northern direction after Barcelona city (see Figure 3.1). Therefore, swell trains reaching B-iw(S) might have been refracting (and dissipating) from the very first moment they reached the coast of Barcelona. If swell trains refracted for over 80 km, that would explain the strong attenuation of swell at B-iw(S) and not at E-iw(D), even though this last instrument was located in shallower water.

Additionally, the coast to the north could have produced an effect similar to diffraction due to the blocking of the northern components of swell. This effect was not expected to be very important compared to refraction because the obstacle (coast) did not produce large gradients of energy, with areas of lower wave energy on its lee side, due to the coastal geometry itself.

Swell attenuation was not always observed. In the example depicted in Figure 5.1, for example, swell at B-iw(S) was not attenuated, possibly due to the higher peak frequency of the swell systems. In other words, such higher frequencies would only refract at even shallower water depth. The effect of the coastal geometry could not be fully verified with the directional shift associated to refraction because there were no directional measurements available at B-iw(S).

In other situations (e.g. 11 Dec 2007) H_s was also larger at E-iw(D) compared to B-iw(S), but winds were blowing offshore and no swell system was recorded. In these situations, the reason for the wave height difference was related to the wind direction and the effective fetch at each buoy. In other words, when wind direction was from the northern sectors (rather than north-west), then the fetch was longer and H_s were higher at E-iw(D) compared to B-iw(S).

Summarizing, wave height at two instruments that were 30 km apart along the coast, at similar depths and similar distances to the coast, could differ up to almost 50%. The reasons for these differences were seen to be the variability of the wind field (coastal wind jets) at the two buoy positions and the attenuation of swell trains arriving at B-iw(S) from eastern directions. Coastal wind jets were characterized by higher wind speeds along the fetch of individual buoys, thus generating locally different wave conditions. Also, in offshore-blowing wind conditions, the deviations of the wind direction from the perpendicular to the coast favoured longer fetches for certain locations compared to the others. Finally, the attenuation of swell close to the coast was mainly caused by refraction and the shadowing effect of the coastline to the north (and associated diffraction).

5.1.2. Peak wave direction differences

The peak direction of wave records (θ_p) was also representative of the high spatial variability of the wave fields. As shown in Figure 5.3, a significant deviation of θ_p was recorded between the measurements at buoys E-iw(D) and A-dw(D) (significance was estimated using a t-test at the 95% confidence level). The largest differences were recorded during Storm nº 3, the northwest, fetch-limited wave growth event (see Table 5.1). Then, the wave trains approached station E-iw(D) with a direction, on average, 26º more from the north than at A-dw(D). Instead, pure easterly wave trains (i.e. Storm nº 4) approached E-iw(D) with an average 7º difference towards the East. Southerly wave trains (e.g. 3 Jan. 2008) approached E-iw(D) with an average 17º deviation towards the east (although more variability around the mean values was recorded; see Figure 5.3).

Table 5.1 Average peak wave direction for the three characteristic directional sectors: east, south and northwest. Data were measured at the buoys A-dw(D) and E-iw(D).

Buoy	East $0^o \leq \theta_p \leq 130^o$	South $135^o \leq \theta_p \leq 225^o$	North-west $270^o \leq \theta_p \leq 360^o$
A-dw(D)	82.5º	183.6º	295.8º
E-iw(D)	89.2º	166.6º	321.8º
Difference	6.7º	17º	26º

In the region of study, I considered three mechanisms to be possibly responsible for the reported shifts in wave direction: different wind direction, wave refraction and slanting fetch conditions. First, I addressed the possibility of a different wind direction at each buoy's location due to the locally high wind variability. However, as shown in Figure 5.3, the comparison of the variability of wind direction and the variability of wave direction indicated that wave direction tended to persist, relatively independent of wind direction. Although independence of waves from wind direction is not surprising in swell-dominant states (eastern- and south-coming waves), it is somewhat unexpected in growing sea states (northwest-coming waves). In fact, Young et al. (1987) concluded from numerical simulations that for wind direction changes less than 60º wave direction adjusts smoothly to the wind direction; and for wind direction changes larger than 60º a new wind-sea system develops in the new wind direction. In the particular case presented in this work, because the direction of growing waves was so different from the direction of the generating wind, additional mechanisms had to be steering wave direction away from wind direction, as discussed below.

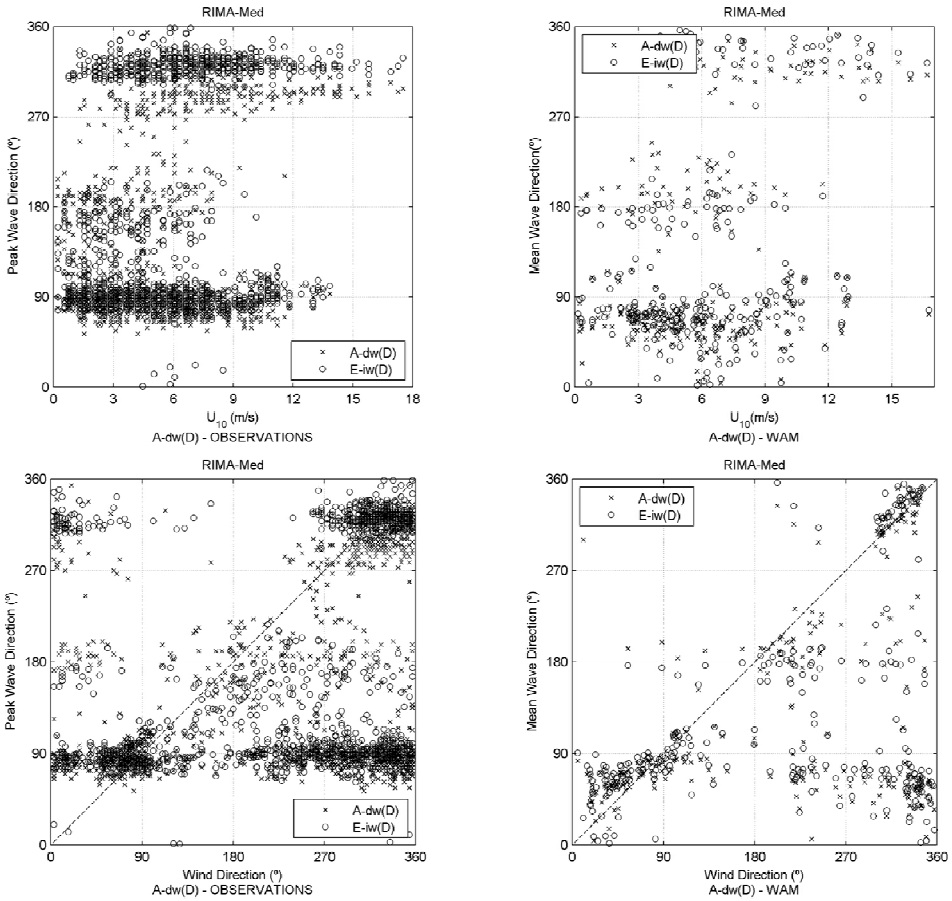

Figure 5.3 Scatter plots of wave direction against wind speed (panels on the top row) and wind direction (panels on the bottom row) from observational data (panels on the left side) and from numerical simulations (panels on the right side). The direction convention is the direction where winds and waves are coming from. Note that the observations were characterized by peak direction, whereas the numerical simulations were characterized by mean direction.

Second, I explored the effect of refraction, which is the prototypical process inducing change in waves' direction in varying depths. Compared to the previous section, in this case I focused on the directional difference between buoys E-iw(D) and A-dw(D), and not on the wave height difference between E-iw(D) and B-iw(S). The observations indicate that wave trains tended to travel in the direction perpendicular to the bathymetric isolines in shallow (or intermediate) waters, as expected due to shoaling and refraction. In effect, the sign of the wave direction shift at E-dw(D) (e.g. to the north during Storm nº3) agreed with the expected deviation due to refraction of wave trains (shallowing of the bathymetry around the Ebro Delta). To verify the effect of refraction on wave direction, its value at buoy A-dw(D) was taken as the unchanged reference value because this buoy was located in deep waters. Thus, wave direction at A-dw(D) was not (or very little) affected by bottom processes such as wave refraction.

According to the linear dispersion relationship of water waves, at 60 m depth, only wave trains whose peak period is longer than 8.5 - 9 s (peak frequencies lower than 0.1 Hz and wavelengths longer than 120 m long) 'feel' the bottom and should refract. According to Snell's law, changes in wave direction (angle

of approach) depend on peak period and water depth. At buoy E-iw(D), for peak periods ranging from 7 s to 12 s, the directional change would be 0.1º to 3º, quite far away from the 26º difference recorded. Note also that wave trains being generated from north-western wind conditions were usually shorter and peak periods were lower than 7 s. Then, the 26º shift recorded during north-west wave conditions could not be only due to wave refraction because such short wave lengths do not 'feel' the bottom and are barely refracted.

Third, and last, I explored the role of slanting fetch conditions in determining wave direction during offshore-blowing wind situations. The term 'slanting fetch' (see for example Ardhuin et al. 2007) refers to wind blowing offshore but not perfectly perpendicular to the coast. Slanting fetch results in a redistribution of the wave energy across directions to match the direction of the longest fetch (usually along the coast). The effects of slanting fetch were also addressed by Pettersson et al. (2010). In their work, they represented the directional data in the same way used in Figure 5.3. Pettersson et al. (2010) reported a steering effect of wave direction due to the fetch geometry (narrow lake) and they concluded that wave directions orientate along the longest fetch component, independently of wind direction due to slanting fetch effects.

In the records (see Figure 5.3), wave directions were highly variable in low wind speed conditions but, at high wind speeds there was a clear steering and orientation along three main wave directions: east, south and northwest. The differences in wave direction could be explained through differences in the length of the fetch at each buoy's position. During eastern storm events (longest fetch), wave direction at buoys A-dw(D) and E-iw(D) was similar and so was the fetch's length; the difference recorded was 7º, but it could be due to refraction and/or to the uncertainty of the measures. During southern storms there was a slightly stronger deviation (17º) to the west at E-iw(D) and to the east at A-dw(D); which could be explained by the blocking effect of Ibiza Island on pure southern fetch, as shown in Figure 5.4. During north-west storms the wave direction difference between buoys was stronger, in agreement with the shorter fetchs involved, and the largest differences in fetch between the buoys. The differences in fetch length in offshore blowing winds were due to the coastal geometry. For wind directions between 270º and 360º, note in Figure 5.8 that the longest fetch at E-iw(D) was shifted to the north, compared to the fetch at A-dw(D), because the Ebro Delta was located on E-iw(D)'s west side. The longest fetch at A-dw(D) was shifted towards the west, because the Coast of Tarragona shortened the fetch on the north side.

Summarizing, it was reasonable to explain the differences in peak wave direction in this region due to an effect of refraction and, predominantly, to an effect of slanting fetch; i.e. a reorientation of wave energy along the direction of the longest fetch.

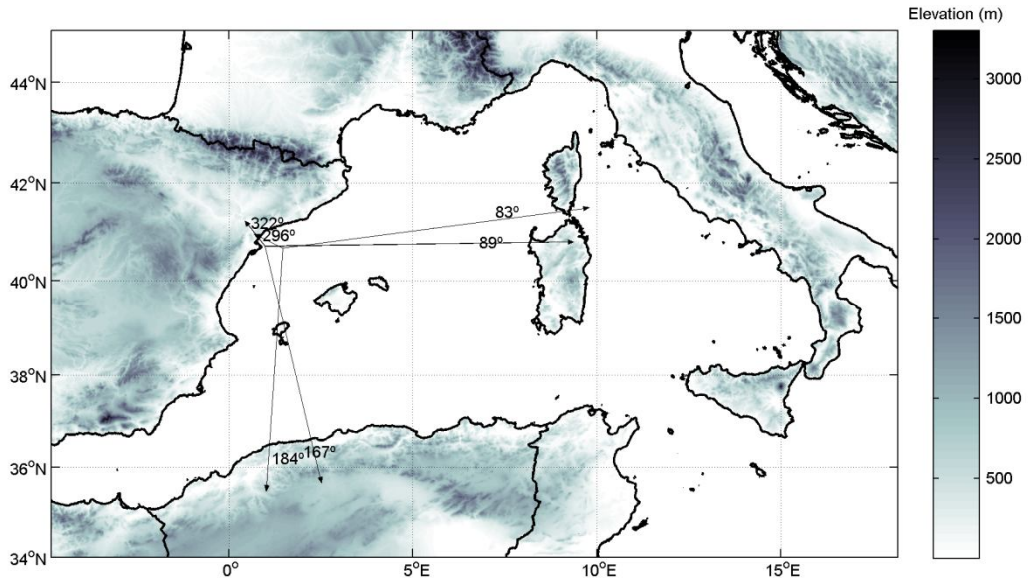

Figure 5.4 Average peak wave direction registered at buoys A-dw(D) and E-iw(D) and graphical illustration of the fetch for each direction in Table 5.1. Ibiza Island is located just below the crossing of the two south-pointing arrows.

5.2. Temporal gradients

In the Catalan Coast, temporal wind variability at large time scales (seasonal) was described by Guadayol and Peters (2006), who used meteorological stations over land to describe coastal wind conditions. In this section I characterize temporal gradients of the wind and wave data records during RIMA-Med in terms of shorter-scale variability (hourly time scales). I did not address even shorter-scale variability because the frequency of measurement was 1 h. Also, shorter-scale variability is part of turbulence studies and gustiness (in the case of wind speed); see for example Abdalla and Cavaleri (2002) and Ponce de León and Ocampo-Torres (1998), and it is out of the scope of this work.

The RIMA-Med time series showed that wind speed records presented sharper temporal gradients, compared to the wave height time series, which were smoother (less variability; compare for example Figure 4.1 and Figure 4.2). This result partly agreed with the fact that waves are the integrated effect of winds both in space and in time. The wave response to changes of wind speed is observed in Figure 5.1 (left panel) during the coastal wind jet addressed in previous section. In this case, the response was quite fast (1 – 2 h), but the result could not be generalized to all situations due to the lack of data for comparison. In fact, different wave responses were expected depending on the maturity of the waves (longer responses for older waves).

For this reason, and in order to quantify the local time response of waves to changes in wind speed, I performed a correlation analysis between wave height and wind speed at A-dw(D) for two different storm events (wave conditions). The degree of correlation for sea and swell conditions is plotted in Figure 5.5

and it shows that during fetch-limited wave growth conditions (Storm nº3) the highest degree of correlation between winds and waves is not lagged in time. Thus, the response of wind sea waves to wind is generally immediate (within 1 h). Instead, the maximum correlation between wave height and wind speed in swell-dominated wave conditions (Storm nº4) is lagged by 2 h. In other words, old swell waves generally take between 2 h and 3 h to respond in some way to wind speed changes (the correlation degree for 3 h time lag being only slightly lower than for 2 h; see Figure 5.5). The shape of the cross-correlation function (and the slope of its tail) is also very enlightening because it illustrates that in swell-dominated conditions a late wave response to winds is much more common than in sea-dominated conditions.

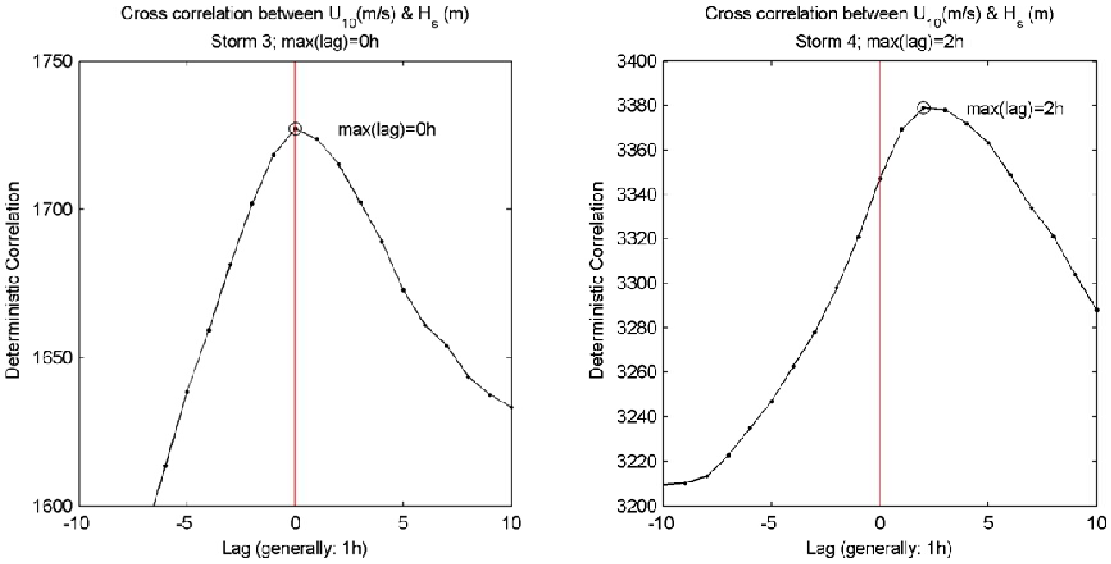

Figure 5.5 Cross-correlation between wave height and wind speed measured at buoy A-dw(D) during fetch-limited growth (Storm nº3; left) and swell conditions (Storm nº4; right). It shows the time response of wave height to wind speed changes.

To characterize temporal gradients I also used histograms of differential values at time lags of 1 h, 2 h and 3 h during RIMA-Med. The changes in U_{10} and H_s for the considered time lags were calculated to describe how fast wind and wave records change in time. The ratio of change in time (t) was an absolute value that was calculated as follows:

$$\text{Ratio of change } U_{10} = \text{abs}\left[\frac{U_{10}\ (t=\text{lag})\ - U_{10}\ (t=0)}{U_{10}\ (t=0)}\right] \qquad \textbf{[5.1]}$$

$$\text{Ratio of change } H_s = \text{abs}\left[\frac{H_s\ (t=\text{lag})\ - H_s\ (t=0)}{H_s(t=0)}\right]$$

The resulting histograms in Figure 5.6 indicated that in one hour time 40% of the time wind speed increased/decreased by half its value (50%). Also, at least 20% of the wind speed values increased/decreased by twice their value (100%), or more, in only 1 h. The probability of faster changes

rose if 2 h and 3 h time lags were considered. In other words, comparing wind speed at time zero and its value 2 or 3 hours later, in 25% and 30% of the observations (respectively) wind speed was seen to double its value (100% increase).

The meteorological stations that showed more variability (less persistence) were the land stations, due to topographic effects on the wind field, as pointed out by Koçak (2002).The lowest variability was recorded at buoy A-dw(D) which was located in the open sea and, thus, less affected by the topography.

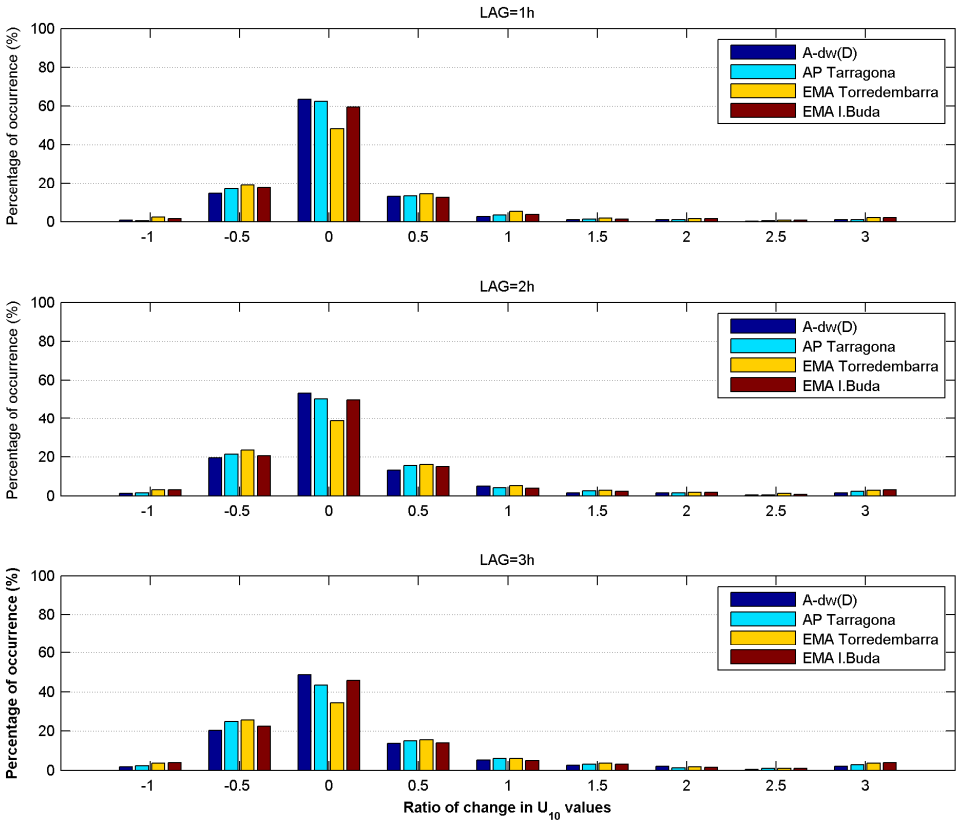

Figure 5.6 Histograms of the difference of U_{10} between the present time and a certain time lagged by 1 h (upper panel), 2 h (middle panel) and 3 h (lower panel) at the four meteorological stations.

The reported high temporal variability of the wind speed data was not linearly transferred to the wave data, as already pointed out above. In fact, more than 96% of the time wave height remained within 50% of the wave height recorded one hour earlier (Figure 5.7). Even more, for the same 1 h time lag, more than 80% of the time wave height increased/decreased less than 25%. Nonetheless, a small percentage of the data showed that sudden rises also occurred, especially at buoy A-dw(D), where the highest wave height variability in time was recorded.

The sharpest wave height changes were recorded at the most offshore buoy, which was exposed to a larger number of wave conditions. Quantitatively, at buoy A-dw(D), the percentage of time during which

wave height increased twice its value was less than 1% for 1 h time lag, 1.3% for 2 h time lag and almost 3% after 3 h (see Figure 5.7).

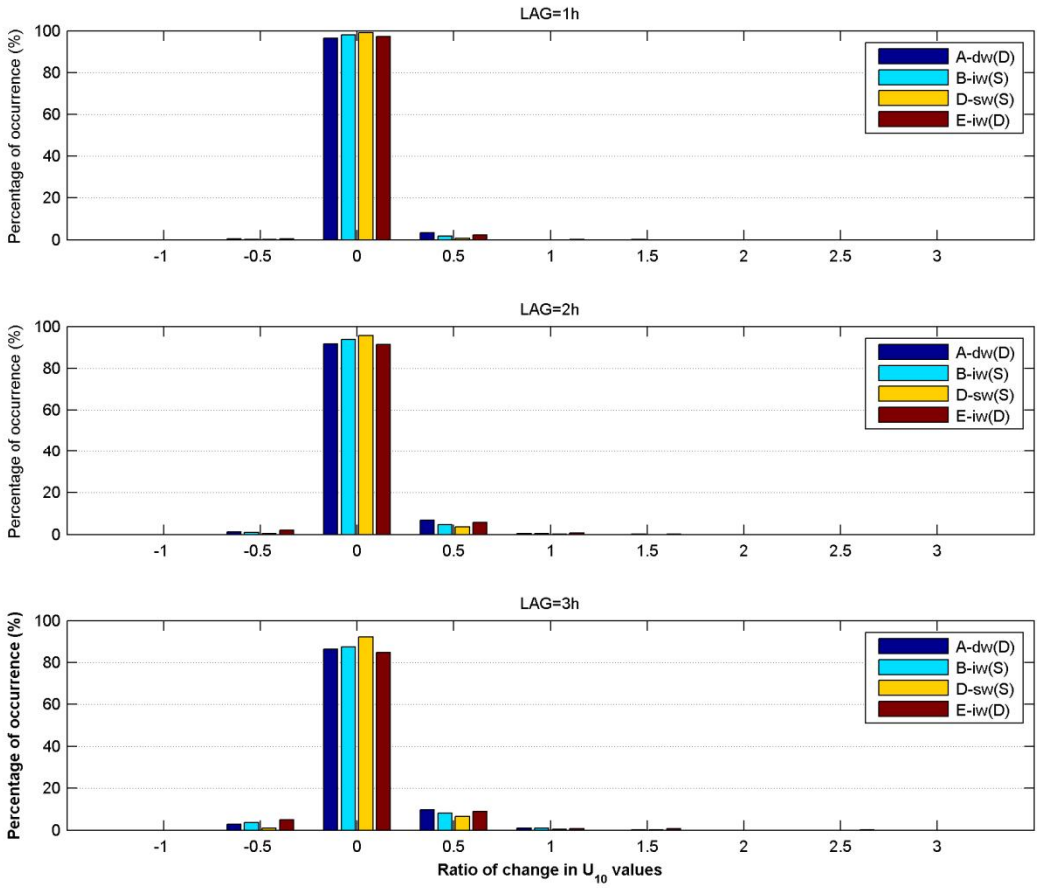

Figure 5.7 Histograms of H_s difference for time lags of 1 h (upper panel), 2 h (middle panel) and 3 h (lower panel) at the four wave instruments.

5.3. Implications for wave modelling

The sharp gradients in the region of study had direct implications on regional wave modelling. In this chapter, to describe the effect of the characteristic features described above on operational predictions I address several main issues related to numerical modelling. Additionally, at some points, I compare the observations with the results from the operational wave forecasting system in the region (MASS atmospheric model and WAM wave model; see Section 4.5).

5.3.1. Coastal wind jets

In a previous section I described, on one side, wave height differences between points separated by 30 km, both, along the coast and in the offshore direction. These differences indicated that the spatial scales of the coastal wind jets were, at most, 30 km wide. Thus, the adequate spatial resolution of a regional model should be at least 30 km, which should not be mistaken with the model's grid size. In fact, the

model's grid spacing should be at least two, or three, times smaller than the spatial resolution; i.e. 15 or 7.5 km.

Additionally, note in Figure 5.8 that the local valleys' width is approximately 8 km; the valley north of Tarragona is slightly narrower, and the valley of the Ebro River is slightly broader. A wind jet being funnelled through these valleys would broaden once exiting the narrow areas and progressing down towards the flatter coastal zone and into the sea. Thus, to resolve wind jets due to local orography (river valleys) of approximately 10 km wide, and without assuming the horizontal broadening of the wind jet, the grid size of the numerical models should be between 5 km and 3.3 km.

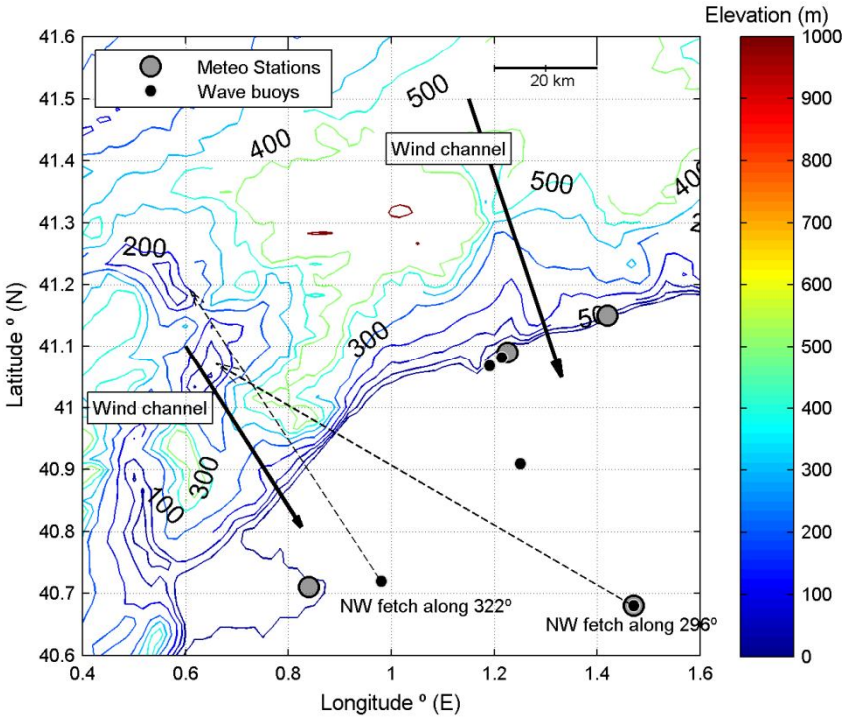

Figure 5.8 Orography of the coastal zone in the region of study. Contour lines are provided for heights above sea level of 0, 20, 50, 100, 200, 300, 400, 500 and 600 m. Solid arrows indicate the position of the river valleys that favour wind channelling. Dashed lines indicate the direction of the average peak wave direction during NW blowing winds at buoys A-dw(D) and E-iw(S). Notice that distances are approximate due to the projection of the map.

The temporal scales of a wind jet was also recorded during RIMA-Med. The characteristic wind speed was seen to increase and decrease within 6 h, which was also the input frequency of the operational wind fields (i.e.6 h). Thus, properly capturing coastal wind jets such as this one with the existing operational models could be almost considered a matter of coincidence. Therefore, these results suggested that using wind fields at least every 3 h was necessary if aiming to capture the temporal scales of coastal wind jets in the region of study.

In previous subsections it was also shown that wind speeds were highly variable at the hourly time scale, but wave heights were less variable. Nonetheless, in wind wave growth conditions, wave energy responded within the same hour to wind speed. Therefore, increasing the wind input frequency from 3 h to 1 h would permit rapid responses of waves to changing winds, if the wave model reaction time was, accordingly, short enough.

5.3.2. Swell attenuation

In a previous section, a remarkable attenuation of swell at buoy B-iw(S) was reported, compared to E-iw(D) and A-dw(D). The effects of in-situ shoaling were not thought to be the main reason of the attenuation because of the depths at which the buoys were located and the low peak periods involved. Instead, the results point to a dominating effect of refraction due to the shadowing effect of the coast to the north of buoy B-iw(S), and a slight effect of diffraction at large scales.

In spectral wave models, refraction is acceptably reproduced but diffraction is limited and requires an additional modification of the action balance equation (The WISE Group 2007). For this reason, for example, Monbaliu et al. (2000) modified the original WAM for high spatial resolution applications to include the effects of refraction. Nonetheless, strong refraction processes still require phase-resolving models. In general conditions, The WISE Group (2007) indicated that refraction was generally well simulated over narrow continental shelves in the absence of currents, but they also pointed out that important errors occurred due to sharp changes of water depth on the scale of a wavelength.

In the region of study, the most limiting conditions in terms of wave refraction occurred during North-westerly winds due to the shorter wave lengths involved. During these situations the wave length was about 76 m, according to linear wave theory and considering that the peak period of growing wind waves at the most offshore buoy was generally shorter than 7 s. Eastern wave trains (usually attributed to swell systems) were characterized by longer periods (12 s) and longer wave lengths (220 m), which are less limiting in terms of simulating wave refraction. Therefore, in order to avoid inaccurate wave estimations due to refraction processes, it was important to avoid changes in water depth sharper than 76 m in two neighbouring grid points. The easiest approach to avoid sharp gradients of water depth would be to decrease the wave model's grid size, even though it entrains, for example, an increase of the computational cost. This approach would also require having a bathymetric field of enough quality and conveniently updated.

5.3.3. Slanting fetch

Slanting fetch effects were thought to be the most probable mechanism responsible for the differences in wave direction between the buoys A-dw(D) and E-iw(D) because the observed differences (up to 26º in offshore blowing wind conditions) could not be due to wind direction or local refraction. Also, wave direction tended to orientate along the direction of the longest fetch. Slanting fetch effects in numerical

simulations, although not fully studied, were already addressed by Ardhuin et al. (2007), among others. These authors concluded that the models reproduce fairly well the directional change due to slanting fetch effects. Although slanting fetch effects are closely related to non-linear interactions, these authors showed that the so-called DIA approximation (commonly used in operational models) produces acceptable results. Also, they reported that the only effect of an increase of the model's directional resolution (from 10º to 5º) brings to a reduction of 3º of the directional energy spread.

To assess the performance of wave models in the region of study in terms of slanting fetch, I used the operational simulations of the WAM model during storm nº3. The difference of the wave direction recorded at the two buoys A-dw(D) and E-iw(D) was about 26º. The operational models only partially reproduced such difference, being the final estimated difference equal to 12º. Note that although the operational output of wave models was mean wave direction, it should not differ importantly from peak wave direction in wave growing conditions. These results indicated that slanting fetch in regional wave models could still be further adjusted to better match the observations. Although out of the scope of the present work, these results call for an in-depth study of the directional capabilities of operational models in the region, under variable wind conditions.

Table 5.2 Average mean wave direction for the three characteristic directional sectors: east, south and northwest. Data were numerically calculated using the WAM model. The output was linearly interpolated at the buoys' location.

Buoy location	East $0º \leq \theta_m \leq 130º$	South $135º \leq \theta_m \leq 225º$	North-west $270º \leq \theta_m \leq 360º$
A-dw(D)	64.8º	190.9º	321.5º
E-iw(D)	68.5º	177.0º	333.5º
Difference	3.7º	13.9º	12º

5.4. Summary and final remarks

The main objective of characterizing the mesoscale spatial and temporal variability in the Catalan region was describing the particular processes occurring at scales of 10 – 100 km and 1 h – 1 day and exploring the main implications for wave modelling. Such detailed characterization was mainly intended for wave modellers aiming to improve wave forecasting, but could also be of interest to other persons studying physical and biological processes in the coastal region. Also, although the results presented are characteristic of the Catalan Coast, these features probably exist in similar orography-controlled regions with similar temporal and spatial scales.

The main spatial features in the NW Mediterranean were coastal wind and wave jets, attenuation of swell at certain locations, and large differences of peak wave direction mainly due to slanting fetch processes. Coastal wind jets were seen to generate locally high wave heights that might have important effects on maritime activities. For example, a particular coastal wind jet lasted about 6 h and stretched along about

30 km. The imprint of coastal wind jets on wave conditions was restricted in space and could be responsible for wave height differences up to 50% between instruments located 30 km apart. The most probable reasons for swell attenuation at an intermediate-depth location close to the coast were the influence of the coast to the north (due to the blocking effect of the coast on the northern-coming swells and refraction of swell). The differences in peak wave direction (up to 26º during offshore-blowing wind conditions) were most possibly caused by slanting fetch effects for several reasons. First, wave direction was rather independent of wind direction. Second, local refraction was not expected to change wave direction more than 3º. And third, wave direction tended to align and orientate along the maximum fetch of the three main directions of local storms (east, south and northwest).

A characteristic of the temporal gradients was that 40% of the wind speed records increased (or decreased) 50% (or more) its initial value in a period of time of 1 h. Wave height time series were much smoother: 96% of the time wave height remained within 50% of the previous value. The cross-correlation of the wind speed and wave height time series indicated that the time response of waves to winds was relatively fast during fetch-limited events (within 1 h) and slower during swell dominated conditions (2 - 3 h).

The amount of variability recorded in the region of study has several implications for wave modelling. First, to reproduce physical processes such as coastal wind jets and swell attenuation it is necessary to increase the spatial and temporal resolution of wind and wave models. The results suggested that the appropriate spatial resolution should be about 5 km. Wind input frequency should be at least 3 h, although an increase to 1 h could be meaningfully explored. An increase of the spatial resolution would increase the probability of capturing the full extension of coastal jets, coastal features and sharp gradients of wind speed and bathymetry. An increase of the wind input frequency (temporal resolution) would prevent loss of information in short duration storms and coastal jets.

Note that this is not the first time that it was suggested to increase the resolution of operational models to improve wave forecasting (see e.g. Bolaños and Sánchez-Arcilla 2006, Bolaños et al. 2007). Also Abdalla and Cavaleri (2002) reported that increasing the spatial and temporal variability of U_{10} consequently increases average H_s. However, in this region, some of the missed features in the simulations were not only related to the models' resolution but also to the estimation of propagation mechanisms (e.g. swell attenuation, slanting fetch). To conclude this chapter, note that the results from this chapter suggest that an increase of the wave models' resolution should improve the amount of variability captured by both wind and wave models, thus supporting the approach taken further on in Chapter 6. An improvement of wave estimations in variable conditions would be, however, constrained to accurately modelling fast responses of waves to winds and properly reproducing wave propagation processes such as refraction and slanting fetch. This last point is addressed in terms of wave growth in Chapter 8.

6. Increasing the spatial and temporal resolution of the forcing winds

Wave forecasting along the Spanish Catalan coast is known to be of limited accuracy especially during fetch-limited conditions, partly due to the high variability of the wind fields. In this chapter wave estimations were improved under geometrically restrained conditions using accurate wind fields and higher resolution wind and wave models. The resolution increase aimed to avoid smoothing wind and wave peak values, to capture wind and wave spatial structures typical of sharp-gradient regions and to consequently improve the estimation of wave parameters.

The analysis was supported by hindcasting fetch-limited storm conditions characterized by highly variable winds. Wind fields at three spatial grid resolutions (18 km, 12 km, 4 km) and three wind input frequencies (6 h, 3 h, 1 h) were used to drive spectral wave models at four spatial resolutions (18 km, 12 km, 4 km, 1 km). Increases in spatial and temporal resolutions were independently assessed.

This chapter is structured as follows. The particular storm event used in this chapter is described in detail the section 6.1. Section 6.2 describes the modelling strategy that was followed and the different simulations performed. The improved performance of the models is presented in section 6.3 for wind speed and section 6.4 for wave height. Section 6.5 describes the performance of the higher resolution models in specific situations associated to sharp gradients such as coastal wind jets, slanting fetch and diffraction. Note that Section 6.5 complements Section 5.3 in previous chapter (implications for wave modelling) and it extends the previous discussion since, at this point, the spatial and temporal resolutions were already adjusted to resolve local gradients. In last section 6.6 a brief summary of the results is provided.

6.1. The case study

The present work focused on fetch-limited conditions and the possibilities to improve wave estimates by better resolving mesoscale variability. For this reason, I selected a particular wave storm event, characteristic of the region of study. The case study was a complicated storm in terms of wave predictions since it mainly consisted of a highly variable northwest offshore wind field (thus, fetch-limited wave growth). Note that Northwesterly events are very common in the region and especially difficult to predict because of their intense nature and abrupt occurrence. The selected event occurred between the 7 Dec. and the 13 Dec. 2007 and corresponded to storm nº3; according to the storm identification performed in Section 4.1.

During the case study, fetch-limited wave heights reached values higher than 2 m (lasting almost 24 h), which is the wave height threshold (average duration) of wave storms in the region (e.g. Sánchez-Arcilla et al. 2008). The event selected for analysis was characteristic of the rapid developing wind patterns common in the NW Mediterranean. It presented sharp veering winds, wave gradients (in time and space) and fetch-limited wave generation, which together make wave forecasting a daunting task with errors well in excess of those found for open sea conditions. The event started on 7 Dec. 2007 when a high pressure system over the Azores and a low pressure system north of the UK forced north-western winds off the Catalan coast. Late on the 8 Dec. and early on the 9 Dec. a fast developing low pressure system located over Italy forced an area of low wind speeds and variable wind directions over the Catalan coast (denoted here as 'calm' period). On the 10 Dec. the Italian low merged with the northern low increasing westerly and north-westerly wind speeds over the region of study. On the 11 Dec. the low centre moved east shifting wind direction first to the north and then to the northeast before dying away the 12 Dec. The synoptic situation is depicted in Figure 6.1.

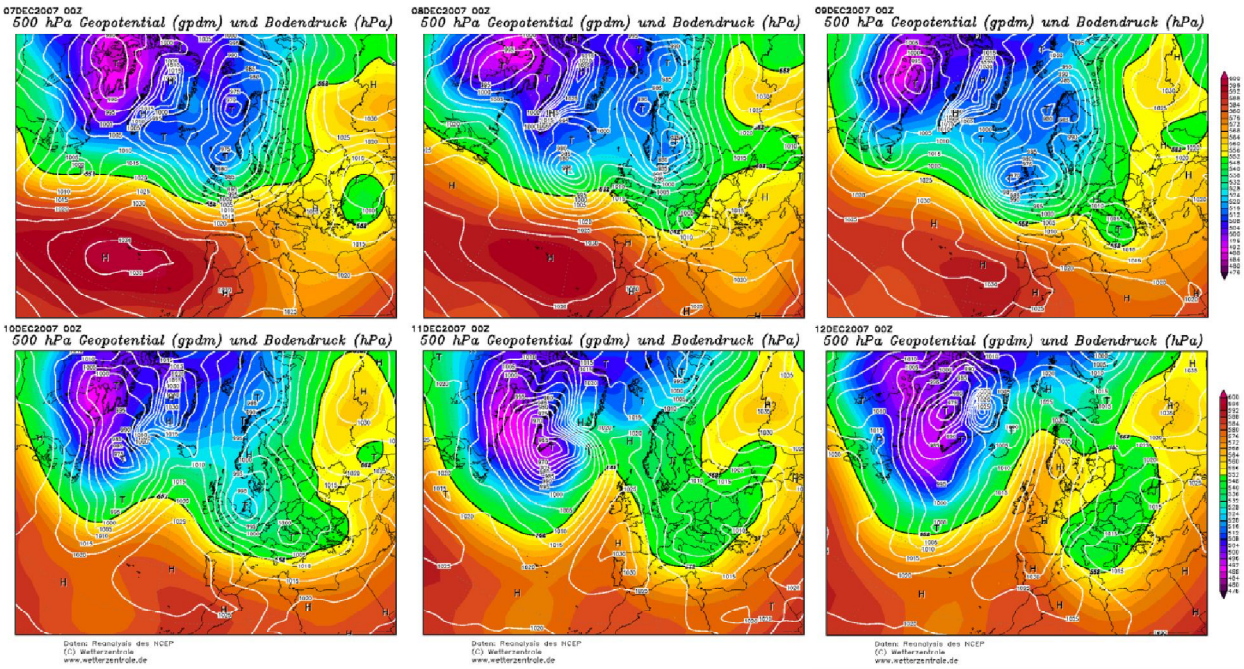

Figure 6.1 Synoptic evolurion of the meteorological situation during the storm event of interest (7 Dec. – 13 Dec. 2007). The panels represent the surface pressure (colour scale) and the 500 hPa geopotential height (contour lines) over the North Atlantic Ocean, Europe and the Mediterranean Sea. They were downloaded from Wetterzentrale.de (Wetterzentrale 2012**) and correspond to NCEP-reanalysis.**

The wind and wave measuring instruments available in the study area during the event of interest were used to evaluate the performance of the numerical simulations. The measuring instruments were already described in Chapter 3, but note here that in this part of the work the effectively used wave instruments were A-dw(D), B-iw(S), D-sw(S) and E-iw(D). These instruments were located at different depths and distances from the coast, along the main direction of the offshore blowing wind (see Figure 3.1). The four

different meteorological stations described in Section 3.2.2 and depicted in Figure 3.1 were also used, as well as wind data from the Quickscat satellite blended with ECMWF simulations.

The wind time series recorded during the storm event are shown in Figure 6.2. Notice that the wind speed values at the offshore buoy (A-dw(D)) and at the coastal-sea station (H-met) were higher than at the two coastal-land stations (T-met and U-met). Wind speed records at the first two stations registered two main peaks: the first one on the 8 Dec. at 00 h; and the second peak on the 10 Dec. around 10 h. At H-met a third important peak was registered on the 9 Dec. at 12 h. The highest wind values were measured at A-dw(D) (nearly 18 m/s), the most offshore station. Slightly lower wind values were recorded at H-met, which was located on the harbour's external breakwater. H-met was located at the in-shore limit of the generation area. Wind direction during the case study was relatively constant around 295º. Late on the 8 Dec. and early on the 9 Dec., during the 'calm' period, turning winds were registered: from the NW to the SW and then from the NE within a 12 h-period.

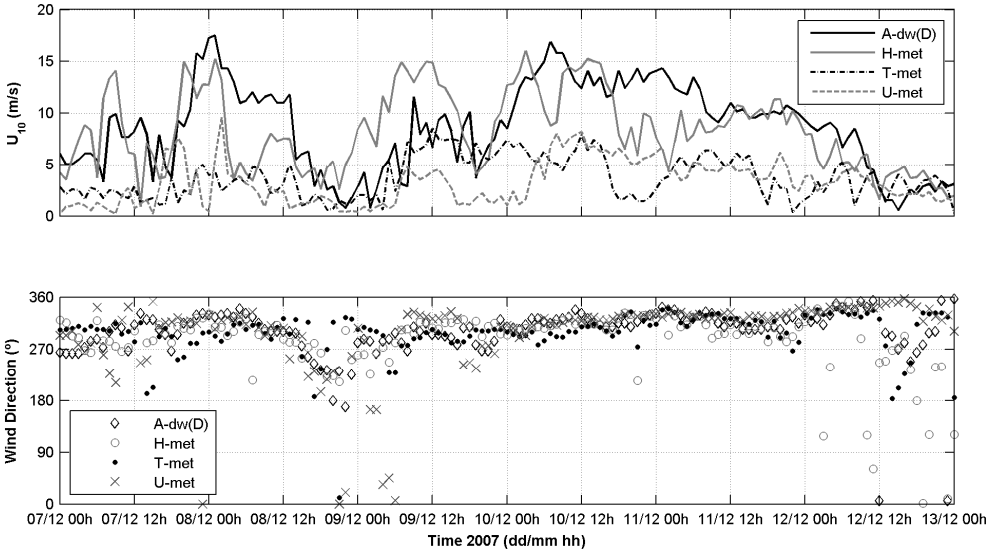

Figure 6.2 Wind speed (upper panel) and wind direction (lower panel) from 7 Dec. to 13 Dec. 2007 at the four meteorological stations close to the instrumental set in Figure 6.5.

Wave instruments also registered two wave height peaks on the 8 Dec. at 00 h and the 10 Dec. at 10 h, and a third but lower peak on the 9 Dec. at midday (Figure 6.3). Peak wave directions were mainly from the NW except during the 'calm' period for which the dominant wave trains were from the SW and the E. Peak periods ranged from 4 s to 7 s, depending on the location (Figure 6.3). During the 'calm' period, a secondary wave train with T_p around 8 s was recorded at the most coastal buoy (D-sw(S)). This buoy was located at a very short fetch position for NW winds (less than 1 km). For this reason the wave energy recorded at this buoy was considered an estimation of the residual swell energy in the system.

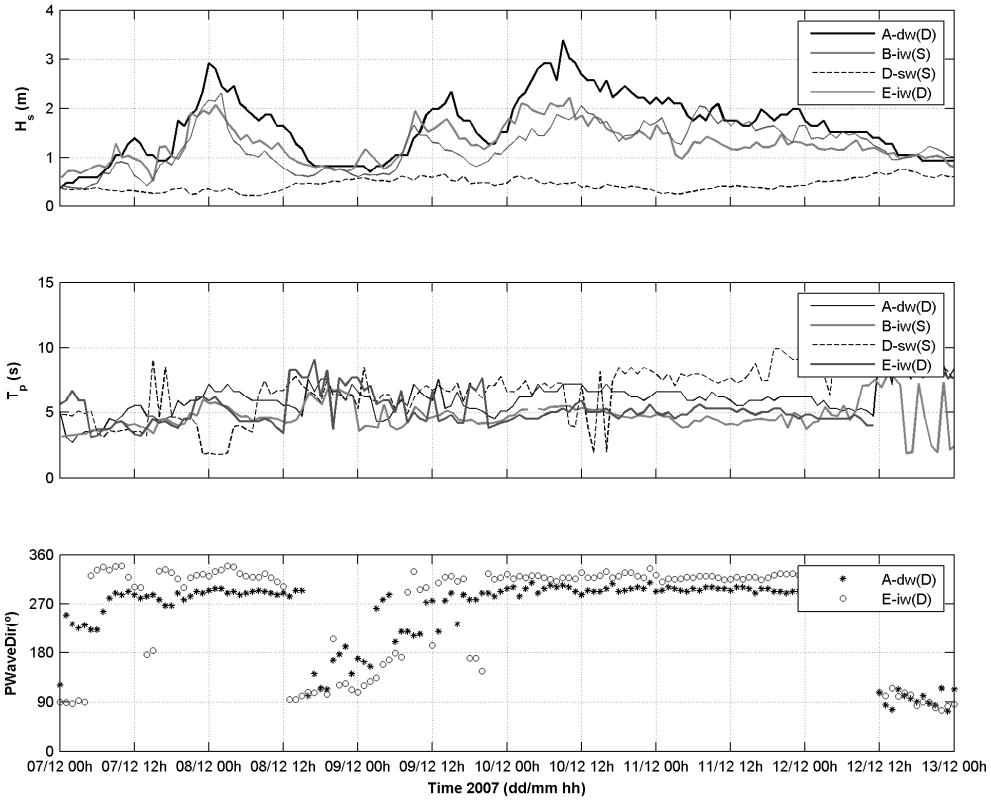

Figure 6.3 Significant wave height (upper panel), peak period (middle panel), and peak wave direction (lower panel) from 7 Dec. to 13 Dec. 2007 at the different wave instruments in Figure 6.5.

The most energetic wave period was recorded late on the 8 Dec. and after the 11 Dec. (peak periods higher than 7.5 s). The energy on the 8 Dec. was less than 0.5 m of wave height (at D-sw(S)). At the end of the study period, late on the 12 Dec., the 'swell' wave height went up to 1 m. Swell trains came either from the east or the south sectors. This event was considered as mainly unimodal and fetch limited because the rare swell recorded was much less energetic than the sea peak. Also, a comparison of a model simulation with and without nesting in a larger domain (with swell) showed that the overall differences were not relevant (< 0.02 m at the peaks).

6.2. Modelling strategy

To check the effects of increasing the spatial resolution of the input wind fields I compared wave estimations obtained by forcing the wave model both with high resolution wind inputs from atmospheric models, and with in-situ wind observations. Bear in mind that the main objective of this approach was to better resolve the spatial variability of the region and to improve wave estimations as an end-result. Within this approach the computational cost was not an important limiting factor.

The set of simulations used in this work is summarized in Table 6.1. I used the atmospheric models MASS and MM5 and the wave models WAM and SWAN, as described in Section 3.3. The grid size of the wind models was decreased down to 4 km and the wind input frequency was increased to 1 h. The whole set of simulations were compared for three main purposes 1) comparing two wave models, 2) describing the improvements of wave estimations due to an increase of the spatial resolution and the input frequency of the forcing wind fields, and 3) assessing the wave estimations when using real wind input data from meteorological stations but no spatial variability. The set of comparisons is summarized in Table 6.2.

Table 6.1 Wind and wave model settings for the different numerical simulations performed in the case study.

Run name	Wind input			Wave output	
	Source	Spatial resolution (km)	Input frequency (h)	Wave model	Spatial resolution (km)
WAM SWAN	MASS	18	6	WAM SWAN	18
MM5 12km/6h MM5 12km/3h	MM5	12	6 3	SWAN	12
MM5 4km/3h MM5 4km/1h	MM5	4	3 1	SWAN	1
A+SWAN H+SWAN T+SWAN U+SWAN	A-dw(D) H-met T-met U-met	Constant over the whole domain	1	SWAN	1

Table 6.2 Purpose of the comparison of numerical simulations, whose details are summarized in Table 6.1.

Purpose of the comparison	**Name of the simulations compared**	
Compare two wave models	WAM	
	SWAN	
Check spatial resolution increase	SWAN	MM5 12km/3h
	MM5 12km/6h	MM5 4km/3h
Check wind input frequency increase	MM5 12km/6h	MM5 4km/3h
	MM5 12km/3h	MM5 4km/1h
Quantify the improvement with real forcing data but no spatial resolution		MM5 4km/1h
		A-dw(D)

In Table 6.1 and Table 6.2 note that in the first couple of simulations the same forcing wind fields from the operational MASS atmospheric model were used to compare two different wave models: WAM and SWAN. This comparison served two purposes: first, it helped choosing one of the two models to study this particular event. Second, it was used to compare the two different formulations of wind input and

dissipation implemented by in each model (JAN in WAM and KOM in SWAN). This comparison, although out of the scope of this chapter, is discussed again in more detail in Chapter 9.

The results from the wave model comparison are presented in the first two columns of Table 6.4 and Table 6.5. The results indicated that both wave models under-estimated the wave height at all locations, although SWAN's estimations were slightly better than WAM's. The best estimations were provided by both models at the most offshore buoy A-dw(D) (longest fetch position). These results also indicated that the differences between JAN (in WAM) and KOM (in SWAN) physical parameterizations were not relevant, as discussed again in Chapter 9.

These results agreed with the model comparison performed for operational purposes by Bolaños et al. (2007), who concluded that WAM predicted the spectral shape better, while SWAN predicted the integrated spectral parameters better. Bolaños (2004) reported under-estimations of the mean period in SWAN that were caused by over-estimations of the energy at high-frequencies. The results confirmed that SWAN under-estimations of peak period were also larger than those in WAM (Table 6.5). The simulated time series (not shown) indicated that both models missed the first H_s peak of the storm, in agreement with the under-prediction of the corresponding U_{10} peak in MASS. The second and third H_s peaks were also highly under-predicted but U_{10} could not be directly blamed for this.

In this work, I used SWAN instead of WAM to discuss the models' problems in variable wind conditions because 1) SWAN predicted slightly better H_s; 2) WAM wind growth formulations were also implemented in SWAN and could be compared more easily; and 3) SWAN used a semi-implicit scheme that was less restrictive than WAM with time step and spatial resolution.

The main physical processes (source functions) active during this experiment were wind input, dissipation through whitecapping and quadruplet interactions. The non-linear interactions were resolved using the DIA approximation. The integration time step was set to 20 min, the numerical scheme was a first order scheme (BSBT) and the number of iterations was set to 15.

6.3. Accuracy assessment of the input wind fields

The accuracy of the simulated wind fields used in this work was verified by comparing the wind speed time series at the location of the different meteorological stations with the observations using statistical tools and visual analysis. The statistical analysis was based on the slope of the scatter plot and the *R2* coefficient that describes the amount of variability captured (refer to Section 4.3 for the details of both parameters). The input wind fields compared were those summarized in Table 6.1; namely, MASS, at 18 km spatial resolution and 6 h temporal resolution, and MM5 at 12 and 4 km spatial resolution and 6 h, 3 h and 1 h temporal resolutions.

Before evaluating the numerical simulations, note that the wind speed measured at buoy A-dw(D) (see Figure 6.2) presented an increase from 5 m/s to 15 m/s in less than 3 h. It would have been naive

expecting to properly reproduce the reported growth rate using the 6 h temporal resolution of wind models. Based on the observational data described in the previous chapter, it was clear that the wind input frequency had to be increased to at least 3 h (and up to 1 h) to properly model wave growth in the area. Also, the scale of the local orography implied that high spatial resolution was needed to resolve local topographical features, such as capes and river channels in the coastal mountain range. In Chapter 5 it was shown that the smallest river valley (just behind Tarragona) was about 10 km wide. Therefore, a grid size of 4 km was fine enough to resolve the wind jets generated in the area.

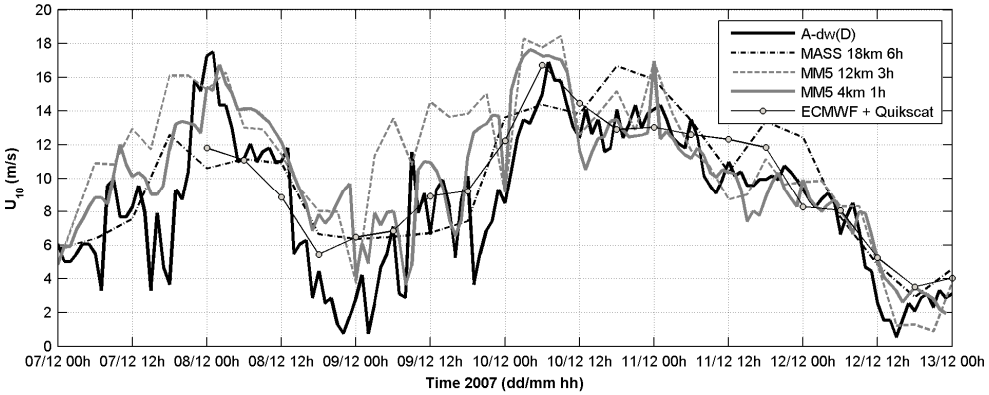

Figure 6.4 Modelled wind speed from MASS 18km/6h, MM5 12km/3h, MM5 4km/1h, ECMWF+QuikSCAT data and observations at the location of offshore buoy A-dw(D) from 7 Dec. to 13 Dec. 2007.

As shown in Figure 6.4, the higher temporal variability of MM5 wind fields (3 h, 1 h) compared to the operational MASS (6 h) was clearly beneficial in the visual comparison with measured U_{10} time series at the most offshore buoy A-dw(D). MM5 simulations reproduced significantly better the highest values of U_{10} both in magnitude and timing. The reason of the marked differences between the output of the two atmospheric models (MASS and MM5) was attributed to the improved settings in MM5; namely, the initial conditions from reanalysis and the much higher resolution of MM5's finest grid (4 km; 1 h). In particular, the finest-resolution simulation reproduced local wind jets that were not reproduced by MASS (see Figure 6.5). The growth and decay rates of the wind speed peaks (see Figure 6.4) were also accurately simulated.

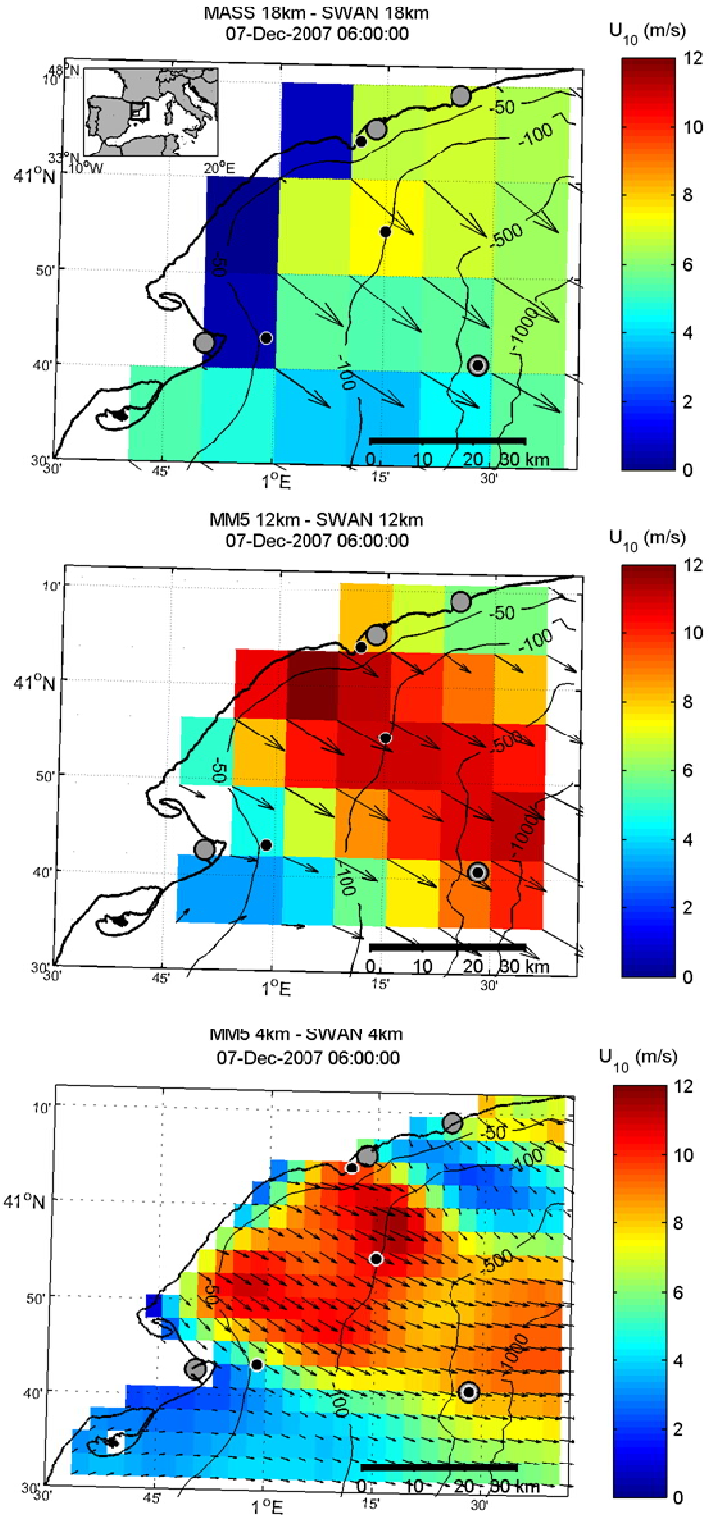

Figure 6.5 Wind fields comparison of the three atmospheric models and their spatial resolutions during a characteristic coastal wind jet: (top panel) MASS-18km; (middle panel) SWAN-12km; (bottom panel) SWAN-4km. Colour and arrows show a snapshot of wind velocity and direction on the 7 Dec. 6h 2007. Wave recording instruments (black dots) and meteorological stations (grey dots) are depicted. Bathymetry is shown as black contour lines. In the top panel, the inner figure depicts the domain of WAM and SWAN-18km (western Mediterranean); the thick-lined square delimits the SWAN-4km grid and the thin-line squared box delimits the close-up of the study area.

The atmospheric models (MASS and MM5 at the different resolutions) statistically over-estimated the wind speed observations (see Table 6.3). Large U_{10} over-estimations where observed at the land stations (T-met and U-met) in comparison with the coastal-sea station H –met and the most offshore buoy A-dw(D), where the best U_{10} estimations were achieved. Comparing MM5 at different resolutions, the U_{10} over-estimations were reduced in the nested and highest-resolution simulation. The lowest over-estimation rates were given by the MASS model, which had a coarser temporal resolution. Nonetheless, the *R2* coefficient (which is independent of the scale) indicated that, compared to MASS, the MM5 simulations explained a larger percent of the variability contained in the observations. These results agreed with the visual analysis of the time series (see Figure 6.4) which indicated that MASS estimates were less accurate than MM5 simulations.

Table 6.3 Comparison of the logarithm of the modelled wind speed (U_{10}) and the observations from 7 Dec. to 13 Dec. 2007. Boldfaced values correspond to the slope of the regression equation minus 1 (*slope-1*; positive/negative values indicate an over/under-prediction of the observations). Regular values correspond to the coefficient *R2*.

U_{10}	MASS 18km – 6h		MM5 12km – 6h		MM5 12km – 3h		MM5 4km – 3h		MM5 4km – 1h	
A-dw(D)	**0.19**	0.37	**0.27**	0.55	**0.33**	0.44	**0.27**	-0.19	**0.28**	-0.08
H-met	**0.23**	-0.95	**0.16**	0.21	**0.09**	-0.01	**-0.04**	-0.18	**-0.14**	-0.34
T-met	**1.73**	-3.22	**1.14**	-0.72	**1.05**	-0.79	**1.08**	-0.81	**0.98**	-0.60
U-met	**2.78**	-2.21	**2.20**	-1.13	**2.41**	-1.85	**1.79**	-1.60	**1.40**	-1.17

Table 6.4 Comparison of the logarithm of the simulated and the observed wave heights (H_s) from 7 Dec. to 13 Dec. 2007. Details of each simulation are given in Table 6.1. Boldfaced values correspond to the slope of the regression equation minus 1 (*slope-1;* positive/negative values indicate an over/under-prediction of the observations). Regular values correspond to the coefficient *R2*.

H_s	WAM		SWAN		MM5 12km/6h		MM5 12km/3h		MM5 4km/3h		MM5 4km/1h	
A-dw(D)	**-0.18**	0.5	**-0.15**	0.42	**0.07**	0.70	**0.09**	0.77	**-0.11**	0.73	**-0.13**	0.74
B-iw(S)	**-0.31**	0.41	**-0.23**	0.37	**0.01**	0.56	**-0.03**	0.57	**-0.15**	0.56	**-0.18**	0.56
E-iw(D)	**-0.29**	0.54	**-0.28**	0.52	**-0.08**	0.63	**-0.04**	0.56	**-0.25**	0.57	**-0.23**	0.62

Table 6.5 Comparison of the logarithm of the simulated and the observed peak period (T_p) from 7 Dec. to 13 Dec. 2007. Details of each simulation are given in Table 6.1. Boldfaced values correspond to the *slope* of the regression equation minus 1 (*slope-1*; positive/negative values indicate an over/under-prediction of the observations). Regular values correspond to the coefficient *R2*.

T_p	WAM		SWAN		MM5 12km/6h		MM5 12km/3h		MM5 4km/3h		MM5 4km/1h	
A-dw(D)	**-0.12**	0.28	**-0.22**	0.33	**-0.12**	0.14	**-0.12**	0.36	**-0.21**	0.37	**-0.21**	0.48
B-iw(S)	**0.07**	-0.13	**-0.06**	-0.04	**0.00**	-0.9	**-0.01**	-1.00	**-0.11**	-0.71	**-0.1**	-0.32
E-iw(D)	**-0.07**	0.32	**-0.18**	-0.08	**-0.16**	-0.9	**-0.15**	-0.77	**-0.30**	-0.34	**-0.27**	-0.40

The results from the comparison of MM5 at 12 km spatial resolution and the nested MM5 at 4 km resolution indicated that increasing the spatial resolution reduced the over-estimation of U_{10} from 33% to 27% at the offshore buoy A-dw(D) (see Table 6.3), thus improving the results. Note that Signell et al.

(2005) and Cavaleri and Bertotti (2003) suggested using higher resolution models to obtain higher U_{10} and to compensate the usually under-estimated U_{10} at the scales they were working with (aprox.190 - 30 km). In the present case study, the increase of spatial resolution was done at smaller scales (12 km to 4 km). This increase reproduced the local topography better and it reduced U_{10} over-estimations at sea. The final result was the same as that reported in previous studies: wind speed estimations at sea were improved when increasing the model's resolution. The most accurate wind fields available for the case study corresponded to the highest-resolution MM5 simulation (4 km; 1 h).

6.4. Evaluating the simulated wave parameters

6.4.1. Increasing the grid size

As shown in the previous section, compared to wind observations, higher-resolution wind inputs were not always statistically better than coarser wind fields (Table 6.3) because the higher level of variability in the high-resolution fields biased the results. An alternative method to evaluate the improvement of the wind fields at sea is to use the less-variable wave fields they generate. Historically, this was done for three main reasons. First, it was assumed that wave models were more accurate than meteorological models (Cavaleri and Bertotti 1997). Second, at offshore locations there were traditionally more wave measurements than wind measurements. And third, wave data are the integrated results, in space and time, of the driving wind fields. For these reasons, but mainly because the main target of this work is wave predictions in sharp gradient conditions, this section describes the effects of increasing the spatial resolution of the wind input in estimating the local wave fields.

Previous sub-section showed that ad-hoc MM5 4km/1h wind fields simulated U_{10} better than MASS operational data (Figure 6.4). While estimating the wave conditions during the case study, the simulated H_s were under-estimated at all locations (Table 6.4) even though all simulated wind fields over-estimated the wind observations at the meteorological stations (Table 6.3, Figure 6.4).

Statistically, the best estimated H_s values were obtained when using U_{10} from the MM5 model at 12 km resolution, partially, because these wind fields provided the largest overestimations of U_{10}. Figure 6.6 verifies that the three peak values of H_s were better estimated when using MM5-12km. Instead, increasing the wind spatial resolution from 12 km to 4 km, although improving U_{10} estimations, it also increased the under-estimation of both H_s and T_p. In fact, a 33% over-estimation in U_{10} from MM5-12km resulted in an 8% over-estimation of H_s at A-dw(D). But a 27% over-estimation of U_{10} from MM5-4km resulted in a 10% under-estimation of H_s at the same buoy. T_p under-estimation was also enhanced with higher resolution wind fields, but not as pronounced, suggesting that the simulated T_p was less sensitive to a wind decrease than H_s (see Table 6.5).

Summarizing, the best input wind fields available, MM5 4km, did not produce the best wave estimations because the wave model tended to under-estimate wave parameters and, thus, a decrease of the wind

over-estimation just enhanced the already known under-estimation of the waves. These results suggested that improvements within the wave model were essential to improve wave estimations, especially in regions of sharp gradients. Also, as addressed again in Section 9.1.3, decreasing the grid size of the wave model (1 km) did not significantly improve the estimations of the wave parameters if the grid size of the wind input was not decreased (4 km). Instead, H_s decreased slightly more due to the higher diffusivity of the BSBT scheme for larger discretizations of the computational grid.

Note that, because the residual swell was not removed from the statistical comparison, the statistical percentages here presented were not absolute values and were only valuable to compare one simulation with another; consequently, they could not be directly compared with previous studies.

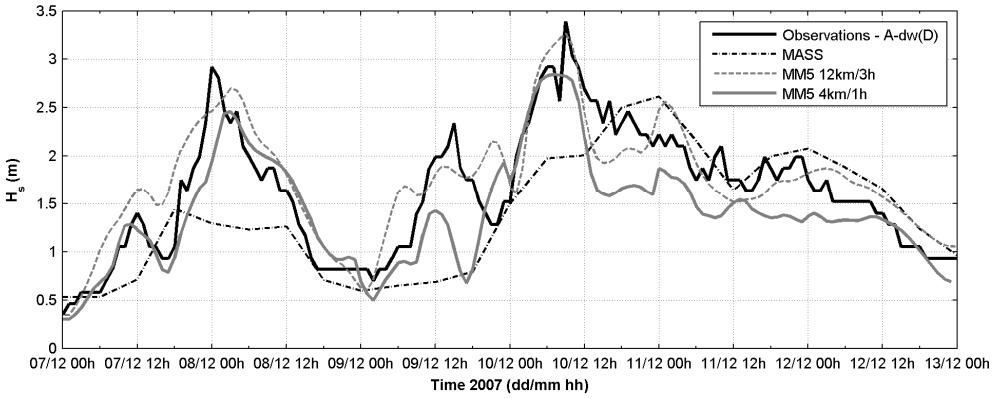

Figure 6.6 Wave height from 7 Dec. to 13 Dec. 2007 estimated using wind inputs from three different sources: MASS-18km, MM5-12km and MM5-4km. SWAN was run at 1 km spatial resolution using the BSBT numerical scheme.

6.4.2. Increasing the wind input frequency

In this section I investigate the improvement of wave estimations (and their variability) due to an increase in the frequency of wind input. The careful analysis of the recorded wind speed time series during the study period indicated that U_{10} could increase by a factor of two in one hour (Figure 6.2 and Section 5.2). Bear in mind that the wind observations available in this study were the mean over 10 min records every hour. Smaller variations of wind speed within the hour describe smaller scale processes (turbulence or gustiness). In this study I increased the temporal resolution of the wind input from the operational 6 h to 1 h, thus focusing on the mesoscale rather than on the small scale of wind gustiness (which can be seen as a much smaller time scale which is out of the scope of this work).

To study the importance of increasing the frequency of wind input to the wave model I compared H_s and T_p from SWAN when forced with MM5 12 km input both every 3 h and every 6h (for which I used the wind fields from +00 h to +18 h, every 6 h). The results in Table 6.4 and Table 6.5 indicated that increasing the frequency of wind input resulted in increased H_s and T_p at all locations. The differences were not important statistically, but they were especially relevant in the visual analysis during the peaks

of the storm, where the maximum values were better estimated, as shown in Figure 6.7. Increasing the input frequency in MM5-12km from 6 h to 3 h permitted to increase the wave height about 0.44 m during the third peak of the storm. The under-estimation of the maximum value (3.4 m) decreased from 17% (6 h) to 4% (3 h). At the intermediate-water buoys, the difference was not so important but it was still relevant (approximately 0.2 m; not shown). T_p was seen to be less influenced by a temporal resolution change than H_s.

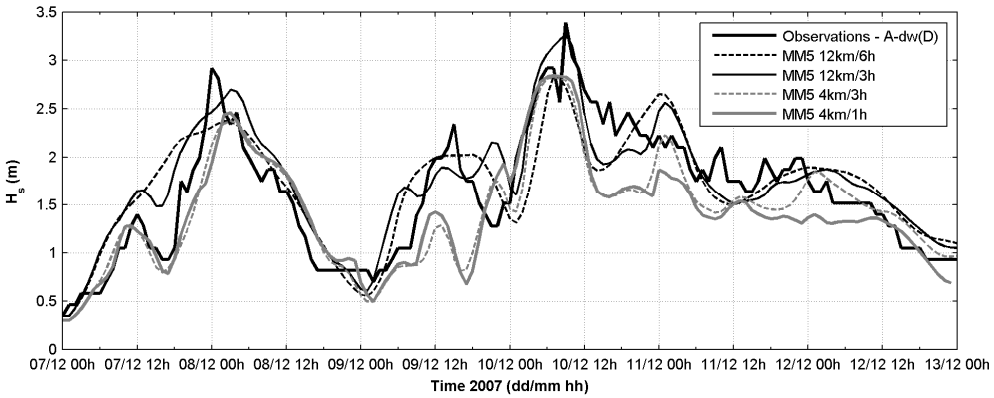

Figure 6.7 Wave height from 7 Dec. to 13 Dec. 2007 estimated using MM5 at different spatial resolutions (12 km, 4 km) and different temporal resolutions (6 h, 3 h, 1 h). SWAN was run at 1 km spatial resolution using the BSBT numerical scheme.

An increase of the input frequency from 3 h to 1 h was analyzed in terms of the high resolution MM5-4km wind fields (Figure 6.7) showing that only minor improvements were achieved. The maximum values of the three main H_s peaks increased slightly, but the improvements were not very important and H_s under-estimation remained large (up to 0.5 m at the peak) and unacceptable for many engineering applications.

An interesting behaviour of the wave model occurred during the last two days of the storm: the wind input every 3 h generated two sudden wave height peaks (11 and 12 Dec.) that disappeared when the wind input every 1 h was used (Figure 6.7). The wave peaks seemed to be a consequence of two wind peaks simulated by MM5-4km (see Figure 6.4). These two peaks were not recorded either in the wind or in the wave measurements; thus, the simulated wind peaks were not real. Even though the model did wrongly simulate the two wind peaks (both in the 3 h and the 1 h inputs) it was interesting to note that the wave model only reproduced the peaks when using the 3 h input.

The different response of the wave model to the wind input every 3 h compared to 1 h indicated that the wave model needed a certain amount of time (3 h) to adjust to the simulated wind fields and to increase accordingly. Instead, when the wind input was every hour, the wave model did not have enough time to respond to the wind signal (peak) and a corresponding wave peak was not simulated. This result indicated that changes in simulated H_s were slower compared to changes in the wind input. In this specific case, a

slow response of the wave model compensated the errors in the wind speed and the unrealistic peaks of MM5 4km/1h were not converted to unrealistic wave height peaks. But then, the validity of the wave model to reproduce sharp variations in wind speed is questioned. Remember that, as shown in the previous chapter, growing waves responded almost immediately (within 1 h) to changes in wind speed. According to the observations, wave models should respond faster to the wind input; i.e. earlier in the time domain. However, if wave models would respond faster to changes in wind speed then wave modellers would be even more dependent on the accuracy of the input wind fields.

Note also that the response of waves in the spatial domain (i.e. short fetches) was also too slow compared to the observations because wave height under-estimations were also reported at the shorter-fetch buoys B-iw(S) and E-iw(D). Note, however, that the results in Table 6.3 also indicated that H_s under-estimations at short fetches were less important for coarser resolution models (even over-estimations were reported) compared to the higher resolution models. Niclasen (2006) already pointed out the need to improve the slow response of wave models in short fetches. He reached this conclusion after comparing wave growth curves from observations and SWAN (using JAN formulation), because observed wave height grew faster than simulated in SWAN. Note that wave growth curves during the present case study were also compared with the simulated rates in next Chapter 7; observed rates also turned out to be slightly faster than those simulated in SWAN.

Meanwhile, the question to be answered is how fast a wave model should respond to a change in wind speed. Or, alternatively, how long should an input wind field remain constant to generate a wave field that can last in time. Right now, if the wind input changes very fast (as it certainly does in the real situations considered) the simulated wave field might not have enough time to respond and grow accordingly. Considering that wind to wave transfer under gusty wind conditions is enhanced (Abdalla and Cavaleri 2002), it seems valuable to explore alternative parameterizations of wind variability in time (e.g. gustiness and mesoscales) to enhance wave growth in the region of study. These results further supported the need to calculate local wave growth and to adjust the models accordingly, as presented in next chapters.

6.4.3. Using wind measurements to estimate wave growth

Traditionally, there have been some doubts on whether in-situ measurements would be a better wind source to estimate local wave conditions. In spite of the drawbacks associated to loosing the spatial variability in a variable region (such as the study area), and the over-estimations observed in the wind models, I decided to explore the advantages of using real wind input data in search of valuable information about the regional wind fields. This approach proved to be very valuable to investigate wind fields within the first 50 km off the coast and to provide additional information on coastal wind jets (next subsection). In this experiment I used wind data from each meteorological station to force the whole

domain in four separate runs, with a single value constant in space and an input wind frequency of 1 h (frequency of the observations).

At the very beginning, I expected to over-estimate H_s when using the winds from the offshore buoy A-dw(D) and to under-estimate H_s when using data from the other three meteorological stations because U_{10} was expected to increase from the coast towards offshore (Flamant et al. 2003). In other words, according to Flamant et al. (2003), wind speed at A-dw(D) was expected to be higher than wind speeds along the fetch. However, it became soon clear that wind speed at A-dw(D) was not the highest wind speed along the fetch because H_s was under-estimated in each case; see for example H_s time-series during the second peak of the storm which are depicted in Figure 6.8.

In fact, the reported H_s under-estimations were much larger than when using the wind fields from any of the considered wind models (an exception occurred on the 9 Dec. during a coastal wind jet event, as discussed in next subsection). The largest H_s under-estimations (80-90%) were obtained when using coastal-land stations (T-met and U-met) as input wind data. Using U_{10} from coastal-sea stations (A-dw(D) and H-met) resulted in H_s underestimations of about 40%.

The fact that H_s was also under-estimated when using winds from the most offshore station (buoy A-dw(D)) indicated that the wind speed at this buoy was probably not the highest wind speed along the fetch, as it was indeed suggested by the wind model (Figure 6.5). Note, that Flamant et al. (2003) measured surface wind speed along a transect perpendicular to the coast in the Gulf of Lion (north of the study region), and they observed that wind speed increases steadily up to approximately 50 km from the coast associated to the land/sea roughness transition. Further offshore they observed another 50 km of perturbed and variable flow that was followed by a sharp wind speed decrease and a sudden increase at larger distances from the coast.

Back to the results, I believe that at buoy A-dw(D) the measured wind speed values were not the highest values along the fetch, as expected within the land/sea transition zone. In fact, buoy A-dw(D) was probably outside the land/sea transition zone due to the local orography, and the linear increase of wind speed from the coast up to this buoy could not be considered to be valid anymore. The simulated wind fields (e.g. in Figure 6.5 bottom panel) proved this hypothesis to be valid. The above results also proved that wind speed at buoy A-dw(D), although at open sea, should not be used to simulate wave conditions in the whole area. Without doubt, H_s and T_p were much better estimated when using modelled winds because of the spatial variability they provided, with wind speed maxima somewhere along the fetch and not at the furthest offshore observation point (Figure 6.5).

The presented results highlighted again the importance of resolving the spatial variability of the input wind fields, which at the present time could only be partially verified by in-situ measurements. They also

supported the use of modelled wind fields as the most reliable wind source available to estimate mesoscale wave conditions.

6.5. Performance in situations associated to sharp gradients

6.5.1. Coastal wind jets

The simple exercise in the previous subsection (using wind observations constant in space to force the wave model) showed an interesting behaviour at the second H_s peak (9 Dec. 2007) when compared with the results from MM5-4km simulations. The second H_s peak was recorded at all buoys but the maximum wave height attained was different (up to 0.5 m difference). In the previous chapter I studied such difference to conclude that it was due to the effect of a localized coastal wind jet. In this chapter, I observed that the wave model estimations during the same period were only accurate when H-met winds were used as input in SWAN. Note that H-met was located on a breakwater at the beginning of the fetch length and just in front of a river valley (which favours wind jets). When MM5 winds were used to force the wave model, the second H_s peak was only properly modelled at B-iw(S), the buoy closest to H-met and to the coast, but not at the other instruments (see Figure 6.8).

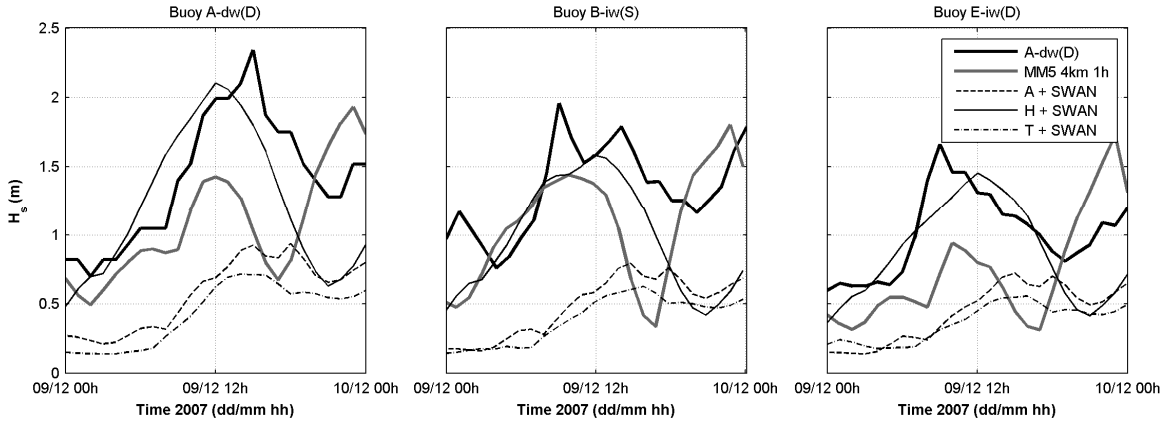

Figure 6.8 Detail of wave height's second peak during a coastal wind jet event (9 - 10 Dec. 2007) at positions A-dw(D) (left), B-iw(S) (middle) and E-iw(D) (right). The observations are compared with wave model simulations ran using different wind inputs: MM5-4km or wind measurements at the meteorological stations.

These results confirmed that there was an important wind jet blowing from the coast that was registered at H-met and that was simulated (but not completely) by MM5. I presumed that the wind jet was estimated by the MM5 model, although a little bit further offshore than the H-met position for two main reasons. First, the comparison of U_{10} time series indicated that the wind peak at H-met position was indeed estimated (although slightly under-estimated). Second, the H_s peak at B-iw(S) was accurately simulated when using winds from MM5.

Two considerations must be taken into account. First, the fact that such an H_s peak was under-estimated using MM5 winds at the further offshore buoy A-dw(D) (and not at B-iw(S)) suggested that the spatial

extension of the simulated wind jet was either not long or not strong enough to generate higher waves at the offshore buoy A-dw(D) (as observed). Second, the fact that the H_s peak at A-dw(D) was only properly estimated when using winds from H-met indicated that the real wind jet should have had either much higher instantaneous wind speeds than simulated, or there should have been high similar-magnitude wind speeds all along the fetch that decreased just before the ocation of the buoy A-dw(D). However, these two options were rather improbable, as discussed below.

The first possibility (higher wind speeds) was not likely because ECMWF-blended data showed similar, or even lower, wind speed values along the fetch. Note, however, that the coarse spatial resolution (0.25º) of remote sensing data, although providing valuable spatial information of the wind speed magnitude (limited by its close distance to the coast), smoothed down local peaks and wind jets. Also, the fact that remote sensing data is blended with ECMWF model limits the representativity of the spatial structure of the real wind field. In any case, higher point-wise and space-limited wind speeds would only be possible, from a physical point of view, if the physical settings in the atmospheric models were adjusted (e.g. lower sea surface roughness permitting higher wind speeds).

The second possibility (i.e. high winds all along the fetch and then a sharp decrease) was also improbable, because such sharp gradients are not physically realistic unless there is a specific reason, not found for a wind jet blowing over the open sea without physical barriers. Orography, sea roughness and mesoscale weather patterns are the processes known to affect wind at sea but they are not able to produce such a sharp decrease of wind speed.

There was a third possible explanation for the lack of persistence of the wind jet on simulated waves at A-dw(D) (compared to the observations). This third reason was a limitation of the wave model in incorporating locally high wind speeds (due to the numerical wave model "inertia"). In the previous section, a similar model limitation was discussed in terms of a slow wave model response in time, instead of in space. In any case it should be acknowledged that, during the case study, wave model limitations were, again, as probable as the inaccuracies of the simulated wind fields.

These results, even considering the partially-unknown accuracy of the spatial structure of the estimated wind fields, indicated that the remaining and consistent under-estimations of H_s and T_p could not be reduced by just using higher resolution wind fields. The wind imprint on the modelled waves appeared to last less than in Nature and a possible reason could be an under-estimation of the transfer of energy from the wind towards the waves (net wind input).

6.5.2. Slanting fetch and wave diffraction

Wave growth in variable wind conditions is also affected by the directional variability of the wind. For example, deviations of the wind direction from the orientation perpendicular to the coast are seen to produce the so-called 'slanting fetch' effect. This concept was introduced in the previous chapter, where I

mentioned the accurate simulation of the directional change associated to slanting fetch obtained by Ardhuin et al. (2007).

More specifically, Ardhuin et al. (2007) performed a model hindcast of a specific fetch-limited event in slanting fetch conditions and concluded that the model includes the presence of waves from the along-shore direction due to the slanting fetch effect. In slanting fetch situations and sharp wind gradients, these authors reported wave energy over-estimations (KOM source term). According to their work, a 10º deviation of the wind direction from the shore normal is as important as a 10% change in wind speed. Other authors such as Bottema and van Vledder (2008) and Gagnaire-Renou et al. (2008) also reported over-estimations of the spectral models in slanting fetch situations. Notice that according to their work, slanting fetch effects would not be responsible for the under-predictions observed in the present case study.

In the present case study I suspected that slanting fetch effects existed because of the wave direction differences between buoys A-dw(D) and E-dw(D) as described in previous chapter. The recorded difference in peak wave direction (26º) was differently estimated by the different-resolution wave models; i.e. coarser resolution models (18 km) estimated a 14º difference, whereas finer resolution simulations estimated differences larger than 30º.

The wave directions resulting from the different simulations suggested that the directional differences between buoys were well approximated if the waves had 'enough time' (or grid nodes) to turn and to adjust to the coastal geometry (slanting fetch and refraction). All in all, in this work, further studies involving slanting fetch could not be addressed in depth because no directional data was available at the more coastal buoys (where the effect of slanting fetch was expected to be stronger).

Refraction processes, in turn, are generally well described over narrow continental shelves in the absence of currents, except if sharp changes of water depth on the scale of a wavelength occur, as reviewed by The WISE Group (2007). Note that this limitation was easily overcome with the increase of the model's spatial resolution.

An additional and equally important effect, given the jet-like nature of the wind fields, was due to the wind imprint on the wave pattern, since there should be an important gradient in wave energy across the wind jet (i.e. roughly parallel to the coast). The correct reproduction of this feature requires dealing with a diffraction process for which spectral wave models are not particularly well suited, as mentioned in the previous chapter. The resulting veering in wave propagation direction (away from the strongest-winds along the wind jet), and the wave height difference between the jet-region and off-side the wind jet is a complex process. This process did not seem to be well reproduced by the present numerical model, but there was no proper data available for comparison within this work. In any case, it is a physical process that should be occurring in the area and, thus, affecting the simulated waves.

6.6. Summary of the obtained results

Wave growth under variable wind conditions is a complex problem from the wave modelling point of view. In this chapter, work was done towards improving the modelling capabilities under such conditions, and it was shown that the accuracy of wave models was different from the accuracy of atmospheric models. Compared to coarse discretizations (e.g. 18 km, 6 h) improving the initial conditions and increasing the resolution (in time and space) of the input wind fields improved the estimations of both wind and waves.

However, for already high resolution runs (e.g. 4 km, 3 h), further refinements of the wind fields only improved wave predictions if the wind had 'enough' time to act on the waves (simulated waves did not respond fast enough to winds that changed every hour). In the future, there must be a balance between the wind field reproducing the meteorological storm and the capability of the wind to 'generate' waves (otherwise, even though the winds get 'better', waves would only get worse because of the slow model response, compared to the observations).

The best U_{10} estimations were obtained from the highest resolution atmospheric model (MM5 4km/1h) nested in reanalysis wind fields from ECMWF. However, to properly reproduce the maximum values of the considered wave event, it was needed to considerably over-estimate U_{10} (approximately 30% as provided, for example, by MM5 12km).

In spite of the limitations in the accuracy of wave models, a frequency increase of the wind input (from 6 h to 3 h) improved the estimation of the maximum values (peaks) of the wave storm. In this sense, a time frequency resolution increase was more effective than a spatial resolution increase (from 12 km to 4 km). Nonetheless, increasing the input frequency (to 1 h using in-situ observations) without increasing the spatial resolution was either way inefficient.

The under-estimation of H_s (and T_p) for over-estimated U_{10} was attributed to two factors: the first one was that even though modelled wind data at the measuring stations was quite accurate (or even over-estimated), it did not provide locally high enough wind speeds (coastal wind jets) or sharp gradients along the fetch. Although a certain degree of uncertainty still lay within the wind fields, the probability of higher gradients or higher wind speeds along the fetch was very low. The second factor considered was an inefficient parameterization of the source terms in wave models (net wind input), as pointed out by many authors in different wind conditions (e.g. Rogers et al. 2003). Note also that a slow transfer of energy from wind to waves was to be expected associated with slow wave model responses.

Also, because an increase in U_{10} was not always directly related with an increase in H_s or T_p at all the locations, wave growth at early stages was expected to be more important than what the actual formulations could model, as reported by other authors. In this sense, a lot of work is being currently done t improve the source terms in the wave models (e.g. Ardhuin et al. 2010, Banner and Morison 2010,

Donelan et al. 2006, Tsagareli et al. 2010), which will hopefully also improve wave modelling in variable wind conditions.

T_p appeared to be less sensitive to changes in U_{10} than H_s and, thus, this parameter could be less suitable to analyse wave modelling improvements during fetch-limited conditions. But for this same reason, it could seem logical to focus the efforts on improving the capability of the wave models to properly estimate T_p and to use it afterwards to validate and verify wave models under a broader range of meteorological conditions.

The fact that T_p was more under-predicted than H_s, suggested that for restricted domains it could be important to increase both the energy transfer from the wind to the waves and the transfer of energy from high to low frequencies. The mechanism directly responsible for the energy transfer in the spectrum is the non-linear transfer term, which is comparatively well adjusted, but directly dependent on the input-dissipation balance. Therefore, here I point again to the balance between wind input and dissipation of energy as the most important factor responsible for the observed under-estimations at short fetches during fetch-limited conditions and sharp wind gradients.

7. Calculating the rate of wave growth in the Catalan Coast

Observational evidences suggest that wave growth is enhanced in situations that deviate from the mostly homogenous wind conditions for which the default settings of wave models are tuned (Babanin and Makin 2008). Because it was possible that in variable wind conditions the wave growth rate also differed from the reference values used to tune wave models even in 'limited' situations, in this chapter I calculated the well-known non-dimensional wave growth curves (commonly used to tune wave models) using local observations. The objective was to adjust the growth rate of the numerical simulations to the observations, as presented in next chapter.

The wave data used in this chapter mainly corresponded to the specific offshore wind event addressed in the previous section (storm nº 3). This event was recorded at the three different instruments at different positions along the fetch. The analysis was supported using data from the whole RIMA-Med campaign and using, additionally, a 5-year long data set recorded at the most offshore buoy A-dw(D). The resulting wave growth rates derived from the observations were compared with those reported by other authors and with those obtained with simulated wind and wave data. The results from the comparison indicated that wave growth in this region was slightly faster than considered by other authors and faster than simulated by the wave model, although the differences were not statistically significant.

This chapter is structured as follows: section 7.1 summarizes the methodology and the results from previous field experiments in the state of the art. Section 7.2 briefly presents the wind and wave data set used in this experiment (observations and simulations). Section 7.3 describes the calculated energy and frequency development rates and discusses the accuracy of the data selected (energy and frequency, fetch and wind speed). Section 7.4 presents the development rates obtained for different external forcings (wind speed tendency, stability of the atmosphere and slanting fetch conditions) and internal wave properties (presence of swell, wave age and wave steepness). Last section provides a brief summary of the results presented in this chapter.

7.1. Non-dimensional growth curves

The non-dimensional growth curves as a method to study wave growth along the fetch were first suggested by Kitaigorodskii (1962) (see, e.g. KC92). The corresponding scaling laws are commonly used nowadays and represent non-dimensional energy and frequency (dependent variables) along non-dimensional fetch (independent variable). The typical scaling laws, however, are not the only ones. For

example, DO85 used inverse wave age instead of non-dimensional fetch. Also Badulin et al. (2007), Hanson and Phillips (1999), among others, used alternative non-dimensional variables to calculate wave growth such as the wave dissipation rate or the total wave input, respectively. Other methods are additionally discussed in Section 9.3.2.

Nonetheless, within the spectral wave modelling community, the non-dimensional wave growth functions of Kitaigorodskii (1962), and more specifically the parameterizations provided by KC92, are a reference method to calculate wave growth. For this reason, in this work I used the so-called non dimensional wave growth curves to study wave growth in the region of study and to adjust the growth rate in the numerical simulations in order to improve wave estimations (in next chapter).

7.1.1. Theoretical basis

The method used in this chapter to approximate wave growth in the region of study is taken from KC92, which is based on the first theoretical similarity suggested by Kitaigorodskii (1962) and is used to describe the non-dimensional evolution of wave parameters along the fetch. The resulting scaling laws therein described use gravity and the wind speed to non-dimensionalize main wave parameters (wave energy and peak frequency) and the fetch. Non-dimensional wave energy ($\overline{\mathrm{E}}$), peak frequency ($\overline{f}$), and fetch ($\overline{\mathrm{X}}$) are calculated as follows:

$$\overline{E} = \frac{g^2 \cdot E}{U^4} \qquad \overline{f} = \frac{U \cdot f_p}{g} \qquad \overline{X} = \frac{g \cdot X}{U^2} \qquad \textbf{[7.1]}$$

The energy of the waves (E) corresponds to the integral of the sea component in the frequency spectrum (also known as m_0). f_p is the peak frequency, g is the gravity and U is the wind speed.

The non-dimensional energy ($\overline{E}$) and the frequency ($\overline{f}$) can be considered as a function of non-dimensional fetch $\overline{\mathrm{X}}$ and are usually plotted on logarithmic axes. Then, the regression line that fits the data can be written as follows:

$$\log\left(\overline{E}\right) = a_{0,1} + b \cdot \log\left(\overline{X}\right) \qquad \log\left(\overline{f}\right) = a_{0,2} + c \cdot \log\left(\overline{X}\right) \qquad \textbf{[7.2]}$$

The slopes of the regression lines (b, c) correspond to the development rate of the dimensionless energy (and the frequency) along the dimensionless fetch. The frequency development rate can also be called frequency downshift rate. On linear axes the development rates can be written as:

$$\overline{E} = a_1 \cdot \overline{X}^b \qquad \textbf{[7.3]}$$

$$\overline{f} = a_2 \cdot \overline{X}^{c} \qquad \textbf{[7.4]}$$

The y-intercept of the non-log expressions [7.3] and [7.4] is $a_n = \exp\left(a_{0,n}\right)$.The development rates (*b* and *c*) describe the rate of growth of the energy, and the frequency, along the fetch. Although many authors (e.g. KC92) refer to it as the growth rate, I was hesitant to use this term under the studied conditions because of the lack of direct physical interpretation of the method, as discussed further on in Section 9.3. The widespread use of the term justified employing it, but not without the corresponding caution.

7.1.2. Field experiments: state of the art

As mentioned by Holthuijsen (2007), the first experiments in fetch-limited situations were performed in the 50's by Bretschneider (1952), Sverdrup and Munk (1946, 1947). Since then, many other authors measured wave growth in similar conditions (see, for example, in Badulin et al. 2007 for a review of such experiments). Nowadays, the most widely used contribution on this subject is due to KC92, who grouped some of the most relevant experiments up to that time, including Hasselmann et al. (1973) (JONSWAP; hereafter JON73) and DO85.

To that date, the development rates obtained from each experiment differed significantly. KC92 re-analyzed five data sets from different fetch-limited experiments and suggested common relationships between the non-dimensional variables that depended on the stability of the atmosphere, thus reducing the scatter observed. The development rates calculated in KC92 are close to, but lower than, **1** (see Table 7.1).

Table 7.1 Non-dimensional energy growth functions calculated in earlier field experiments (* as reviewed in KC92).

Authors	Development rate (*b*)	Origin (a_1)	Characteristics
Hasselmann et al. (1973) – JON73 *	1	1.6·10-7	
Kahma (1981) – K81 *	1	3.5·10-7	
Kahma and Calkoen (1992) – KC92 *	0.77	9.3·10-7	Stable atmosphere
	0.94	5.4·10-7	Unstable atmosphere
Donelan et al. (1985) – DO85 *	1	2.8·10-7	Stable atmosphere
	1	3.8·10-7	Unstable atmosphere
Hwang and Wang (2004)	0.81	6.2·10-7	1st order function
	$1.8 - 2 \cdot 0.06 \cdot \ln \overline{X}$	$e^{-17.6} \cdot \overline{X}^{0.06 \cdot \ln \overline{X}}$	2nd order function

After KC92, further field experiments reported significantly different development rates and their authors pointed to alternative sources of scatter such as the variability and gustiness of wind speed, surface currents, etc. (see e.g. Abdalla and Cavaleri 2002; Haus 2007). A more recent (and critical) review of

fetch-limited field experiments, and the growth curves calculated therein, is given in Badulin et al. (2007). They support the reticence of Donelan et al. (1992) towards accepting the non-dimensional curves as an accurate method to describe wave growth, as discussed again in Section 9.3. Refer to Table 7.1 and Table 7.2 for a summary of some of the development rates calculated in previous field experiments.

Table 7.2 Non-dimensional frequency downshift functions calculated in earlier field experiments (* as reviewed in Badulin et al. 2007).

Authors	Abbreviation	Downshift rate (-10**c*)	Origin (a_2)	Characteristics
Hasselmann et al. (1973)	JON73	3.3	3.5	
Kahma (1981)	K81	3.3	3.2	
Kahma and Calkoen (1992)	KC92st	2.4	1.9	Stable atmosphere
	KC92un	2.8	2.3	Unstable atmosphere
Donelan et al. (1985)*	DO85	2.3	1.9	Stable atmosphere

7.2. Synopsis of the experimental data used

In this chapter, observational data recorded in the region of study (the coastal area of Tarragona) was used to calculate the local non-dimensional wave growth functions. Additionally, simulated data from previous chapter was provided for comparison. This section is specifically dedicated to contextualize the data sets already introduced in previous chapters and to provide additional information relevant to the present analysis; the main reason is furnishing the reader with a complete overview of the particular data to favour the understanding of the chapter.

7.2.1. Observational data

Observations were taken from the RIMA-Med field campaign and from the 5-year long data record at buoy A-dw(D). To describe wave growth in all possible conditions, the three following data sets were used: a) the RIMA-Med dataset, which contains the smaller subset: b) the 'Fetch-limited dataset'; and c) the 5-year long dataset. The data records were considered as independent groups of data and individual growth curves were calculated for each dataset exclusively, as explained below.

First, however, remember that the RIMA-Med field campaign recorded wave data at different positions along a transect perpendicular to the coastline during approximately two months. The wave-measuring instruments and meteorological stations available during RIMA-Med are depicted in Figure 3.1. The field campaign is described in Chapter 3 of the present work. The RIMA-Med dataset was only used to calculate the growth rates in situations of crossed seas (wind sea and swell).

Instead, the main focus of this chapter was the 'Fetch-limited data set' recorded during the storm event that started on the 7 Dec. 2007 and ended on the 13 Dec. 2007 (referred to as storm nº3 in Chapter 2 and thoroughly simulated in Chapter 6). Remember here that the storm nº3 was characteristic of pure wave

growth conditions in the region of interest, with strong offshore winds (from the northwest) that generated wave heights up to 3.5 m at the offshore buoy A-dw(D) (see Figure 7.1).

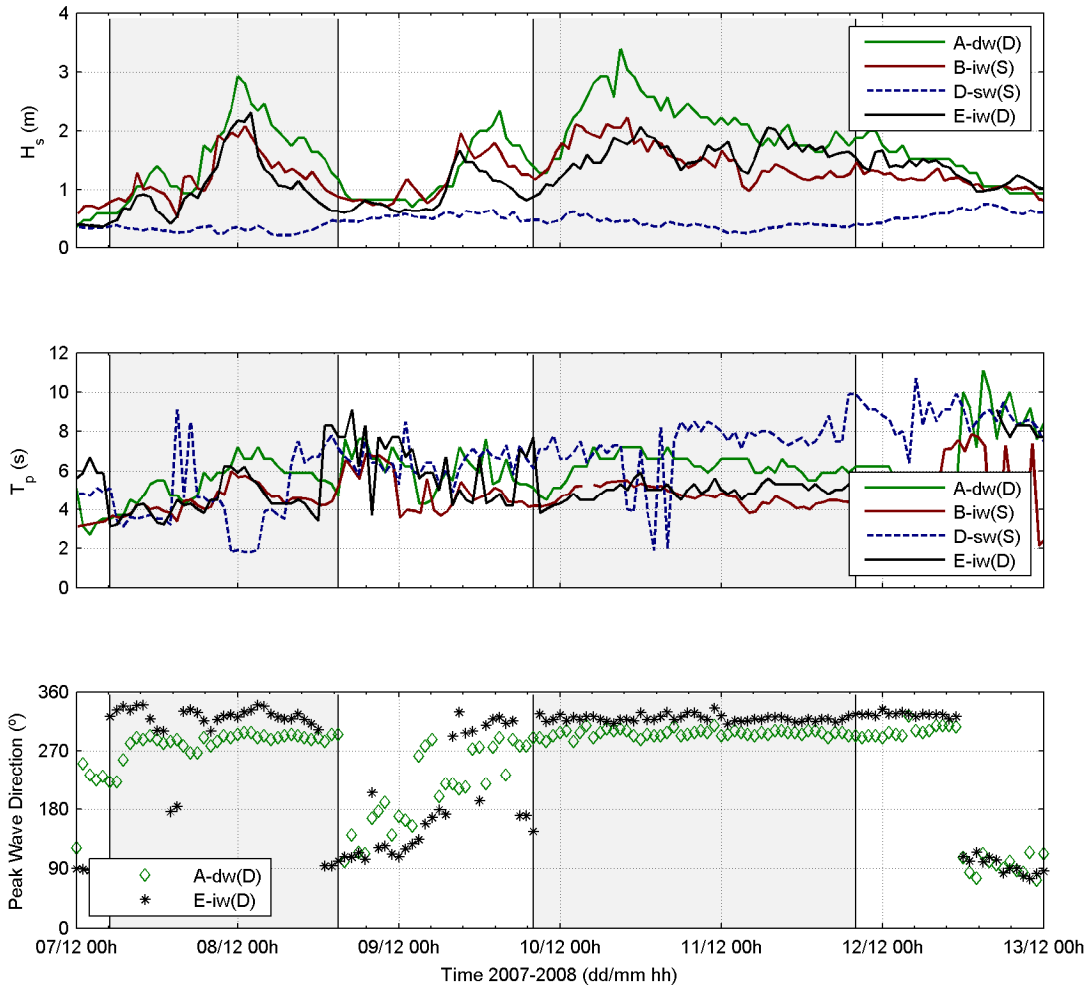

Figure 7.1 Significant wave height (upper panel), peak period (middle panel), and peak wave direction (lower panel) from 7 Dec. to 13 Dec. 2007 at the different wave instruments. The grey background indicates the period considered within the data subset (7 Dec. 5 h – 8 Dec. 15 h and 9 Dec. 20 h – 11 Dec. 20 h).

The so-called 'Fetch-limited data set' did not comprise the whole storm nº3 because those records containing the residual swell on the 8 Dec. were excluded. Such interfering swell was identified through a detailed visual analysis of the directional spectra from buoys A-dw(D) and E-iw(D). Consequently, only wind sea data from North-western directions was considered in the 'Fetch-limited data set', which was limited to the periods 7 Dec. 5 h – 8 Dec. 15 h and 9 Dec. 20 h – 11 Dec. 20 h (depicted by the darker regions in Figure 7.1). This dataset was especially valuable because wind and wave conditions were relatively close to the ideal conditions encountered in the reference experiments; i.e. buoy measurements at different distances from the coast, wind direction perpendicular to the coast and no significant swell.

To calculate the wave growth curves in a wider range of atmospheric and oceanographic conditions I additionally used the 5-years long data set recorded at buoy A-dw(D), which contained both meteorological and oceanographic data at 1 h intervals. The data set was described in more detail in Chapter 3. The main short-coming of this data set was the availability of measurements at only one buoy and, thus, at only one point along the fetch. However, the main advantage was that the large amount of data reduced the scatter of the calculated curves and it provided statistical significance to the analysis (see below).

I mentioned above that the growth curves were independently calculated for the different data sets. The reason is that shorter data-sets contained wave information at different positions along the fetch, whereas the longest data set only contained information at a single point. Due to this limitation I differentiated two different ways of calculating the growth curves; these were named 'multi-fetch' and 'single-fetch' datasets. Multi-fetch datasets contained wave data at different distances from the coast (fetch) and single-fetch datasets contained wave data at only one position (or buoy).

Multi-fetch datasets were only possible during RIMA-Med. The single-fetch datasets could be calculated during RIMA-Med, when taking wave data from individual buoys only, or during the 5-year long data set. Theoretically, the single-fetch datasets could not be used to calculate the growth curves using the methodology presented by Kitaigorodskii (1962). For this reason, DO85 used the inverse wave age as independent variable instead of non-dimensional fetch. However, KC92 recalculated the single-fetch data in DO85 in terms of the classical growth curves and obtained comparable growth rates. Based on KC92's work it can be concluded that similar growth rates could be calculated using either 'single-fetch' or 'multi-fetch' datasets.

However, fuelled by the strong reticence of Badulin et al. (2007) in using 'single-fetch' data sets to calculate wave growth rates, in this chapter I took the 'single-fetch' growth curves at each buoy during the 'fetch-limited' data set and I compared them with the growth curves for the whole data set (multi-fetch). The aim was to assess the suitability of using single-fetch versus multi-fetch data sets. It is shown below that the growth rates obtained using only one position along the fetch (single-fetch) were indeed higher than those obtained from datasets containing measurements at different positions along the fetch (multi-fetch). All in all, the comparison of the datasets indicated that the 5-year dataset (single-fetch) was still useful to compare wave growth in different conditions (e.g. stability of the atmosphere, swell, etc.).

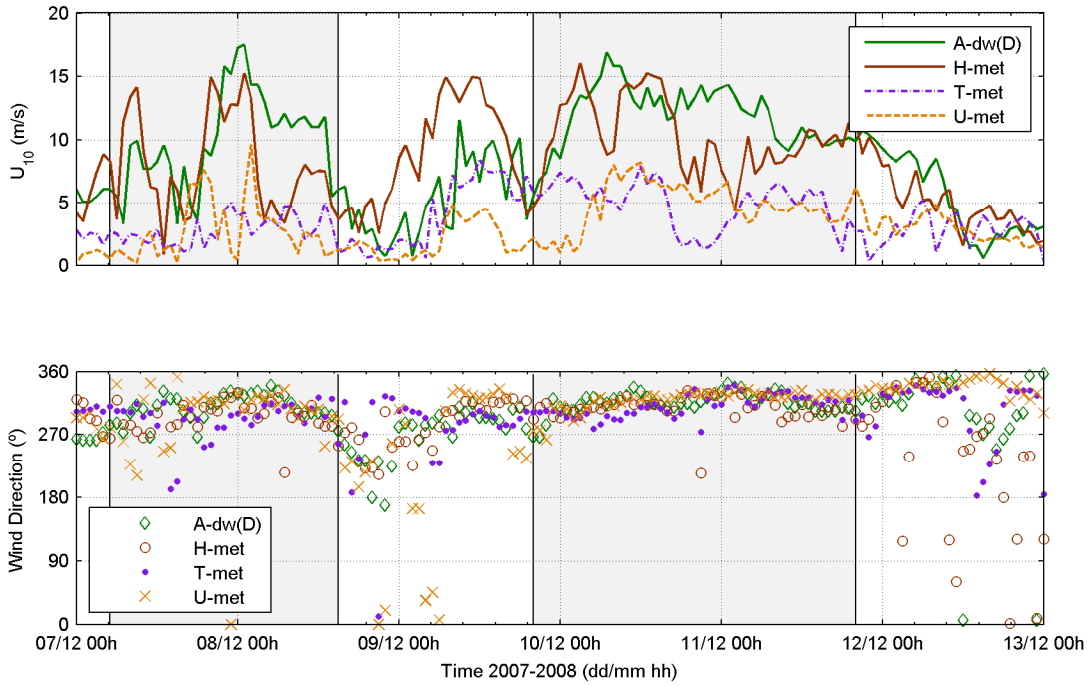

Figure 7.2 Wind speed (upper panel) and wind direction (lower panel) from 7 Dec. to 13 Dec. 2007 at the four meteorological stations in the area of study. Grey background indicates the period considered within the subset of data (7 Dec. 5 h – 8 Dec. 15 h and 9 Dec. 20 h – 11 Dec. 20 h).

7.2.2. Numerical simulations

The results from the numerical simulation of storm nº3 called 'MM5 4km/1h' (in agreement with the nomenclature in previous chapter; see Table 6.1) were used in this chapter to calculate the wave development rate in the wave model and to compare it with the observations. Mark that the development rates from the simulations presented in this work are not necessarily representative of the development rate of the SWAN model in all kind of growth conditions, but they are only representative of the specific numerical simulation considered.

According to previous chapter, the simulated wind speeds were closely (or slightly over-) predicted, whereas wave height and wave period were under-predicted. The growth curves derived from the simulated wind and wave data are plotted in Figure 7.3 (right side) and are summarized in Table 7.3 and Table 7.4. In these tables, each column presents the development rate (and the 95% confidence limits) calculated using in-situ wind and wave data for each individual buoy (single-fetch curves) and for all buoys (multi-fetch curves). The Y-origin of each curve is given in Appendix A. Buoy D-sw(S) was not included in the calculations because its position was too close to the land-sea boundary (one grid point) and the accuracy of the wave model at this location was uncertain.

The development rate in the tables is followed by the ± 95% confidence interval, which indicated that there was a 95% of probability that the fit took any of the values within that range. The confidence

interval is also a measure of the scatter of the data points; in other words, large intervals occur when the scatter is large. From now on, any reference to significant differences refers to the 0.95 significance level, unless specified otherwise.

The development rate calculated using simulated data at all buoy locations (last column of first row in Table 7.3; *s1*) was very similar (0.8) to the reference rate derived by KC92 in stable atmospheric conditions (0.77; see Table 7.1). The differences between the downshift rates were not striking either (compare Table 7.2 and Table 7.4).

The fact that the simulated wave heights (and peak periods) were smaller than the observed ones (as reported in the previous chapter), while the simulated development rates were not significantly different from the rates reported in earlier experiments (Table 7.1), suggested that the development rates in the region of study were faster than presently considered in the wave model and in the state of the art. These results provided further justification for the increasing need to calculate the development rates in the region of study and to adjust the growth rate of the wave model to the observed ones.

As shown in Table 7.3 and Table 7.4, the development rates calculated using simulated single-fetch data differed considerably from each other (0.74 to 1.1 – energy curves), even though the differences were not significant. These results provided the first evidence that calculating the growth curves using a 'single-fetch' data set rather than 'multi-fetch' data sets might not produce the same development rates. This is discussed again in Section 9.3.1.2.

Simulations *s2* and *s3* (see Table 7.3 and Table 7.4) were used in section 7.3.2.2 to analyze the importance of using in-situ versus offshore wind measurements to non-dimensionalize the variables. This comparison was especially important given the high spatial variability of the winds in the region, as shown in previous chapters; for example, Figure 6.4 depicts the numerical simulation of a typical coastal wind jet in the area. Do not forget that theory imposes that the wind speed used to non-dimensionalize the variables should be representative of the wind speed generating the waves. The presented results indicate that using simulated wind data from the position of the offshore buoy A-dw(D), rather than in-situ wind speed, to non-dimensionalize the variables, did not make a big difference (1% for multi-fetch data).

Table 7.3 Energy development rate (*b*), and 95% confidence interval, of the non-dimensional growth functions calculated using simulated wave energy (SWAN model – MM5 4km/3h). Single-fetch data sets were calculated at the position of buoys A-dw(D), B-iw(S) and E-iw(D) and multi-fetch data set contained data from all three buoys. The non-dimensional variables were scaled using either simulated wind in-situ (MM5 model), at the position of buoy A-dw(D) or at a position close to H-met meteorological station.

Nº	Location of scaling wind	A-dw(D) B	B-iw(S) B	E-iw(D) b	All buoys b
s1	MM5 in-situ	0.91±0.32	1.1±0.28	0.74±0.21	0.8±0.1
s2	MM5 at buoy A	0.91±0.32	0.65±0.26	0.75±0.42	0.79±0.11
s3	MM5 at H-met	1.8±0.22	1.7±0.23	1.98±0.32	1.46±0.15

Table 7.4 Same as Table 7.3 – it displays the frequency downshifting rate (*c*10*).

Nº	Location of scaling wind	A-dw(D)	B-iw(S)	E-iw(D)	All buoys
s1	MM5 in-situ	-3.23±1.04	-3.78±0.74	-2.69±0.56	-2.65±0.25
s2	MM5 at buoy A	-3.23±1.04	-2.59±0.84	-2.97±1.3	-2.6±0.3
s3	MM5 at H-met	-5.29±0.64	-4.86±0.64	-5.34±0.82	-4.16±0.4

7.3. Selecting the dimensional variables

There are two basic assumptions associated with the non-dimensional curves of wave growth (see e.g. KC92). The first one is that wind conditions are "ideal", which means that wind speed is constant in magnitude and direction, homogeneous in space and unlimited in time. The second one is that the dimensional wave parameters (energy or wave height and peak frequency) are generated along the given fetch by the chosen wind speed (which is assumed to be homogeneous and representative of the whole generation area).

In this work, I calculated the growth curves using the 'Fetch-limited dataset' because it represented the closest I could get to ideal conditions in the region of study. This data set was also useful because it contained pure wind sea data at different locations along the fetch and the wind direction (multi-fetch). The estimated curves are plotted in Figure 7.3 (left panel). The estimated development rates were slightly faster but comparable to the reference functions reported by other authors (Table 7.1) and to the curves calculated from simulated data (Table 7.3, Table 7.4 and Figure 7.3 -right side-). The development rates obtained (slope of the fit) are summarized in the first row of Table 7.6 (observations; energy) and Table 7.7 (frequency). The complete functions (including the y-intercept given in Appendix B) take the form:

$$\overline{E} = 6.42 \cdot 10^{-7} \cdot \overline{X}^{0.94} \quad \textbf{[7.5]}$$

$$\overline{f_p} = 2 \cdot \overline{X}^{-0.281} \quad \textbf{[7.6]}$$

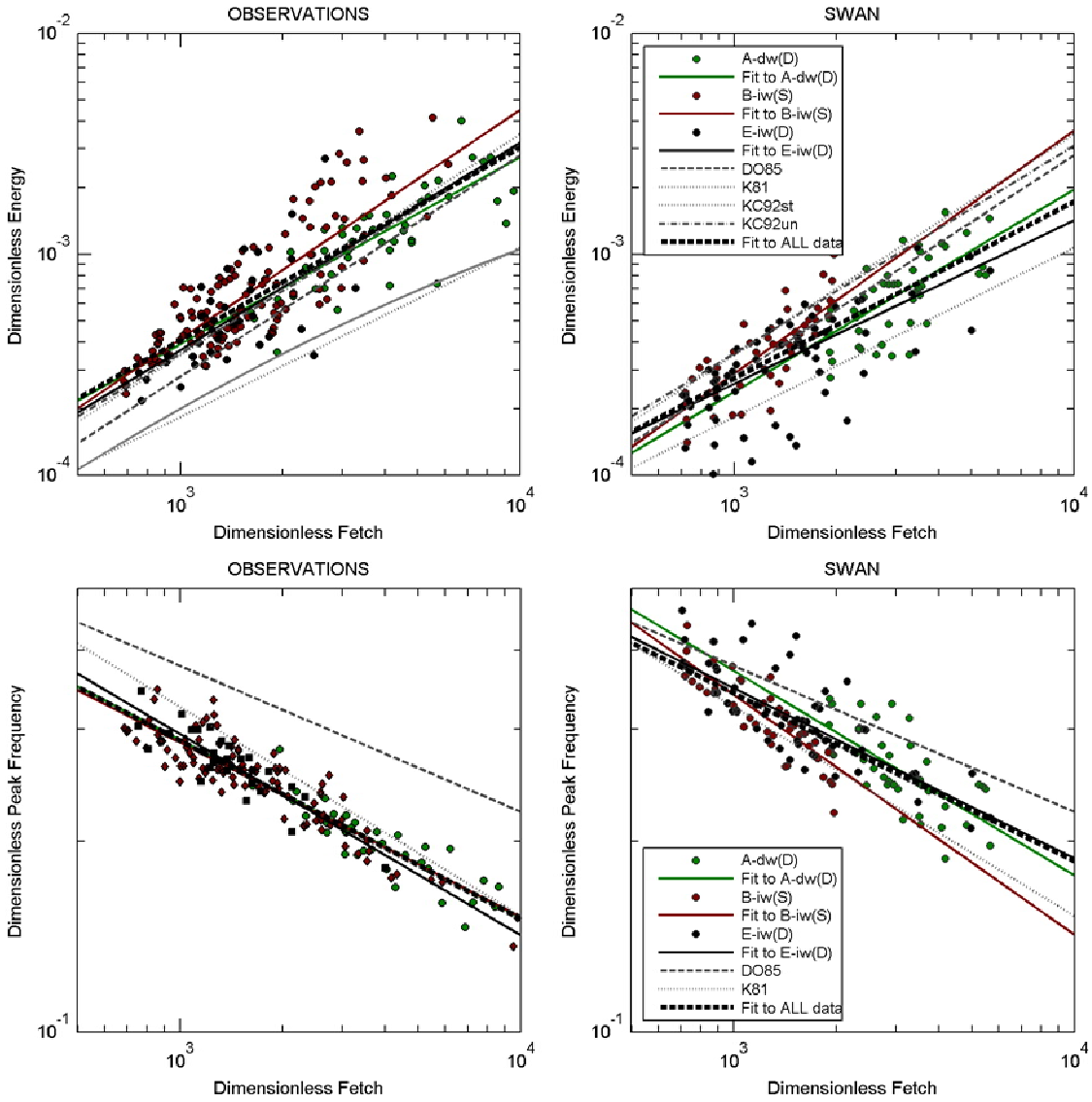

Figure 7.3 Non-dimensional wave growth curves from observations (left panels) and from numerical simulations (right panels). Simulated data was obtained using MM5 4km/3h. Top panels show the energy growth curves and lower panels show the peak frequency curves.

Note, however, that to obtain the development rates above I first selected accurately the dimensional variables in order to get as close as possible to the so-called 'ideal conditions'. The reason was that, otherwise, the calculated development rates tended to increase due to deviations from the ideal conditions. In other words, the closer I got to the ideal conditions, the closer were the development rates to the reference functions in Table 7.1. These results indicated that to estimate the development rates in the region of study it is required an accurate selection of the dimensional variables (energy, wind speed and fetch) and the wind conditions in order to fulfil the homogeneity of the wave growth conditions assumed by the method. Namely, 1) using pure wind sea only and no swell, 2) selecting the value of wind speed which was the best representative of the wind that generated wave growth in ideal conditions, and 3) adjusting the value of fetch.

In this section I describe the difficulties related to selecting the dimensional variables (energy and peak frequency, wind speed and fetch) in the region of study and I justify the variables taken to calculate the local wave growth functions (equations [7.5] and [7.6]).

7.3.1. Wave energy and peak frequency

The non-dimensional growth curves require pure wind sea conditions in order to adequately describe the wave growth. For this reason, in the present calculations wind sea systems only were selected, as a first step before exploring the influence of swell (addressed later on in section 7.4.4). In the Catalan coast it was especially important to separate the wave systems because bimodal situations of coexisting sea and swell are especially common and can occur 50% of the time (Bolaños et al. 2009). Sea and swell can be approximately separated through a wide variety of methods. A good review of these methods can be found in Portilla et al. (2009).

Briefly, the basic methodology to separate sea and swell consists of two steps. The first step splits the spectra into partitions (one partition for each peak of the spectrum); and then it combines partitions that are related. In the literature, the parameters used to combine partitions (or not) differ slightly. In this work, I basically used the methodology suggested in Portilla et al. (2009) with a few modifications: I used the peak frequency of each partition (instead of the mean frequency) as a criterion to combine partitions. Also, I combined partitions whose peak frequency was closer than 0.015 Hz to the separation frequency (lowest frequency between two energy partitions) and/or which energy was lower than 8% the total energy of the spectrum. The exact methodology used in this work is described in detail in Annex III.

While the first step of the separation method is intended to identify significant wave systems in the spectrum, the second step is intended to classify each system as sea or swell. There exist several different methods to perform the second step (some of which are reviewed in Portilla et al. 2009). In this study I first used a fixed frequency (separating frequency f_s) above which wave systems were classified as swell. Although this is a common method in regions where sea and swell are located at very different frequencies, it is less suitable in the Catalan coast where the peak frequencies of both sea and swell are relatively close. I observed, for example, that the variability of the wind speed magnitude favoured the presence of old wind sea peaks, which were energy peaks that were being generated just before a sudden drop of wind speed.

To take a conservative approach and to remove the low wind speed situations with non-related high energy peaks, in this work I decided to use the parametric growth curves derived by KC92 to classify the wind sea and the swell. In particular, the expected peak frequency for the measured wind speeds ($f_{p,KC92}$) was calculated using the wave development rates reported in KC92 (for the composite data set). Then, the separation frequency (f_s), above which the wave systems would be considered as sea, was determined as follows:

$$f_s = 0.7 \cdot f_{p,KC92} \quad \textbf{[7.7]}$$

The expected peak frequency was multiplied by 0.7 to add a 30% margin of uncertainty to the growth curves from KC92. In this way, I included lower peak frequencies (more developed waves) for given wind speeds than considered by KC92. According to this method, a significant partition was classified as sea when its peak frequency was larger than the separation frequency defined by the local wind speed.

Using the KC92 growth laws to separate sea and swell has two main shortcomings. The first one is that the resulting sea data is inevitably biased to fit the KC92 growth functions, at least the peak frequency curves. This is the main reason for introducing the 30% margin of uncertainty between the peak frequency and the separation frequency. In this way, partitions that KC92 would otherwise consider to be swell (according to KC92), are considered to be sea. Thus, even though the data may still be slightly biased towards KC92, it is also possible to distinguish faster rates of wave growth than those considered in KC92.

The second inconvenience of using KC92 curves to separate sea and swell is the tight dependence of the method on wind speed. This is especially important in regions where it is difficult to obtain representative wind measures along the fetch. In this work I used wind speed measures at the most offshore buoy A-dw(D) because, as shown below in section 7.3.2, the wind speed at this position was the most representative value of wind speed along each buoy's fetch.

Note that, in the sea/swell classification procedure, fetch was not adjusted to wind direction in order to avoid an even stronger dependence of the wind sea on the wind speed value used to separate the wave systems. The main consequence was that more wave systems with low peak frequencies were considered to be wind sea (instead of swell or old wind sea) than the other way around.

Further adjusting the data set to ideal wind conditions could be achieved by restricting the wave directions to shore normal sectors. In this case, this restriction was not used because directional data was not available from all instruments.

7.3.2. Wind speed

The wind speed value that is directly related to wave growth is an important source of scatter of the non-dimensional growth curves (e.g. Komen et al. 1994). On one side, to describe the turbulent boundary layer there is controversy on whether the wind speed at 10 m elevation (U_{10}) should be taken, rather than the wind speed at half the wavelength ($U_{\lambda/2}$) or the friction velocity (U^*). On another side, an additional source of uncertainty in variable wind regions is the location at which the wind speed value is measured, and whether it is or not representative of the wind speed that generated those particular wave conditions. In this section, I discuss the possible measures of wind speed and the position at which wind speed was measured, and I briefly discuss the suitability of using wind speed along wave direction (in agreement

with DO85). To focus on close-to-ideal wind conditions only, I selected wind directions blowing along the shore-normal direction (315º±15º).

7.3.2.1. Scaling wind velocity

The many discrepancies related to the choice of the best wind speed that describes the turbulent boundary layer were already discussed by Komen et al. (1994) and Hwang (2006). The controversy turns around the three different measures of wind speed: U_{10}, $U_{\lambda/2}$, or U^*. Note that $U_{\lambda/2}$ is the wind speed at a height equal to half a wavelength, and U^* is a velocity scale related to wind stress. This section mainly focused on choosing the best wind speed to scale the variables in the region.

Hwang (2006) compared U_{10} and $U_{\lambda/2}$ and determined that $U_{\lambda/2}$ is strongly dependent on the drag coefficient (C_d) and the sea state (wavelength), but it is not related to the non-dimensional variables. Instead, from numerical simulations they reported that U_{10} calculations are more uncertain due to the dependence on both C_d and the sea state. Young and Verhagen (1996) compared U_{10} and U^* and concluded that less uncertainty is introduced when using U_{10}. Babanin and Soloviev (1998) justified using U_{10} over U^* based on the justification given in Donelan et al. (1985), according to which U_{10} is more useful to characterize the wind "effects on the 'energy containing' gravity waves".

In this study it was not possible to exactly calculate U^* due to lacking measurements of the turbulent components of wind speed. In such situations, according to Drennan et al. (2003), to calculate U^* (and the drag coefficient) it is necessary to make the assumption of pure wind-sea conditions, thus adding an additional source of uncertainty.

Note that in this study a logarithmic wind profile was assumed, and the drag law of Smith and Banke (1975) was used to extrapolate wind speed from 3 m to 10 m. Thus, U_{10}, U^* and $U_{\lambda/2}$ were all dependent on the drag coefficient to a certain degree. I decided to use U_{10} because it is the value most commonly used to scale the variables and it is easier to compare with previous studies.

7.3.2.2. In-situ or offshore wind sources

In wind conditions that are very close to the ideal situation, selecting the wind speed value that is generating waves is an easy task because point measurements at specific locations are assumed to be representative of the wind speed along the whole fetch. This assumption was accepted in some of the previous studies where the non-dimensional curves were calculated (e.g. Ewans and Kibblewhite 1990; Violante-Carvalho et al. 2002). The wind speed used to scale the variables was then usually taken from in-situ wind measurements. Instead, Dobson et al. (1989) used a function to describe the wind variations along fetch (across the marine boundary layer). Whereas Young and Verhagen (1996) and Breugem and Holthuijsen (2007) used the average wind speed along the fetch.

In the region of interest, the assumption of homogeneity could not be easily accepted because of the high spatial variability of the wind and wave data described in Chapter 5. In this case, the wind variability was not only due to the marine boundary layer, and could thus not be easily approximated by a simple function of fetch. To select the wind speed measure that was representative of the whole area, I non-dimensionalized the variables using the wind speed records from the four meteorological stations and I compared the resulting development rates. I used observational and simulated data from RIMA-Med.

The results show that, when the wind speed was taken from the meteorological stations on land or at the shoreline, the development rates calculated were much larger (b>1) than the rates suggested by previous authors ($b \leq \mathbf{1}$). Instead, when the wind speed was taken at the offshore buoy A-dw(D), the development rates were close to the previously reported ones, suggesting that offshore wind values were more representative of the wind speed along the fetch than land stations, in agreement with Babanin and Soloviev (1998).

To verify the hypothesis that the wind measurements at the offshore buoy were sufficiently representative of the wind speed values at each buoy's location, I calculated the non-dimensional curves using the numerically simulated wind and wave values. Wind values for scaling were taken in-situ, at buoy A-dw(D) position and at the coastal position of meteorological station H-met.

On the one side, the resulting development rates in Table 7.3 and Table 7.4 confirmed that using wind data at A-dw(D) to scale the variables provided similar development rates than using in-situ wind data. Then, the simulated development rates were not significantly different from the values given in KC92 for stable wind conditions. On the other side, using wind data from coastal station H-met produced significantly larger development rates (>>**1**), further confirming the better suitability of using wind speeds at A-dw(D) to approximate wind speed in the region.

These results confirmed the idea that offshore wind values were more representative of the wind speeds along the fetch than coastal wind measurements and were, thus, more adequate to scale the non-dimensional variables. In this work, no approximations to wind speed across the boundary layer, or average values, were made to avoid introducing unnecessary uncertainties in the calculations.

7.3.2.3. Wind speed along the wave direction

Some authors considered wind speed along the wave direction (only) as the single responsible for wave growth (e.g. DO85, Walsh et al. 1989, Hanson and Phillips 1999). In this work I also calculated the growth curves using the component of wind speed along wave direction but only for comparison purposes and only using data from directional buoys A-dw(D) and E-iw(D) (where wave direction was available). The slope of the growth curves obtained when taking the measured wind speed along the direction of the waves ($b = 0.96 \pm 0.09$) was not significantly different compared to the standard curves derived for the RIMA-Med subset. Instead, the development rate calculated using the wind speed along the wave

direction for the 5-years data set was much larger and significantly different (b = 1.21 + 0.03) than the standard rates and larger than the rates reported in the literature. In this work, the wind speed along the wave direction was not used because of the unavailability of wave direction at all instruments. Nonetheless, the inconsistent growth rates calculated using buoy A-dw(D) long data set suggest that this term could substantially increase the scatter of the data points and should be further studied.

7.3.3. Fetch

In ideal wind conditions, the wind is blowing perpendicular to the coast (which is assumed to be infinitely long) and the fetch is equal to the minimum distance from the buoy to the coast (along the perpendicular line). However, in variable wind conditions the wind direction can change and the distance to the coast (along the wind direction) can change accordingly.

The many definitions of fetch were studied, among others, by Breugem and Holthuijsen (2007) who compared the two approximations used in Young and Verhagen (1996). The first definition approximates the value of the fetch at the most upwind position (shortest fetch) based on the experimental curves suggested by JON73. Afterwards, increasing values of fetch are calculated adding the physical distance between measuring stations to the initial fetch. This measure of fetch reduces the scatter of the data points within the growth curves, but it incorporates the uncertainty associated to the use of the JON73 curves. The second measure of fetch is based on the geometry of the coast but it considers the distance from the location of observation to the upwind coast along the main axis of the lake, which is only valid in restricted fetch geometries (see Pettersson 2005).

Focusing on the more geometric definitions of fetch, in this work I additionally considered three approximations of fetch, with their corresponding limitations in variable wind conditions. The first one is the pure geometric definition of fetch as the minimum distance to the coast, independently of wind direction, an approximation only valid in ideal situations.

The second definition is related to the possibility that the wind effectively generating wave growth is the component of wind speed along the direction of waves (as suggested in DO85), which would imply that fetch is the minimum distance to the coast along the wave (and not the wind) direction. This definition of fetch was not further considered in this work due to the unavailability of wave direction at all instruments. Nonetheless, keep in mind that in the region of interest the wave direction tended to orientate along the direction of the longest fetch, as described in DO85 and Walsh et al. (1989) for slanting fetch conditions. This characteristic of wave growth in variable wind conditions is addressed again in 7.4.3 where the rates of wave growth are calculated for different angles of the wind compared to the shore-normal direction.

The third definition of fetch was given by the change in wind direction along the fetch and its influence on a so-called effective fetch. In simple wind conditions, fetch could be then calculated as the distance to the coast in the direction parallel to the wind direction (at the offshore buoy), as defined in Dobson et al.

(1989). In this work, to reduce the influence of the fetch value in changing wind directions, I calculated fetch according to the last definition, i.e. as the distance to the coast along the wind direction, and I limited the range of wind directions to those which were perpendicular to the coast (315º±15º).

Note that at buoy A-dw(D), a ±15º range of wind directions could change the value of fetch by as much as 10 km (see Table 7.5). In short data sets, e.g. 'Fetch-limited dataset', the narrow directional range selected provided development rates that were comparable to those reported by other authors. Instead, the development rates calculated using wider directional ranges, although they were calculated with larger amounts of data, they also tended to increase and depart from the rates reported by previous authors. In large data sets (5-year long data set) the definition of fetch was less important because the scatter of the data points and the differences compared to previous authors did not increase significantly.

Table 7.5 Fetch (X) in km along three directions from each buoy to the coast (α) and non-dimensional fetch ($\bar{X}$) for a 10 m/s wind speed blowing along the shore normal.

Buoy	X Distance to the coast (km) along the direction:			$\bar{X}$ for α=315º and U_{10}=10 ms^{-1}
	300º	315º	330º	
A	59	56	49	$5.5 \cdot 10^3$
B	27	24	21	$2.4 \cdot 10^3$
D	1	1	1.1	$0.1 \cdot 10^3$
E	23	22	24	$2.2 \cdot 10^3$

7.4. Other factors conditioning wave growth

Traditionally, the scatter of the data points in the growth curves and the different development rates reported in the literature are attributed to the environmental characteristics of each experiment (which I call external forcings) and the characteristics of the sea state (which I call internal properties of the wave field). For example, in Walsh et al. (1989) they blamed the stability of the atmosphere, the non-homogeneity of the wind fields, and the asymmetry of the fetch about the wind direction (slanting fetch). These authors also discussed the limited suitability of combining laboratory and field measurements. Later on, KC92 reconciled the discrepancies in previously reported development rates by separating the data according to the stability of the atmosphere.

Other authors exploring external forcings include, among others, Ardhuin et al. (2007), who suggested that slanting-fetch effects may also contribute to enhanced wave development rates, and Haus (2007), who reported reduced development rates in the presence of strong currents. The different wave growth under strong currents was also reported by Battjes et al. (1987). Ponce de León and Ocampo-Torres (1998) and Abdalla and Cavaleri (2002), in turn, described enhanced wave growth due to gustiness of the wind using numerical simulations.

Also, the impact of the geometry of the domain on wave growth was explored in depth limited regions by Young and Verhagen (1996) and Bottema and van Vledder (2009), among others. Breugem and Holthuijsen (2007) reanalyzed the data in Young and Verhagen (1996) and concluded that the narrow width of the fetch was responsible for the lower wave heights measured, compared to broader (ideal) fetch geometries. These results agree with the work performed by Pettersson (2005) in the Gulf of Finland.

In this section I calculated the development rates during some of these conditions to explore their importance in the region of study. Some factors were, however, not taken into account for evident reasons. For example, I did not consider the effect of currents on wave growth because local currents are not very strong (~ 10 cm/s at 100 m depth according to Bolaños et al. 2009). Gustiness was not considered either due to the lack of information on small scale wind variability. Depth-limited conditions were not addressed because the local bathymetry deepens very fast (see for example Figure 3.1) and deep water could be assumed for all waves growing from the coast towards open sea.

I grouped the possible situations affecting wave growth in two groups: external environmental forcings and internal wave properties. The external forcings group include the tendency of wind speed (increasing/ decreasing wind speed values), the stability of the atmosphere and slanting fetch conditions. The internal properties of the wave field include the effect of swell (mixed seas) on wave growth, and the different wave age and wave steepness conditions.

To approximate wave growth under the considered conditions I mostly calculated the energy and peak frequency development rates during the 'Fetch-limited dataset' corresponding to close-to-ideal wind sea conditions. The exception is the study of the influence of swell on wind-sea growth, for which I used data records from the whole RIMA-Med field campaign. Also, to further support the analysis, I used wave data from buoy A-dw(D) during the 5-years period 2004 – 2009 from a single-fetch point of view.

The development rates calculated in this study are collected in Table 7.6 and Table 7.7, where b corresponds to the energy development rate and c corresponds to the rate of frequency downshift. $a_{0,1}$ and $a_{0,2}$ correspond to the y-origin of the fit. Each value in the tables is followed by the 95% confidence interval, which again indicates that there is a 95% of probability that the fit could take any of the values within that range.

The first three columns of Table 7.6 and Table 7.7 contain the development and downshift rates calculated using wave data from one of the three instruments available only (A-dw(D), B-iw(S) and E-iw(D)), as single-fetch datasets. The rates on the fourth column were calculated using data from all instruments, thus they form a multi-fetch dataset. The fifth, and last, column contains the rates for the single-fetch long data set at A-dw(D) from 2004 until 2009.

The results obtained provided further information beyond just approximating wave growth in each particular meteorological and oceanographic condition because they permitted to compare single- and multi-fetch datasets. Although the limitations of single-fetch datasets are addressed again in Section 9.3.1.2, it is just mentioned here that their main drawback was that the range of non-dimensional fetch was only possible due to the different wind speeds recorded.

On one side, the general comparison of the results showed that single-fetch datasets during the 'fetch-limited dataset' were not characterized by a consistent behaviour; i.e. the differences between the pairs of situations analysed did not always coincide with the differences obtained with the multi-fetch dataset. Also, the confidence ranges of single-fetch data sets were very large thus indicating that the uncertainty of the calculations was also large. The large scatter and uncertainty of these calculations were most probably due to the limited amount of data records used.

On the other side, the comparison showed that the 'single-fetch' development rates calculated tended to be faster than those approximated using the 'multi-fetch' data set. In spite of the limitation due to the size of the short 'single-fetch' datasets, notice that this tendency also existed when comparing the multi-fetch data set and the 5-year long single-fetch dataset, for which the size limitation of the dataset was importantly reduced.

Although the differences were not significant, I believe that the higher rates were partly due to the uncertainties derived from the selection of the dimensional variables (as discussed in previous section 7.3). In particular, the wind sea/swell separation method used might need a more accurate tuning given the large amount of data considered (5 years), and the directional information of the waves might have to be included in the wind sea/swell classification method. Other causes of the higher rates of single-fetch data sets could be the inherent limitations of the method, as discussed in section 9.3.

From now on, when using the term 'single-fetch data set', I refer to the 5-year-long data set from buoy A-dw(D), unless otherwise specified. The development rates from the 5-year-long data set, however, were not (and should not be) used to quantify wave growth in the region. Instead, they were used to search for significant differences during the environmental situations and the sea state conditions analyzed, given the larger size of the dataset.

Once the differences between single- and multi-fetch datasets were clarified, in the following sections I focused on the two last columns of Table 7.6 and Table 7.7 and I discussed the development and downshift rates in the different meteorological and oceanographic conditions addressed.

Table 7.6 Energy development rate (*b*), and 95% confidence interval, of the non-dimensional growth functions calculated using observed data. Single-fetch data sets were calculated at the position of buoys A-dw(D), B-iw(S) and E-iw(D) and multi-fetch data set contained data from all three buoys. Bold values highlight the differences that are significant (95% level).

		A-dw(D)	B-iw(S)	E-iw(D)	All instruments	A-dw(D) (2004/2009)
ALL		1.02±0.17	1.01±0.12	1.11±0.37	0.94±0.08	1.01±0.04
Atmospheric stability	Unstable	1.14±0.23	0.96±0.21	1.4±0.44	0.94±0.1	1.01±0.04
	Stable	1.31±0.52	0.94±0.29		0.87±0.25	0.9±0.08
Wind speed tendency	Increasing	0.81±0.35	1.44±0.21	1.92±0.57	1±0.17	1.02±0.1
	Decreasing	0.86±0.28	0.81±0.15	1.69±0.58	0.82±0.11	0.97±0.05
	Constant	0.7±0.94	1.05±0.21	0.38±2.46	0.99±0.16	1.04±0.07
Slanting fetch	±5º	1.09±0.24	1.13±0.22	1.18±1.1	1.01±0.15	1.07±0.06
	±15º	1.02±0.17	1.01±0.12	1.11±0.37	0.94±0.08	1.01±0.04
	±30º	1.01±0.19	0.99±0.1	1.05±0.36	0.93±0.07	1.04±0.03
	±45º	1.09±0.14	1.02±0.09	1.05±0.36	0.97±0.06	1.03±0.03
Bimodality (RIMA-Med)	Pure Sea	0.95±0.11	0.99±0.1	1.17±0.22	0.94±0.06	**1.01±0.04**
	Sea(dominant) +swell	1.22±0.97	0.76±0.17	1.34±0.39	0.98±0.18	**1.14±0.05**
	Sea + swell (dominant)	1.1±0.36	1.39±0.14	0.99±0.62	0.97±0.17	**1.01±0.05**
Wave age (C_p/U)	C_p/U <1	0.98±0.16	1.03±0.14	1.11±0.37	0.92±0.08	0.81±0.05
	C_p/U >1					0.99±0.16
Wave steepness (H/L)	0.01-0.02					1.01±0.61
	0.02-0.03					1.18±0.1
	0.03-0.04	1.09±0.17	0.92±0.15	0.80±0.4	0.95±0.08	1.04±0.05
	0.04-0.05	0.76±0.65	1.19±0.19	1.7±0.45	1.15±0.15	0.96±0.14

7.4.1. Stability of the atmosphere

The effect of the stability of the atmosphere on wave growth in the region of study was explored through the calculation of the development rates for stable and unstable atmospheric conditions, separately. The stability of the atmosphere can be estimated using the bulk Richardson number (KC92, Young 1998; Liu and Ross 1980):

$$R_b = \frac{g\left(T_a - T_w\right)/z_T}{T_a\left(U/z\right)^2} \qquad \textbf{[7.8]}$$

Where z and z_T refer to the height at which wind and air temperature are measured and T_a and T_w refer to the temperature of air and water. Negative (positive) values of the Richardson number indicate unstable (stable) atmospheric conditions. Because the sign of the Richardson number is basically given by the temperature difference between air and water only, in this work I approximated the atmospheric stability simply using the sign of the temperature difference. The atmosphere is said to be unstable when the water

is warmer than the air. Otherwise, atmospheric conditions are stable (including neutral conditions). Neutral conditions refer to no difference of temperature between air and water.

Previous authors such as KC92, Liu and Ross (1980) and Young (1998) reported higher development rates in unstable conditions, whereas Ewans and Kibblewhite (1990) concluded that the stability of the atmosphere had no effect on wave growth. Table 7.6 indicates that, in this region, faster energy development rates occurred in unstable atmospheric conditions (see also Figure 7.4), even though the differences were not significant at the 95% level for any of the datasets compared (single- or multi-fetch and long or short periods of time).

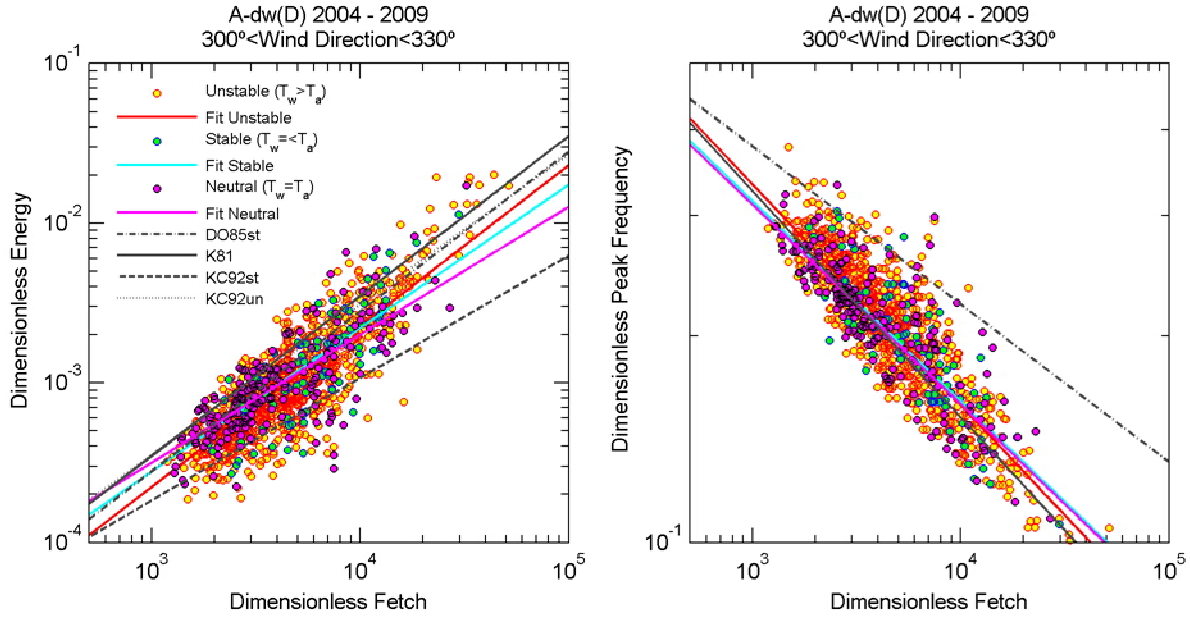

Figure 7.4 Energy (left panel) and peak frequency (right panel) growth curves for different atmospheric stability conditions, which depend on the water temperature (T_w) and the air temperature (T_a). Data were measured at buoy A-dw(D) during the period 2004 - 2009. Black lines show the empirical functions calculated in previous field experiments (Table 7.1). The development rates calculated for each atmospheric condition are given in Table 7.6 and Table 7.7.

7.4.2. Wind speed tendency

I used the term wind speed tendency to refer to changes of wind speed from one time step to a following one, and I differentiated increasing, decreasing and constant tendencies. The influence of the wind speed on wave growth was studied previously by other authors in different contexts. For example, Ewans and Kibblewhite (1990) studied self-similarity in growing, decaying and steady spectra and concluded that the spectral shape was preserved in all situations. Uz et al. (2002) performed a battery of laboratory tests under different wind speed tendencies. They reported that, compared to steady wind conditions, wave height was higher in increasing wind speed conditions due to higher wind stress (and roughness). In rapidly changing situations, Uz et al. (2002) concluded that higher wind stress could also occur for decreasing wind conditions if the surface wave field was not yet in equilibrium with the wind forcing (if

the surface was still 'rough'). Hanson and Phillips (1999) calculated the development rates of wave energy in rising and falling wind speeds against inverse wave age (U/C_p). They concluded that wind seas were more developed in falling wind speed situations, compared to constant situations.

In this work, the tendency of wind speed was calculated comparing the simultaneous wind speed value with the mean of the following 3 h. Wind speed differences smaller than ±0.5 m/s were considered 'constant wind' conditions. Positive (negative) differences above this limit were categorised as having an 'increasing' ('decreasing') wind speed tendency.

The energy development rates in Table 7.6 and Table 7.7 indicated that wave growth during 'constant' wind conditions was similar and not significantly different from 'increasing' wind conditions. The rates obtained were close to those described by pioneering authors such as JON73 and DO85. Energy development rates approached values of **1**, and peak frequencies oscillated between -0.24 and -0.33.

Development rates in 'decreasing' wind conditions were seen to be slower than in 'increasing' and 'constant' wind conditions suggesting that wave energy and frequency decreased more slowly than they increased for the same rates of wind speed change, as reported by Hanson and Phillips (1999). In this case, the reported difference was only significant for the frequency downshift rate between constant and decreasing wind speed. Again, the scatter of the curves was considerably large.

7.4.3. Slanting fetch

The term 'slanting fetch' refers to wind blowing offshore, but not perfectly perpendicular to the coast. The slanting fetch effect is related to the variability of the wind direction and its deviations from the shore-normal direction. Slanting fetch was studied in depth by Ardhuin et al. (2007) who reported a redistribution of the wave energy across directions to match the direction of the longest fetch (along the coast). According to their work, a 10º deviation of the wind direction from the shore normal is as important as a 10% change in wind speed. Their results show noticeable deviations from the curves summarized in KC92 and point to higher wave heights along the coast in slanting fetch conditions.

The behaviour of wave direction in slanting fetch conditions was further explored in Pettersson et al. (2010), whose results show that wave direction tends to orientate along the fetch's longest direction. Note for reference that slanting fetch conditions were also addressed by other authors such as Holthuijsen (1983), Dobson et al. (1989), Pettersson (2004), Bottema and van Vledder (2008), Gagnaire-Renou et al. (2008).

In the region of study, slanting fetch occurred because wind direction was highly variable compared to the shore normal and because of the position of the buoys in relation with the geometry of the coastline. In fact, in agreement with Pettersson et al. (2010), the wave directions recorded in the region tended to orientate along a characteristic direction that was different from the predominant wind direction. In Figure

7.5, note that wave direction at buoy A-dw(D) tended to orientate along the specific directions 70º, 200º and 295º (for strong wind speeds). These results agreed with the plots calculated using shorter datasets in Figure 5.3.

In this section I compared the development rates for increasing angles of wind direction (± 5º, 15º, 30º and 45º), following the work of Dobson et al. (1989). In agreement with Ardhuin et al. (2007), I expected to obtain increasing development rates for increasing angles (see Table 7.6 and Table 7.7). However, the development rates were not significantly different for the considered angle windows; even though the scatter of the curves was reduced (the confidence intervals were smaller).

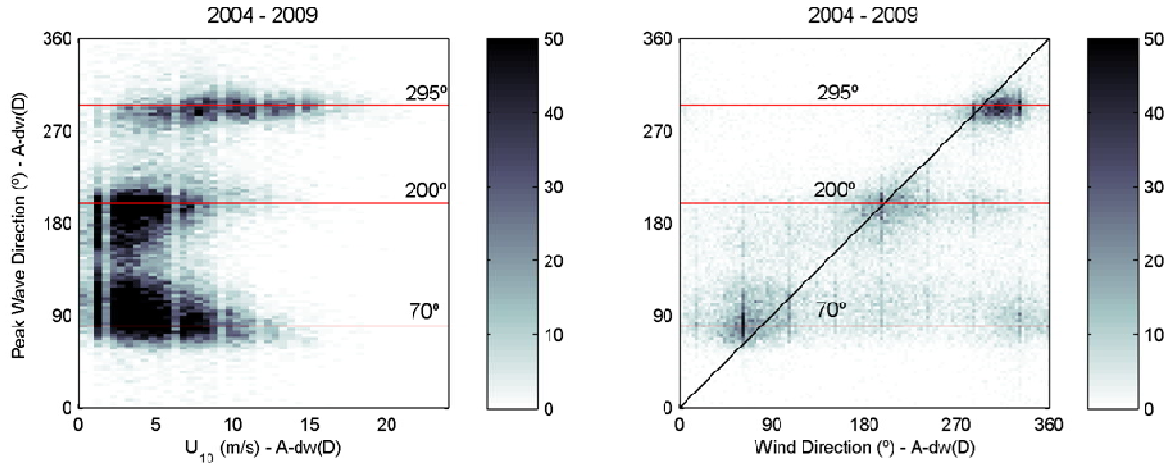

Figure 7.5 Scatter plots of peak wave direction as a function of wind speed (left panel) and wind direction (right panel) showing the effects of slanting fetch. Data were measured at buoy A-dw(D) during the period 2004 – 2009.

7.4.4. Bimodality of the wave spectra

The effect of swell on sea growth using fetch-limited experiments was explored many times in the past. The results were uneven and the effect of swell on sea is, at the present time, not yet clear. For example, Ewing (1980) computed a cross-correlation between swell and sea and found no correlation between the time series. Dobson et al. (1989) calculated the non-dimensional growth curves and reported misleadingly low development rates when sea and swell were not accurately separated. Hanson and Phillips (1999) reported no relationship between non-dimensional energy and swell. They concluded that the reason was the scaling law they used (DO85), which masks any existing relationship. Violante-Carvalho et al. (2002) also reported no effect of swell on sea growth, but Violante-Carvalho et al. (2004) observed a slight reduction of sea energy in situations of sea and swell alignment.

In laboratory experiments, Mitsuyasu and Yoshida (2005) indicated that wind waves were intensified by an opposing swell, whereas they were attenuated by a following one. Later on, Ardhuin et al. (2007) argued again that a moderate swell had no significant effect on sea growth and Jouon et al. (2009) confirmed that swell did not contribute to the high frequency components of the spectra.

Table 7.7 Same as Table 7.6 – it displays the frequency development rate (*c*10*).

		A-dw(D)	B-iw(S)	E-iw(D)	All instruments	A-dw(D) (2004/2009)
ALL		-2.81±0.53	-2.75±0.27	-3.17±0.72	-2.81±0.18	-3.22±0.1
Atmospheric stability	Unstable	-3.32±0.66	-2±0.48	-2.99±0.99	-2.72±0.24	-3.22±0.11
	Stable	-3.62±1.31	-3.45±0.47	-1.9	-3.18±0.43	-2.92±0.21
Wind speed tendency	Increasing	-3.15±1.39	-3.41±0.45	-3.95±0.98	-3.13±0.31	-3.2±0.24
	Decreasing	-2.72±0.75	-2.27±0.39	-2.75±1.49	**-2.45±0.28**	-3.16±0.15
	Constant	-1.93±2.58	-3.30±0.47	-0.70±2.61	**-3.2±0.36**	-3.26±0.18
Slanting fetch	±5º	-3.44±0.64	-2.94±0.42	-3.9±1.6	-3.08±0.26	-3.34±0.16
	±15º	-2.81±0.53	-2.75±0.27	-3.17±0.72	-2.81±0.18	-3.22±0.1
	±30º	-2.85±0.52	-2.65±0.22	-2.83±0.79	-2.75±0.16	-3.31±0.08
	±45º	-2.95±0.4	-2.7±0.2	-2.83±0.8	-2.79±0.15	-3.30±0.08
Bimodality (RIMA-Med)	Pure Sea	-3.08±0.37	-2.86±0.23	-3.26±0.43	-2.95±0.15	**-3.22±0.1**
	Sea(dominant) +swell	-3.23±2.23	-3.3±0.49	-3.6±0.7	-3.29±0.4	**-3.49±0.12**
	Sea + swell (dominant)	-3.76±0.71	-4.6±0.25	-3.23±0.97	**-3.59±0.3**	-3.29±0.15
Wave age (C_p/U)	C_p/U<1	-2.71±0.51	-2.66±0.3	-3.17±0.72	-2.74±0.2	-2.66±0.14
	C_p/U>1					-2.46±0.3
Wave steepness (*H/L*)	0.01-0.02					-2.85±1.6
	0.02-0.03					-3.11±0.23
	0.03-0.04	-2.93±0.57	-2.38±0.37	-1.8±0.78	-2.59±0.23	**-2.88±0.13**
	0.04-0.05	-2±1.55	-2.8±0.45	-3.85±1.21	-2.77±0.35	**-2.23±0.35**

In this work, to explore the effect of swell on wind sea I compared the development rates of the curves in situations of pure wind sea with those of mixed sea states. In mixed sea states, sea- and swell-dominated conditions were differentiated from each other depending on which component was more energetic. Note that bimodal situations did not occur during the 'Fetch-limited dataset' and therefore, in this case only, the development rates were calculated during the whole RIMA-Med field campaign (in Table 7.6 and Table 7.7), during which a few bimodal storm events were recorded, as described in Section 4.1.

The resulting energy development rates indicated that wave growth was faster in bimodal conditions, especially if the sea was more energetic than the swell (see Table 7.6). When the wind sea was more energetic than the swell the development rate difference was high, compared to pure wind sea systems. These results indicated that swell enhanced wind sea growth especially at the last stages of wave growth, during which swell was no longer more energetic than sea. Table 7.7 also shows that the rates of peak frequency downshift were significantly faster in sea-dominated bimodal situations.

7.4.5. Wave age

Wave age is defined as the ratio of the celerity of the spectral peak (C_p) and the wind speed. The celerity of the spectral peak was calculated using the peak period (T_p) and following linear wave theory (in deep waters $C_p = g*T_p / 2\pi$). The wave age of growing seas is considered to be less than **1** ($C_p/U < 1$) (Komen et al. 1994; Holthuijsen 2007). When the waves run faster than wind ($C_p/U > 1$) they are not expected to grow anymore. Above $C_p / U > 1.2$, Pierson and Moskowitz (1964) refer to fully developed conditions (according to Donelan et al. 1992). Hwang and Wang (2004) already stated that the wave energy development rates are clearly dependent on fetch, duration and wave age. For this reason, in this section I calculated the development rate of energy and peak frequency for different ranges of wave age.

In a first approach, I selected five different ranges of wave age: younger than 0.5, from 0.5 to 0.75, from 0.75 to 1, from 1 to 1.5 and older than 1.5. Because the wave age is a function of wind speed, in Figure 7.6 the different wave ages span along the plot in differentiated bands (large vertical scatter). The development rate of each of these groups was up to 50% smaller than the rates previously reported (in this work and in previous works) and the scatter of the fit increased dramatically. These results indicated that non-dimensional wave development was not a matter of a single wave age only, but a succession of wave ages: from young stages to fully developed conditions.

Therefore, in a second approach, I separated wave growth in growing seas ($C_p/ U < 1$) from almost-developed sea states ($C_p/U > 1$). In this case, energy and frequency development rates of growing seas were seen to be similar to the previously reported rates (although slightly smaller) (see Table 7.6 and Table 7.7). During the 'Fetch-limited dataset' almost no wave measurements above the limit of wave growth ($C_p/ U > 1$) were recorded. Instead, in buoy A-dw(D) dataset there was a considerable amount of developed data. In particular, at buoy A-dw(D) (2004/2009) 'young' waves were recorded for wind speeds higher than 6 m/s and 'old' waves were recorded above 10 m/s (not shown).

The large amount of 'developed' wave data in the 5-year long dataset suggested the possibility that the sea/swell separation method was unsatisfactory to separate sea from swell in the wide range of conditions considered. More specifically, I suspected that some swell might have been considered to be wind sea, thus slightly increasing the development rates calculated using the long-record single-fetch data set from buoy A-dw(D) (compared to multi-fetch data during RIMA-Med).

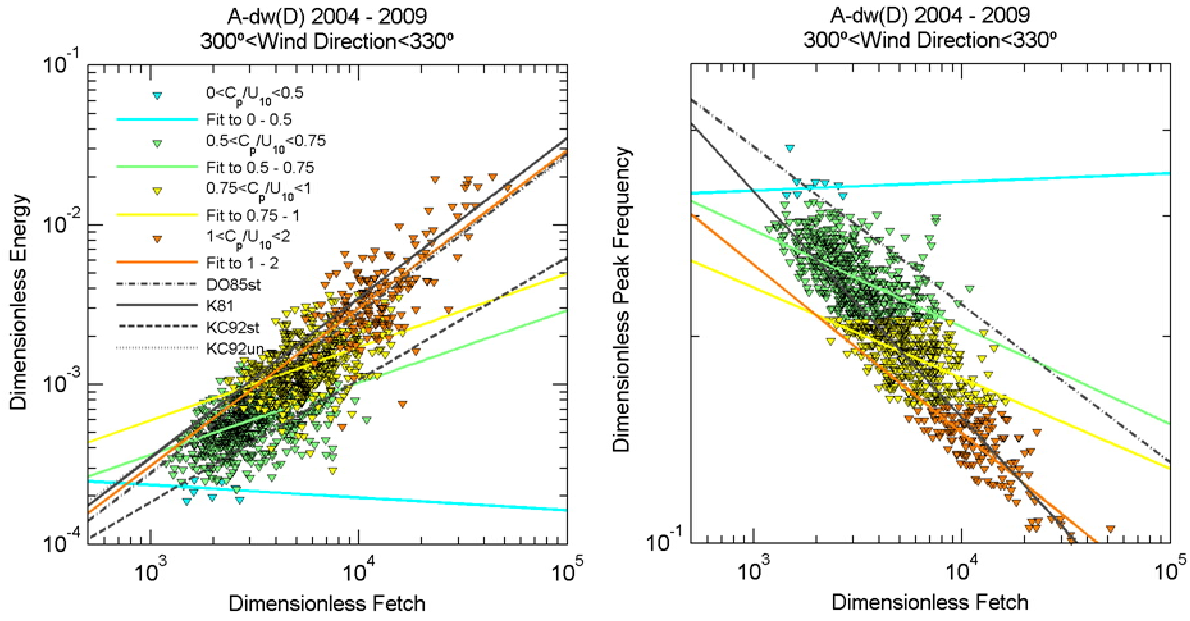

Figure 7.6 Energy (left panel) and peak frequency (right panel) growth curves for different wave age conditions. Note that the slope of the fit increases for increasing wave age. Data were measured at buoy A-dw(D) during the period 2004 - 2009. Black lines show the empirical functions calculated in previous field experiments (Table 7.1).

7.4.6. Wave steepness

Wave steepness refers to the ratio of wave height over wave length (H_s/L_p). The wavelength was calculated using the peak period and according to linear wave theory (in deep waters $L_p = g*T_p^2/2\pi$). In this section I calculated the energy and frequency development rates for different wave steepness ranges from 0.01 to 0.06.

García et al. (1993) described the wave steepness in this region ranging from 0.01 to 0.06, steeper waves corresponding to growing wind waves (sea). In agreement, wave steepness in the region of study, and during RIMA-Med subset, was lower than 0.06 and, in general, lower than 0.05.

The observations indicated that at buoys A-dw(D) and E-iw(D), during the 'Fetch-limited dataset', the range of wave steepness was limited to 0.03 – 0.05. At A-dw(D), the majority of the waves felt within the 0.03-0.04 steepness range. During the long-data record at A-dw(D), a larger amount of gentle-sloped waves were recorded, which confirmed the hypothesis that a certain amount of swell (or 'old sea') was indirectly included in the calculations, and could be responsible for the higher growth rates, compared to multi-fetch data.

The energy development rates in Figure 7.7 were not significantly different for the considered wave steepness (neither using multi-fetch nor single-fetch data; see Table 7.6). Instead, the rates of frequency downscaling in Table 7.7 were significantly higher for less steep waves (0.03 - 0.04 range) when calculated using buoy A-dw(D) long-record data set. In Figure 7.7, be aware that steep waves (young sea)

tended to be plotted on the left hand side of the frequency curves because they corresponded to short wave lengths, and thus, high peak frequencies.

The results suggested that the rate of frequency downscaling was faster during the first stages of wave growth but the energy growth was not necessarily faster. This result was not consistent with the results from the multi-fetch data set thus calling for a more detailed study on wave growth in different wave steepness conditions (or wave age).

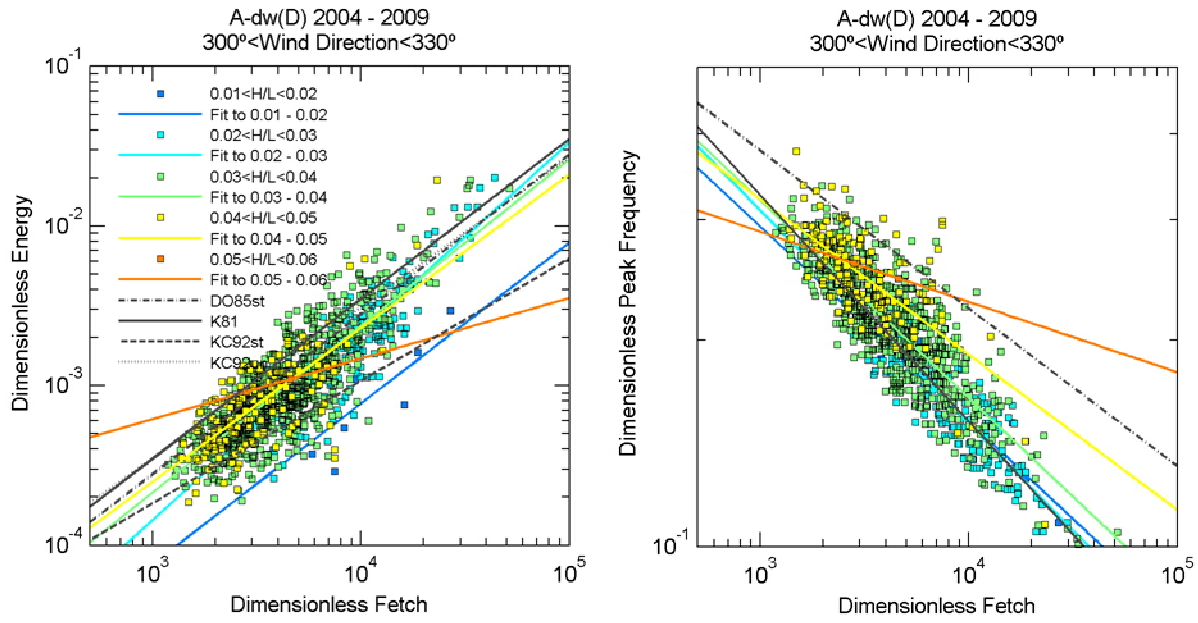

Figure 7.7 Energy (left) and peak frequency (right) growth curves for different steepness ranges. Note that the slope of the fit decreases for increasing steepness. Data were measured at buoy A-dw(D) during the period 2004 - 2009. Black lines show the empirical functions calculated in previous field experiments (Table 7.1). The development rates calculated for each steepness range are given in Table 7.6 and Table 7.7.

7.5. Summary of the results

In this chapter I used the scaling law proposed by Kitaigorodskii (1962), and the non-dimensional curves used in JON73 to study wave growth in a region characterized by variable wind and wave conditions. The development rates obtained were consistently, but not significantly, higher compared to the rates derived from previous wave growth experiments and from simulated data.

For this region, in order to reduce the scatter of the data points, I carefully selected the dimensional variables that approximated the ideal conditions encountered in the reference studies. Also, I explored the influence of other factors conditioning wave growth, such as the stability of the atmosphere, to better understand wave growth in the region of study. The wave growth curves calculated in this work (energy and peak frequency) were comparable to the curves recorded in earlier experiments when the ideal conditions of homogeneity and persistence of the wind conditions could be assumed (pure wind sea and wind directions along the shore normal).

In general, the development rates calculated in this study did not change significantly depending on the external forcings and internal wave properties considered. Significantly different energy development rates were only obtained for long-term single-fetch data from buoy A-dw(D) when comparing pure wind sea and mixed sea and swell conditions. The results indicated that wave energy grew faster in the presence of a less energetic swell system (frequency downshift was also faster). All in all, the results obtained for multi-fetch and single-fetch data sets did not always agree, thus calling for a more detailed study of wave growth under the different conditions addressed.

The development rates calculated using simulated data were found to be slightly, but not significantly, slower compared to the observations, thus supporting the feasibility to improve wave estimations by adjusting wave growth in the model. The adjustment of the simulated rate of wave growth to the observed wave growth (calculated for all kind of conditions) is described in the next chapter.

Appendix A. Y-intercept of the growth curves from simulated data

Table 7.8 Y-origin (a_2) values and 95% confidence interval, of the non-dimensional growth functions calculated using simulated wave energy (SWAN model – MM5 4km/3h). Single-fetch data sets are calculated at the position of buoys A-dw(D), B-iw(S) and E-iw(D) and multi-fetch data set contains data from all buoys. The non-dimensional variables were scaled using either simulated wind (MM5 model) in-situ, at the position of buoy A-dw(D) or at a position close to H-met meteorological station.

Simulation n^o	Location of scaling wind	A-dw(D)	B-iw(S)	E-iw(D)	All buoys
s1	MM5 in-situ	4.3·10-7±1.8·10-6	1.4·10-7±3.6·10-7	1.6·10-6±2.5·10-6	1.1·10-6±7.4·10-7
s2	MM5 at buoy A	4.3·10-7±1.8·10-6	3.4·10-6±1.1·10-6	1.4·10-6±1.4·10-5	1.2·10-6±1·10-6
s3	MM5 at H-met	4·10-10±9.1·10-10	2.2·10-9±4.4·10-9	2.4·10-10±8.4·10-10	1.1·10-8±1.6·10-8

Table 7.9 Same as Table 7.8 – it displays the Y-origin (a_1) values.

Simulation n^o	Location of scaling wind	A-dw(D)	B-iw(S)	E-iw(D)	All buoys
s1	MM5 in-situ	3.45±3.21	4.64±2.57	2.23±0.93	2.12±0.39
s2	MM5 at buoy A	3.45±3.21	1.99±1.28	2.74±2.89	2.06±0.46
s3	MM5 at H-met	18.27±10.33	10.06±5.13	14.75±9.66	6.31±2.03

Appendix B. Y-intercept of the growth curves from observed data

Table 7.10 Y-intercept ($a_{0,1}$) of the wave energy growth curves and the 95% confidence interval. Blank spaces indicate that there were not enough data points to calculate the fit.

		A-dw(D)	B-iw(S)	E-iw(D)	All instruments	A-dw(D) (2004/2009)
ALL		-15±1.4	-14.69±0.89	-15.54±2.7	-14.26±0.61	-15.38±0.33
Atmospheric stability	Unstable	-15.95±1.88	-14.41±1.5	-17.63±3.16	-14.26±0.73	-15.36±0.34
	Stable	-17.75±4.51	-14.11±2.34		-13.66±2.03	-14.38±0.69
Wind speed tendency	Increasing	-13.13±2.97	-17.7±1.57	-21.42±4.25	-14.56±1.28	-15.36±0.84
	Decreasing	-13.83±2.25	-13-34±1.05	-19.5±4.08	-13.42±0.8	-15.09±0.45
	Constant	-12.48±7.64	-15.2±1.57	-10.34±17.9	-14.73±1.24	-15.61±0.57
Slanting fetch	±5º	-15.65±2.04	-15.6±1.67	-16.12±8	-14.81±1.16	-15.87±0.52
	±15º	-15±1.4	-14.69±0.89	-15.54±2.7	14.26±0.61	-15.38±0.33
	±30º	-14.94±1.53	-14.59±0.72	-15.16±2.6	-14.2±0.53	-15.7±0.26
	±45º	-15.59±1.19	-14.77±0.66	-15.16±2.6	-14.47±0.5	-15.61±0.24
Bimodality (RIMA-Med)	Pure Sea	-14.47±0.95	-14.54±0.78	-15.97±1.62	-14.23±0.49	-15.38±0.33
	Sea(dominant) +swell	-17.35±9.07	-13.13±1.45	-17.51±3.27	-14.86±1.48	-16.73±0.43
	Sea + swell (dominant)	-16.63±3.56	-18.84±1.31	-14.85±5.51	-15.02±1.59	-15.83±0.53
Wave age (C_p/U)	C_p/U<1	-14.74±1.35	-14.83±1.01	-15.54±2.7	-14.13±0.64	-13.80±0.42
	C_p/U>1		-113.2		-113.2	-14.89±1.52
Wave steepness (H/L)	0.01-0.02					-16.43±5.63
	0.02-0.03					-17±0.86
	0.03-0.04	-15.58±1.42	-14.22±1.08	-13.58±2.95	-14.49±0.66	-15.64±0.43
	0.04-0.05	-12.77±5.29	-15.96±1.43	-19.67±3.44	-15.67±1.14	-14.93±1.14

Table 7.11 Y-intercept ($a_{0,2}$) of the peak frequency growth curves and the 95% confidence interval. Blank spaces indicate that there were not enough data points to calculate the fit.

		A-dw(D)	B-iw(S)	E-iw(D)	All instruments	A-dw(D) (2004/2009)
ALL		0.7±0.44	0.65±0.2	0.97±0.52	0.69±0.14	1.12±0.09
Atmospheric stability	Unstable	1.1±0.53	0.11±0.35	0.84±0.71	0.63±0.18	1.12±0.09
	Stable	1.46±1.14	1.21±0.38		1.01±0.35	0.86±0.18
Wind speed tendency	Increasing	0.99±1.16	1.13±0.33	1.57±0.73	0.94±0.24	1.09±0.2
	Decreasing	0.63±0.6	0.29±0.28	0.65±1.05	0.42±0.21	1.08±0.13
	Constant	0.02±2.1	1.09±0.36	0.84±1.9	1.01±0.25	1.16±0.15
Slanting fetch	±5º	1.23±0.53	0.8±0.31	1.52±1.15	0.91±0.2	1.23±0.13
	±15º	0.7±0.44	0.65±0.2	0.97±0.52	0.69±0.14	1.12±0.09
	±30º	0.72±0.43	0.57±0.16	0.72±0.57	0.64±0.12	1.21±0.07
	±45º	0.8±0.33	0.6±0.15	0.72±0.57	0.67±0.11	1.21±0.07
Bimodality (RIMA-Med)	Pure Sea	0.91±0.32	0.72±0.17	1.04±0.32	0.8±0.11	1.12±0.09
	Sea(dominant) +swell	1.12±2.11	1.16±0.41	1.33±0.58	1.12±0.31	1.41±0.11
	Sea + swell (dominant)	1.69±0.71	2.39±0.23	1.1±0.87	1.47±0.29	1.31±0.14
Wave age (C_p/U)	$C_p/U<1$	0.62±0.42	0.58±0.22	0.97±0.52	0.65±0.14	0.68±0.11
	$C_p/U>1$					0.33±0.29
Wave steepness (H/L)	0.01-0.02					0.74±1.47
	0.02-0.03					0.97±0.21
	0.03-0.04	0.79±0.47	0.35±0.28	0.02±0.58	0.51±0.17	0.85±0.11
	0.04-0.05	0.08±1.25	0.69±0.33	1.46±0.87	0.67±0.26	0.43±0.28

8. Adjusting the simulated rate of wave growth

In the previous chapter it was shown that the development rates calculated from local observations tended to be higher than the rates derived in other field experiments, and higher than calculated using simulated data. Although no specific situations during which wave growth was faster were clearly identified, it became clear that adjusting the simulated wave growth rate to the locally calculated rate could still improve wave estimations. The results below indicated that tuning the dissipation term to adjust the model's growth rate to the observations slightly improve wave estimations. However, the under-estimation of the wave parameters was not completely overcome. Note here that the calibration presented did not attempt to tune the model exactly to the growth curves. Instead, the aim was to show that the improvement was indeed possible.

Calibrating spectral wave models (their source terms) using the non-dimensional wave growth curves is not a novelty and it has been commonly (and recently) used in the literature. Take for example the calibration of the new dissipation formulations derived by Van der Westhuysen et al. (2007) and Ardhuin et al. (2010). These authors, however, used the growth rates derived by other authors to describe wave growth for the general case; i.e. quasi-homogeneous wind conditions. In this study, I calculated the wave growth curves characteristic of the region of study and I adjusted the regional model accordingly. To this end, I used local observations and wind directions along the shore normal (315º±15º). The growth functions derived for this region were presented in Chapter 7; see eq.[7.5] and [7.6].

The calculated development rates (exponent of the independent variable) are slightly faster than the rates reported by KC92 and faster than the rates obtained from simulated data. The simulated data used in the present chapter corresponded to the simulations obtained using the higher resolution input wind fields (MM5 4km/1h). The wave growth functions derived using simulated data are given in equations [8.1] and [8.2].

$$\overline{E}_{MODR1h\_1} = 4.7 * 10^{-7} \cdot \overline{X}^{-0.92} \qquad \textbf{[8.1]}$$

$$\overline{f_p}_{MODR1h\_1} = 2.57 \cdot \overline{X}^{-0.290} \qquad \textbf{[8.2]}$$

Although the differences between simulated and observed data are not statistically significant, the graphical representation in Figure 7.3 shows that simulated data is generally below the theoretical curves.

Bear in mind that low non-dimensional values mean that simulated energy (peak frequency) is lower (higher) than the observations. This result could explain the common under-estimations shown in Chapter 6. Consequently, tuning the regional wave model to the slightly faster development rates calculated was expect to locally increase (decrease) the simulated energy (peak frequency) and to improve the estimations. Therefore, in what follows I adjust the model's growth rate to the slightly faster development rates derived from the RIMA-Med subset of data to prove that the improvement was indeed possible. The extent of the improvement is also assessed.

Note, however, that during RIMA-Med the confidence intervals of the calculated growth rate were large because of the limited amount of data used in the calculations. Therefore, and although not considered in this work, an alternative possibility could be the calibration of the wave model with the single-fetch data curves calculated at buoy A-dw(D) (2004 – 2009). The growth curves derived from observations at A-dw(D) only are given in equations [8.3] and [8.4].

$$\overline{E}_{A-dw(D)} = 2.1^{*}10^{-7} \cdot \overline{X}^{1.01} \qquad \textbf{[8.3]}$$

$$\overline{f_p}_{A-dw(D)} = 3.1 \cdot \overline{X}^{-0.322} \qquad \textbf{[8.4]}$$

The advantage of using the curves calculated from the 5-year long dataset at A-dw(D) is the reduced uncertainty of the curves, which is possible because of the large amount of data used in the calculations. However, the main drawback of this approach is, as mentioned above, the possibility that the dataset contains swell systems which were erroneously considered as sea. Therefore before considering using these curves further, it would be necessary to first calibrate again the sea-swell separation method in order to better discern the wind sea from the swell in such large data sets.

8.1. Dissipation due to whitecapping

In this work I decided to tune the dissipation term in wave models in order to adjust the simulated growth rates to the observed ones. Although this decision was already justified in Chapter 2, remember here that of all parameterizations involved in wave energy input in spectral wave models (wind input, dissipation and non-linear interactions), the dissipation due to whitecapping is the least well-know term. Because the other source terms are better known physically, dissipation adjusts the energy balance in order to agree with the growth rates given in the literature.

At present times, a lot of work has been done towards improving the understanding and the parameterization of the dissipation source term (e.g. Ardhuin et al. 2010, Banner and Morison 2010). However, the exact physical description of the dissipation due to whitecapping has not yet been agreed on. Thus, it still is a convenient option to calibrate wave models locally using the dissipation coefficients.

In this work, to drive the SWAN wave model I used the source terms suggested by Komen et al. (1984) (KOM). To adjust these terms to the observations, I focused on the tuneable coefficients used in the expression for dissipation due to whitecapping, which is mainly controlled by the steepness of the waves. The whitecapping is expressed by The WAMDI Group (1988) as follows:

$$S_{ds,w}(\sigma,\theta) = -\Gamma\tilde{\sigma}\frac{k}{\tilde{k}}E(\sigma,\theta) \quad \textbf{[1.5]}$$

Where Γ is a steepness dependent coefficient, k is the wave number and $\tilde{\sigma}$ and $\tilde{k}$ refer to the mean frequency and the mean wave number, respectively. Γ was adapted by Günther et al. (1992), based on Janssen (1991) (according to The SWAN team 2009), and is written as:

$$\Gamma = C_{ds}\left((1-\delta)+\delta\frac{k}{\tilde{k}}\right)\left(\frac{\tilde{s}}{\tilde{s}_{PM}}\right)^{p} \quad \textbf{[1.6]}$$

Where δ, p and C_{ds} are tuneable coefficients and $\tilde{s}$ is the overall wave steepness. The steepness of the Pierson-Moskowitz spectrum (1964) is $\tilde{s}_{PM} = \sqrt{3.02\cdot10^{-3}}$. The tuneable coefficients in equation [1.6] were obtained in KOM by closing the energy balance equation in idealized wave growth conditions (growing and fully developed waves) for deep waters. In other words, the tuneable coefficients depend on the expression of the wind input. Note also that different tuneable coefficients could be expected in non-ideal wave growth conditions.

The default values of the tuneable coefficients for KOM wind input are $\delta = 0$, $p = 4$ and $C_{ds} = 2.36\cdot10^{-5}$. Accordingly, equation [1.6] takes the form:

$$\Gamma = C_{ds}\left(\frac{\tilde{s}}{\tilde{s}_{PM}}\right)^{4} = C_{ds}\left(\frac{\tilde{s}^{4}}{stpm^{2}}\right) \quad \textbf{[1.7]}$$

$$\text{stpm} = \tilde{s}_{PM}{}^{2} = 3.02\cdot10^{-3} \quad \textbf{[1.8]}$$

In SWAN 40.72ABCD it is possible to easily tune C_{ds} and *stpm*. Note that the larger the C_{ds} and the smaller *stpm*, the larger is the dissipation. The dissipation coefficient C_{ds} is a linear coefficient of the amount of energy to be dissipated. The steepness parameter *stpm* should be thought of as the maximum steepness above which waves would break and dissipate energy through whitecaps. Small values of *stpm* indicate that waves start breaking when they are less steep than for larger steepness limits (*stpm*).

To calibrate SWAN adjusting the dissipation parameters of the KOM whitecapping formulation I aimed to decrease C_{ds} and to increase *stpm*. The reason was that simulated growth rates were lower than the

observed ones and, therefore, the goal was to reduce the amount of whitecapping in the simulations (and to increase the generally under-estimated wave values).

8.2. Adjusting the tuneable coefficients

The objective of the tuning exercise is to demonstrate that wave simulations could be locally improved if the wave growth rates of the model are adjusted to match the wave growth rates derived from in-situ observations. This exercise does not aim to find the best tuneable coefficients that permit to simulate the observations. The reason is that this sort of calibration is not only dependent on the tuneable coefficients of whitecapping themselves, but also on the numerical settings of the wave model (e.g. grid size, time step) as discussed in next chapter. Therefore, a systematic calibration of whitecapping would be suitable for each particular prediction system.

In SWAN, the default values of the tuneable parameters are:

$C_{ds} = 2.5 \cdot 10^{-5}$

$stpm = 3.02 \cdot 10^{-3}$

Bearing in mind that growth rates in SWAN wave model were to be increased from 0.92 to 0.94 (energy) and decreased from -0.290 from -0.281 (peak frequency), I ran SWAN again using three different dissipation coefficients C_{ds} = 2, 2.5; and 3 and two different steepness limits *stpm* = 3 and 3.5. The different parameters were tested in several model simulations, whose names are summarized in Table 8.1. The numerical run using SWAN default values is called R1h-1. This simulation corresponds to the highest resolution simulation compared and discussed in Chapter 6. The growth rates resulting from each numerical simulation are given in Table 8.2 for energy and Table 8.3 for peak frequency.

The results in Table 8.2 and Table 8.3 indicate that the growth rate of the simulations could be increased if the tuneable coefficients in SWAN are adjusted. In the next section the wave height and the peak period time series were evaluated, both visually and statistically, to assess how much the calibrated growth rate improves wave predictions.

Table 8.1 Name of the SWAN model simulations ran with different coefficients in the whitecapping expression [7]

C_{ds} [$\cdot 10^{-5}$] \ *stpm* [$\cdot 10^{-3}$]	3	3.5
2	R1h-3	R1h-7
2.5	R1h-1	R1h-8
3		R1h-9

Table 8.2 Energy growth rates and 95% confidence interval obtained for each simulation summarized in Table 8.1.

C_{ds} [$\cdot 10^{-5}$] \ *stpm* [$\cdot 10^{-3}$]	3	3.5
2	0.93±0.06	0.95±0.06
2.5	0.92±0.06	0.94±0.06
3		0.92±0.06

Table 8.3 Peak frequency downshift rates (*10^{-1}) and 95% confidence intervals obtained for each simulation summarized in Table 8.1.

C_{ds} [$\cdot 10^{-5}$] \ *stpm* [$\cdot 10^{-3}$]	3	3.5
2	-2.900±0.17	-2.813±0.21
2.5	-2.903±0.15	-2.857±0.19
3		-2.881±0.16

8.3. Performance assessment of SWAN

The improvement of the wave predictions could be visually assessed in Figure 8.1 and Figure 8.2. It is shown that the maximum values of the storm event were better estimated with the calibration in run R1h_7, compared to default run R1h_1 and compared to the other combination of tuneable coefficients. Statistically, the simulations calibrated with the different dissipation parameters were assessed using scatter plots of the simulated variables. The simulated wave height (or peak period) were plotted against the measurements at each buoy (not shown). The parameters representative of the scatter plots were the *slope-1* and *R2*, which indicated the over-/under-estimation of each simulation and the scatter of the data points along the best-fit line (see section 4.3).

The statistical fit parameters in Table 6.4 and Table 6.5 are summarized in Figure 8.3 and Figure 8.4. The results confirmed, statistically, the improvement achieved with the calibration of the wave model according to the observed wave growth rates. The improvements were especially relevant for run R1h_7, which presents the best fit (lowest *slope-1* values or deviations from the fit) and comparably high *R2* values (amount of variability captured in the simulation). In this case, wave height increased about 18% and peak period increased about 4%. All in all, the under-estimation of the peak values in Figure 8.1 and Figure 8.2 indicated that numerical estimations still need to be improved; both in terms of H_s and T_p. The consistent under-estimation of the peak periods was particularly relevant.

Table 8.4 Comparison of the logarithm of the simulated and the observed wave heights (H_s) from 7 Dec. to 13 Dec. 2007. The coefficients used in each simulation are given in Table 6.1. Boldfaced values correspond to the slope of the regression equation minus 1 *slope-1* (positive/negative values indicate an over/under-prediction). Regular values correspond to the determination coefficient *R2*.

H_s	R1h_1		R1h_3		R1h_7		R1h_8		R1h_9	
A-dw(D)	**-0.13**	0.74	**-0.07**	0.42	**0.05**	0.72	**-0.04**	0.73	**-0.10**	0.74
B-iw(S)	**-0.18**	0.56	**-0.13**	0.56	**-0.01**	0.55	**-0.1**	0.55	**-0.16**	0.56
E-iw(D)	**-0.23**	0.62	**-0.18**	0.61	**-0.06**	0.61	**-0.14**	0.61	**-0.21**	0.62

Table 8.5. Comparison of the logarithm of the simulated and the observed peak period (T_p) from 7 Dec. to 13 Dec. 2007. The coefficients used in each simulation are given in Table 6.1. Boldfaced values correspond to the *slope* of the regression equation minus 1 *slope-1* (positive/negative values indicate an over/under-prediction). Regular values correspond to the determination coefficient *R2*.

T_p	R1h_1		R1h_3		R1h_7		R1h_8		R1h_9	
A-dw(D)	**-0.21**	0.48	**-0.20**	0.47	**-0.17**	0.35	**-0.18**	0.40	**-0.21**	0.49
B-iw(S)	**-0.10**	-0.32	**-0.09**	-0.39	**-0.05**	-0.35	**-0.08**	-0.37	**-0.10**	-0.32
E-iw(D)	**-0.27**	-0.40	**-0.26**	-0.45	**-0.23**	-0.41	**-0.24**	-0.48	**-0.27**	-0.40

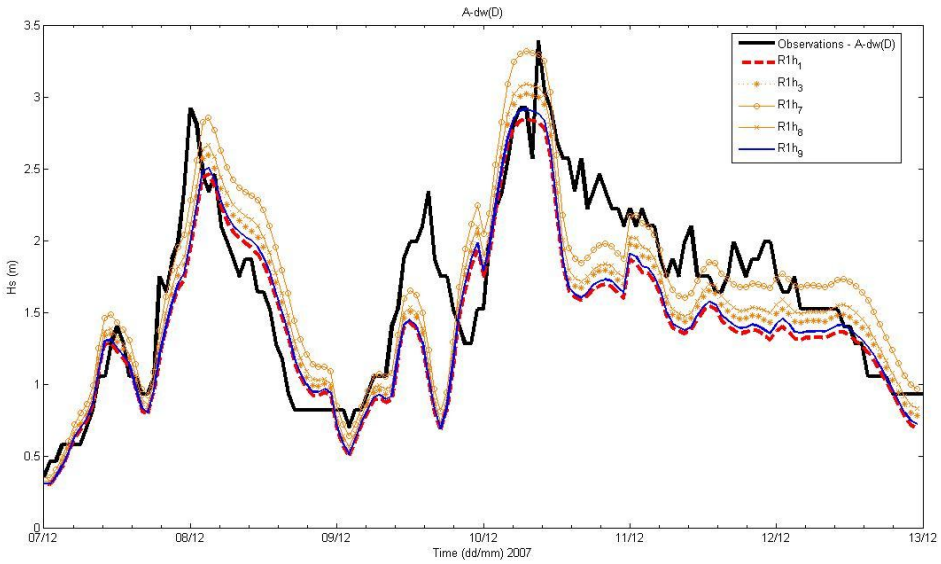

Figure 8.1 Observed and simulated wave height at offshore buoy A-dw(D) during the fetch-limited wave storm occurred from 7 to 13 Dec. 2007.

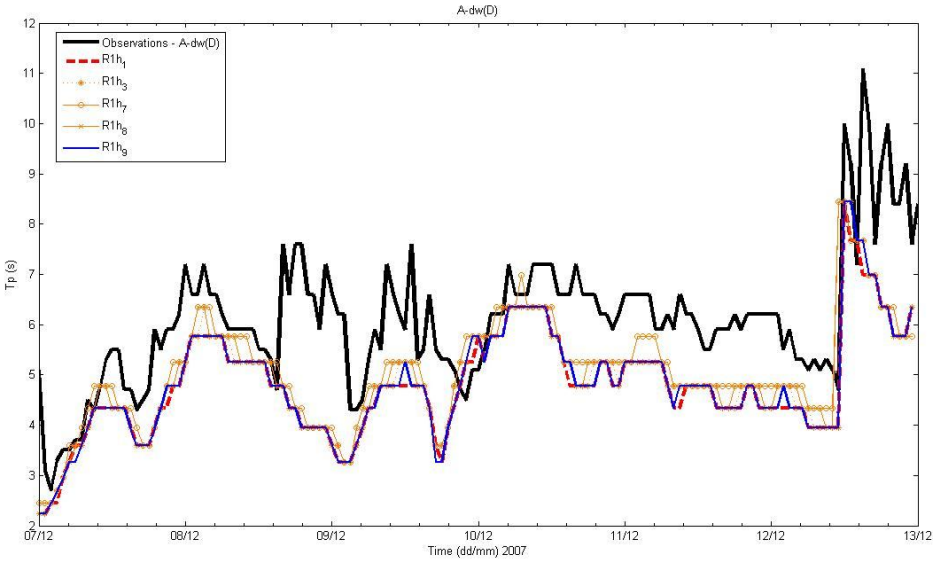

Figure 8.2 Observed and simulated peak period at offshore buoy A-dw(D) during the fetch-limited wave storm occurred from 7 to 13 Dec. 2007.

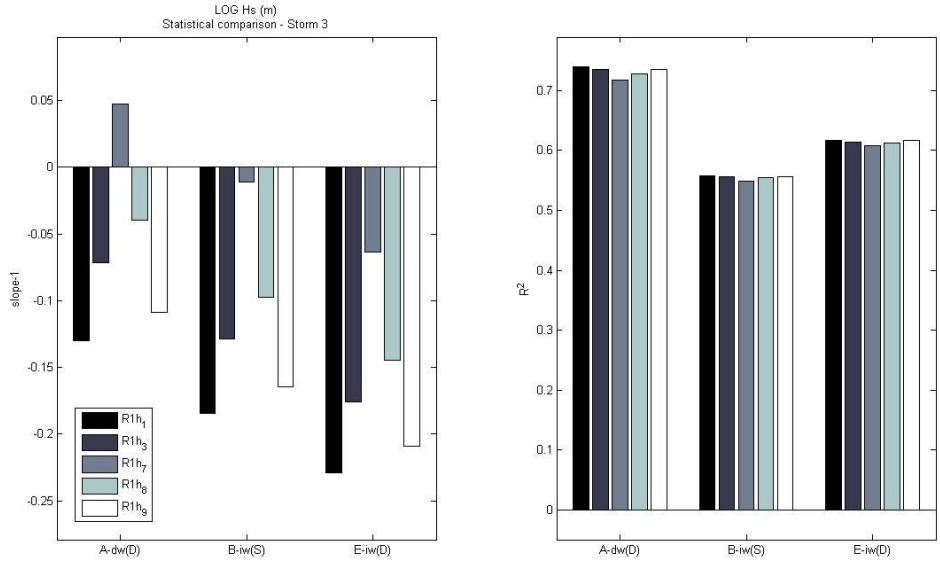

Figure 8.3 Statistical parameters for the comparison of wave height obtained from several model runs, which were calibrated with the different parameters summarized in Table 8.1. Each group of bars correspond to the different buoys/locations used for comparison: A-dw(D), B-iw(S) and E-iw(D). On the left side the *slope-1* obtained from the scatter plot of the loglog variables is plotted. On the right side, the *R2* value is plot, which is a measure of the scatter of the data points along the best-fit line.

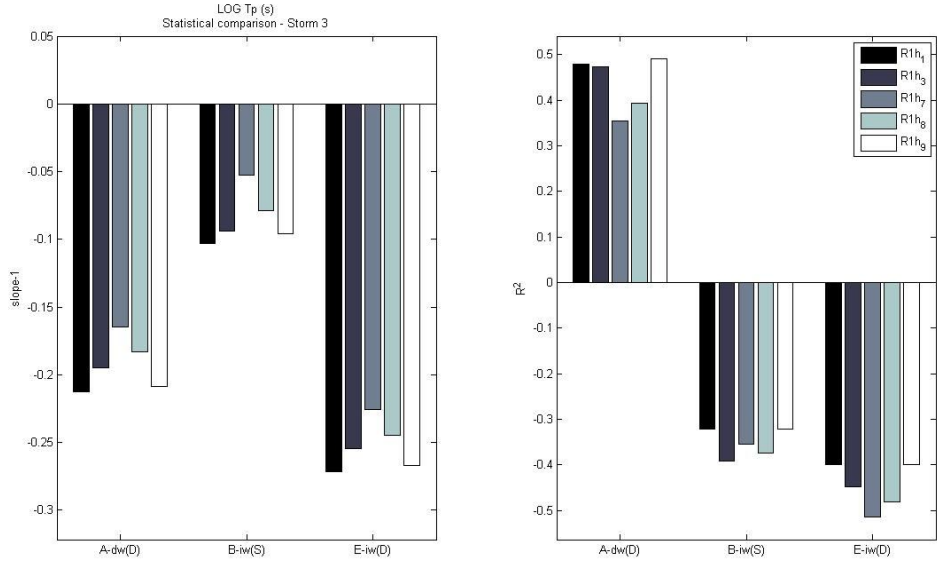

Figure 8.4 Statistical parameters for the comparison of peak period obtained from several model runs, which were calibrated with the different parameters summarized in Table 8.1. Each group of bars correspond to the different buoys/locations used for comparison: A-dw(D), B-iw(S) and E-iw(D). On the left side the *slope-1* obtained from the scatter plot of the loglog variables is plotted. On the right side, the *R2* value is plot, which is a measure of the scatter of the data points along the best-fit line.

8.4. Summary of the results

In the previous chapter I used the scaling law proposed by Kitaigorodskii (1962), and the non-dimensional curves used in JON73 to derive the wave growth curves in a region characterized by variable wind and wave conditions. The development rates obtained were consistently different compared to those derived in previous wave growth experiments and from the simulated data. Due to these differences, I calibrated the tuneable dissipation coefficients of whitecapping processes in SWAN to match the locally derived growth curves.

The results from the calibration of whitecapping in SWAN indicated that the growth rate from the simulations could be increased and could be adjusted to the locally observed growth rates. Accordingly, the estimation of the wave parameters improved and the differences between observed and simulated wave height and peak period were reduced. Although the improvements achieved were moderate and the common under-estimations of the wave parameters were still observed, especially in terms of peak period, the possibility to improve wave estimations was nevertheless proved.

9. Discussion

The path taken in this work is just one of the possible ways towards improving wave estimations in the study area. Although this path was considered the most efficient approach to locally improve wave estimations given the characteristics of the region, it was not exempt from complications and shortcomings. Remember that the general objective of this dissertation is to improve local wave estimations by including mesoscale gradients (variability) into wave growth simulations. The two approaches taken were, first, increasing the model's resolution (grid size and wind input frequency) and, second, adjusting the simulated wave growth rate to the observations. In earlier chapters I showed that improving wave estimations was indeed possible and both approaches contributed, partially, to noticeable progress. However, wave height and wave period still tended to be under-estimated thus indicating that there still was room for improving wave modelling.

Keep in mind that numerical estimations of wave parameters are subject to three main sources of error, as enumerated for example in The WISE Group (2007): the input wind fields, the numerical settings of the simulations, and the physical processes embedded in the model (e.g. wind input and dissipation formulations, and non-linear interactions). In this work, the input wind fields (the first main source of error) were considered to be 'the best it could get'. Indeed, in Chapter 6 the relatively good accuracy of the input wind fields was proved in comparison with measurements both from coastal and at-sea meteorological stations. The good accuracy was achieved both by using initial conditions from re-analysis and by decreasing the grid size (nesting) and increasing the wind output, which permitted to better capture the local gradients.

In spite of the good point-wise accuracy achieved in the simulation of the wind fields, their lack of precision in representing the true wind patterns was evident. For example, it was shown that not all wind jets were accurately predicted and that the overall time series were slightly over-estimated. The main possible reason was the difficulty of simulating winds in mountainous coastal regions, as already pointed out by many authors before (e.g. Cavaleri and Bertotti 1997). Therefore, wind modellers still have work ahead towards improving wind in coastal regions.

All in all, also for slightly over-estimated input wind fields, wave parameters were seen to remain under-estimated. Moreover, the accuracy of the wave estimations was seen to be poorer than that of the input wind fields. These facts provided evidence towards the increasing need for focusing on wave models and

questioning their performance in very demanding situations like those analyzed in this work. Operational wave modelling for larger areas and relatively homogeneous situations, such as those encountered in open oceans, are mainly limited by the wind forecast rather the than wave forecast. Instead, in this chapter, once accepting that the input wind fields used in this work were more accurate than the corresponding wave predictions, the focus was set on exploring the limitations of the wave model itself.

According to The WISE Group (2007), further sources of error in wave models could be the numerical settings and the physical formulations therein implemented. In this work, numerical limitations were especially relevant in association with the increase of the wind input resolution carried out in Chapter 6. The resolution increase of the input wind fields was seen to entail, at least, a matching increase of the wave model's grid size. But small grid sizes usually required a decrease of the integration time step (to avoid numerical diffusion) with the corresponding increase of the model's computational time. These issues are an important limitation to be considered when increasing the resolution of the input wind fields, as discussed in section 9.1.

The second source of error mentioned in The WISE Group (2007) is the parameterization of the physical processes in wave models. The physical processes include the propagation mechanisms (including refraction, shoaling and diffraction) and the wind input and energy dissipation processes (i.e. the balance of energy). In this work, I adjusted the balance of energy according to the wave growth rate derived from observations. In particular, in Chapter 8 I modified the dissipation parameters in the expression for whitecapping to tune the rate of wave growth in the model. Of course, tuning the whitecapping term is not the only way to tune the balance of energy in the wave models; the remaining "source terms", i.e. energy input and non-linear interactions, also play an important role. The limitations of the source terms and their role in representing the balance of energy are described in section 9.2.

Adjusting the rate of wave growth in the model to the observations improved the estimated wave condition but it was not based on physical grounds. In fact, if this solution was to be implemented in sharp-gradient regions around the globe, it would require constant retuning for each individual region. Note that, although recent references point out the need to enhance the growth rate under gradient conditions (see Annenkov and Shrira 2009), the study of wave growth in the region (as presented in Chapter 7) did not result in a more physically-sound adjustment of the wave models. The restricted results of this study, and the limited improvement of wave estimations after tuning the balance of energy, could also be due, in part, to the restricted applicability of the non-dimensional wave growth curves. Thus, in section 9.3 I address the limitations of the non-dimensional curves in terms of describing wave growth, particularly in variable wind conditions.

9.1. Limitations of increasing the wind input resolution

Increasing the wind input resolution in a numerical model has several implications beyond those of increasing the computational grid (in space and in time). These implications are discussed in this section using the simulations described in Chapter 6 and using a battery of test cases in ideal but fetch-limited conditions. The simple test cases were used to describe the differences in H_s and T_p estimations when using the different settings in SWAN; namely, grid size, integration time step and numerical scheme. The different numerical and physical settings of the wave model were changed from test to test to assess its relevance in the model's output (the compared settings are summarized in Table 9.1).

The test cases represented a one-dimensional idealized domain of the case study (fetch-limited wave growth) in both stationary and non-stationary conditions. The domain was 60 km long and the input wind speed was set constant to 10 m/s. Be aware that in stationary conditions the wave model iterates until the wave field is stationary (i.e. unlimited time). In non-stationary conditions the action balance equation is solved for a user-defined time step. Non-stationary runs can also iterate, for each time step, until the change in local H_s and T_p from the previous iteration to the next one is small. The study case in Chapter 6 was calculated in non-stationary conditions, except once, when it was run in stationary mode (see section 9.1.1). The test runs in this section were run both in stationary and non-stationary modes. The results from the test runs were evaluated at checkpoints that were located at distances from the coast similar to the buoys in the case study: 50 km, 20 km, and 1 km.

Table 9.1 Numerical and physical settings explored in the test cases for stationary and non-stationary runs.

Numerical scheme	Spatial resolution (km)	Integration time step (min)	Physics	Non-linear interactions
BSBT	18	60	KOM	DIA
S&L	12	30	WESTH	XNL
SORDUP	4	20	JAN	
	1	10		
		1		

Before getting into the importance of the numerical settings used in the simulations, let me shortly review the general working procedure of the numerical models considered. Spectral wave models, such as SWAN and WAM, calculate the evolution of the wave energy spectra in time and space using the action balance equation. This equation contains the basic energy propagation mechanisms (including diffraction and refraction) and it describes the balance of the wave energy through the so-called source terms. The source terms characterize the energy input from wind to waves, the energy dissipation, mainly through whitecapping in deep-water regions, and the energy redistribution along spectral directions and frequencies due to non-linear interactions among wave components. For a more detailed description of wave models refer to Komen et al. (1994), and The SWAN team (2009).

To solve the wave action equation several numerical schemes can be implemented in the wave models. The model's final solution, however, is tightly related to the selected numerical settings. For this reason, in this section I address the different numerical settings of the SWAN model related to the change of resolution implemented to increase the variability of the input wind fields: the grid size and the integration time step. An additional numerical setting discussed is the numerical scheme used to solve the energy propagation in the geographical space, which is tightly related to both the spatial and temporal grids.

9.1.1. Numerical scheme

SWAN uses different numerical schemes to solve the propagation in the spectral space and the propagation in the geographical space. Propagation in the spectral space is resolved using a hybrid central/upwind scheme particular to SWAN. Propagation in the geographical space, instead, can be solved using three different numerical schemes: BSBT, S&L and SORDUP. Each one of these three schemes was conceived for different target situations and each one has its own limitations, as summarized in Table 9.2. The reader is referred to Rogers et al. (2002) for a more complete discussion on the subject, note that the basic differences between schemes are the order of the numerical scheme (lower order schemes having higher numerical diffusion) and the stability of the scheme. Large numerical diffusion is usually responsible for under-estimation of maximum values and over-estimation of minima. The stability of the scheme is usually related to the Courant number (CN) which is the product of the group velocity (C_g) and the integration time step (Δt) divided by the spatial resolution (Δx):

$$CN = C_g \cdot \frac{\Delta t}{\Delta x} \qquad \textbf{[9.1]}$$

Table 9.2 Characteristics of the numerical schemes available in SWAN model.

Numerical scheme	Numerical diffusivity	Stability	Preferred integration time step	Preferred grid size
BSBT	High	Unconditionally stable	Large and small	Large and small
S&L	Low	CN < 10	Small	Small
SORDUP	Low	Unconditionally stable	Stationary	Large and small

The default numerical scheme in SWAN for non-stationary simulations is S&L (after Stelling and Leendertse 1992; see The SWAN team 2009). S&L is a third order numerical scheme, which is conditionally stable because a diffusion term is added to prevent the Garden Sprinkler Effect (GSE; see also Janssen 2008). This effect describes the splitting of the swell systems into individual swell systems (in the directional space) during swell propagation at coarse spectral resolutions. Because this effect is only important at large oceanic scales, in more local domains, when the Courant number is larger than 10

(stability condition of S&L), it is recommended to use the first order upwind scheme Backward in Space Backward in Time (BSBT) (The SWAN team 2009).

The BSBT is recommended for non-stationary simulations at small scales because it is unconditionally stable (at least when the source terms are set to 0, i.e. no energy input or dissipation is considered, as reported by Rogers et al. 2002). However, if larger scales are also considered, Rogers et al. (2002) showed that the first order schemes (such as BSBT) tend to under-estimate the maxima and to over-estimate the minima due to large numerical diffusion. To overcome this problem small integration time steps are recommended.

Alternatively, Rogers et al. (2002) suggest using a sequence of stationary runs (e.g. second order upwind scheme SORDUP) for local scales and almost stationary conditions (such as fetch-limited situations). Although this approach is less suitable if duration limited situations are likely, SORDUP is unconditionally stable and less diffusive than BSBT. Note that in the present case study, in variable wind conditions, it was very difficult to tell apart fetch and duration limited situations because wind speed was rarely constant over time or space. Remember also that fetch limited conditions assume a constant wind blowing over a limited fetch for unlimited time, whereas duration limited growth assumes a constant wind blowing over unlimited fetch for limited time. In variable conditions, instead of stationary conditions, sea states from mixed origins are expected. Thus, the stationary approach did not seem the most convenient to simulate the case study considered. Nonetheless, I ran the case study in stationary mode to verify the unsuitability of this approach in the region of interest.

The results from the series of stationary computations (every 3 h) indicated that some H_s peaks were estimated earlier in time than recorded (1 - 3 h) (as expected; not shown). Also, the estimation of certain maxima and minima was enhanced because the model was set to reach stationary conditions for each single wind field. Stationary runs were very dependent on the input wind fields used and whether they represented the wind speed peak values or not. Also, stationarity assumed that waves responded immediately and completely to wind speed changes, which was not always true, as it was shown in Figure 5.5 of Section 5.2. In any case, the H_s under-estimations of the main peaks observed in non-stationary runs were not improved using a set of stationary runs. These limitations, together with the larger computational time needed, made the stationary approach less suitable to model wave conditions in variable wind situations.

The case study in Chapter 6 was run using the BSBT numerical scheme because it was easier to find a compromise between accuracy and computational time for lower order numerical schemes. Although computational cost was not limiting, the settings used provided results that were very close to the best estimations achievable with the present tools, as it is shown below.

9.1.2. Integration time step

The real-situation case study (storm nº3) was generally run with an integration time step of 20 min; this value was chosen based on several considerations. First, the selected integration time step was chosen so that the numerical velocity ($\Delta x / \Delta t$) of the model was able to simulate the physical velocity of the wave trains to be estimated. The physical velocity was the representative velocity of the wave trains in the region and it was calculated using the relationships from KC92 for a given fetch distance and wind speed. According to KC92's parameterization, for wind speeds of 10 m/s, and 55 km fetch, one would expect peak wave periods smaller than 5 s at the most offshore buoy. Assuming linear theory equations to be valid in fetch-limited growth conditions, wave group celerity for such peak periods would be less than 4 m/s. In 20 min these waves would travel less than 5 km. Therefore, for a wave model's grid size of 4 km and an integration time step of 20 min, the physical velocity was estimated to be only slightly higher than the numerical solving velocity of the model.

The relationship between numerical and physical velocities could be expressed in terms of the Courant number (CN) defined in equation [9.1]. For the above grid size and time step CN was equal to 1.2, which indicated that no stability problems were to be expected for a 20 min time step and S&L numerical scheme. However, if the grid size was to be decreased to 1 km, to better resolve the coast and bathymetrical singularities, stability problems could arise with the higher order S&L scheme (if the time step was not accordingly reduced). This reasoning also justified using the unconditionally stable BSBT scheme to simulate the case study.

The sensitivity of the BSBT scheme in SWAN to the integration time step was explored using the test cases in non-stationary conditions. The results from these tests are shown in Figure 9.1 and indicated that wave height increased faster and reached higher equilibrium values when shorter integration time steps were selected. The large differences reported were due to the high diffusivity of the numerical scheme (BSBT) for large integration time steps. In fetch-limited situations, when the integration time step was set to 20 min the wave height needed almost 10 h to reach the full development (Figure 9.1). When the integration time step was reduced to 1 min, fetch-limited wave height was reached in almost 5 h (not shown), no matter the grid size of the model. In other words, the larger the integration time step, and the smaller the grid size, the longer it took for the BSBT scheme to reach stationary conditions.

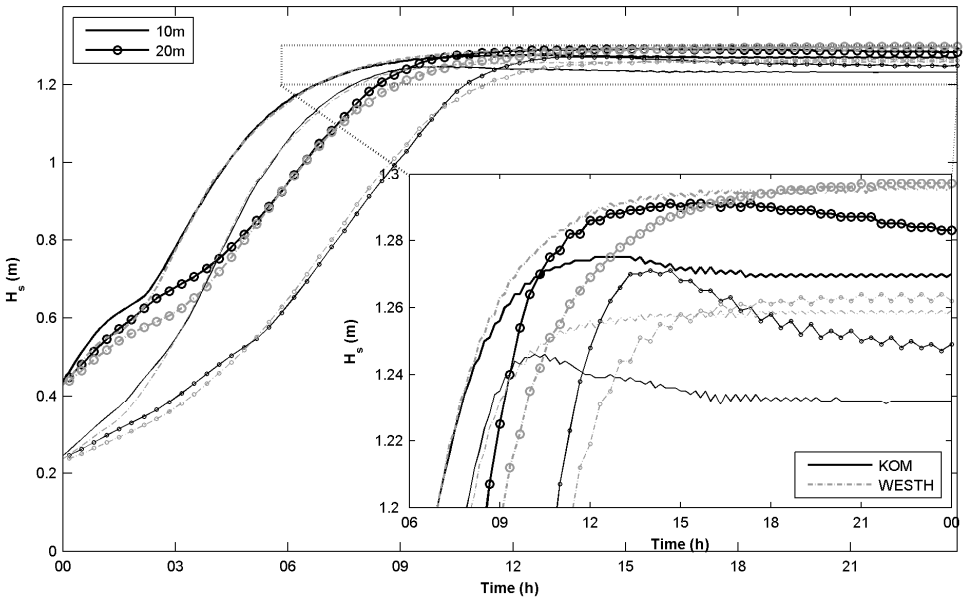

Figure 9.1 Wave height from a non-stationary test case in fetch limited conditions and constant wind speed (10 m/s). Data corresponds to a position 50 km offshore. Two spatial resolutions are shown: 4 km (thicker lines and bigger circles) and 1 km. The input and dissipation formulations are KOM (black lines) and WESTH (grey lines). Two integration time steps are plotted: 10 min (no marker) and 20 min (circles). The inner panel is a close-up of the last hours (from 9 h – 24 h), when the simulation reached stationary conditions.

The effect of the integration time step in the simulation of the real case study was different than in the test cases. Figure 9.2 depicts simulated H_s time series using high resolution wind fields (4 km / 3 h) and running SWAN at 1 km spatial resolution, using a first order numerical scheme and different time steps. In terms of timing, the difference between 20 min and 1 min time steps was focused on the peak of the storm, which was reached 1 h earlier (case study) instead of 5 h earlier (test case). In terms of wave height, slightly larger differences were observed in the real case study compared to the test cases. Although the difference was not very important, remark that in the case study, wave height simulated using 1 min time step was 0.05 m higher than using 20 min. Note, however, that this small improvement involved a 20-times increase of the computational cost.

The results of the case study also indicated that if very large integration time steps were considered (1 h) the peaks of the storm in terms of wave height were missed, as expected for high diffusivity schemes and large time steps. In this case, for the same input winds, the difference in growth time using either 1 h- or 20 min-time steps was 2 h and the wave height difference was about 0.5 m (look for example in Figure 9.2 at the third peak of the storm on the 10 Dec.).

Summarizing, at shorter time steps, wave growth rates and maximum wave heights increased. For the simulations of the case study the computational time step was set to 20 min as a compromise between the

accuracy and the computational time, the ability to describe the physical processes (wind and wave peaks) and the timescale of the measured processes (frequency of the measurements: 1 h).

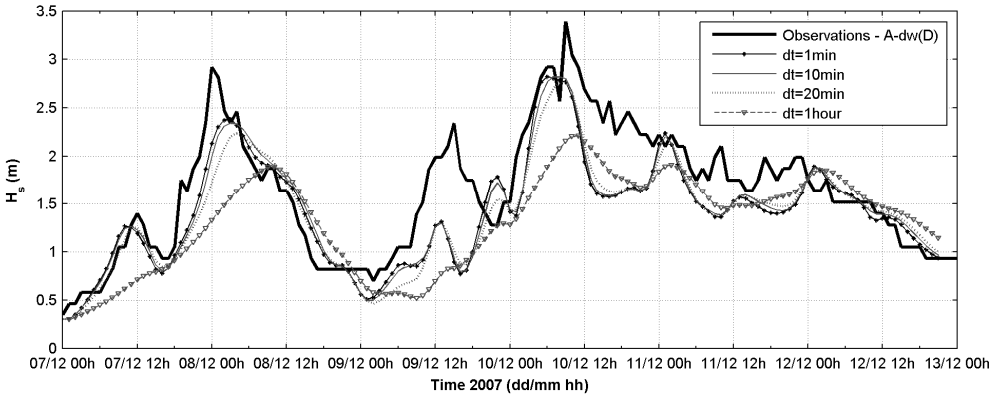

Figure 9.2 Wave height from 7 Dec. to 13 Dec. 2007 estimated using SWAN at 1 km spatial resolution and four different integration time steps: 1 h, 20 min, 10 min, and 1 min. Input wind fields were provided by MM5-4km/3h. SWAN was run using the BSBT numerical scheme and KOM physical formulations.

9.1.3. Grid size

The inaccuracies of the numerical simulations in terms of the grid's size were also explored using the test model settings discussed above. In the stationary test case shown in Figure 9.3, H_s and T_p were slightly lower for finer spatial resolutions (e.g. 1 km), as expected in terms of numerical diffusivity of the BSBT scheme. In the real-situation case study, in agreement with the test results, the higher resolution models slightly enhanced the under-estimation of the maxima and minima of the time series. Nonetheless, decreasing the grid size of the wave model did not produce a relevant difference in the statistical fit parameters compared to coarser resolution simulations. T_p estimations were also slightly worse with the higher spatial resolution runs (both statistically and visually).

The choice of the wave model's grid size was a compromise between the need to resolve the spatial features of the wind field and the coastal geometry, and the diffusivity of the numerical scheme. The reason is that finer resolution models used more grid points to represent the same physical distance and thus, the higher diffusivity of first order schemes resulted in under-estimation of the maxima. To counter-act the high diffusivity of the propagated wave trains when using the BSBT scheme, the integration time step was to be accordingly reduced.

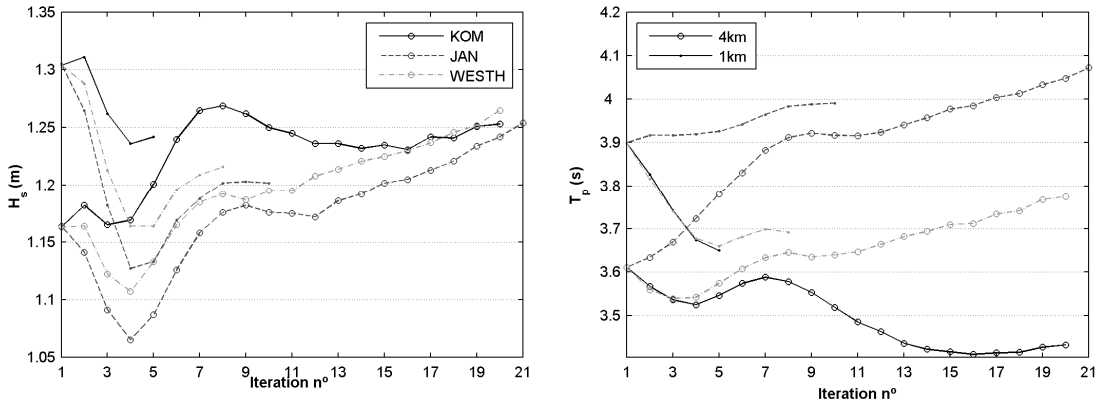

Figure 9.3 Significant wave height (left panel) and peak period (right panel) calculated from a test case in stationary conditions and constant wind speed (10 m/s). Data corresponds to a position 50 km offshore. Two spatial resolutions are shown: 4 km (big circles) and 1 km (small circles). The input and dissipation formulations are KOM (black), JAN (dark grey) and WESTH (light grey).

Summarizing, if the spatial resolution of the models is increased, the integration time step should decrease, either to reduce the numerical diffusion of the numerical scheme or to avoid stability problems. However, the results presented in this section confirmed the limited value of increasing the spatial resolution of the wave model above that of the input wind fields, unless the particular features of the coastal geometry were to be resolved. Also, further decreasing the time step, if anything, would only slightly adjust the maximum values of the wave parameters and the timing of the storm peaks, at expenses of increasing the computational time. To conclude, in the study case, the common under-estimation of the wave parameters could not be essentially attributed to the numerical settings chosen.

9.2. Limitations of the parameterization of the source terms

In Chapter 8 of the present work I showed that tuning the dissipation coefficients of the SWAN wave model to match the simulated and the observed growth rates improved the estimation of the wave parameters. The reported improvement, however, was not large enough to over-come the under-estimation of the wave parameters, which still persisted. The first possible source of error considered was the parameterizations that describe the balance of wave energy in the wave model (i.e. the source terms), as addressed in this section. The second source of error considered was the accuracy of the wave growth rate calculated, as addressed in next section 9.3. The physical processes (source functions) active during the case study and the test cases were wind input, dissipation through whitecapping and quadruplet interactions.

The expression for whitecapping in SWAN differs depending on the wind input parameterization because it depends on a parameter that is estimated by closing the energy balance equation (source terms included) in fully developed conditions (see The SWAN team 2009). Quadruplet interactions are a nonlinear wave-wave interaction process that is commonly estimated using the Discrete Interaction

Approximation (DIA) proposed by Hasselmann et al. (1985). All three source terms are balanced and should be considered altogether as a single wave input term. The reader is referred, for example, to the work of Rogers et al. (2003) for an interesting discussion on the balance of source terms and its limitations. In this work, in particular, I focused on the expression for the dissipation as the tuning knob of wave models due to the well-known uncertainty linked to its parameterization (The WISE Group 2007). In this section I explored the different parameterizations of the source terms implemented in SWAN wave model and I addressed the accuracy levels that could be achieved as they were presently implemented.

9.2.1. Wind input and whitecapping

There are three different wind input and dissipation formulations implemented in SWAN 40.72ABCD. The default, and most used, parameterization is due to Komen et al. (1984) (KOM). The second formulation, which is the default in WAM, depends on the existing sea state and was described by Janssen (1989, 1991) (JAN). The third and newest formulation is a modification of KOM to improve the dissipation term and was described by Van der Westhuysen et al. (2007) (WESTH).

The test cases described in section 9.1 were used here to assess the performance of each physical parameterization in terms of H_s and T_p. The results in Figure 9.3 showed that H_s grew higher and faster when using WESTH. However, at the most offshore position, H_s estimated using the WESTH formulation was only 1% higher than with KOM, and 7% higher than with JAN. T_p was larger when JAN formulation was used. Again at the most offshore buoy, T_p was 9 % higher with JAN than when using WESTH, and 24% higher than with KOM. Notice that when using KOM formulations convergence was reached faster; i.e. a smaller number of iterations was needed to reach the fetch-limited value. Note that the percentages are approximate; they were calculated using the wave height achieved after reaching convergence in stationary mode (see Figure 9.3).

In Figure 9.1, H_s values were estimated using a 24 h non-stationary simulation for both KOM and WESTH parameterizations. Note that the differences observed between both formulations were similar in non-stationary and stationary conditions. Also, JAN formulations in SWAN experienced convergence problems in non-stationary runs due to the numerical scheme implemented as discussed further on.

The differences reported between the parameterizations are representative of the different equilibrium of the source terms (input, dissipation and non-linear interactions) in each formulation and how they balance each other. For example in non-stationary runs, Figure 9.4 shows that the non-linear interactions at the spectral peak were more important in JAN than in the other formulations (up to three times larger). This effect is related to the pronounced shape of the wind input spectral peak in JAN (as suggested by Badulin et al. 2005). In effect, notable differences were also observed when comparing the amount of wind input and wave dissipation in each formulation, as depicted in Figure 9.4.

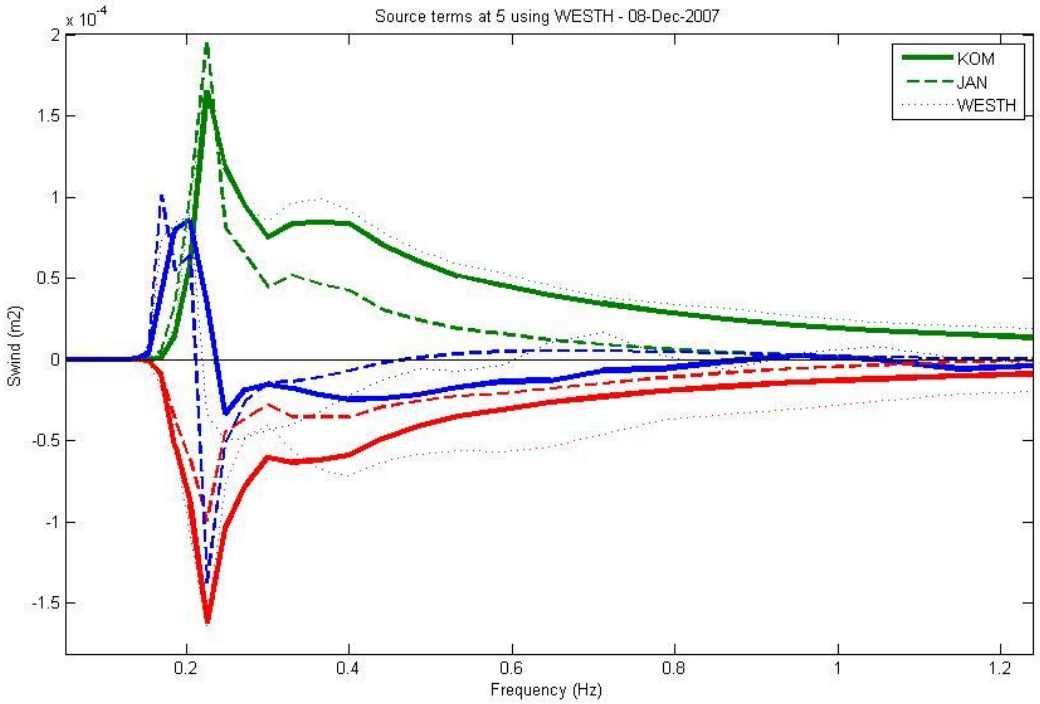

Figure 9.4 Source terms in SWAN wave model calculated using the three implemented physical parameterizations (KOM, JAN and WESTH) during a simple test case in fetch-limited wave growth conditions. The green lines describe the energy input from wind to waves, the red lines represent the energy dissipation due to whitecapping and the blue lines depict the energy transfer due to the non-linear interaction term.

The differences reported between the parameterizations implemented in SWAN explained why there still is no agreement within the wave modelling community; the reason is that the exact process of wind input and dissipation is still unclear. Fortunately, the balance of the three source terms, although individually disparate, lead to more than acceptable estimations of the integrated wave parameters, as shown throughout this work. Nonetheless, it is inevitable to think that this important lack of knowledge could be the reason for the mis-estimation of the wave parameters in complicate wave growth conditions, as already mentioned many times.

For example, the inaccuracy of the source terms (KOM and JAN) and their balance was thoroughly addressed in Rogers et al. (2003). Additionally, at present times, a significant effort is being done within the wave modelling community towards improving the model's source terms (e.g. Ardhuin et al. 2010, Banner and Morison 2010, Donelan et al. 2006, Tsagareli et al. 2010). Meanwhile, in this work I chose to use the frequently used KOM formulations in spite of the limitations reported by other authors (e.g. Ardhuin et al. 2010) because they converged faster, had no identified stability problems, and they had been thoroughly used and validated in the literature and are, thus, directly comparable to what could be called the standard 'state of the art'.

9.2.2. Non-linear interactions

To calculate the amount of uncertainty within the implementation of the non-linear interactions term, I tested some of the different methods included in SWAN; namely, the DIA approximation (as mentioned above) and the XNL approach. The XNL approach calculates the exact interactions and was implemented in SWAN by Van Vledder (2006). The XNL approach is more accurate than DIA but it also is 10^3 to 10^4 times more expensive computationally. The results from the test cases (not shown) indicated that during simplified fetch-limited conditions, compared to the exact method (XNL), the DIA approximation estimated higher H_s and T_p (between 4% and 13% depending on the wind input formulation).

Although DIA is an approximation to reduce the computational time needed to solve the full equation, its accuracy appears to be satisfactory enough and it is the best operational tool available (i.e. acceptable computational cost). Moreover, from the present results it follows that the DIA approximation could not be responsible for the under-estimations of the wave parameters reported. Note that the difference between both methods was larger for KOM than WESTH or JAN, which emphasizes again the importance of addressing altogether the balance between wind input and dissipation terms plus the non-linear interactions term.

9.2.3. Numerical scheme and action density limiter

SWAN uses different numerical schemes to solve the propagation of the energy in the geographical space (see section 9.1.1 above), in the spectral space (hybrid central/upwind scheme particular to SWAN), and to resolve the source terms. To approximate the source terms SWAN uses an almost implicit numerical scheme, which in turn uses the so-called action density limiter to ensure convergence. This limiter restricts the maximum energy change per time step: KOM and WESTH parameterizations limit it to a fraction of the omni-directional Phillips spectrum (Booij et al. 1999) and JAN uses the dynamic limiter suggested by Hersbach and Janssen (1999).

The two different limiters used in SWAN, which depend on the parameterization of the source terms, are discussed in Tolman (2002), and the references quoted therein, and in Zijlema and van der Westhuysen (2005). It is relevant to note that, in the literature, large under-estimations of the models have been related to the effect of these limiters. The inaccuracy of wave models due to the limiter is seen to be especially relevant at very early stages of wave growth and, thus, under variable wind conditions. In Hargreaves and Annan (2001) they discussed different solutions (including removing the limiter) but they acknowledge that the limiter works fine in many applications, one exception being the high resolution coastal applications (such as the present case study). The implications of the limiter in SWAN are also addressed in The SWAN team (2009) but no definite solution or alternative is generally accepted.

Note that the integration time step mentioned in previous sections also has a crucial effect on the action density limiter, as discussed in Tolman (2002) and Niclasen (2006). These authors report larger under-

estimations for larger time steps. Although the under-estimations decrease with smaller integration time steps, the computational cost is expected to increase accordingly. In Niclasen (2006) they also describe a non-convergent behaviour of SWAN with the JAN parameterization (for large time steps; i.e. more than 10 min) that they attribute to a deficiency in the implementation of the limiter (see below).

Our results also suggest that the role of the action density limiter could also be a major source of error within the wave models, especially in the region of study. Because the limiter is tightly related to the parameterization of the balance of energy, the large uncertainties it entails provided further evidence towards pointing to the source terms as a major source of error in wave forecasting.

9.2.4. Stability issues

During the simulation of the case study, I noticed that the stability of the BSBT numerical scheme was seriously compromised when JAN formulations were used. In particular, for time steps larger than 5 min JAN failed to converge and the estimated wave height reached abnormally high values. In other words, the BSBT scheme with JAN formulation in the source terms was only conditionally stable. The reported instability was observed to be different for the different spatial resolutions, as expected according to the Courant number stability condition.

A stability analysis of the different numerical schemes used to solve the propagation was already performed by Rogers et al. (2002). These authors concluded that BSBT was unconditionally stable if no source terms were included in the right side of the wave action equation. Rogers et al. (2002) also validated the results with source and sink terms and concluded that although the numerical schemes worked just as well with or without source terms, it was possible –'even likely'- that the numerical analysis was invalid when these terms were included. Rogers et al. (2002) were, thus, opening the door to a possible stability problem of the so-called 'unconditionally stable' numerical schemes. Indeed, the results presented in the present work suggest that the BSBT scheme was not unconditionally stable when the source terms were set according to JAN.

Niclasen (2006) already studied the excessive wave heights during storm events obtained when using JAN's physics and pointed to an implementation deficiency of JAN's formulation in SWAN. More specifically, they referred to the implementation in SWAN of the action density limiter (originally formulated for WAM by Hersbach and Janssen 1999). Niclasen (2006) suggested to omit high frequencies or to decrease the computational time step to prevent the implementation error and concluded that the most 'economical' time step giving good results was about 10 min. Because his conclusions were obtained using SWAN's default numerical scheme (S&L) it was likely that the convergence problem occurred for both the BSBT (used in this work) and the S&L numerical schemes.

Summarizing, the parameterization of the source terms in spectral wave models contained a large degree of uncertainty, especially when simulating fetch-limited wave growth (as already reported by Rogers et

al. (2003) for different wind conditions). On one side, the different parameterizations implemented in SWAN, and commonly used in the literature, were seen to estimate very different values of each specific source term (input, dissipation, non-linear interactions) in the same simple conditions. Fortunately, because the source terms balance each other, the estimations of the integrated parameters were not very different from one formulation to the other. On the other side, the numerical schemes used to solve the source terms were seen to be highly dependent on a rather unphysical parameter (the action density limiter) which, in turn, could lead to stability problems. All in all, the parameterization of the source terms was associated to a large degree of uncertainty which, if a ranking was to be made, would probably take it to the first element of the list; i.e. the source terms would be the first element in wave models needing to be improved. Additionally, the large uncertainty described, and the fragile balance of the source terms, easily explains the limited improvements achieved in this work when adjusting the growth rate in the model.

9.3. Limitations of the non-dimensional growth curves

In previous sections I addressed the limitations inherent to the wave model itself and their role in the restricted improvement achieved in estimating wave parameters. I also concluded that the large uncertainties within the parameterization of the source terms could be responsible for the limited improvements achieved when tuning dissipation in the model. Additionally, the limited improvement achieved could also be related to the growth curves used to tune the wave model, as shown below. The method used to describe wave growth in the region (the non-dimensional growth curves) is also restricted, especially in variable wind regions.

The wave growth rate calculated in Chapter 7 is subject to two main sources of uncertainty. The first one is the suitability of the data used, which deviates from the 'ideal' wind conditions required. The second, and main, one is the disadvantages of the non-dimensional growth curves as a method to study wave growth. The suitability of the data used could be questioned for several reasons. For example, the dataset lacked directional information and wind measurements at all buoy positions. Also, wind conditions were neither homogeneous nor stationary, thus departing from the ideal conditions for which the non-dimensional growth curves were designed. These shortcomings were especially important given the high variability of wind and waves in the region of study, but they were seen to be reduced after accurately selecting wave energy, peak frequency, fetch and wind speed. Moreover, the numerous studies in the literature also had to deal with real conditions (which are rarely ideal) and they still obtained comparable growth rates.

The second source of uncertainty of the growth curves is the intrinsic shortcomings of the methodology, which although already known, had been barely addressed altogether and discussed as a whole. This is the main reason why, in this section, I describe these shortcomings in detail and I discuss the reasons for

which they could limit the growth curves as a tool to study the wave growth at the small scales and variability conditions of interest. The outcome of this analysis contributes to improve the wave forecasting in the region since it points out the need to find alternative ways to characterize the wave growth in 'gradient' regions.

9.3.1. Limitations of the current procedure

The non-dimensional curves are widely used in the literature since JON73 and the large differences between the expressions calculated in the different field experiments are well known. Although a lot of authors attempted to reduce the reported differences and the scatter of the curves, the truth is that a single relationship applicable to all conditions and locations has not yet been found. For example, Bottema and van Vledder (2008) questioned the ability of the considered growth curves to properly describe their experimental data and they urged for additional measurements to quantify the range of validity of the existent expressions because of their widespread use to tune wave models. The differences found in this study, and presented in earlier chapters, are an additional and clear example of the level of uncertainty within these curves.

Furthermore, Badulin et al. (2007) emphasized the early doubts expressed in Donelan et al. (1992) towards the validity of a single growth function to describe wave growth in all situations/conditions. According to the weakly turbulent law, Badulin et al. (2007) argued that no universal function should be expected for wave growth. Instead, they derived a fixed relationship between the rate of energy development (b) and the rate of frequency downshift (c) (see equation 2.38 in Badulin et al. 2007).

$$b = \frac{10 \cdot c - 1}{2} \qquad \textbf{[9.2]}$$

The function reported by Badulin et al. (2007) (equation [9.2]) is plotted in Figure 9.5, where it is compared with the rates derived in this work (in Chapter 7) and the rates reported by some authors previously (vertical and horizontal lines in the plot). The comparison showed that the development rates calculated for the region of study (and reported in Table 7.3 and Table 7.4) differed considerably from the empirical rates reported earlier on. As depicted in Figure 9.5, most of the growth rates calculated in this study lay above, and beyond, the highest growth rates reported by previous authors: the horizontal line $b = 1$ is the largest rate of energy development, and the vertical line $c = 0.33$ is the fastest rate of frequency downshift. Figure 9.5 confirms that the rates calculated in this study were, in general, much higher than those from KC92 both in stable and unstable atmospheric conditions, as mentioned in previous chapters.

Last, but not least, notice that the growth rates plotted in Figure 9.5 are largely scattered along the relationship [9.2] (diagonal blue line) presented by Badulin et al. (2007). Note that Badulin et al. (2007) compared their suggested theoretical relationship with earlier experiments and they reported large

deviations for experiments which could not be explicitly regarded as fetch-limited. Deviations were observed, for example, for data sets which included different wind/wave conditions (e.g. KC92 composite dataset which included stable and unstable atmospheric conditions). Deviations in the present dataset could also be due to the complexity of wave growth in the region.

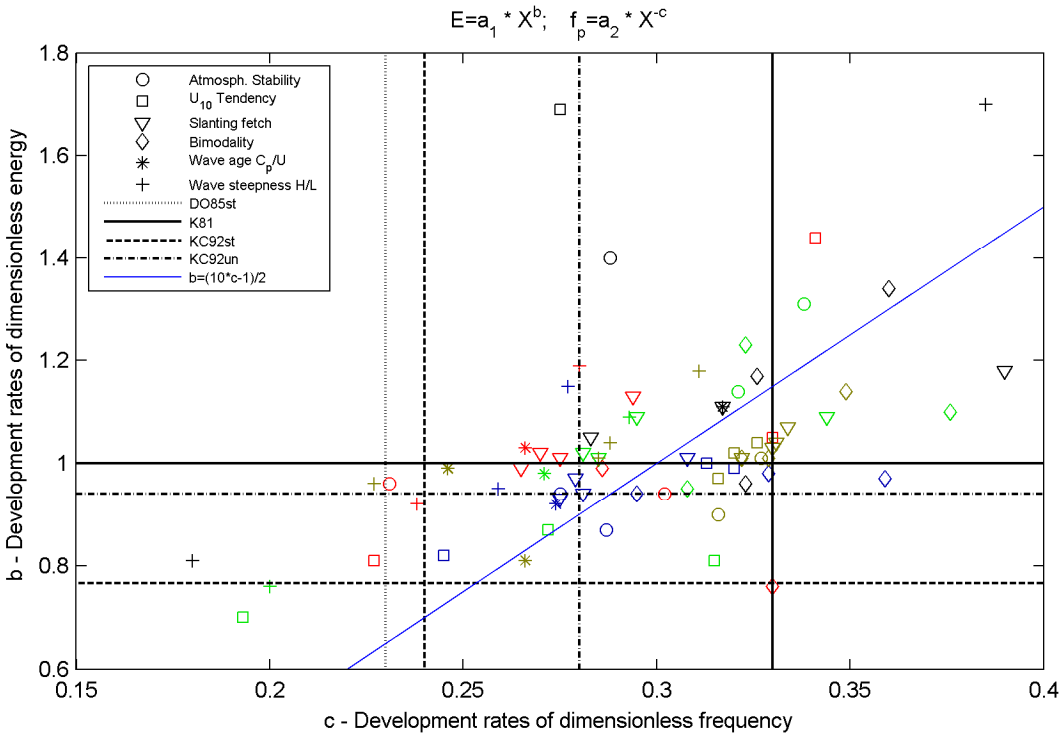

Figure 9.5 Graphical representation of the large differences between the development rates observed in this study. The development rates of dimensionless energy (b) and peak frequency (c) along dimensionless fetch are plotted for the different internal wave properties and external forcings analyzed (and reported in Table 7.6 and Table 7.7). Note that not all the rates in the tables are plotted in this figure because they are out of the figure limits. Horizontal and vertical lines indicate the reference energy and frequency development rates reported by other authors in earlier experiments (see Table 7.1). The diagonal line indicates the theoretical relationship derived in Badulin et al. (2007) (see equation [9.2]). The colour scale indicates the data sets used to calculate the rates: A-dw(D) in green (RIMA-Med) and brown (2004 - 2009); B-iw(S) in red; E-iw(D) in black; all RIMA data in blue.

In this direction, in Chapter 7 I explored the influence of the dimensional data on the growth curves and the deviations from ideal fetch-limited conditions. Also, I explored the effect of different external environmental forcings and internal wave properties but it was not possible to reduce the scatter of the curves and the differences compared to earlier experiments, as clearly shown in Figure 9.5. In this chapter, to focus on the observed differences and to better understand wave growth in the region, I examine closely the data points within the multi-fetch curves and their associated energy spectrum. Although not shown, I also plot the progression in time of the non-dimensional values in order to represent temporal variations in a similar way to that presented in Hwang et al. (2011). The results, in spite of their variability, brought to light the many limitations of the considered methodology as a method

to describe wave growth. These results called for an in-depth description of each single constraint of the method itself.

The following sections address the inherent limitations of the growth curves, paying particular attention to the particularities of variable wind situations. First, I describe the well-known spurious correlations and, then, I address the problem of using wind speed to widen up the range of non-dimensional fetch (especially in single-fetch datasets). Also, I discuss the intrinsic relationship between the dimensional variables and the lack of physical interpretation of the curves as they are commonly used. Last, I briefly discuss some growth processes particular to wave growth in variable wind conditions, which could not be satisfactorily isolated in the previous section but which could also limit the applicability of the curves (i.e. diffraction, duration-limited conditions and the presence of old sea).

9.3.1.1. Spurious correlations

One of the best well-known limitations of the non-dimensional curves is the so-called "spurious correlation". This term refers to the inherent correlation between the non-dimensional terms on x- and y-axis (see for example Kahma and Calkoen (1992) and Young and Verhagen (1996), or Kenney (1982) for a sound discussion). Spurious correlations can lead to misleading relationships between the non-dimensional variables, as discussed below. The origin of the spurious correlation is the common factor g/U^2 used to non-dimensionalize both energy and fetch. In the case of the frequency growth curves the common factor inducing the spurious correlations is g/U. To demonstrate the origin of the spurious correlation it is necessary to start from the non-dimensional variables defined in previous Chapter 7, which are written again below:

$$\overline{E} = g^2 \cdot E / U^4 \qquad \textbf{[9.3]}$$

$$\overline{X} = g \cdot X / U^2 \qquad \textbf{[9.4]}$$

Expressing U in terms of non-dimensional fetch and replacing it in the expression for the non-dimensional energy ([9.3]) the following simplified equations are obtained:

$$\overline{E} = \frac{g^2 \cdot E}{\left(g \cdot X / \overline{X}\right)^2} \qquad \textbf{[9.5]}$$

$$\overline{E} = \frac{E}{X^2} \cdot \overline{X}^2 \qquad \textbf{[9.6]}$$

In a log-log representation, equation [9.6] could be written as equation [9.7], where the factor of **2** between the variables in both axes becomes evident. In other words, even if no correlation between the variables existed, there would always be a misleading spurious correlation due to the factor g/U^2 on both sides of [7.2], which inherent relation is equal to 2.

$$\log\left(\overline{E}\right) = \log(\mathrm{E} / \mathrm{X}^{\mathbf{2}}) + \mathbf{2} \cdot \log\left(\overline{X}\right) \qquad \textbf{[9.7]}$$

In the same way, the spurious correlation between non-dimensional peak frequency and non-dimensional fetch is equal to **-1/2**, because its common factor is *g/U*.

$$\log\left(\overline{f}\right) = \mathbf{1} / \mathbf{2} \cdot \log(\mathrm{X} \cdot f_p{}^{\mathbf{2}} / \mathrm{g}) - \mathbf{1} / \mathbf{2} \cdot \log\left(\overline{X}\right) \qquad \textbf{[9.8]}$$

Fortunately, in this work, the development rates generally derived from the observation (slope of the fit function) were approximately **1** for the energy and approximately **1/3** for the peak frequency, which are values far enough from the spurious correlations (**2** for energy and **1/2** for peak frequency) and avoid misleading interpretations. Note that because the spurious correlation is inherent to the scaling law used, whenever the observed correlation is close to the spurious one (within the 95% confidence intervals), both correlations (real, if any, and spurious) cannot be told apart.

For example, all growth functions derived with data from buoy D-sw(S) were too close to the spurious correlation to provide any valuable information about real wave growth: the spurious correlation resulting from the dimensional energy and fetch was quadratic (*b*=**2**). Buoy D-sw(S) was located very close to the coast in a partially sheltered bay, at the entrance of the harbour. On the one side, fetch-limited data at this location was often contaminated with longer waves coming from other offshore directions. On the other side, the buoy was not able to measure high frequency waves generated in fetches shorter than 1 km (early stages of wave growth). The reason is that, according to KC92's growth laws, at the buoy's fetch and for the range of wind speeds considered, the expected peak frequency is too close to the instrument's frequency resolution.

The development rates calculated using data from buoy E-iw(D) were also often spurious. At this buoy, the reasons were thought to be the low representativeness of the wind speed used to non-dimensionalize the data, and the limited amount of pure sea data since, at this location, more than 50% of the sea states are usually bimodal (according to Bolaños et al. 2009).

9.3.1.2. Using wind speed to enhance non-dimensional fetch coverage

Many experimental studies, after the revealing JONSWAP experiment (JON73), such as the reference paper from DO85, used data from a single measuring instrument only (single-fetch). In such experiments, variation in the non-dimensional fetch was artificially introduced through consideration of variations of

wind speed. Experiments of this sort were presented by Ewing (1980), Ewans and Kibblewhite (1990), Babanin and Soloviev (1998), Ataktürk and Katsaros (1999), Hanson and Phillips (1999) and Violante-Carvalho et al. (2002).

A range of wind speeds are traditionally used to widen up the range of non-dimensional fetch values because higher wind speeds need longer fetches to reach the same fetch-limited state than lower wind speeds at shorter fetches. In low wind speed situations waves are soon limited by fetch (short fetches), but the difference compared to the fully developed state should be comparable to the difference in higher wind speeds. As a consequence, for the same amount of energy (or frequency), high (low) wind speeds are associated with low (high) dimensionless fetches and energies, thus creating a range of non-dimensional fetch values 'artificially'.

Notice that within the log-plot of the non-dimensional growth curves, high wind speed situations are plotted on the lower-left side of the plot and lower wind speed values are plotted on the upper-right side, because in equations [9.3] and [9.4] wind speed is in the denominator. According to the authors that use single-fetch data only (see above), the relationship between both non-dimensional terms is the same development rate that is obtained using different instruments measuring at different physical fetches (multi-fetch). In the case study here presented this assumption proved not to be always valid, because the development rates obtained using single-fetch data tended to be slightly higher than the development rates obtained using multi-fetch data (as shown in Chapter 7). There are three main reasons for the different development rates obtained using single-fetch data in this study. The first one is the unsuitability itself of using a single fixed instrument to describe wave growth along the fetch instead of, for example, just describing wave growth as a function of wind speed. This shortcoming was already pointed out by Badulin et al. (2007), who excluded single-fetch data sets from their analysis. Badulin et al. (2007) attributed the comparable development rates obtained in such experiments to simple coincidence.

The second cause of the different development rates obtained from single-fetch curves was linked to the lack of in-situ wind measurements. Remember that wind speed at buoy A-dw(D) was used both to separate wind sea and swell and to scale the dimensional variables from all buoys. Even though I showed in section 7.3.2.2 that wind speed at buoy A-dw(D) could be used as a measure of wind speed at the other buoy's location, it might not be representative enough of the along-fetch variability, not even in terms of the non-dimensional curves. This lack of representativity could be responsible for the slightly different development rates observed.

In fact, notice that if the wind speed at A-dw(D) was higher than real wind speed at the buoys (due to increasing wind speed in the transition zone), then the non-dimensional energy would be lower than in reality. Then, the non-dimensional data points would be plotted below the reference curves on the left-hand side of the plot. The opposite would occur if wind speed at A-dw(D) was lower than in-situ wind

speed: higher non-dimensional energy would be observed (above the reference curves). Indeed, in section 6.4.3 I reported that maximum wind speed values along coastal jets occurred somewhere in between buoy A-dw(D) and the coast. Thus, wind speeds at the buoy were lower than along the fetch, thus favouring non-dimensional data points above the reference curves and, eventually, inducing to higher rates of wave growth.

The third cause of the different development rates obtained at buoy A-dw(D) only was thought to be an inaccurate separation of wind sea and swell in all kind of wind conditions (as suggested e.g. in section 7.4.5). If more energy was considered to be wind sea than there really was, then the non-dimensional data points would fall above the curves calculated in earlier experiments. This could either increase the growth rate (slope of the fit line) or just shift the fit line along the y-axis.

9.3.1.3. Relationships between the scaling variables

I mentioned above that wind speed was used to scale the variables to favour the non-dimensional comparison of wave growth at both long and short fetches and low and high wind speeds. Although non-dimensional growth curves have been presented as a method to describe the non-dimensional wave growth along non-dimensional fetch, wave growth in fetch-limited conditions is not only directly dependent on fetch, but also on wind speed. Therefore, growth functions not only represent the relationship between the wave parameters and fetch, but they also characterize the relationship between waves and wind speed.

Note, for example, that the relationship between the wave parameters and the wind speed was magnified by the high exponent of the wind speed in the scaling relations (wind speed is raised to the power of **2** to scale fetch, **4** to scale energy and **1** to scale frequency; see [9.3] and [9.4]). These exponents are necessary to non-dimensionalize the variables, but they enhance the relationship between energy and fetch or energy and wind speed. This enhancement is especially worrying in the case of energy because of the large exponents used to non-dimensionalize the variables. In fact, I observed that the relationship between wind speed and energy could mask the relationship with fetch. For this reason, in this section I addressed the masking effect in detail in order to analyze how it could affect the growth rate.

To address the importance of the relationship between wind speed and energy I assumed the relationship $E \propto {U_{10}}^2$ (this exponent corresponds to fetch-limited growth, according to Cavaleri and Bertotti 2003). It is shown below that such a relationship between the variables tended to arrange the non-dimensional parameters along a straight line whose slope would be equal to **1**. Note that b = 1 is the value of the development rate calculated in the first field experiments (see Table 7.1).

Typically, the non-dimensional growth function looks like:

$$\log\left(\frac{E\cdot g^2}{U^4}\right)=a_0+b\cdot\log\left(\frac{X\cdot g}{U^2}\right) \quad \textbf{[9.9]}$$

Incorporating the relationship $E = {U_{10}}^2$, the previous equation takes the form:

$$\log\left(\frac{U^2\cdot g^2}{U^4}\right)=a_0+b\cdot\log\left(\frac{X\cdot g}{U^2}\right) \quad \textbf{[9.10]}$$

The rearrangement of the terms leads to:

$$\log\left(\frac{g}{U^2}\right)+\log(g)=a_0+b\cdot\log(X)+b\cdot\log\left(\frac{g}{U^2}\right) \quad \textbf{[9.11]}$$

When the constant terms are grouped in a parameter called *D*, such as:

$$D=\log(g)-a_0-b\cdot\log(X) \quad \textbf{[9.12]}$$

The resulting equation takes the form below and it is true for *b* equal to **1**.

$$\log\left(\frac{g}{U^2}\right)=b\cdot\log\left(\frac{g}{U^2}\right)-D \quad \textbf{[9.13]}$$

Therefore, growth rates equal to **1** are to be expected for any growing waves whose energy is proportional to the squared value of the wind speed. Note that the opposite is not straight forward: a *1:1* slope does not necessarily imply that the relationship between energy and wind speed is a square exponential. In this work, deviations of the development rate from the *1:1* slope were a sign of the dependence of wave energy on other factors such as wind gradients, the stability of the atmosphere, the presence of swell, etc.

The effect of the wind-energy relationship is accentuated if data from only one buoy is taken. Then, the relationship between energy/frequency and fetch was very weak (fetch only varies due to wind direction) and the non-dimensional curves mainly describe wave growth due to wind speed (and not fetch). Even for multi-fetch data sets it is important to be aware of the addressed relationship and to remember that non-dimensional curves describe wave growth as a function of both fetch and wind speed, even though in dimensionless terms, it is generally referred to non-dimensional wave parameters and fetch.

Note also that there may also exist a relationship between fetch and wind speed within the marine boundary layer (U_{10} increasing with fetch, as reported by Flamant et al. 2003). This relationship was expected to be much less strong than the one between energy and wind speed, especially because in the previous chapter it was shown that wind speed within 50 km off the coast was significantly variable due to the coastal orography (not fetch). In other words, in this region the variability of the wind speed along

the fetch was thought to be beyond the steady increase due to the roughness change of the sea surface and the development of the marine boundary layer. In other regions, where the difference of the wind speed between land and sea was a tight function of fetch (or distance to the coast), the intrinsic relationship between fetch and wind speed could also be taken into account.

9.3.1.4. The physical interpretation

The complex relationships between dimensional variables lead to a poor physical representation of the wave growth rate obtained from the non-dimensional curves. Remember that wave growth curves are used to describe growth of non-dimensional wave parameters along non-dimensional fetch, but they should be used carefully to describe physical (and dimensional) wave growth along fetch. I emphasize it because the term development rate, often referred to as 'growth rate', could be misleading and could induce to erroneous interpretations of the results, as detailed below.

The main reason for the lack of physical interpretation is the position of the wind speed in the quotient of the scaled terms (remember that it is raised to the power of **2** (fetch) and **4** (energy); see [9.3] and [9.4]). To non-dimensionalize the energy, the energy itself is divided by wind speed (inverse relation), even though the physical relationship between both variables is directly proportional (energy increases if wind speed increases). Two different behaviours result from this controversy. On the one side, the position of wind speed in equations [9.3] and [9.4] forces high wind speeds to be plotted on the left side of the growth curves (where the non-dimensional values are lower). On the other side, high energy values are usually plotted towards the upper-right hand side of the curves. In this opposing relationship, the wind speed plays a more important role because it is raised to the power of **4**, and it masks the effect that wave energy is higher for longer fetches and/or higher wind speeds. The unanswered questions could be written as follows: Why are non-dimensional energies high? Because energy is high or because wind is low?

The case of non-dimensional frequency is similar because wind speed is multiplying the frequency to scale it even though, physically, high wind speeds are related to low frequencies. In this case, however, wind speed is only raised to the power of **1**, and the masking effect is probably less important.

The inverse relationship is also important to remember because, as a consequence, positive slopes (development rates) of the growth curves describe growth of dimensionless quantities, but do not directly describe physical growth of dimensional parameters. The reason for this emphasis is that higher development rates (steeper slopes) do not necessarily imply that wave growth is 'faster' but rather, that wave energy at low wind speed situations is higher, and energy at high wind speeds is lower, than reported by other authors. Of course, this interpretation is not straight forward because the relationship between energy and fetch, or other external forcing or internal wave properties, also plays an important role as described above.

Summarizing, the lack of direct physical interpretation of the non-dimensional growth curves is due to, first, the fact that wind speed scales the variables on both axis. Second, it is due to the higher exponent of the wind speed compared to the energy in the scaling procedure. Third, it is due to the inverse relationship between wind speed and energy (or frequency) in the scaling law, as opposed to the direct relationship that exists in Nature.

9.3.1.5. Particularities of wave growth in variable wind conditions

In addition to the complex relationships described above, there are additional physical processes that are suspected to affect the wave growth (and the growth curves) in variable wind conditions. The effect of these processes on wave growth cannot be easily separated from the wave data analysed, as it was done in section 7.4, e.g. atmospheric stability, because no easy indicators were available in this study to proceed accordingly. This restriction limits, of course, the method's performance to study wave growth. In this subsection, the physical processes typical of variable wind conditions are described in terms of their possible effect on modifying the slope of the non-dimensional curves. The accurate description of the physical processes permitted to better understand the non-dimensional curves obtained and threw some light on local wave growth mechanisms.

9.3.1.5.1. Diffraction

Diffraction is a typical process of wave propagation that describes the turning of wave direction due to a diffusion of wave energy from high-level energy regions to low-level energy regions. Although, typically, diffraction situations occur at the entrance of harbours and at the tip of breakwaters, I suspected that a similar effect (at larger scales) could exist in regions of spatially variable wind fields and coastal wind jets.

In the region of study, jet-like wind structures are characteristic (as shown in previous chapters). I expected jet-like wave patterns to be generated accordingly, but also, I expected wave energy to diffract from the jet-like regions to the neighbouring areas where weaker wind speeds produced lower wave heights.

Such diffraction processes were expected to generate a broader directional spectrum, compared to homogeneous wind conditions. Also, the dimensional wave energy and peak frequency were expected to either increase or decrease depending on the location of the measurement point relative to the position of the wind jet (inside or outside the wind jet, respectively). In terms of the non-dimensional curves I expected diffraction processes to cause an increase of the vertical scatter of the non-dimensional wave variables (energy and frequency).

Note also that more jet-like structures were expected to occur during strong wind conditions. If this would be the case, the scatter of the wave energy would be enhanced towards the lower left-hand side of the

plot, as it is indeed observed in Figure 7.4. Note, however, that the larger scatter of dimensionless energy at high winds could also be due to the larger number of data points compared to low wind speeds (which were indirectly removed through the sea/swell separation method; see section 7.3.1).

9.3.1.5.2. Duration vs. fetch-limited

Remember, again, that fetch-limited conditions assume a constant wind blowing over a limited fetch for unlimited time, whereas duration limited growth assumes a constant wind blowing over unlimited fetch during limited time. In variable conditions, wave fields might not always reach equilibrium with the wind forcing and, thus, sea states of mixed origins are expected.

A reference study for duration-limited growth was carried out by Hwang and Wang (2004), who fitted a linear and a second order functions to duration-limited curves in non-dimensional form (see Table 7.1). These authors also addressed the issue of converting fetch- to duration-limited curves, thus confirming the validity of the space-time conversion. Nonetheless, they also stated that the development rates were clearly fetch-, duration-, and wave-age-dependent. In Hwang et al. (2011) the emphasis was given to variable wind conditions and they provided a valuable discussion about the duration- or fetch-limited conditions. These authors noticed that, after a wind change, the wind sea quickly adjusts to the ideal fetch-limited wave growth functions. Also, after discussing the relationship between fetch- and duration-limited growth, these authors concluded that fetch- and duration-limited curves are not equivalent in variable wind situations.

Badulin et al. (2007) performed a more theoretical study of duration-limited growth and found that the relationship between the development rate and the downshift rate was not the same as in pure fetch-limited conditions, thus questioning the validity of the space-time conversion. In a more practical direction, Le Roux (2009) included the duration as an independent parameter and suggested a parametric expression to estimate wave parameters for any combination of wind velocity, fetch and duration, while also taking into account the atmospheric and water properties. All these earlier studies indicate that the role of duration-limited growth in variable wind situations is not yet well understood or approached.

Therefore, the first step I took to address the duality fetch- versus duration-limited growth in the region of study was to look for the separation point between both sea states. Note for example that there exist parametric expressions that were specifically formulated to calculate whether a sea state is limited by fetch or time. The first one of these functions was derived from the set of expressions in the U.S. Army Corps of Engineers (1984) by Hurdle and Stive (1989). The second one was given in Resio et al. (2002). Although both expressions give quite different minimum values below which wave growth is expected to be duration limited, for U_{10} lower than 10 m/s and fetch longer than 20 km, the estimated minimum durations are always longer than 1 h (see Figure 9.6). According to these expressions, and strictly speaking, in the region of study wave growth should be more duration-limited rather than fetch-limited.

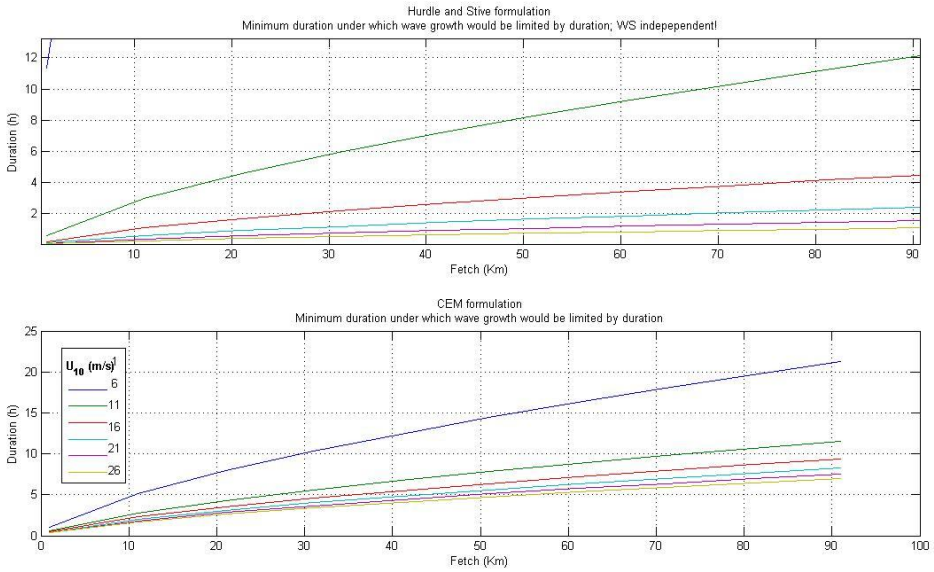

Figure 9.6 Minimum duration required to surpass duration-limited condition for the given wind speeds and fetch. Top panel represents the functions derived by Hurdle and Stive (1989)**; Bottom panel represent the functions presented in** Resio et al. (2002)**.**

Note, however, that Lin et al. (2002) described the response time of waves to changing winds to be 1 h only, in agreement with the results presented in Figure 5.5. The difference between Lin et al.'s work and Resio et al.'s work was no other than the energy of the waves at the time of the wind change (the 'initial conditions'), which for the parametric expressions was no energy at all. Instead, if the 'initial conditions' were large (energetic), then fetch-limited situations should be reached much faster than otherwise.

If duration-limited situations were indeed common, the non-dimensional data points would be placed below the reference curves because wave energy would not have time enough to reach the fetch-limited state (as observed in Hwang et al. 2011). Instead, wave energy in this study was generally similar (or higher) than reported by other authors. Therefore, either wave growth rates were much faster than considered before or, more probably, wave energy was not duration-limited.

In any case, note that theoretically, higher wind speeds need shorter minimum durations and lower wind speeds need longer durations to reach the same steady state of energy and frequency. This means that it is more probable to encounter larger scatter (duration-limited data) for lower wind speeds (located on the right-hand side of the plotted curves) because of the longer times they needed to reach the equilibrium. In fact, in the present case study, if duration-limited conditions were common, lower energies than in pure fetch-limited conditions would also be concentrated at lower wind speeds (right hand-side of the plot). Hence, the dimensionless data points would tend to decrease the development rate of the observed curves. Again, this did not seem to fit the case reported in this study, as shown for example in Figure 7.4.

9.3.1.5.3. The role of 'old sea'

In this study I used the wave growth curves from KC92 to classify the sea systems as wind sea or as swell, even though this was not an exact method and it could induce to considerable scatter. As discussed in section 7.3.1, KC92's curves were used to remove low wind speed situations during which simultaneous too high energy was considered to be 'old sea'. Note that I use the term 'old sea' to refer to wave systems that were growing just before a sudden decrease of wind speed.

In variable wind conditions where wind increases and decreases in very short periods of time, I expect 'old sea' to be 'active' again (and keep growing) when the wind increases again (the 'initial conditions' referred to in previous subsection). Therefore, in variable wind conditions, and just after a wind increase, I expect to encounter higher wave energy for the same wind speeds (than KC92, for example) because the 'initial conditions' of wave growth are more energetic than no wave energy at all. If the wave energy is higher for similar-magnitude wind speeds, then wave growth would also tend to be faster. After a while, when the fetch-limited equilibrium is reached again, no significant differences are to be expected.

Indeed, in the curves calculated from the observations (see Figure 7.4, for example) a considerable amount of energy was observed above the reference curves reported by other authors, but the resulting development rates were not much higher. The reason is the time required to reach equilibrium again, which is expected to be much shorter when there already is a significant amount of wave energy to start from (see Lin et al. 2002). Therefore, the role of old sea on wave growth affects moderately the equilibrium conditions in fetch-limited situations (as represented by the growth curves). Old sea, however, influences the growth rate at the initial stages of wave growth (duration- and fetch-limited), for which different growth curves would be required (if this method was to be used).

9.3.1.6. Summary

After exploring the limitations of the non-dimensional curves in detail, I concluded that the main limitation is the role of wind speed to scale the variables. There are four main reasons. First, the wind speed induces spurious correlations due to the common scaling factor on both the dependent and the independent terms. Second, the intrinsic relationship between the dependent variable (E or f_p) and the wind speed as a scaling variable strongly influences the derived development rate along dimensionless fetch. Third, the fact that varying wind speed widens up the non-dimensional fetch range influences the physical meaning of 'development rates along the fetch' because it converts one-point measures to fetch dependent measures. This conversion was shown to be inadequate because development rates tended to be higher when only one-point measurements were used compared to multi-fetch data sets. Fourth, wind speed is an in-situ measure and its representativity along the fetch is uncertain. For this reason, when the wind speed at buoy A-dw(D) was taken to be representative of the wind speed at the positions B-iw(S) and E-iw(D), the growth rates at these other locations were higher. The lack of representativity of the

wind speed could also be responsible for part of the large scatter of the development rate of multi-fetch data sets.

Altogether, using the wind speed to scale the variables strongly limits the methodology and hampers the accurate description of wave growth in non-dimensional and dimensional (physical) terms. Additionally, the scatter of the growth curves increases due to the physical processes typical of variable wind conditions such as diffraction, duration-limited waves and 'old sea' energy. However, the specific contribution of each process to the overall scatter of the curves still needs further observational evidence.

Diffraction and old sea were expected to enhance wave growth, compared to ideal wind conditions. Duration-limited situations, instead, were expected to produce lower energy (higher peak frequency) than purely fetch-limited conditions. In this case, however, I expected the wave systems to rapidly adjust to changing winds due to the higher wave energy of the initial state, compared to the no-energy state of duration limited curves, thus reducing the effect of duration-limited situations on fetch-limited growth curves. These processes influence the scatter of the curves and its slope although they do not provide 'individual' information about wave growth in the studied conditions.

All in all, the short-comings of the non-dimensional growth curves as a method to describe wave growth, and the considerable scatter resulting from the variability of the wind conditions limit the suitability of this approach to study wave growth in purely physical terms. Therefore, further refinements of wave models in variable wind conditions could not only be achieved using the typical non-dimensional wave growth curves and the limited data available. These results encourage additional work towards finding more suitable methods to characterize wave growth.

9.3.2. Alternative methodologies

Some authors used alternative growth functions either to reduce the scatter of the plots or to express wave growth in terms more suitable to their field experiments. For example, DO85 studied the relationship of the non-dimensional dependent terms (energy and frequency) with the inverse wave age (U_c/C_p), as the independent term. The main reason was overcoming the limitation of having one-point measures only. Note that U_c is the component of the 10 m wind speed in the direction of the waves at the peak of the spectrum ($U_{10}\cdot\cos\varphi$), where φ is the directional difference between wind and waves, and C_p is the celerity of the waves at the spectral peak.

The expressions derived by DO85 were written in terms of the laws derived in JON73 by KC92, who showed that the development rates are comparable to each other. However, KC92 noted that the spurious correlation of the law proposed by DO85 is closer to the real relationship between the terms, and thus, DO85's relationship is less suitable to derive trustworthy growth laws. Nonetheless, some authors also used DO85's approach to reduce the scatter of the curves including Dobson et al. (1989), Hanson and Phillips (1999), Violante-Carvalho et al. (2002) and Pettersson (2005). DO85's approach to wave growth

was also used to calibrate some of the dissipation functions in the literature (e.g. Banner and Morison 2010).

In this work, I additionally calculated non-dimensional wave growth along inverse wave age, in agreement with the work of DO85 (Table 9.3). The objective was to observe the local differences in wave growth that were to be expected when using different expressions of wave growth. The growth rate derived for multi-fetch data resulted to be very close to the rate reported in DO85. The growth curves for single-fetch data were exactly the same as reported in Donelan et al. (1992). These results indicated that taking the DO85 growth laws would not provide a better adjustment of the models to the observations. The main reason is that the method was not able to tell apart differences between wave growth in the region of study and wave growth in DO85.

Table 9.3 Non-dimensional energy growth functions as a function of inverse wave age calculated in previous field experiments (left column) and in the present work (right column).

Previous field experiments		Present data set	
$\overline{E} = 2.7 \cdot 10^{-3} \cdot \left(U_c / C_p\right)^{3.3}$	DO85	$\overline{E} = 3.2 \cdot 10^{-3} \cdot \left(U_c / C_p\right)^{3.3}$	Subset RIMA-Med
$\overline{E} = 2.3 \cdot 10^{-3} \cdot \left(U_c / C_p\right)^{3.2}$	Donelan et al. (1992)	$\overline{E} = 2.3 \cdot 10^{-3} \cdot \left(U_c / C_p\right)^{3.2}$	A-dw(D) 2004 - 2009

Other approaches to wave growth were carried on by Hanson and Phillips (1999), who replaced the wind speed with the wave dissipation rate in order to non-dimensionalize the variables and to reduce the scatter. Instead, Badulin et al. (2007) used the total wave input and suggested using different non-dimensional terms to calculate wave growth. Also Le Roux (2009) suggested empirical functions to estimate the wave parameters for any wind speed, fetch and duration, but also taking into account the stability of the atmosphere and the water properties. In laboratory experiments, Lamont-Smith and Waseda (2008) performed multivariate regression to their data and found different relationships that were, unfortunately, different from those observed in JON73 datasets (field data).

In this section I explored yet another approach to wave growth in variable wind conditions: adjusting a multivariate regression to the observations. This method calculates the dependent variable as a linear combination of the other variables, plus an independent term. The coefficients obtained for each parameter are a measure of the relative importance of the parameter in modulating the sea state. This method could thus be used to rank each of the considered parameters according to its importance in modulating the sea states. In this work I preliminarily calculated the wave height as a linear combination of fetch, wind speed, wave period and depth. The period of time selected was storm nº3 and wave data was taken from buoys A-dw(D), B-iw(S) and E-iw(D). The resulting linear combination had the following form:

$$H_s = -0.2X + 0.1U_{10} + 2.1T_p - 0.01h - 1 \quad \textbf{[9.14]}$$

This equation indicates that the least important term affecting wave growth was depth (h), as expected in deep waters. It also indicates that wave height was highly related to wave period and, to a lesser degree, it was related to fetch and wind speed. Also, the independent term was quite important, thus suggesting that there exist other factors, which were not considered here, that might also significantly affect H_s. Note however that a low coefficient does not necessarily indicate a lack of relationship between the variables. It only indicates that the physical influence, if any, could not be told apart. Again, keep in mind that the obtained function does not consider the full range of factors such as wind and wave directions.

In future work I strongly suggest exploring additional methods to characterize wave growth. For example, an ANOVA test could be performed to gain understanding on the different parameters affecting wave growth. In particular, an ANOVA test would be especially useful to study the long-term data set because it could take into account all atmospheric and sea states such as the tendency of the wind speed, the stability of the atmosphere or the wave age, the wave steepness and the swell energy. This type of test is a statistical tool that considers the different states as switches that affect the relationship (slope) between two variables X and Y (say for example the dimensionless energy and fetch, or the inverse wave age). The output from the ANOVA test would provide valuable information on the significance (or not) of each 'switch' on the relationship between the two variables. In this case, also, no significance would mean that the method is not suitable to determine whether there is or there is not a physical effect of the 'switch' on sea growth.

It is important to note that these methods (multivariate regression and ANOVA) are statistical tools only. It means that they cannot estimate the physical properties of wave growth (such as growth rate in time) and they can 'only' provide statistical information on the existing processes. All in all, they could be used as a preliminary step towards better understanding wave growth in these regions. A more accurate knowledge on the physics of wave growth in variable wind conditions is still required to improve its characterization and estimation.

To conclude this section, note that the non-dimensional growth curves are a valid and widely used approximation of wave growth, but whose limitations are also important. Adjusting the simulated wave growth rate to the observations proved to be an acceptable tool to tune the model, but it could not be thought of as the only valid solution, or a long-term solution, to improve wave estimations in variable wind conditions.

9.4. Overall considerations

The results in previous chapters indicated that wave estimations in fetch-limited conditions and sharp wind gradients did improve when increasing the resolution of the wind input fields and when adjusting the simulated wave growth rate to the observations. In spite of the improvement achieved, there remained an under-estimation of wave parameters for slightly over-estimated wind speeds. The reasons for this

under-estimation were discussed in terms of the limitations of the increase of resolution (numerical settings of the wave models) and the adjustment of the wave growth rates (parameterization of the source terms and wave growth curves), as summarized below.

In short, the main numerical constraints of the wave model are the high diffusivity of low order schemes, which require a reduced integration time step for decreasing grid sizes, and the stability of high order schemes, which need to fulfill the Courant number condition (thus reducing the grid size and the time step simultaneously). During the case study, the under-estimation of the maximum values of the event was reduced and the timing of the storm peak was improved by selecting the best configuration of the numerical settings. However, the wave parameters remained generally under-estimated.

The parameterization of the source terms entrains a larger degree of uncertainty derived from the lack of knowledge of the exact processes describing the transfer of energy between wind and waves, in particular within the dissipation term. Also, the numerical scheme used to solve the source terms is constrained by the need of an unphysical term: the action density limiter. These facts, as said before, call for a strong need of better understanding of the mechanisms of wind wave growth.

In this direction, the capability of the non-dimensional curves as a method to estimate wave growth is limited mainly due to the large scatter of the measurements, to the deviations from ideal wind conditions and, to the limited suitability of using wind speed as the scaling variable. Particularly demanding situations within wave growth were seen to be the duration-limited stages of wave growth and the old sea systems.

Last, as shown in Section 7.4.4, it is particularly interesting to note that the influence of swell systems significantly contributed to speed up the rate of frequency downshift and, to a lesser extent, the rate of wave energy growth. These results are in agreement with the much better performance of JAN formulation in estimating the peak period. Also, these results support the suitability of estimating the energy input term as a function of the sea state to improve, in particular, the estimation of the peak period, in agreement with JAN parameterizations.

Summarizing, the results from this work indicate that wave growth in variable conditions and small scales (from hour to days) still need to be further studied. It is for instance necessary to find a suitable method to capture the physical characteristics of wave growth in the studied conditions. Also, the mechanisms leading to the energy balance in wave models should be further developed once more observations become available. In this sense, the resulting method should be able to capture the particularities of wave growth in variable wind conditions, especially during the early stages of wave growth.

10. Conclusions and future work

Improving wave predictions in the NW Mediterranean has proved and will keep on proving to be a tough, difficult but not impossible task. In this work, wave estimations in fetch limited conditions were improved by focusing on the wind and wave gradients characteristic of the region. On the one hand, the higher temporal and spatial resolution of the forcing wind fields captured much better the higher scales of wind speed and it avoided smoothing down the highest wind speed peaks. On the other hand, the rate of wave growth in the region of study was faster than the simulations and faster than the rates derived for more homogeneous wind conditions. Taking these considerations into account to simulate a particular storm event in the region, the results presented throughout this document confirmed that the estimation of wind wave growth in sharp gradient regions improved by increasing the wind resolution and by adjusting the model's wave growth rate to the locally observed rate.

Additionally, this work revealed interesting characteristics of the sharp wind and wave gradients in the NW Mediterranean and particularities of wind wave growth under such conditions. The major findings and the most important contributions of this work to the state of art are listed below:

- Coastal wind jets, of short duration (less than 6 h) and limited effect on wave growth (less than 50 km), were characteristic features of the coastal region during offshore blowing wind conditions. Other features observed, which are typical of complex geometry regions, were slanting fetch mechanisms and wave propagation processes (e.g. swell attenuation, diffraction and refraction).
- In the Catalan Coast, 50% of wind speed values were seen to increase/decrease twice/half its value in less than 1 h (sharp temporal gradients) whereas wave records were much smoother than the wind time series. In fact, although growing waves (wind sea) responded relatively fast (within 1 h) to wind speed changes, more mature waves responded more slowly (2 - 3 h).
- The growth functions of non-dimensional wave energy calculated for the region of study were slightly faster compared to the curves reported by other authors and faster than those calculated from numerical simulations. Although not significantly different, the wave energy growth rate of the observations was 2% faster than estimated in the numerical simulation. The local expressions for non-dimensional energy and frequency growth are:

$$\overline{E} = 6.42 * 10^{-7} \cdot \overline{X}^{0.94} \quad \textbf{[10.1]}$$

$$\overline{f_p} = 2 * 10^{-7} \cdot \overline{X}^{-0.281} \quad \textbf{[10.2]}$$

- The wave growth rates obtained indicated that wave growth in variable wind conditions was faster compared to more homogeneous wind conditions. Additionally, deviations from the 'ideal' fetch-limited conditions (e.g. swell, changing wind speed) induced to misleadingly high growth rates and caused large scatter of the data points along the fit.
- The limited applicability of the non-dimensional curves to describe wave growth is based on the scatter of the calculated curves and their tendency to report higher development rates in less 'ideal' growth conditions. In particular, the important role of the wind speed in the scaling procedure hamper the suitability of the non-dimensional curves as a method to approximate wave growth under the studied conditions.
- Increasing the temporal and spatial resolution of the wave modelling system prevented 'information' losses in short duration storms because it captured, both, the wind and wave gradients in the geographic dimension and the sharp increases/decreases of the wind speed. The resolution increase also increased the amount of variability captured by the model (and reduced the model's bias).
- The best wind speed estimations were obtained from the highest resolution atmospheric model (MM5 4km/1h) nested in reanalysis wind fields from ECMWF. However, to approximately estimate the maximum values of the wave storm event it was necessary to considerably over-estimate wind speed (30-40%; for example when using MM5 12km).
- A frequency increase of the wind input, from 6 h to 3 h, improved the estimation of the maximum values (peaks) of the storm about 13%. In this sense, an increase of the frequency resolution was more effective than a spatial resolution increase (from 12 km to 4 km), which only improved the timing of the peaks but not the maximum values achieved. Nonetheless, increasing the input frequency even more (up to 1 h using in-situ observations) without increasing the spatial resolution was either way inefficient.
- Adjusting the numerical settings (e.g. spatial discretization, integration time, etc.) was especially relevant to refine the estimation of the wave parameters. If the computational cost was not limiting, shorter time steps improved the estimation of the storm's maximum values and better simulated the timing of the peaks.

- Adjusting the wave growth rate in the model to the observations improvedthe wave height about 18 % and peak frequency about 4%. Although the main improvements occurred during the peaks of the storm, they were somewhat limited due to 1) the inherent inaccuracies of the current parameterization of the source terms and 2) the difficulties of the non-dimensional wave growth rate to accurately describe wave growth in variable wind conditions.

- The physical source terms presently implemented in the spectral wave models are far from consistent even though the total balance of energy is well approximated. In particular, the disparity of the amount of energy and the spectral shape of the main parameterizations for energy input and dissipation are the best example of the current uncertainties within wave growth. Also, the need to use unphysical parameters (such as the action density limiter) to approximately simulate wave growth confirms that the source terms are a potential and main source of error within wave forecasting, especially in sharp-gradient regions.

The results presented in this work proved that improving wave estimations in the region, and in other gradient-regions, is indeed possible. Also, and most importantly, the results showed a path to be followed in the near future to effectively improve operational wave forecasting. Indeed, increasing the resolution and the accuracy of the input wind fields will lead to more accurate wave estimations operationally. In this direction, operationally better input wind fields can be achieved by improving atmospheric simulations or including real time assimilation, for example. The computational cost of higher resolution models can be reduced by running parallel simulations, for instance. To improve the estimation of wave growth locally, regional wave models can be tuned to better simulate the regional rate of wave growth. Also, wave data assimilation can be conveniently used as a tool to achieve more immediate results in terms of maximum storm values.

The results presented in this work not only provided direct and practical applications towards improving present-day wave forecasting in the region but they also opened a wide range of perspectives towards improving wave forecasting in the future. From the physical point of view, it is clear that further research in the physics of wind and wave interaction is needed, as it is being claimed by many authors (see for example Cavaleri 2009). In particular, it is important to better understand the wave growth and energy dissipation processes in variable wind conditions in order to extend the limits of knowledge and, later on time, apply this knowledge to practical applications.

In this direction, this work provided interesting details about wave growth in the region, thus easing the path towards a better physical comprehension of wave growth in sharp-gradient regions. For instance, the results obtained indicate that increasing efforts should be directed towards better describing the interaction between wind and waves in a wide number of temporal and spatial scales. Independently of the suitability of sticking to the spectral description of surface waves or the parameterization of the source

terms as they are presently implemented, further insight into these processes would surely lead to improved forecasting. Note that, although these issues are common nowadays in discussions within the wave modelling community (e.g. Cavaleri 2009, 2006), there still is work to do.

A long-lasting open issue within operational forecasting in the NW Mediterranean is the accurate prediction of crossing sea conditions (bimodal spectra). In this work it was shown that the wind sea part of the energy spectra (i.e. growing waves) could be improved if the sharp-gradients of the region were taken into account (either using high resolution wind fields or adjusting the rate of wave growth). If these same steps were taken when estimating bimodal wave conditions, wave estimations would improve accordingly; at least in terms of the wind sea part of the spectra. However, further improvements in this direction will be necessary linked to a more accurate knowledge of the interaction between sea and swell; in particular when both systems are very close in the frequency domain.

Note also that, aiming to push the limits of knowledge in wave growth conditions and sharp-gradient regions, the amount of data measured during RIMA-Med could still provide further and valuable information about relevant physical processes. A re-evaluation of these data from new perspectives and/or using new/different methodologies would surely provide further interesting details about wind wave growth. Note, also, that more accurate and physically-grounded parameterizations of the wave energy input terms (balance of energy) are of high priority in order to improve wave forecasting. To this end, it is important to slowly but surely fill in the lack of knowledge within wind wave growth and the physical processes therein involved (e.g. wave response to changing winds).

In this direction, adequate and extensive field campaigns are more necessary than ever. It is not only important to measure waves along the coast and towards offshore, but it is also highly important to measure winds at sea (incluing wind stress). Indeed, understanding wave growth will hardly be possible without in-situ wind measurements. To this end, and to supply comprehensive spatial information of both wind and waves, remote sensing data is, at present, commonly used in field campaigns around the globe (e.g. Ocampo-Torres et al. 2011). In this direction, however, special efforts are needed to characterize the mesoscale processes in the transition zone, between the coastal fringe and the open ocean, at scales of less than 10 kilometres and less than 6 hours. In field campaigns it is also increasingly important to reduce the range of uncertainty of the measurements because the wind and wave models' bias is constantly decreasing. Indeed, if the amount of uncertainty within the measurements is as large as the degree of uncertainty of the models, there will be no more room for improvement and a dead end will be reached.

But not all future efforts need to be directed towards the physical aspects of wave growth; the numerical aspects of wave models still play an important role within wave forecasting. Present day numerical models are mainly restricted by the computational cost, and the limitations of the numerical schemes. Nowadays, computational capacities increase at amazing speeds but the range of spatial and temporal

scales to be simultaneously estimated also increase. Therefore, it might be wise to follow the worldwide tendency towards energy efficiency or, in this case, computational efficiency. This goal, however, might not be achievable with the tools presently available or the representation of the sea surface currently used. In this sense, new ideas and approaches are highly necessary, as the wave modelling community plead (see e.g. Cavaleri 2006).

To conclude, keep in mind that improving wave forecasting is not only important for present day applications as they are currently known, but it can also widen up the range of activities that take place at sea to levels that are hardly imagined. Right now, the accuracy range of wave predictions is relatively large and the time window is no more than a few days ahead. The tiny steps taken in this work, although focused in short-scale predictions may eventually also improve mid- and long-term predictions. For instance, better hindcasting wave conditions during the last few decades might lead to relatively fast improvements in wave forecasting in the next few decades. And not only this: can you, for example, picture the day when shipping routes will be planned months ahead? Or surfing trips, fishing activities, wind/wave power production or even field campaigns? Can you imagine the day when activities at sea are planned, and the risks assessed, depending on half a meter wave height difference? Today, it might sound incredible, but work is in progress.

Annex I Calculating wind speed at 10 m elevation

Wind speed at buoy A-dw(D) (U_z) was measured at a 3 m elevation (z = 3 m). Measured wind speed was extrapolated to 10 m elevation (U_{10}) using the iterative procedure described in Leake (2007):

$$U_{10} = U_z \frac{\mathbf{log}(z / z_0)}{\mathbf{log}(10 / z_0)} \qquad \textbf{[A I- 1]}$$

Eq. [A I- 1] results from taking the quotient of the equation which describes the logarithmic profile of the surface wind speed at an elevation of 10 m and z. The logarithmic profile of the surface wind speed takes the following form (see Komen et al. 1994):

$$U_z = \frac{U^*}{\kappa} \mathbf{log}(z / z_0) \qquad \textbf{[A I- 2]}$$

The roughness length (z_0) was calculated after Charnock (1955) relationship (Charnock's constant α_{CH} equal to 0.04):

$$z_0 = \frac{\alpha_{CH} \cdot U^{*2}}{g} \qquad \textbf{[A I- 3]}$$

The friction velocity (U^*) is related to wind speed at 10 m elevation (U_{10}) through the drag coefficient as follows (see Komen et al. 1994):

$$U^{*2} = C_D U_{10}^{\ 2} \qquad \textbf{[A I- 4]}$$

Where the drag coefficient was calculated after the Smith and Banke (1975) drag law using the following expression:

$$C_D = 10^{-3} \left(0.63 + 0.066 \cdot U_{10}\right) \qquad \textbf{[A I- 5]}$$

Annex II Quality control of the raw time series and the energy spectra

The raw time series of RIMA-Med and buoy A-dw(D) data sets were submitted to a strict quality control to remove possibly erroneous records. The quality control on the raw data was based on the procedure described in Casas-Prat and Holthuijsen (2010) (see also Casas-Prat 2008). Eight different errors in the time series were looked for:

1. Length of the time series shorter than expected from the recording time and the sampling frequency.
2. Existence of 'spikes' in the time series. To search for 'spikes' the vertical acceleration of two consecutive data points was calculated. A 'spike' occurred when the vertical acceleration is larger than half the gravitational acceleration (1/2*g).
3. Existence of 'gaps' in the time series. A 'gap' was defined as three (or more) consecutive values with zero values.
4. Smaller $H_{s,1/3}$ compared to H_{min}. In Casas-Prat (2008), H_{min} = 0.5 m. In this work, H_{min} was set to 0.2 m.
5. Existence of 'freak waves' in the time series. A freak wave occurred when H_{max} was higher than 2.83 times $H_{1/3}$ during less than three consecutive values.
6. Mean frequency larger than half the Nyquist frequency, to avoid aliasing:

$$\frac{f_{Ny}}{f_m} > 2.2 \qquad \textbf{[A II. 1]}$$

7. Spectral energy at the first discrete frequency of the spectrum was larger than 0.004 m^2/Hz. This criterion was set to avoid irregular spectral shapes due to, for example, bumps caused by boats.
8. Water depth was shallower than half the wavelength :

$$h < L_0/2 \qquad \textbf{[A II. 2]}$$

The routine to search for errors in the raw time series was implemented in a MATLAB function called QC_complete.m. This routine searched for the eight different errors in the time series. To do so, it used the WAFO toolbox (Brodtkorb et al. 2000) because it intrinsically calculated the frequency spectrum.

This work used the MATLAB routine QC_fast.m because if one error was encountered it skipped the remaining search operations. The objective of this function was not to identify what sort of errors existed but whether there was an error (of any sort) or not. This routine was used to accelerate the calculations.

The routine QC_raw.m searched for the first three errors only to avoid calculating the frequency spectrum from the raw time series.

Additionally, when splitting the frequency spectra (using SPLITseaswell_Alomar.m) four more errors were searched for in the spectra:

9. The energy value of the first discrete frequency of the spectrum (m^2/Hz) was higher than 0.1% of the total energy of the spectrum, or higher than 10 – 3 m^2/Hz.
10. The energy value of the last discrete frequency of the spectrum was higher than 0.1% of the total energy of the spectrum, or higher than 10 - 3 m^2/Hz.
11. The energy value of the first discrete frequency of the spectrum was equal to the peak (maximum) value of the energy spectrum.
12. No data was available.

This additional quality control was also implemented in an independent MATLAB function called QC_spec1D.m. MATLAB functions were written for MATLAB R2010a.

Annex III Sea – swell partitioning

Sea states can be represented as the superposition of multiple wave systems. To represent the sea state as a whole it is common to use the energy spectra. The 1D spectrum represents the energy distribution along frequencies and the 2D spectrum represents the energy distribution along both frequencies and directions. The information given in the energy spectra is usually combined in several integral parameters (e.g. wave height and peak period) that properly describe characteristics of single energy systems (unimodal spectra). However, if more than one energy system coexists within the same sea state (e.g. bimodal spectra) the integrated parameters of the spectrum are not representative of the sea state.

In variable wind conditions, it is common to observe different wave systems (or wave trains) at the same time. For this reason, the energy spectra usually present more than one energy peak at different frequencies and/or directions. These sea states are called bimodal, or even trimodal (i.e. three peaks). In such conditions the adequacy of using the integral parameters is limited and it is preferred to separate the different wave systems and treat them independently.

There exist two sorts of energy systems as a function of the generation zone and their characteristic physical processes: wind sea and swell. Wind sea (sometimes simply referred to as ‘sea’) is locally generated and it is still growing. Swell is generated in remote regions, it is not affected by generation processes, and it just propagates in space. Sea is generally steeper (shorter peak periods) than swell and its peak direction is usually similar to wind direction. Although several studies point to strong interactions between both systems, at present, sea and swell are generally treated as two independent systems. The reason is that each system affects differently the many coastal activities (mainly because of its different wavelengths).

Separating sea and swell is important in disciplines such as maritime engineering and structural design, coastal protection, fishing activities and marine sports. In numerical modelling and wave predictions is common to separate sea and swell because the main processes affecting each system are clearly different and they are unevenly studied. The interaction processes between the ocean, the atmosphere and the oceanic circulation (currents) are also affected by the characteristics of the energy systems. Also, sea swell separation is increasingly important in numerical assimilation procedures because each system should be assimilated independently.

Sea – swell partitioning permits to associate a characteristic wave height and peak period to each sea system. Spectral partitioning and identification of the wave systems can be achieved using the characteristic properties of each wave system, for example, peak period and direction. The next sections review the state of the art of spectral partitioning and they describe the method used in this dissertation to separate RIMA-Med data set and the 5-years data set from buoy A-dw(D).

III.i State of the art

A recent review about sea-swell partitioning was given by Portilla et al. (2009), who examined extensively the present state of the art and suggested optimized methods for both 1D and 2D spectral partitioning and sea-swell identification. Spectral partitioning consists of splitting the significant energy peaks (energy maxima) that can be either sea or swell. The combination of less energetic peaks with more relevant ones is done according to certain criteria that are described further on. Note that the amount of secondary peaks not associated to an independent wave system depends on the frequency resolution of the method used to calculate the spectra (from the raw time series of sea surface elevation) and depends on the windows used to smooth (average) the spectra. Sea-swell identification refers to the classification of the significant peaks resulting from the partitioning into sea or swell, which depends on different characteristics that are also described further on.

The review of the state of the art provided here is mainly based on the work by Portilla et al. (2009). Nonetheless, in what follows, other relevant methodologies are given to provide a more complete overview of the existing methods. As a first step, the focus was set on 1D frequency spectra mainly because they were available at all buoys in the Catalan region (as opposed to 2D spectra, which were only available from directional instruments).

III.ii Partitioning methods

Originally, there existed two partitioning methods only. The first one, suggested by Gerling (1992), first searched the lowest thresholds in a spectrum, and then partitioned the spectrum accordingly. Each ‘partition’ was considered significant when it was consistent in time and space. This method required directional and wind information, which are not always available. The second method was described by Hasselmann et al. (1996) and, although very similar in concept to that of Gerling (1992), it emulated the watershed algorithm to partition the 2D spectra according to the local peaks (catchment areas). They suggest merging partitions that satisfy the following conditions:

1. The two peak frequencies are only one grid cell apart;
2. The trough between two energy peaks is not sufficiently pronounced;
3. The square spectral distance between two peaks is shorter than the spread of any of the two systems.

Although both methods are very similar, assessing the significance of the partitions using the first method is more complex because more data is needed to assess the persistence in time of the energy systems (time series). The second method, however, needs to be adjusted to each situation. Also, as the spectral resolution increases the partitioning becomes more problematic.

Other authors used the ideas in Hasselmann et al. (1996) but with different settings to combine partitions (calibration) like Voorrips et al. (1997), which adapted the algorithm to 1D spectra; Violante-Carvalho et al. (2002) and Rodríguez and Guedes Soares (1999) for 1D spectra only; and Hanson and Phillips (2001) and Aarnes and Krogstad (2001) for 2D spectra.

In 2D partitioning (frequency and direction) Portilla et al. (2009) introduced an image-processing tool in the combining algorithm which can be thought as a filtering method. As a first step towards implementing the separation of sea and swell operatively in the Catalan coast the focus was on separating sea and swell from 1D frequency spectra only.

In 1D partitioning (frequency spectra), additionally to Voorrips et al. (1997) algorithm, which is Hasselmann et al. (1996) algorithm adapted to 1D spectra, Violante-Carvalho et al. (2002) used other criteria to detect significant peaks but with the same limitations than the initial algorithm. On another side, Rodríguez and Guedes Soares (1999) presented an alternative method to detect significant peaks. This method was based on the variance of each peak and whether it lied within certain confidence intervals (of the spectral calculation) or not. The method mainly filtered the signal using a convolution function that Portilla et al. (2009) found to be too aggressive for 1D spectra.

In 1D partitioning, and after reviewing the state of the art, Portilla et al. (2009) suggested improved criteria for merging partitions which were previously partitioned according to the inverse catchment method of Hasselmann et al. (1996). Portilla et al. (2009) concluded that the method they suggested was more accurate than any of the pre-existing ones. In addition to the methods reviewed in Portilla et al. (2009), and reviewed above, in Bolaños et al. (2005) and Rotés (2004) they discussed other methods to partitionate the spectra and to combine non-significant partitions in the region of interest. They referred to the contributions of Guedes Soares and Nolasco (1992) and Houmb and Due (1978).

In this work, the partitioning method described by Portilla et al. (2009) was selected and it was implemented in a MATLAB routine (with several modifications) to be easily used for 1D frequency spectra. In general terms, the method consisted of first identifying all peaks in the spectrum using the maximum/minimum method. All maxima (which derivative is zero) were considered a peak. Each peak, or partition, was limited by a minimum and a maximum separation frequency. Each partition was characterized by a peak frequency (f_p [Hz]), a separation frequency (the lowest preceding frequency; f_s [Hz]), and the total energy contained in the partition (E [m^2]). The objective of the partition algorithm was to combine non-significant partitions with significant ones and to end up with the most significant

partitions only (sea/swell). Remember that, in this case, a significance refers to the perdurability in time and space of an energy partition. In Portilla et al. (2009), each partition was combined with the neighbouring partition whose mean frequency (f_m) was closer to the partition's f_m.

Depending on the frequency resolution of the spectrum there were more or less initial partitions. When the frequency resolution was coarse, there were fewer initial partitions and it was easier to combine non-significant partitions with significant ones, but the risk was smoothing down less energetic (although significant) peaks. Instead, when the frequency resolution was too high, a large number of initial partitions were identified and it became more difficult to combine partitions with neighbouring ones.

The criteria suggested in Portilla et al. (2009) to combine partitions (which they call spurious peaks) are the following:

1. Combine all partitions whose f_p is larger than a certain threshold (i.e., 0.35–0.4 Hz); the reason for this measure is that there usually exists high variability in the tail of the spectrum, which is not generally associated with a consistent energy system. However, peaks in the tail belong to the wind sea part and it might necessary to adjust these values to the location of the recording instrument, and the peak frequency of the expected wind sea peak;
2. Combine partitions whose total energy is low (i.e., lower than 5% of the total energy);
3. Combine partitions that have few spectral bins before or after the peak (i.e., less than 2 bins);
4. Combine partitions that are placed between two other (neighbouring) partitions and have a lower peak energy level than these two neighbours.

In this work, three additional criteria were added to calibrate the algorithm for the buoys in the Catalan Coast:

5. Combine partitions whose f_p is very close to fs (closer than i.e. 0.015 Hz); but only if more than the expected number of partitions is found (e.g. 2 or 3 wave systems);
6. Combine each partition with the closest neighbour partition in terms of peak frequency rather than mean frequency. f_p was considered to be more representative of the nature of the energy peak than f_m;
7. Combine partitions whose total energy is lower than 8% of the total energy.

III.iii Identification methods

To identify the characteristics/origin (sea or swell) of each partition, Portilla et al. (2009) used the environmental and physical features of the waves and energy spectra, such as wave steepness, width of the spectral peak, etc.

It must be noted that the definition of sea and swell is rather important when identifying the origin of the peaks. Especially in the NW Mediterranean where swell events are usually associated to eastern wave trains, also when an eastern wind is still blowing, and thus, the wind-input term (Bidlot 2001) is positive. This definition contradicts Bidlot's (2001) definition: “the so-called wind waves (or wind sea) are the wave components that are still under the influence of the local forcing wind.”

The different methods described in the state of the art of Portilla et al. (2009) are here only briefly summarized. For further information please refer to Portilla et al. (2009).

1. Wave age. This method can be used only if wind information is available. This method is used by WAM numerical model, it is based on Komen et al. (1984)’s formulation, and it identifies wind sea depending on wave age (U_z/C_p):

$$\beta \frac{U_z}{c_p} \cos(\theta - \psi) > 1 \qquad \textbf{[A III - 1]}$$

The cosine term refers to the wind direction ψ along the wave direction (θ). U_z is the wind speed and cp the phase speed ($c_p = g/(2\pi f)$). β is a calibration factor <1.3 (with some variations; see Portilla et al. 2009).According to Portilla et al. (2009), other authors also used wave age to identify wind sea (e.g. Donelan et al. 1985 and Drennan et al. 2003.

2. Fixed frequency. This method separates swell as those wave systems which peak frequency is lower than a fixed separation frequency such as 0.1 Hz. It should only be used in regions where sea and swell are markedly different.

3. Pierson-Moskowitz (PM) peak frequency. This method splits sea system according to the maximum frequency value that can be reached for the given wind sea values (Pierson-Moskowitz (PM) peak frequency). The PM peak frequency is calculated as follows:

$$f_{PM} = 0.13 \frac{g}{U_{10}} \qquad \text{where typically} \qquad f_s = 0.8\, f_{PM} \qquad \textbf{[A III - 2]}$$

According to Portilla et al. (2009), this method is used by Earle (1984) and Quentin (2002) and might overestimate wind sea.

4. Wave steepness. Wang and Hwang (2001) used a splitting frequency f_s based on wave steepness. Because they observed that the peak of the steepness function is related to wind speed, they suggested an expression for f_s as a function of the peak of the steepness function f_m (only):

$$f_s = 4.112\left(f_m\right)^{1.746} \qquad \textbf{[A III - 3]}$$

This method is especially useful because it does not require wind data. However, according to Portilla et al. (2009), Gilhousen and Hervey (2001) pointed that this method over-estimates wind sea under certain conditions, and added an additional criterion to improve the algorithm. Portilla et al. (2009) found rather arbitrary using the higher of the splitting frequencies calculated from the two criteria suggested, and did not considerate this method any further.

5. JONSWAP spectrum. Violante-Carvalho et al. (2002) proposed to fit a JONSWAP spectrum to the high frequency spectral components to detect the peak that corresponds best to wind sea. For bi- or tri-modal spectra they add two additional conditions:
    a. Wind and wave directional information
    b. Equilibrium range parameter

This method is useful because it does not require wind data.

6. Wind and wave directions. Voorrips et al. (1997) also suggested a 1D identification method that used wind and wave directional information, but is thus only applicable for 2D spectra rather than 1D.

7. JONSWAP spectrum modified. Portilla et al. (2009) suggested using Method 5 from Violante-Carvalho et al. (2002), which introduced an additional criterion related to the magnitude of the fitting parameter (of the JONSWAP spectrum). Portilla et al. (2009) also tested Method 3 (and reported swell under-estimations in sea states) and 4 (reported swell over-estimation in periods of wind sea states).

8. Parametric growth curves. The method suggested for the Catalan coast consisted in separating sea and swell based on the parametric growth curves from Kahma and Calkoen (1992). This method needs in-situ wind data information to calculate the expected peak period for the given wind speed. Wave systems which peak period is larger than 0.7 times the expected peak period are also considered as sea. Otherwise, they are classified as swell.

Bolaños et al. (2005) and Rotés (2004) discuss additional methods that are mainly based on the wave steepness. For unimodal spectra (only one peak) they used the method of Lopatoukhin et al. (2002). For bimodal spectra (two energy peaks) they used the Maximum Steepness method described by Buckley (1988). However, these methods were not convincing and, thus, they were not further considered. Note for example that Portilla et al. (2009) concluded that the existing methods are not very consistent and the combination of different methods is still necessary to obtain more robust results.

III.iv RIMA-Med and A-dw(D) data sets

RIMA-Med field campaign (30 Oct. 2007 – 10 Jan. 2008) measured wind and wave data at several locations in front of Tarragona's harbour. A-dw(D) raw data was available from 20 Aug. 2004 to 25 Nov. 2009. Sea surface time series were retrieved, raw wave data were analysed using WAFO toolbox, and the energy spectra were calculated. 1D spectra were then partitioned and the resulting wave systems were classified (identified) as sea or swell.

Wave systems were separated mainly using the partitioning algorithm described in Portilla et al. (2009). The separation algorithm suggested by Portilla et al. (2009) was written in a MATLAB routine called SPLITseaswell_Portilla09.m. The data from the RIMA-Med campaign were separated using the same algorithm but modified (see previous section) and renamed as SPLITseaswell_Alomar.m.

The three additional criteria used in this work (compared to those in Portilla et al. 2009) are 1) using the peak frequency instead of the mean frequency; 2) the minimum energy of a partition was set to 8% of the total energy (instead of 5%); and 3) the minimum frequency difference between separation frequency and peak frequency was set to 0.015 Hz.

The input of SPLITseaswell_Alomar.m is a 1D frequency spectrum (or a matrix with a spectral time series), and additional settings. Its output is in matrix form (or a structure array if more than one spectrum is being partitioned) with the following information for each partition identified:

1. Energy [m^2];
2. Peak frequency [Hz];
3. Mean frequency [Hz];
4. Separation frequency [Hz];
5. Frequency difference between the peak and the separation value [Hz];
6. Peak energy [m^2/Hz].

The partition and identification procedures were combined in a single MATLAB function called ID_seaswell_1D.m. The output of this function is a structure array with the following information:

<Part.Results> is a matrix with all the partitions with as many rows as the product of time (date) and the spectral partitions and 11 columns, which contain the following variables:

1. Date
2. Significant wave height (m)
3. Mean wave direction (º)
4. Peak wave direction (º)

5. Mean period (s)
6. Peak period (s)
7. Wind speed (m/s)
8. Wind direction (º)
9. TIPO – It refers to the number of partitions of the spectrum and it can have one of the following numbers:
    1. Unimodal (1 peak)
    2. Bimodal (2 peaks)
    3. More than 2 peaks
10. WhatPP – It classifies the partition as sea or swell, and ranks its importance depending on the coexisting wave systems in the same spectrum. Note that the number before the decimal point refers to the nature of the partition:
    1. Wind sea
    2. Swell
    3. Error

The numbers after the decimal point refer to the coexisting partitions in the same spectrum and are ranked starting with the nature of most energetic partition. Thus, possible values of whatPP are:[1; 1.11; 1.12; 1.21; 2; 2.12; 2.21; 2.22; 3; 3.333];

11. Error type:
    1. No error;
    2. The first value in the spectrum is higher than a certain limit;
    3. The last energy value is higher than a maximum energy (or a percentage of the total energy in the spectrum);
    4. The first value of the spectrum is equal to the maximum value;
    5. There are no valid values in the spectrum;

<Part.info> contains info about the structure of the output and the limit values used in the MATLAB function.

11. References

Aarnes, J. E., and Krogstad, H. E., 2001. Partitioning sequences for the dissection of directional ocean wave spectra: A review. Part of work package 4 (Wp4) of the EnviWave research programme under the EU Energy, Environment and Sustainable Development programmepp. EVG-2001-00017, pp. 23.

Abdalla, S., and Cavaleri, L., 2002. Effect of wind variability and variable air density on wave modeling. J. Geophys. Res. 107, pp. 3080.

Abdalla, S., Janssen, P., and Bidlot, J. R. 2003. Use of satellite data and enhanced physics to improve wave predictions.Coastal engineering 2002: solving coastal conundrums: proceedings of the 28th International Conference, 7-12 July 2002, Cardiff, Wales, World Scientific Publishing, Cardiff, UK pp. 87-96.

Annenkov, S. Y., and Shrira, V. I., 2009. 'Fast' nonlinear evolution in wave turbulence. Phys. Rev. Lett. 102, pp. 024502.

Ardhuin, F., Herbers, T. H. C., van Vledder, G. P., Watts, K. P., Jensen, R., and Graber, H. C., 2007. Swell and Slanting-Fetch Effects on Wind Wave Growth. J. Phys. Oceanogr. 37, pp. 908-931.

Ardhuin, F., Rogers, E., Babanin, A. V., Filipot, J., Magne, R., Roland, A., van der Westhuysen, A., Queffeulou, P., Lefevre, J., Aouf, L., and Collard, F., 2010. Semiempirical dissipation source functions for ocean waves. Part I: definition, calibration, and validation. J. Phys. Oceanogr. 40, pp. 1917-1941.

Ardhuin, F., Stutzmann, E., Schimmel, M., and Mangeney, A., 2011. Ocean wave sources of seismic noise. J. Geophys. Res. 116, pp. C09004.

Ardhuin, F., Bertotti, L., Bidlot, J., Cavaleri, L., Filipetto, V., Lefevre, J., and Wittmann, P., 2007. Comparison of wind and wave measurements and models in the Western Mediterranean Sea. Ocean Eng. 34, pp. 526-541.

Ataktürk, S. S., and Katsaros, K. B., 1999. Wind Stress and Surface Waves Observed on Lake Washington. J. Phys. Oceanogr. pp. 633-650.

Babanin, A. V., and van der Westhuysen, A., 2008. Physics of "saturation-based" dissipation functions proposed for wave forecast models. J. Phys. Oceanogr. 38, pp. 1831-1841.

Babanin, A. V., and Makin, V. K., 2008. Effects of wind trend and gustiness on the sea drag: Lake George study. J. Geophys. Res. 113, pp. C02015.

Babanin, A. V., and Soloviev, Y. P., 1998. Field Investigation of Transformation of the Wind Wave Frequency Spectrum with Fetch and the Stage of Development. J. Phys. Oceanogr. 28, pp. 563-576.

Badulin, S. I., Babanin, A. V., Zakharov, V. E., and Resio, D., 2007. Weakly turbulent laws of wind-wave growth. J. Fluid Mech. 591, pp. 339-378.

Badulin, S. I., Pushkarev, A. N., Resio, D., and Zakharov, V. E., 2005. Self-similarity of wind-driven seas. Nonlinear Processes in Geophysics. 12, pp. 891-945.

Banner, M. L., and Morison, R. P., 2010. Refined source terms in wind wave models with explicit wave breaking prediction. Part I: Model framework and validation against field data. Oc. Mod. 33, pp. 177-189.

Battjes, J. A., Zitman, T. J., and Holthuijsen, L. H., 1987. A Reanalysis of the Spectra Observed in JONSWAP. J. Phys. Oceanogr. pp. 1288-1295.

Bauer, E., and Weisse, R., 2000. Determination of high-frequency wind variability from observations and application to North Atlantic wave modeling. J. Geophys. Res. 105, pp. 26179-26190.

Bentamy, A., Ayina, H., Queffeulou, P., Croize-Fillon, D., and Kerbaol, V., 2007. Improved near real time surface wind resolution over the Mediterranean Sea. Ocean Science. 3, pp. 259-271.

Bertotti, L., and Cavaleri, L., 2009. Large and small scale wave forecast in the Mediterranean Sea. Nat.Hazards Earth Syst.Sci. 9, pp. 779-788.

Bidlot, J., 2001. ECMWF wave-model products. ECMWF Newsletterpp. 91, pp. 9-15.

Bolaños, R., 2004. Tormentas de oleaje en el Mediterráneo: Física y predicción. PhD Thesis. Universitat Politècnica De Catalunya.

Bolaños, R., Rotés, A., and Sanchez-Arcilla, A. 2005. Spectral wave climate at northern Spain's Mediterranean coast.Ocean Waves Measurements and Analysis, 5th International Symposium WAVES, ASCE, Madrid, Spain.

Bolaños, R., and Sánchez-Arcilla, A., 2006. A note on nearshore wave features: Implications for wave generation. Prog. Oceanogr. 70, pp. 168-180.

Bolaños, R., Sanchez-Arcilla, A., and Cateura, J., 2007. Evaluation of two atmospheric models for wind–wave modelling in the NW Mediterranean. J. Marine Syst. 65, pp. 336-353.

Bolaños, R., Sánchez-Arcilla, A., Gomez, J., and Cateura, J. 2004. Limits of operational wave prediction in the north-western Mediterranean.Proceedings of the 29th International Conference on Coastal Engineering 2004, ICCE, Lisbon, Portugal. Jane McKee Smith. World Scientific, National Civil Engineering Laboratory, Lisbon, Portugal, pp. 818-829.

Bolaños, R., Jorda, G., Cateura, J., Lopez, J., Puigdefabregas, J., Gomez, J., and Espino, M., 2009. The XIOM: 20 years of a regional coastal observatory in the Spanish Catalan coast. J. Marine Syst. 77, pp. 237-260.

Bolaños, R., Osuna, P., Wolf, J., Monbaliu, J., and Sanchez-Arcilla, A., 2011. Development of the POLCOMS–WAM current–wave model. Ocean Modelling. 36, pp. 102-115.

Booij, N., Ris, R. C., and Holthuijsen, L. H., 1999. A third-generation wave model for coastal regions 1. Model description and validation. J. Geophys. Res. 104, pp. 7649-7666.

Bottema, M., and van Vledder, G., 2008. Effective fetch and non-linear four-wave interactions during wave growth in slanting fetch conditions. Coast. Eng. 55, pp. 261-275.

Bottema, M., and van Vledder, G. P., 2009. A ten-year data set for fetch- and depth-limited wave growth. Coast. Eng. 56, pp. 703-725.

Bretschneider, C. L., 1952. The generation and decay of wind waves in deep water. Trans. Am. Geophys. Union. 33, pp. 381-389.

Breugem, W. A., and Holthuijsen, L. H., 2007. Generalized Shallow Water Wave Growth from Lake George. J. Waterw. Port Coast. Ocean Eng. 133, pp. 173-182.

Brodtkorb, P. A., Johannesson, P., Lindgren, G., Rychlik, I., Ryden, J., and Sjö, E. 2000. WAFO - a Matlab Toolbox for the analysis of random waves and loads.Proc. 10th Int. Offshore and Polar Eng. Conf., ISOPE, Seattle, USA, pp. 343-350.

Buckley, W. H., 1988. Extreme and climatic wave spectra for use in structural design of ships. Nav. Eng. J. 100, pp. 36-58.

Casas-Prat, M., 2008. Overview of ocean wave statistics. Minor Thesis. Universitat Politècnica De Catalunya.

Casas-Prat, M., and Holthuijsen, L. H., 2010. Short-term statistics of waves observed in deep water. J. Geophys. Res. 115, pp. C09024.

Cavaleri, L., 2009. Wave modeling-missing the peaks. J. Phys. Oceanogr. 39, pp. 2757-2778.

Cavaleri, L., and Bertotti, L., 2006. The improvement of modelled wind and wave fields with increasing resolution. Ocean Eng. 33, pp. 553-565.

Cavaleri, L., and Bertotti, L., 2004. Accuracy of the modelled wind and wave fields in enclosed seas. Tellus A. 56, pp. 167-175(9).

Cavaleri, L., and Bertotti, L., 2003. The characteristics of wind and wave fields modelled with different resolutions. Q. J. R. Meteorol. Soc. 129, pp. 1647-1662.

Cavaleri, L., and Bertotti, L., 1997. In search of the correct wind and wave fields in a minor basin. Mon. Weather Rev. pp. 1964-1975.

Cavaleri, L., and Sclavo, M., 2006. The calibration of wind and wave model data in the Mediterranean Sea. Coast. Eng. 53, pp. 613-627.

Cavaleri, L., 2006. Wave modeling: where to go in the future. Bull. Am. Meteorol. Soc. 87, pp. 207-214.

Charnock, H., 1955. Wind stress on a water surface. Q. J. R. Meteorol. Soc. 81, pp. 639-640.

Codina, B., Aran, M., Young, S., and Redaño, A., 1997. Prediction of a mesoscale convective system over Catalonia (Northeastern Spain) with a nested numerical model. Meteorol. Atmos. Phys. 62, pp. 9-22.

Datawell BV, 2009. Datawell Waverider Reference Manual.

Dobson, F., Perrie, W., and Toulany, B., 1989. On the deep-water fetch laws for wind-generated surface gravity waves. Atmos. Ocean. 27, pp. 210-236.

Donelan, M. A., Skafel, M., Graber, H. C., Liu, P., Schwab, D., and Venkatesh, S., 1992. On the growth rate of wind-generated waves. Atmos. Ocean. 30, pp. 457-478.

Donelan, M. A., Hamilton, J., and Hui, W. H., 1985. Directional Spectra of Wind-Generated Waves. Philosophical Transactions of the Royal Society of London.Series A, Mathematical and Physical Sciences. 315, pp. 509-562.

Donelan, M. A., Babanin, A. V., Young, I. R., and Banner, M. L., 2006. Wave-Follower Field Measurements of the Wind-Input Spectral Function. Part II: Parameterization of the Wind Input. J. Phys. Oceanogr. 36, pp. 1672-1689.

Drennan, W. M., Graber, H. C., Hauser, D., and Quentin, C., 2003. On the wave age dependence of wind stress over pure wind seas. J. Geophys. Res. 108, pp. 8062.

Earle, M. D., 1984. Development of algorithms for separation of sea and swell. National Data Buoy Centerpp. MEC-87-1, pp. 1-53.

Ewans, K. C., and Kibblewhite, A. C., 1990. An Examination of Fetch-Limited Wave Growth off the West Coast of New Zealand by a Comparison with the JONSWAP Results. J. Phys. Oceanogr. pp. 1278-1296.

Ewing, J. A., 1980. Observations of wind-waves and swell at an exposed coastal location. Estuarine and Coastal Marine Science. 10, pp. 543-554.

Flamant, C., Pelon, J., Hauser, D., Quentin, C., Drennan, W. M., Gohin, F., Chapron, B., and Gourrion, J., 2003. Analysis of surface wind and roughness length evolution with fetch using a combination of airborne lidar and radar measurements. J. Geophys. Res. 108(C3), pp. 8058.

Gagnaire-Renou, E., Benoit, M., and Forget, P. 2008. Modeling waves in fetch-limited and slanting fetch conditions using a quasi-exact method for nonlinear four-wave interactions.Proc. 31st Int. Conf. on Coastal Eng. 1-5 September 2008, Hamburg (Germany), pp. 496-507.

García, M. A., Sánchez-Arcilla, A., Sierra, J. P., Sospedra, J., and Gómez, J., 1993. Wind waves off the Ebro Delta, NW Mediterranean. J. Marine Syst. 4, pp. 235-262.

Gerling, T. W., 1992. Partitioning sequences and arrays of directional ocean wave spectra into component wave systems. J. Atmos. Ocean. Technol. pp. 444-458.

Gilhousen, D. B., and Hervey, R. 2001. Improved estimates of swell from moored buoys.Ocean Wave Measurement and Analysis Proceedings of the Fourth International Symposium, ASCE Conf. Proc.

Grell, G. A., Dudhia, J., and Stauffer, D. R., 1994. Description of the fifth-Generation Penn State/NCAR Mesoscale Model (MM5). NCAR Tech. Note, NCAR/TN-398-STR.

Guadayol, O., and Peters, F., 2006. Analysis of wind events in a coastal area: a tool for assessing turbulence variability for studies on plankton. Sci. Mar. (Barc.). pp. 9-20.

Guedes Soares, C., and Nolasco, M. C., 1992. Spectral Modelling of Sea States with Multiple Wave Systems. J. Offshore Mech. Arct. Eng. 114, pp. 278-284.

Günther, H., Hasselmann, S., and Janssen, P. A. E. M., 1992. WAM-model: cycle 4 (revised version). pp. Techn. Rep. No. 4.

Hanson, J. L., and Phillips, O. M., 1999. Wind Sea Growth and Dissipation in the Open Ocean. J. Phys. Oceanogr. pp. 1633-1648.

Hanson, J. L., and Phillips, O. M., 2001. Automated analysis of ocean surface directional wave spectra. J. Atmos. Ocean. Technol. pp. 277-293.

Hargreaves, J. C., and Annan, J. D., 2001. Comments on "Improvement of the Short-Fetch Behavior in the Wave Ocean Model (WAM)". J. Atmos. Oceanic Technol. 18, pp. 711-715.

Hasselmann, K., Barnett, T. P., Bouws, E., Carlson, D. E., Cartwright, D. E., Enke, K., Ewing, J. A., Gienapp, H., Hasselmann, D. E., Kruseman, P., Meerburg, A., Müller, P., Olbers, D. J., Richter, K., Sell, W., and Walden, H., 1973. Measurements of wind-wave growth and swell decay during the Joint North Sea Wave Project (JONSWAP). Dtsch. Hydrogr. Z. 8, pp. 1-95.

Hasselmann, S., Brüning, C., and Hasselmann, K., 1996. An improved algorithm for the retrieval of ocean wave spectra from synthetic aperture radar image spectra. J. Geophys. Res. 101, pp. 615-629.

Hasselmann, S., Hasselmann, K., Allender, J. H., and Barnett, T. P., 1985. Computations and parameterizations of the nonlinear energy transfer in a gravity-wave spectrum. Part II: Parameterizations of the nonlinear energy transfer for application in wave models. J. Phys. Oceanogr. pp. 1378-1391.

Haus, B. K., 2007. Surface current effects on the fetch-limited growth of wave energy. J. Geophys. Res. 112, pp. C03003.

Hersbach, H., and Janssen, P. A. E. M., 1999. Improvement of the Short-Fetch Behavior in the Wave Ocean Model (WAM). J. Atmos. Ocean. Technol. pp. 884-892.

Holthuijsen, L. H., 1983. Observations of the directional distribution of ocean wave energy. J. Phys. Oceanogr. 13, pp. 191-207.

Holthuijsen, L. H., 2007. Waves in Oceanic and Coastal Waters, Cambridge University Press, Cambridge, UK.

Houmb, O. G., and Due, E., 1978. On the occurrence of wave spectra with more than one peak, Division of Port and Ocean Engineering, University of Trondheim, Norwegian Institute of Technology, Trondheim, Norway.

Hurdle, D. P., and Stive, R. J. H., 1989. Revision of SPM 1984 wave hindcast model to avoid inconsistencies in engineering applications. Coast. Eng. 12, pp. 339-351.

Hwang, P. A., García-Nava, H., and Ocampo-Torres, F., 2011. Observations of wind wave development in mixed seas and unsteady wind forcing. J. Phys. Oceanogr. 41, pp. 2343-2362.

Hwang, P. A., 2006. Duration- and fetch-limited growth functions of wind-generated waves parameterized with three different scaling wind velocities. J. Geophys. Res. 111, pp. C02005.

Hwang, P. A., and Wang, D. W., 2004. Field measurements of duration-limited growth of wind-generated ocean surface waves at young stage of development. J. Phys. Oceanogr. pp. 2316-2326.

IFREMER, 2007. ftp://ftp.ifremer.fr/ifremer/cersat/products/gridded/mwf-blended/data/6-hourly/2007/12/ (8/18, 2010).

Janssen, P. A. E. M., 2008. Progress in ocean wave forecasting. Journal of Computational Physics. 227, pp. 3572-3594.

Janssen, P. A. E. M., 1991. Quasi-linear theory of wind-wave generation applied to wave forecasting. J. Phys. Oceanogr. 21, pp. 1631-1642.

Janssen, P. A. E. M., 1989. Wave-induced stress and the drag of air flow over sea waves. J. Phys. Oceanogr. 19, pp. 745-754.

Jouon, A., Lefebvre, J. P., Douillet, P., Ouillon, S., and Schmied, L., 2009. Wind wave measurements and modelling in a fetch-limited semi-enclosed lagoon. Coast. Eng. 56, pp. 599-608.

Kahma, K. K., 1981. A study of the growth of the wave spectrum with fetch. J. Phys. Oceanogr. pp. 1503-1515.

Kahma, K. K., and Calkoen, C. J., 1992. Reconciling discrepancies in the observed growth of wind-generated waves. J. Phys. Oceanogr. pp. 1389-1405.

Kenney, B. C., 1982. Beware of spurious self-correlations! Water Resour. Res. 18, pp. 1041-1048.

Kitaigorodskii, S. A., 1962. Applications of the theory of similarity to the analysis of wind-generated wave motion as a stochastic process. Izv. Akad. Mauk SSSR, Geophys. pp. 105-107.

Koçak, K., 2002. A method for determination of wind speed persistence and its application. Energy. 27, pp. 967-973.

Komen, G. J., Cavaleri, L., Donelan, M., Hasselmann, K., Hasselmann, S., and Janssen, P. A. E. M., 1994. Dynamics and modelling of ocean waves, Cambridge University Press, Cambridge, UK.

Komen, G. J., Hasselmann, K., and Hasselmann, K., 1984. On the existence of a fully developed wind-sea spectrum. J. Phys. Oceanogr. 14, pp. 1271-1285.

Lamont-Smith, T., and Waseda, T., 2008. Wind wave growth at short fetch. J. Phys. Oceanogr. pp. 1597-1606.

Le Roux, J. P., 2009. Characteristics of developing waves as a function of atmospheric conditions, water properties, fetch and duration. Coast. Eng. 56, pp. 479-483.

Leake, J., 2007. Wave modelling within the Coastal simulator. pp. 1-14.

Lin, W., Sanford, L. P., Suttles, S. E., and Valigura, R., 2002. Drag Coefficients with Fetch-Limited Wind Waves. J. Phys. Oceanogr. 32, pp. 3058-3074.

Liu, P. C., and Ross, D. B., 1980. Airborne measurements of wave growth for stable and unstable atmospheres in Lake Michigan. J. Phys. Oceanogr. 10, pp. 1842–1853.

Lopatoukhin, L., Rozhtov, V., Boukhanovsky, A., Degtyarev, A., Saskov, K., Athanassoulis, G., Stefanakos, C., and Krogstad, H. E. 2002. The spectral wave climate in the Barents Sea.ASME, Oslo, Norway, pp. 283-289.

Mitsuyasu, H., and Yoshida, Y., 2005. Air-Sea Interactions under the Existence of Opposing Swell. J. Oceanogr. 61, pp. 141-154.

Monbaliu, J., Padilla-Hernandez, R., Hargreaves, J. C., Albiach, J. C. C., Luo1, W., Sclavo, M., and Günther, H., 2000. The spectral wave model, WAM, adapted for applications with high spatial resolution. Coast. Eng. 41, pp. 41-62.

Niclasen, B. A., 2006. An operational wave model for the Faroe Shelf. PhD Thesis. University of the Faroe Islands.

Ocampo-Torres, F., García-Nava, H., Durazo, R., Osuna, P., Díaz Méndez, G., and Graber, H., 2011. The int OA Experiment: A Study of Ocean-Atmosphere Interactions Under Moderate to Strong Offshore Winds and Opposing Swell Conditions in the Gulf of Tehuantepec, Mexico. Bound. -Layer Meteorol. 138, pp. 433-451.

Ocampo-Torres, F. J., 2001. On the homogeneity of the wave field in coastal areas as determined from ERS-2 and RADARSAT synthetic aperture radar images of the ocean surface. Scientia Marina. 65.

Pettersson, H., 2004. Wave growth in a narrow bay. Finnish Institute of Marine Research. Contributions No. 9, pp. 33.

Pettersson, H., Kahma, K. K., and Tuomi, L., 2010. Wave Directions in a Narrow Bay. J. Phys. Oceanogr. 40, pp. 155-169.

Pettersson, H., 2005. Directional measurements of wave growth in a short and narrow fetch geometry Journal of Atmospheric & Ocean Science. 10, pp. 15.

Pierson, W. J., and Moskowitz, L., 1964. A proposed spectral form for fully developed wind seas based on the similarity theory of SA Kitaigorodskii. J. Geophys. Res. 69, pp. 5181-5190.

Ponce de León, S., and Ocampo-Torres, F. J., 1998. Sensitivity of a wave model to wind variability. J. Geophys. Res. 103, pp. 3179-3201.

Portilla, J., Ocampo-Torres, F. J., and Monbaliu, J., 2009. Spectral Partitioning and Identification of Wind Sea and Swell. J. Atmos. Ocean. Technol. pp. 107-122.

Puertos del Estado, 2008. Tráficos portuarios. Revista De Puertos. 144, pp. 78-82.

Queffeulou, P., and Bentamy, A., 2007. Analysis of Wave Height Variability Using Altimeter Measurements: Application to the Mediterranean Sea. J. Atmos. Oceanic Technol. 24, pp. 2078-2092.

Quentin, C. G., 2002. Etude de la surface océanique, de sa signature radar et de ses interactions avec les flux turbulents de quantité de mouvement dans le cadre de l'experience FETCH. pp. 263.

Resio, D., Bratos, S., and and Thompson, E. (2002). "Meteorology and Wave Climate." *Coastal Engineering Manual. Engineer Manual 1110-2-1100*, L. Vincent, and Z. and Demirbilek, eds.,Washington, DC., II-2-1-II-2-71.

Ris, R. C., Holthuijsen, L. H., and Booij, N., 1999. A third-generation wave model for coastal regions: 2. Verification. J. Geophys. Res. 104, pp. 7667-7681.

Rodríguez, G., and Guedes Soares, C., 1999. A criterion for the automatic identification of multimodal sea wave spectra. Appl. Ocean Res. 21, pp. 329-333.

Rogers, W., Kaihatu, J., Petit, H., Booij, N., and Holthuijsen, L., 2002. Diffusion reduction in an arbitrary scale third generation wind wave model. Ocean Eng. 29, pp. 1357-1390.

Rogers, W. E., Hwang, P. A., and Wang, D. W., 2003. Investigation of wave growth and decay in the SWAN Model: Three regional-scale applications. J. Phys. Oceanogr. pp. 366-389.

Rotés, A., 2004. Clima espectral de oleaje en la costa Catalana. Minor Thesis. Universitat Politècnica De Catalunya.

Sánchez-Arcilla, A., González-Marco, D., and Bolaños, R., 2008. A review of wave climate and prediction along the Spanish Mediterranean coast. Nat. Hazard. Earth Sys. 8, pp. 1217-1228.

Signell, R. P., Carniel, S., Cavaleri, L., Chiggiato, J., Doyle, J. D., Pullen, J., and Sclavo, M., 2005. Assessment of wind quality for oceanographic modelling in semi-enclosed basins. J. Marine Syst. 53, pp. 217-233.

Smith, S. D., and Banke, E. G., 1975. Variation of the sea surface drag coefficient with wind speed. Q. J. R. Meteorol. Soc. 101, pp. 665-673.

Stelling, G. S., and Leendertse, J. J. 1992. Approximation of convective processes by cyclic AOI methods.ASCE, Tampa, Florida, pp. 771-782.

Sverdrup, H. U., and Munk, W. H., 1947. Wind, sea, and swell: theory of relations for forecasting. U.S. Navy Hydrographic Officepp. Publication. No. 601.

Sverdrup, H. U., and Munk, W. H., 1946. Empirical and theoretical relations between wind, sea and swell. Trans. Am. Geophys. Union. 27, pp. 823–827.

The SWAN team, 2009. SWAN scientific and technical documentation. SWAN Cycle III version 40.72ABCD.

The WAMDI Group: Hasselmann, S., Hasselmann, K., Bauer, E., Janssen, P., Komen, G., Bertotti, L., Lionello, P., Guillaume, A., Cardone, V., and Greenwood, J., 1988. The WAM model-a third generation ocean wave prediction model. J. Phys. Oceanogr. 18, pp. 1775-1810.

The WISE Group, Cavaleri, L., Alves, J. -. G. M., Ardhuin, F., Babanin, A., Banner, M., Belibassakis, K., Benoit, M., Donelan, M., Groeneweg, J., Herbers, T. H. C., Hwang, P., Janssen, P. A. E. M., Janssen, T., Lavrenov, I. V., Magne, R., Monbaliu, J., Onorato, M., Polnikov, V., Resio, D., Rogers, W. E., Sheremet, A., McKee Smith, J., Tolman, H. L., van Vledder, G., Wolf, J., and Young, I., 2007. Wave modelling – The state of the art. Prog. Oceanogr. 75, pp. 603-674.

Tolman, H., 2002. Limiters in third-generation wind wave models. J. Atmos. Ocean. Sci. 8, pp. 67-83.

Tolosana-Delgado, R., Egozcue, J., Sáchez-Arcilla, A., and Gómez, J., 2010. Wave height data assimilation using non-stationary kriging. Comput. Geosci. pp. 363-370.

Tsagareli, K. N., Babanin, A. V., Walker, D. J., and Young, I. R., 2010. Numerical investigation of spectral evolution of wind waves. Part I: wind-Input source function. J. Phys. Oceanogr. 40, pp. 656-666.

Tucker, M. J., and Pitt, E. G., 2001. Waves in ocean engineering, Elsevier Science Ltd., Oxford, UK.

U.S. Army Corps of Engineers, 1984. Shore Protection Manual, Coastal Engineering Research Center, Washington, D.C.

Uz, B. M., Donelan, M. A., Hara, T., and Bock, E. J., 2002. Laboratory studies of wind stress over surface waves. Bound. -Layer Meteorol. 102, pp. 301-331.

Van der Westhuysen, A. J., Zijlema, M., and Battjes, J. A., 2007. Nonlinear saturation-based whitecapping dissipation in SWAN for deep and shallow water. Coast. Eng. 54, pp. 151-170.

Van Vledder, G. P., 2006. The WRT method for the computation of non-linear four-wave interactions in discrete spectral wave models. Coast. Eng. 53, pp. 223-242.

Violante-Carvalho, N., Ocampo-Torres, F. J., and Robinson, I. S., 2004. Buoy observations of the influence of swell on wind waves in the open ocean. Appl. Ocean Res. 26, pp. 49-60.

Violante-Carvalho, N., Parente, C. E., Robinson, I. S., and Nunes, L. M. P., 2002. On the growth of wind-generated waves in a swell-dominated region in the south Atlantic. J. Offshore Mech. Arct. Eng. 124, pp. 14-21.

Voorrips, A. C., Makin, V. K., and Hasselmann, S., 1997. Assimilation of wave spectra from pitch-and-roll buoys in a North Sea wave model. J. Geophys. Res. 102, pp. 5829-5850.

Walsh, E. J., Hancock III, D. W., Hines, D. E., Swift, R. N., and Scott, J. F., 1989. An observation of the directional wave spectrum evolution from shoreline to fully developed. J. Phys. Oceanogr. 19, pp. 670-690.

Wang, D. W., and Hwang, P. A., 2001. An operational method for separating wind sea and swell from ocean wave spectra. J. Atmos. Ocean. Technol. pp. 2052-2062.

Wetterzentrale, 2012. "NCEP-reanalysis." http://www.wetterzentrale.de/topkarten/fsreaeur.html.

Wyatt, L. R. 1998a. The SCAWVEX project. ASCE, Virginia Beach, Virginia, USA, pp. 1457-1467.

Wyatt, L. R. 1998b. Variability in wave spectra measured by HF radar.ASCE, Virginia Beach, Virginia, USA, pp. 355-369.

Wyatt, L. R., Green, J. J., and Middleditch, A., 2011. HF radar data quality requirements for wave measurement. Coast. Eng. 58, pp. 327-336.

Young, I. R., 1998. An experimental investigation of the role of atmospheric stability in wind wave growth. Coast. Eng. 34, pp. 23-33.

Young, I. R., Hasselmann, S., and Hasselmann, K., 1987. Computations of the response of a wave spectrum to a sudden change in wind direction. J. Phys. Oceanogr. pp. 1317-1338.

Young, I. R., and Verhagen, L. A., 1996. The growth of fetch limited waves in water of finite depth. Part 1. Total energy and peak frequency. Coast. Eng. 29, pp. 47-78.

Zijlema, M., and van der Westhuysen, A. J., 2005. On convergence behaviour and numerical accuracy in stationary SWAN simulations of nearshore wind wave spectra. Coast. Eng. 52, pp. 237-256.

Abbreviations

ANOVA	Statistical method to calculate the Analysis of Variance
AWAC	Acoustic dopplerWAve and Current profiler
BSBT	Backward in Space Backward in Time numerical scheme
dd	Day
DIA	Discrete Interaction Approximation (Hasselmann et al. 1985)
DO85	Refer to Donelan et al. (1985)
E	East direction
ECMWF	European Centre for Medium-Range Weather Forecasts
EPPE	Ports of the State; *(in Spanish)* Ente Público Puertos del Estado
FFT	Fast Fourier Transform
h	Hours; 1 h = 360 s.
JON73	Refer to Hasselmann et al. (1973)
K81	Refer to Kahma (1981)
KC92	Refer to Kahma and Calkoen (1992)
KOM	Refer to Komen et al. (1994)
JAN	Refer to Janssen (1989, 1991)
LIM	Maritime Engineering Laboratory; (in Spanish) Laboratorio de Ingeniería Marítima

MASS	Mesocale Atmospheric Simulation System (see e.g. Codina et al. 1997)
mm	Month
MM5	Fifth generation Mesoscale Model (see e.g. Grell et al. 1994)
NW	North west
RIMA	Reducing maritime risks using high resolution model; *(in Spanish)* Hacia una reducción de RIesgos MArítimos usando modelado de alta resolución
RIMA-Atl	Field campaign carried on in the Coruña Bay in fall 2008
RIMA-Med	Field campaign carried on in the NW Mediterranean in fall 2007
S	South
S&L	Third order numerical scheme after Stelling and Leendertse (1992)
SMC	Meteorological Service of Catalonia; (*in Catalan*) Servei Meteorològic de Catalunya
SORDUP	Second ORDer Upwind numerical scheme (see Rogers et al. 2002
SWAN	Simulating Waves Nearshore wave model (Booij et al. 1999, Ris et al. 1999)
UPC	Technical University of Catalonia; (*in Catalan*) Universitat Politècnica de Catalunya
W	West
WAM	WAve Model (see e.g. Monbaliu et al. 2000)
WESTH	Refer to Van der Westhuysen et al. (2007)
XIOM	Network for oceanographic and coastal meteorological measurements; *(in Catalan)* Xarxa d'Instrumentació Oceanogràfica i Meteorològica
XNL	eXact Non-Linear transfer method to compute non-linear interactions (see Van Vledder 2006)
yyyy	Year

Variables

$a_{0,n}$	Slope of the linear function fitting the non-dimensional variables in log-axis
a_n	Y-intercept of the non-dimensional growth curves $a_n = \exp\left(a_{0,n}\right)$.
α	Direction from an offshore position to the coast (º)
α_{CH}	Charnock's constant
b	Energy development rate
β	Calibration factor in Komen et al. (1984)
c	Frequency downshift rate
C_{D}	Drag coefficient
C_{ds}	Tuneable coefficient of Γ
CN	Courant Number
C_g	Group velocity (m/s)
C_p	Celerity of the waves peak (m/s)
Γ	Steepness dependent coefficient involved in dissipation through whitecapping
δ	Tuneable coefficient of Γ
Δt	Integration time step (min)
Δx	Spatial resolution (m)
E	Wave energy calculated as the integral of the energy spectra (m^2)
$\overline{E}$	Non-dimensional energy

f_i	Values of the forecast model (fit equation)
f_m	Mean frequency (Hz)
f_{NY}	Nyquist frequency (Hz)
f_p	Peak frequency (Hz)
f_s	Separation frequency (Hz)
$\overline{f}$	Non-dimensional energy
φ	Directional difference between wind and waves (degrees)
g	Acceleration due to gravity g = 9.81 m/s
h	Depth (m)
$H_{1/3}$	Mean of the 1/3 highest waves of a surface elevation time series (m)
H_{min}	Minimum wave height required in the quality control procedure (Annex II) (m)
H_{max}	Maximum wave height in the raw time series (m)
H_s	Significant wave height (m)
k; $\tilde{k}$	Wave number; mean wave number
L_0	Wave length in deep waters (m)
L_p	Wave length of the waves in the peak of the spectrum (m)
m_n	Momentum of n-order
p	Tuneable coefficient of Γ
R^2	Coefficient of determination of a fit model
R_b	Bulk Richardson number to estimate atmospheric stability
$\tilde{s}$	Overall wave steepness
$\tilde{s}_{PM}$	Steepness of the Pierson-Moskowitz spectrum: $\tilde{s}_{PM} = \sqrt{3.02 \cdot 10^{-3}}$

stpm	$= \tilde{s}_{PM}{}^2$
$\sigma, \tilde{\sigma}$	Frequency, mean frequency (rad)
ψ	Wind direction (º)
$S_{ds,w}$	Whitecapping dissipation term in spectral wave models
slope	Slope of a regression equation where the variables where log-transformed.
slope-1	Statistical measure of the proportion of over/under-estimation (bias) of the forecast model (dependent variable) versus the observations (independent variable). It is equal to *slope* minus **1**
t	Time (s)
T_a	Air temperature (ºC)
T_p	Peak period (s)
T_w	Water temperature (ºC)
θ	Wave direction
θ_m	Mean wave direction (degrees from the north in a clockwise sense)
θ_p	Peak wave direction (degrees from the north in a clockwise sense)
U	Wind speed (m/s)
U*	Friction velocity
U_z	Wind speed at height z (m/s)
U_{10}	Wind speed 10 m above the sea surface (m/s)
x	Independent variable in a typical regression equation
X	Fetch (m)
$\overline{X}$	Non-dimensional fetch

y, y_i	Dependent variable in a typical regression equation
$\bar{y}$	Mean of the simulations (dependent variable) in a regression equation
z	Height at which wind is measured (m)
z_0	Roughness length (m)
z_T	Height at which air temperature is measured (m)

List of Figures

List of tables

CIIRC
International Centre
for Coastal Resources
Research

UNIVERSITAT POLITÈCNICA
DE CATALUNYA
BARCELONATECH

Laboratori d'Enginyeria Marítima
UNIVERSITAT POLITÈCNICA DE CATALUNYA